



**HAL**  
open science

# Topology optimisation of electromagnetic devices

Bibi Safoorah Bilquis Mohamodhosen

► **To cite this version:**

Bibi Safoorah Bilquis Mohamodhosen. Topology optimisation of electromagnetic devices. Electromagnetism. Ecole Centrale de Lille, 2017. English. NNT : 2017ECLI0028 . tel-01818091

**HAL Id: tel-01818091**

**<https://theses.hal.science/tel-01818091>**

Submitted on 3 Jul 2019

**HAL** is a multi-disciplinary open access archive for the deposit and dissemination of scientific research documents, whether they are published or not. The documents may come from teaching and research institutions in France or abroad, or from public or private research centers.

L'archive ouverte pluridisciplinaire **HAL**, est destinée au dépôt et à la diffusion de documents scientifiques de niveau recherche, publiés ou non, émanant des établissements d'enseignement et de recherche français ou étrangers, des laboratoires publics ou privés.

N° d'ordre : 341

**CENTRALE LILLE**

## **THESE**

Présentée en vue  
d'obtenir le grade de

## **DOCTEUR**

En

**Spécialité : Génie Electrique**

Par

**MOHAMODHOSEN Bilquis**

**DOCTORAT DELIVRE PAR CENTRALE LILLE**

Titre de la thèse :

**TOPOLOGY OPTIMISATION OF ELECTROMAGNETIC DEVICES**

**OPTIMISATION TOPOLOGIQUE DE DISPOSITIFS ELECTROMAGNETIQUES**

Soutenue le 6 décembre 2017 devant le jury d'examen :

<b>Président</b>	<i>Betty Semail, Professeur, Polytech Lille</i>
<b>Rapporteur</b>	<i>Frédéric Messine, Professeur, ENSEEIHT- Toulouse</i>
<b>Rapporteur</b>	<i>Bruno Dehez, Professeur, Université Catholique de Louvain</i>
<b>Directeur de thèse</b>	<i>Frédéric Gillon, Maître de Conférences HDR, Centralelille</i>
<b>Co-Directeur de thèse</b>	<i>Abdelmounaïm Tounzi, Professeur, Université Lille 1</i>
<b>Membre</b>	<i>Stéphane Vivier, Maître de Conférences HDR, UT Compiègne</i>
<b>Invité</b>	<i>Jean-Claude Mipo, Société Valéo</i>

Thèse préparée dans le Laboratoire L2EP  
avec le soutien financier de la Région Hauts-de-France  
Ecole Doctorale SPI 072



L'établissement Centrale Lille, le laboratoire L2EP, les encadrants de la thèse et moi-même remercions sincèrement la région Hauts-de-France pour le support financier apporté à ces travaux de recherche. Nous remercions également l'état français sans lequel ces travaux de recherche n'auraient pu être réalisés. Je remercie à titre personnel Centrale Lille et le L2EP de m'avoir donné l'opportunité de conduire ma thèse au sein de leur institution.

## Abstract

Topology Optimisation (TO) is a fast growing topic that has been sparking the interest of many researchers for the past two decades in the electromagnetic community. Its attractiveness lies in the originality of finding innovative structures without any layout a priori. This thesis work is oriented towards the TO of electromagnetic devices by elaborating on various aspects of the subject. First of all, a tool for TO is developed and tested, based on the ‘home-made’ tools available at the L2EP. As TO requires a FE and an optimisation tool working together, a coupling is done using both. Furthermore, a TO methodology is developed and tested, based on the Density Method. An academic cubic test case is used to carry out all the tests, and validate the tools and methodology. An approach is also developed to consider the nonlinear behaviour of the ferromagnetic materials with our TO tools. Afterwards, the methodology is applied to a 3D electromagnet, which represents a more real test case. This test case also serves to compare the results with linear and nonlinear behaviour of the materials used. Various topologies are presented, for different problem formulations. Subsequently, the methodology is applied to a more complex electromagnetic device: a Salient Pole Synchronous Generator. This example allows us to see how the problem definition can largely affect TO results. Some topologies are presented and their viability is discussed.

## Acknowledgements

The journey of a PhD student towards the glorious day of being awarded the title of Doctor is a long and strenuous one, during which the support and help of others is simply a *sine qua non*. I wholeheartedly seize this moment to express my gratitude and appreciation towards those who have fuelled my determination, or simply made the road more pleasant.

God, thank You for giving me all the grit I needed to pursue my dreams and attain my goals; You were inarguably the one who knew all of my ups and downs.

Before addressing some words to the people who have been there throughout my PhD, I would like to thank the members of the jury for making the defence day possible despite their numerous commitments. Thank you Pr. Frédéric Messine and Pr. Bruno Dehez for accepting the responsibility of rapporteur to my thesis, for your relevant suggestions and useful interrogations; Stephane Vivier (HDR) and Dr. Jean Claude Mipo for keeping a practical and industrial analysis to the discussion as jury members, and Pr. Betty Semail for her timely presiding of the jury.

I am very grateful to my two thesis directors, Pr. Frédéric Gillon and Pr. Mounaïm Tounzi, for trusting me in undertaking this thesis, which promised to be a challenging one since the very beginning. I can never forget their words of encouragement and conviction which led me to choose this path after my internship with them. I enjoyed working with Frédéric for his patience and passion in transmitting his knowledge to students, his availability, optimism, and invariably good humour. I have learned a lot working with Mounaïm as well who, despite not being on the same Centralelille premises, was always accessible whenever his help was needed. His pertinent analyses and comments have undoubtedly contributed to the good achievement of this work, without forgetting his humane and joyful character. I cannot fail to mention Loïc Chevallier, who has been a huge support during my PhD in terms of *code\_Carmel* development, utilisation and endless hours of debugging, and Julien Korecki for providing helpful tips and information on the use of *Salome* with *code\_Carmel*. In the same way, I am very grateful to Florent Delhayé for his efficient technical help in the utilisation, maintenance and update of *Sophemis*. I cannot forget the teaching staffs of Centralelille and Université Lille1 who have always provided valuable suggestions and advice whenever they were summoned, and also non-teaching staffs for their pleasant humour and administrative support. But the lively office ambience would not have been the same without my lab mates, whether they were here for a short or long term.

The greatest moral support surely came from my family, especially my mom who never stopped encouraging me and believing in what I could achieve. She has been for all these years and still remains my biggest source of motivation in whatever I undertake. I have warm appreciation towards my two brothers who have always been supportive in good and bad moments. My thanks also goes to my close friends from Mauritius, Master ASE, Erasmus and those I have known via other occasions for their precious friendship, whose names I will not mention here for fear of forgetting someone. Last but certainly not the least, heartiest cheers to a special someone for his love and support, especially during the final stretch.

To Mom,  
for your unconditional love and faith in me  
& Dad,  
for believing your little girl could achieve big things

# Table of Contents

ABSTRACT .....	I
ACKNOWLEDGEMENTS .....	II
TABLE OF CONTENTS.....	V
LIST OF FIGURES.....	X
LIST OF TABLES .....	XIII
LIST OF ABBREVIATIONS.....	XIV
<b>INTRODUCTION .....</b>	<b>1</b>
<b>CHAPTER I – STATE OF THE ART .....</b>	<b>4</b>
I.1 INTRODUCTION .....	5
I.2 ORIGIN OF THE TOPOLOGY OPTIMISATION IDEA.....	5
I.3 DIFFERENCES BETWEEN MECHANICAL AND ELECTROMAGNETIC STRUCTURES.....	7
I.4 TOPOLOGY OPTIMISATION METHODS.....	8
<i>I.4.1 Homogenisation Method (HM)</i> .....	8
I.4.1.1 One-Material Microstructures.....	8
Rank Layered Microstructure .....	9
Rectangular Microstructure.....	10
Triangular Microstructure.....	11
Hexagon Microstructure.....	12
I.4.1.2 Bi-material Microstructure .....	12
I.4.1.3 Optimisation Algorithms used with HM .....	13
I.4.1.4 Applications of HM to Electromagnetic Problems.....	13
<i>I.4.2 Density-based Methods</i> .....	14
I.4.2.1 Interpolation Schemes .....	15
I.4.2.2 Density Method for Bi-material.....	19
I.4.2.3 Optimisation Algorithms with Density Method.....	20
I.4.2.4 Application of Density Method to Electromagnetic Problems .....	20
<i>I.4.3 ON/OFF Method</i> .....	21
I.4.3.1 Optimisation Algorithms with ON/OFF Method.....	22
I.4.3.2 Application of ON/OFF Method to Electromagnetic Problems .....	23
<i>I.4.4 Level Set Method</i> .....	23
I.4.4.1 Optimisation Algorithms with Level Set Approach.....	26
I.4.4.2 Application of Level Set Approach to Electromagnetic Problems .....	26
I.5 GENERAL COMPLICATIONS WITH TO .....	27
I.5.1 <i>Intermediate Material</i> .....	27
I.5.2 <i>Local Minima</i> .....	28
I.5.3 <i>Checkerboard Designs</i> .....	28



1.5.4	<i>Mesh Dependencies</i> .....	29
I.6	SUMMARY OF TO METHODS .....	30
	Choice of TO Method.....	31
I.7	NUMERICAL TOOLS .....	31
1.7.1	<i>Code_Carmel – A FE Calculation Code</i> .....	32
1.7.1.1	Maxwell’s Equations.....	32
1.7.1.2	Constitutive Laws of Materials .....	34
1.7.1.3	Boundary Conditions .....	35
1.7.1.4	Formulations .....	36
	Electrostatic Formulation .....	36
	Magnetostatic Formulation .....	37
1.7.1.5	Finite Elements Approach .....	38
1.7.1.6	Nonlinearity.....	39
1.7.1.7	Movements .....	40
1.7.1.8	Energy.....	41
1.7.1.9	Force.....	41
1.7.2	<i>Sophemis – An Optimisation Platform</i> .....	42
1.7.2.1	Full Factorial Design.....	42
1.7.2.2	Latin Hypercube Square .....	43
1.7.2.3	fmincon SQP .....	44
1.7.2.4	Genetic Algorithm (GA) .....	46
I.8	SUMMARY .....	47
<b>CHAPTER II</b>	<b>– METHODOLOGY AND TOOL DEVELOPMENT .....</b>	<b>48</b>
II.1	INTRODUCTION .....	49
II.2	COUPLING OF <i>CODE_CARMEL</i> AND <i>SOPHEMIS</i> .....	49
II.2.1	<i>Overall Process</i> .....	49
II.2.2	<i>Configurations of the Coupling</i> .....	51
	1. Local Utilisation .....	51
	2. Distant Utilisation .....	51
	3. Distant and Distributed Utilisation .....	52
II.3	CHOICE OF TO METHOD – DENSITY METHOD.....	52
	Global TO Process with Density Method .....	54
II.4	NONLINEAR BEHAVIOUR OF MATERIALS FOR TO USING <i>CODE_CARMEL-SOPHEMIS</i> .....	55
	Integrating the Nonlinear Calculation in the TO process.....	57
II.5	3D ELECTROMAGNETIC TEST CASE.....	58
II.6	BEHAVIOUR ANALYSIS OF TO USING DESIGN OF EXPERIMENTS .....	60
II.6.1	<i>Cubic_Case_8</i> .....	60
II.6.2	<i>Design of Experiments</i> .....	62
II.6.3	<i>Analysis of the Convexity of the Variables</i> .....	63
	II.6.3.1 One zone is varied .....	64

II.6.3.2	Two zones are varied.....	66
II.7	DEVELOPMENT OF A METHODOLOGY FOR TO .....	68
II.7.1	<i>Cubic_Case_64</i> .....	68
II.7.2	<i>Mesh Size Investigation</i> .....	70
II.7.3	<i>Introduction of the Feasibility Factor (FF) in the Methodology</i> .....	72
II.7.4	<i>Using FF in the Optimisation Problem Formulation</i> .....	72
II.7.4.1	FF as Constraint .....	73
II.7.4.2	Proposed Formulation with FF .....	75
II.7.5	<i>Comparison of Proposed Methodology with other Density Mappings</i> .....	78
II.7.6	<i>Comparison with ON/OFF Method</i> .....	83
II.7.7	<i>Repeatability of Solutions</i> .....	84
II.7.8	<i>Using Mesh Elements as Variables</i> .....	84
II.8	NONLINEAR BEHAVIOUR OF THE FERROMAGNETIC MATERIALS .....	85
II.9	OTHER PROBLEM FORMULATIONS .....	87
II.10	SUMMARY AND CONTRIBUTIONS .....	90
<b>CHAPTER III – APPLICATION OF TO METHODOLOGY TO A 3D ELECTROMAGNET .....</b>		<b>91</b>
III.1	INTRODUCTION .....	92
III.2	STATE OF THE ART .....	92
III.3	3D FE ELECTROMAGNET MODEL.....	95
III.3.1	<i>Finite Element Model</i> .....	95
Optimisation Variables	.....	97
III.3.2	<i>Mesh Size Investigation</i> .....	97
Computation of Energy.....	98	
Computation of force .....	99	
Cross verification with Reluctance Network.....	100	
III.4	TO OF THE ELECTROMAGNET .....	101
III.4.1	<i>Maximising Energy</i> .....	101
Results .....	102	
III.4.2	<i>Maximising Attractive Force</i> .....	103
III.4.2.1	Linear Behaviour of Ferromagnetic Materials.....	104
III.4.2.2	Nonlinear Case .....	109
III.5	SUMMARY AND CONTRIBUTIONS .....	115
<b>CHAPTER IV – TO OF A SALIENT POLE SYNCHRONOUS GENERATOR .....</b>		<b>116</b>
IV.1	INTRODUCTION .....	117
IV.2	STATE OF THE ART .....	117
IV.3	SALIENT POLE SYNCHRONOUS GENERATOR (SPSG) MODEL .....	121
IV.3.1	<i>FE Model of the Original SPSG</i> .....	121
Magnetic Flux Density in the Air Gap and Spatial Distribution .....	123	

IV.3.2	<i>TO of the Machine</i> .....	126
	Magnetic Flux Density in the Air Gap and Spatial Distribution .....	128
IV.4	OPTIMISATION OF SPSG.....	131
IV.4.1	<i>Recap of TO Process</i> .....	131
	TO Filter .....	132
IV.4.2	<i>Maximisation of B in the Stator</i> .....	133
IV.4.3	<i>Optimisation of Magnetic Flux Density in Air Gap</i> .....	136
IV.4.3.1	Linear behaviour of Materials .....	137
	Example 1 – Average Convergence with Relevant Topology .....	139
	Example 2 – Good Convergence with Poor Topology .....	141
IV.4.3.2	Nonlinear Behaviour of Materials .....	143
IV.5	SUMMARY AND CONTRIBUTIONS .....	146
<b>CONCLUSION</b> .....		<b>147</b>
	SUMMARY AND CONTRIBUTIONS .....	148
	PERSPECTIVES.....	149
	Methodology .....	149
	Tool.....	149
	Applications .....	149
<b>REFERENCES</b> .....		<b>151</b>
<b>APPENDICES</b> .....		<b>- 0 -</b>
APPENDIX A .....		- 1 -
	<i>Calculation of LHS with Sophemis</i> .....	- 1 -
APPENDIX B .....		- 3 -
	<i>Example of Sophemis Model on Matlab for TO</i> .....	- 3 -
APPENDIX C .....		- 5 -
	<i>Example of Sophemis windows</i> .....	- 5 -
	Sophemis window.....	- 5 -
	Optimisation of a model .....	- 5 -
	Live visualisation of evolution of iterations .....	- 6 -
APPENDIX D .....		- 7 -
	<i>Example of files where force is extracted</i> .....	- 7 -
	<i>Example of file where B is extracted</i> .....	- 7 -
APPENDIX E .....		- 8 -
	<i>Example of server showing running of code_Carmel-Sophemis coupling</i> .....	- 8 -
APPENDIX F.....		- 9 -
	<i>Different mesh sizes for 3D FE electromagnet model</i> .....	- 9 -
	Energy obtained using A and $\Omega$ formulations with 3.0 A/mm <sup>2</sup> .....	- 9 -
	Force obtained using A and $\Omega$ formulations with 3.0 A/mm <sup>2</sup> .....	- 10 -

<b>OPTIMISATION TOPOLOGIQUE DE DISPOSITIFS ELECTROMAGNETIQUES .....</b>	<b>I</b>
Introduction .....	I
Etat de l'Art.....	II
Développement de Méthodologie et Outils OT.....	III
Application à un Electroaimant.....	V
Application à une Génératrice Synchrone à Pôles Saillants (GSPS) .....	VI
Conclusion and Perspectives .....	VII

## List of Figures

Figure 1.1 Publications in Electromagnetism from 1992 Till Present [8].....	6
Figure 1.2 Basic Concept of HM in TO using Square Microcell [11] .....	9
Figure 1.3 Example of Rank-1 and Rank-2 Microstructures [12].....	10
Figure 1.4 Rectangular Microstructure in 2D and 3D.....	11
Figure 1.5 Plate Optimisation Model and its Microstructure [13] .....	12
Figure 1.6 (a) Hexagonal Microstructure, (b) FE mesh of a Quarter of the Hexagonal Microstructure [10]..	12
Figure 1.7 Rank Layered Bi-material Microstructures [10].....	13
Figure 1.8 H-shaped Electromagnet (a) Initial Domain; Volume Constraint of (b) 60%, (c) 70% [15] .....	14
Figure 1.9 Example of 2D domain $\Omega$ with Density Method .....	15
Figure 1.10 Comparison of Different Interpolation Schemes .....	18
Figure 1.11 Electrostatic Actuator Design (a) Inital Design, (b) Final Design .....	21
Figure 1.12 Blurring Technique (a) Original Structure, (b) Blurred Structure, (c) Topology Selected according to the Volume Fraction of 0.5 [42].....	22
Figure 1.13 Contour Representation when a Surface Intersects a Plane [59] .....	24
Figure 1.14 (a) Contour at Zero Level Set, (b)-(d) Evolution of a Contour by Splitting [60].....	24
Figure 1.15 Representation of Domain $\Omega$ and Boundary .....	25
Figure 1.16 Optimised Shape and Flux Distribution (a) ON/OFF (b) Level-set Method [70].....	27
Figure 1.17 Checkerboard Patterns with (a) Structural Design, (b) Electromagnetic Design .....	29
Figure 1.18 Example of Mesh Dependency of the TO Design [9].....	29
Figure 1.19 Subgroups of Maxwell's Equations .....	33
Figure 1.20 Schema of Electromagnetic Domain .....	36
Figure 1.21 B(H) Curve using Marrocco Equation .....	40
Figure 1.22 Latin square Example .....	43
Figure 2.1 Flowchart for Overall TO Process .....	50
Figure 2.2 Local Utilisation Layout .....	51
Figure 2.3 Distant Utilisation Layout.....	52
Figure 2.4 Distant and Distributed Utilisation Layout .....	52
Figure 2.5 (a) Example of Initial Domain, (b) Colour Legend for $\rho$ and $\mu r$ .....	54
Figure 2.6 Polynomial Mapping for different Penalisation Coefficients $n$ .....	54
Figure 2.7 Block Diagram of TO Process with Polynomial Mapping .....	55
Figure 2.8 $\mu(H)$ Curve.....	56
Figure 2.9 H(B) Curve .....	57
Figure 2.10 Block Diagram to Highlight Main Differences using Nonlinear Materials .....	58
Figure 2.11 Test Cases with respective number of variables (a) 8, (b) 64 .....	59
Figure 2.12 Magnetic Potential Difference Applied to Nodes .....	59
Figure 2.13 <i>Cubic_Case_8</i> (a) showing 8 zones (variables), (b) showing MPD .....	61
Figure 2.14 MQ v/s Energy for FFD and LHS.....	63

Figure 2.15 (a) Concave, (b) Convex, (c) Desired Shape .....	64
Figure 2.16 Initial Structure with one zone varying .....	65
Figure 2.17 Energy v/s Density for each zone varied .....	65
Figure 2.18 Initial Structure for Two Zones Varied.....	66
Figure 2.19 Energy v/s Density for Two Zones Varied .....	67
Figure 2.20 Example of Continuation Method.....	68
Figure 2.21 Cubic_Case_64 (a) FE Model, (b) Model showing only zones .....	69
Figure 2.22 Magnetic Flux Density Distribution for Maximum Energy (Linear Case) .....	69
Figure 2.23 True Energy v/s Mesh Size of <i>Cubic_Case_64</i> .....	70
Figure 2.24 Feasibility Factor (FF) w.r.t $\rho_i$ .....	72
Figure 2.25 Example of biased solution with <i>FF</i> as constraint .....	73
Figure 2.26 Evolution of (a) Energy, (b) MQ, (c) FF w.r.t the Number of Evaluations .....	74
Figure 2.27 Energy and FF against Weightage Coefficient $\lambda$ .....	76
Figure 2.28 (a) Final Topology, (b) Energy, (c) FF, (d) MQ, (e) Sum of Objectives .....	78
Figure 2.29 Comparison of Density Methods with Proposed Methodology for (a) Energy, (b) MQ, (c) FF, against the Number of Evaluations .....	80
Figure 2.30 Magnetic Flux Density Distribution for Topology with Proposed Methodology (Linear Case) ...	81
Figure 2.31 Effect of Initial Points on Optimal Results .....	84
Figure 2.32 Model using Mesh Element as Variable with (a) Geometry, (b) FE Model .....	85
Figure 2.33 Magnetic Flux Density Distribution with Maximum Energy (Nonlinear Case) .....	86
Figure 2.34 Magnetic Flux Density Distribution of Optimal Topology (Nonlinear Case) .....	87
Figure 2.35 Magnetic Flux Distribution with MPD=15 AT (a) Linear Case, (b) Nonlinear Case .....	89
Figure 3.1 (a) H-Shaped Electromagnet, (b) Design Domain, Optimised Shape with Volume Constraint(c) 60%, (d) 70% [15].....	93
Figure 3.2 (a) C-core Actuator, (b) Initial Domain, Results in (c) Linear Case, (d) Nonlinear Case [18] .....	94
Figure 3.3(a) Initial Domain, (b) Density Method Results (coarse mesh on left & fine on right), (c) LSM (conventional on left and advanced on right) [64] .....	94
Figure 3.4 TO of Magnetic Yoke (a) Design Domain, (b) Optimised Yoke shape, (c) Magnetic Flux Line Plot .....	95
Figure 3.5 (a) Electromagnet Model with Dimensions, (b) Quarter Model, (c) Model with Boundary Conditions .....	96
Figure 3.6 Energy for Different Mesh Sizes .....	98
Figure 3.7 Nodes on which Force is Calculated.....	99
Figure 3.8 Attractive Force v/s Number of Nodes .....	100
Figure 3.9 Reluctance Network for Electromagnet .....	101
Figure 3.10 Case of Maximum Energy in the Electromagnet for Linear Material Behaviour .....	102
Figure 3.11 Optimal Topology while Maximising Energy with MQ = 0.8.....	103
Figure 3.12 (a) $\beta=0.8$ , (b) $\beta=0.6$ , (c) $\beta=0.4$ , (d) $\beta=0.2$ .....	104
Figure 3.13 Magnetic Flux Density Distribution for (a) $\beta = 0.2$ , (b) $\beta = 0.6$ .....	106

Figure 3.14 Convergence Graphs for Linear Case with $\beta = 0.2$ .....	108
Figure 3.15 Position of Non-converged Variables .....	109
Figure 3.16 Magnetic Flux Density Distribution in Nonlinear Case with Variables as Iron .....	110
Figure 3.17 Marrocco Saturation Curve.....	110
Figure 3.18 (a) $\beta=0.8$ , (b) $\beta=0.6$ , (c) $\beta=0.4$ , (d) $\beta=0.2$ .....	111
Figure 3.19 Nonlinear Case $\beta = 0.2$ (a) Overall Objective, (b) Force, (c) FF, (d) MQ, (e) Density of Variables .....	114
.....	
Figure 4.1(a) Design Region of Machine, (b) Cell Division for TO, (c) Final Results .....	118
Figure 4.2 (a) Initial IPM Motor, (b) TO Domain in Red, (c) Material Removed in the Optimisation process (Green), (d) Optimised Shape, (e) Optimised Radial Component .....	119
Figure 4.3 (a) Initial Domain of IPM, (b) Optimised Topology.....	120
Figure 4.4 (a)&(b) Initial Design Space and Positions, Optimised Topologies for (c) 5 Iterations (d) 8 Iterations .....	121
Figure 4.5 SPSG (a) Geometry, (b) Mesh .....	123
Figure 4.6 Spatial Distribution of B in the Machine with (a) Linear, (b) Nonlinear Material Behaviour .....	125
Figure 4.7 Magnetic Flux Density in Air Gap with (a) Linear, (b) Nonlinear Material Behaviour .....	126
Figure 4.8 Domain to be Optimised (a) FE model, (b) Zoom, (c) Geometry.....	128
Figure 4.9 Spatial Distribution of B in the Machine for (a) Linear, (b) Nonlinear Behaviour of Materials ...	129
Figure 4.10 Magnetic Flux Density in Air Gap for (a) Linear, (b) Nonlinear Behaviour of Materials .....	130
Figure 4.11 Block Diagram for Overall TO Process .....	131
Figure 4.12 Zones Numbering .....	132
Figure 4.13 (a) Topology Before Filter, (b) $\rho_{sum}$ for each zone, (c) Filtered topology with $\nu = 0.05$ and $w = 0.95$ , (d) Filtered Topology with $\nu = 0.1$ and $w = 0.9$ .....	133
Figure 4.14 Maximisation of B in the Stator Yoke .....	134
Figure 4.15 Topologies in (a) Linear, (b) Nonlinear, B Distribution in (c) Linear, (d) Nonlinear .....	135
Figure 4.16 Modulus of Sine Curve Imposed .....	136
Figure 4.17 (a) Spatial Points, (b) Convergence of Objective .....	138
Figure 4.18 Unfiltered Results (a) Topology, (b) B Distribution, (c) B in Air Gap .....	138
Figure 4.19 Filtered Results (a) Topology, (b) B Distribution, (c) B in Air Gap .....	139
Figure 4.20 (a) Spatial Points, (b) Convergence of Objective .....	140
Figure 4.21 Unfiltered Results (a) Topology, (b) B Distribution, (c) B in Air Gap .....	140
Figure 4.22 Filtered Results (a) Topology, (b) B Distribution, (c) B in Air Gap .....	141
Figure 4.23 For 13 Spatial Points (a) B in Stator and in Rotor Used in Constraint (b) Objective Convergence, (c) B in Air Gap with 13 points, (d) B in Air Gap with 73 points, (e) Optimal Topology .....	142
Figure 4.24 (a) Convergence of Objective, (b) B in the Air Gap, (c) Unfiltered Topology, (d) B Distribution .....	143
.....	
Figure 4.25 (a) Filtered Topology, (b) B Distribution, (c) B in the Air Gap.....	144

## List of Tables

Table 1.1 Recap of the Interpolation Schemes .....	18
Table 1.2 Combinations for Final Material .....	19
Table 1.3 Example of Full Factorial Design .....	43
Table 1.4 Latin Square Experimental design .....	44
Table 1.5 Recap of Tool Chosen .....	47
Table 2.1 Recap of Mesh Size Investigation Information .....	71
Table 2.2 Biased Solution's Information .....	73
Table 2.3 Comparison of Different Mappings with Proposed Method .....	82
Table 2.4 Results with GA .....	83
Table 2.5 Results with Nonlinear Behaviour of Materials .....	86
Table 2.6 Comparison of Linear and Nonlinear Cases.....	88
Table 3.1 Information about the TO Results with Energy .....	103
Table 3.2 Additional Information about the TO Results .....	105
Table 3.3 Additional Information for Nonlinear Case .....	112
Table 4.1 SPSG Parameters .....	122



## List of Abbreviations

<b>Abbreviation</b>	<b>Full Form</b>
BLDC	Brushless DC Motor
DoE	Design of Experiments
FE	Finite Element
FF	Feasibility Factor
FFD	Full Factorial Design
GA	Genetic Algorithm
HM	Homogenisation Method
IPM	Interior Permanent Magnet
LHS	Latin Hypercube Square
LSM	Level-Set Method
MPD	Magnetic Potential Difference
MQ	Material Quantity
RAMP	Rational Approximation of Material Properties
RN	Reluctance Network
SIMP	Solid Isotropic Material with Penalisation
SPSG	Salient Pole Synchronous Generator
SQP	Sequential Quadratic Programming
TO	Topology Optimisation

# Introduction

---

We are currently living in a very demanding era, pushing the human intelligence towards the invention of more effective technologies and the improvement of existing ones in the pursuit of optimality, if not excellence. We, research scientists, are the most active players in this quest for superiority. With the help of other technologies such as computers, which have now become ineluctable tools, we are capable of engaging into more tedious calculations and simulations, drawing us closer to our goals. This has brought a big boost in engineering in general, including the electrical field which is our main concern.

The electrical engineering laboratory (Laboratoire d'Électrotechnique et d'Électronique de Puissance, L2EP), within which this thesis was carried out, has many ongoing works on the optimisation of electromagnetic devices, such as electrical machines, amongst others. This thesis was therefore oriented towards this same mind-set. Optimisation of machines, for example, is a vast subject which can extend from the optimisation of one simple parameter to the whole machine. Classically, engineers start off from already existing structures and optimise some dimensions to yield a better design. But in doing so, the optimisers always find themselves constrained by the initial shape of the structure, and thus reduces the degree of freedom. Moreover, in a constant search of new structures, we are very often biased by existing ones which can obstruct our sense of innovation. For this reason, we will use a different approach to this type of problem: the Topology Optimisation (TO).

TO is an original way of finding new designs of structures without having any layout a priori on the latter. This infers that the optimisation problem is defined in such a way that the existing structures are not considered in the problem, but the TO process is rather free to find the optimal structure it judges the best, according to the information specified. Scientific researchers in the mechanical/structural field are the pioneers in TO, and have taken many decades before coming up with such a methodology. The results were so interesting that they attracted researchers from various other fields, including electromagnetism.

TO remains till date amongst the most complex forms of optimisation as it requires equal expertise in optimisation algorithms, as well as numerical modelling of structures. In our case, the numerical modelling method used is Finite Element (FE) Analysis. Moreover, depending on the nature of the models, which are electromagnetic in our case, extensive knowledge is also desired in the same field to be able to interpret the results obtained, and hence redirect the works on the right path.

The main aim of this thesis is to develop and acquire the necessary skills and proficiency to be able to optimise the topology of any electromagnetic device, whether simple or complex.

To achieve this, a number of stepwise objectives must be enacted to successfully reach our goal.

The first objective is to develop and test a functional tool for TO of electromagnetic devices. The development of the TO tool will be based on the 'home-made' tools available at the L2EP, namely *code\_Carmel* for solving FE numerical models, and *Sophemis* for solving optimisation problems. A coupling of both will have to be done to create a functional TO tool. To test the latter, it is important to have a simple, yet effective test case to assess its characteristics. For this purpose, an academic 3D test case will have to be developed and parameterised. Its electromagnetic nature should be straightforward and easily understood, and the FE model should also be solved rapidly.

The second objective is to develop a methodology for TO, based on the existing ones such as Density Methods, ON/OFF Methods and so on. The proposed methodology should allow us to overcome the problems usually met with the other methods, for a more effective TO. For a paramount testing of the latter, the academic test case will again be used.

Furthermore, the consideration of the nonlinear behaviour of the ferromagnetic materials is often overlooked in TO due to its tedious setting and high computation time, despite being a very important aspect of electromagnetic modelling. If the electromagnetic device is operating at or near saturation point, and the latter is not considered in the TO process, this might yield incorrect optimal structures. Therefore, the third objective is to adapt the TO tool so that it takes into account the nonlinear behaviour of the materials, and hence allow us to analyse its effects. It will also have to be compared with cases of linear material behaviour to put forward its importance. A 3D electromagnet will be used for this purpose as it represents a more real test case, and hence a more judicious appraisal. The FE model of the electromagnet will also have to be developed and parameterised.

Last but not least, the fourth objective of this thesis work is to apply the developed tools and methodology to a more complex, electrical engineering device: a Salient Pole Synchronous Generator (SPSG). It is desired to see the different topologies obtained w.r.t various optimisation problems. The assessment of the process's behaviour can help us gather enough information to strive towards better solutions in the future.

We will see throughout this manuscript how all these objectives contribute to approach the main aim of this thesis work. The TO process is a complex one, as mentioned before, and should be tackled step by step for productive results. A plan of the work accomplished in the manuscript to guide the reader on the course of the latter is presented here. The manuscript is mainly divided into four chapters:

1. Chapter I: A state of the art of the various existing TO methods is done. The method used to complement the proposed methodology of this thesis work is justified. The 'home-made' numerical tools for FE analysis and optimisation are elaborated, as they will further be used to compose the TO tool developed.
2. Chapter II: The development of the TO tool is detailed, as well as the coupling between *code\_Carmel* and *Sophemis*. A methodology for TO based on the existing methods is proposed. The academic test case is used to test and validate the latter. The consideration of the nonlinear behaviour of the ferromagnetic materials in the TO calculations is developed and explained in this chapter, and tested on the academic test case. Additional investigations are made on various aspects of TO with this model, serving to identify strengths and limitations of the methodology.
3. Chapter III: The TO tool and methodology are used to optimised the topology of the iron core of the 3D electromagnet. Various cases of optimisation problems will be presented. Calculations for linear and nonlinear behaviour of materials are both done, and the results are compared and analysed.
4. Chapter IV: The TO of the rotor top of the SPSG is done w.r.t different optimisation problems, and the viability of the various topologies are analysed.

We will conclude the manuscript with some opinions and assertions we have built up on TO during this thesis work, and with some interesting perspectives for future works on the topic.

# Chapter I – State of the Art

---

## I.1 Introduction

TO has sparked a sudden interest amongst researchers in the past two decades, owing to its originality and ability to produce innovative designs. Before heading to any kind of computation, it is interesting to step into the history of TO to understand its evolution, and the methods associated with it.

The first segment of this chapter is dedicated to the history of Topology Optimisation (TO) over time, and how the different methods evolved till present day. Some TO methods were developed from existing ones, while others were established from popular optimisation methods initially designed for different purposes in other fields. Firstly, the main TO methods shall be introduced without focusing on the field for which it was conceived, whether mechanical, electrical and so on. Afterwards, the main applications w.r.t electrical engineering will be evoked with some examples and findings.

In the second segment, the numerical tools used to carry out the TO process are encompassed. This englobes the classical Finite Element (FE) methods and algorithms mainly used for the purpose of modelling and optimisation. Both tools used are developed at the L2EP within the OMN (Outils et Méthodes Numériques) team. TO normally requires the use of both tools coupled together, but this section will focus on them individually as the coupling is a significant part developed during this PhD work, and hence to be presented in the next chapter.

Finally, the conclusion will hint at the methods retained for the rest of this thesis work, and briefly uncover the content of the following chapter.

## I.2 Origin of the Topology Optimisation Idea

The desire to generate optimal structures dates a long way back when numerical tools did not even exist. Works were already being carried out in the mechanical field to find the limits of reducing the amount of material present in frame structures without degrading the former's tensile stress and strain.

In 1904, Michell [1] proposed a mathematical study to sustain given forces in structures attaining the limits of economy of material. The idea was definitely in a TO mind-set, but was left unexploited for many decades before Rozvany [2] published his work on the optimisation of perfectly plastic and elastic grillages of maximum stress and stiffness with minimum weight solutions. But as for the previous case, the study was essentially a mathematical formulation without practical applications. Later in 1972, Rozvany and Prager [3] studied the

minimum weight design of grillage of perfectly plastic beams that are on the verge of plastic collapse under given loads. They proposed a discretisation of the beams constituting the grillage, but the study was mostly based on changing the number of discretisation, and hence beams. The idea of discretising the optimisation domain was hence introduced.

In 1988, Bendsøe and Kikuchi [4] innovated with the Homogenisation Method (HM) applied to a generalised mechanical TO problem, revolutionising the subject and inspiring the sheer interest of other authors. Afterwards, Bendsøe introduced the Direct approach [5] based on the HM, but easier in application, and therefore more engineer-oriented. The idea was further elaborated in [6] where the authors adapted the Direct Method into SIMP (Solid Isotropic Material with Penalisation) Method for intermediate densities, which will be detailed in the future sections. But it wasn't until 1996 that TO was introduced in the electromagnetism community by Dyck and Lowther [7], presenting the OMD (Optimised Material Distribution) Method.

According to Scopus [8], various fields such as mechanics, electromagnetism, computer science, physics and astronomy, energy, chemistry, neuroscience and econometrics use TO, amounting to some 3600 publications since 1986. The number of papers on TO in electromagnetism holds a fair share as shown in Figure 1.1, for year 1992 till present. This includes conference and journal papers, and we can see a steep rise from around 2007. As for the leading countries in TO in electromagnetism, Scopus surveys the greater number of works from Japan, USA, China and South Korea.

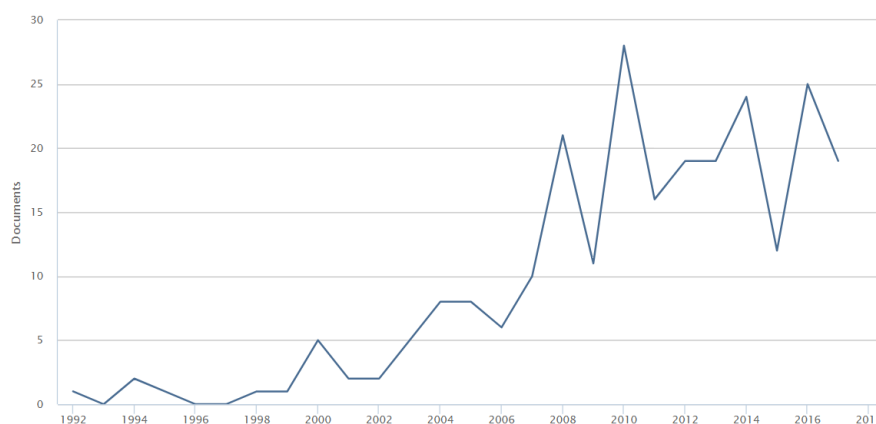


Figure 1.1 Publications in Electromagnetism from 1992 Till Present [8]

The state of the art in the next sections will focus on the TO methods in electromagnetism, but also a few in mechanical since the methods for the former were actually derived from the latter. Despite not having the same way of formulating the problem, they are closely related. The next section will concisely enumerate the main differences between TO in mechanical



and electromagnetism to justify why the methods cannot be directly translated from one to the other.

### **I.3 Differences between Mechanical and Electromagnetic Structures**

Regarding TO, the main dissimilarity is that in mechanical structures, it is often desired to have lighter designs while respecting the given mechanical constraints like tensile stress and strain, whereas in electromagnetic structures, it is rather required to have magnetically optimal structures w.r.t the magnetic force, magnetic flux density, EMF and so on.

Another essential difference is that in electromagnetism, the nonlinearity of the ferromagnetic materials constituting the majority of the devices must be taken into account. Since we are dealing with the permeability of materials, we must take into account the saturation effect. This implies a limitation of the material to allow flow of more magnetic flux at some point due to their saturation. After this point, there is also a change in the material's behaviour. These effects do not have to be considered in mechanical structures, but can be a turning point in electromagnetism.

We can also evoke the importance of the movement of electromagnetic devices such as in motors and generators to produce the expected output, while in mechanical devices such as beams, bridges, frames or housings, they are usually required to be stationary and withstand the prescribed load.

The above factors alone represent a substantial hindrance to TO as they largely increase the computation time for the resolution of the models. Computation time usually varies from model to model, and can take several hours to several days. It could be a good practice to keep a step-wise procedure of finding the optimal topology of electromagnetic structures by gradually increasing the difficulty. For instance, a TO using linear materials is usually the stepping stone due to its relative rapidity. Once the correct problem formulation is found, and the solution obtained corresponds to a suitable one, a TO using nonlinear materials can afterwards be envisaged. Subsequently, if the electromagnetic device involves movements (such as in electric machines), the latter can also be added to the TO calculations for a closer consideration of real conditions.

Before getting into these details, it is fair to first introduce the various existing TO methods to later narrow down our choice for this work.

## I.4 Topology Optimisation Methods

Since the introduction of TO, various authors have proposed diverse methods of tackling the problem. This section reviews the most popular methods in literature. The Homogenisation Method (HM) is covered first, introducing its different variants. Thereafter, the Density Method is presented and its clear relation with the HM is evoked. Subsequently, the ON/OFF Method is discussed, and its link with the Density Method is also explained. Last but not least, the Level-set Method is outlined to see its completely different background when compared to the first 3 methods. For each method, the algorithms used for optimisation, and the applications in electromagnetism are shortly illustrated to provide a wider overview of what has been done in literature.

### I.4.1 Homogenisation Method (HM)

HM was one of the first and most pioneering TO methods introduced in literature by Bendsøe and Kikuchi [4]. It was basically developed for mechanical/structural designs with the aim of reducing material constituting the structures for lighter and stronger ones. It deals essentially with anisotropic/ composite materials, with an interpolation between void and full material. It was founded on theoretical work that proved the existence of solutions could be resolved by modifying the design space to include relaxed designs, for instance in the form of composites [9]. These design spaces made of composites can be modelled by materials with microstructures, and it exists in different types such as rotated, layered or rectangular microstructures amongst others. Hence, this involves the consideration of other parameters such as orientation and dimensions of each microstructure. In a TO problem, each microstructure would normally represent a variable to be optimised, and therefore we have more than one parameter for each variable depending on the microstructure type. The optimal design of structures is closely connected with the study of microstructures and finding the effective homogenised material properties for composite microstructures [4]. The following section reviews some of the existing microstructures.

#### I.4.1.1 One-Material Microstructures

In one-material microstructures, the material model contains one material with one or more voids. If a portion (or percentage) of a region is made of voids, material is not placed there. Otherwise, if there is no porosity in an area, material is placed in that area [10]. An example is given in Figure 1.2 to show the basic concept of HM in TO using a square microcell with centrally placed rectangular hole as the material model. The top of the figure shows the

domain before optimisation, and the bottom, after optimisation. The black area represents material, the white represents void, and the grey area represents intermediate materials. This means that the material found these types of regions is neither fully solid nor void, but is instead consists of a certain percentage of solid and void. This makes it an intermediate material which is not manufacturing-friendly, and hence usually undesired in the final solution. We will go deeper into this matter throughout this thesis work.

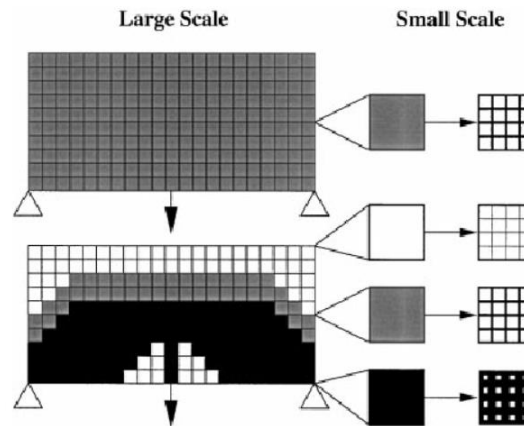


Figure 1.2 Basic Concept of HM in TO using Square Microcell [11]

Various one-material microstructures exist, and some are presented below. They can also directly be implemented into a FE code to be used as main elements of the domain. For instance, instead of using tetrahedral elements, which is the most common practice, it could also be interesting to use the one-material microstructures, and the different parameters of each microstructure would represent the variables of the optimisation problem.

#### *Rank Layered Microstructure*

The basic idea of this category is to find extremal microstructures with maximum rigidity (or equivalent minimum compliance). A layered microstructure of rank- $p$  can be used, with  $p$  ranging from 1 and above, but usually ranks 1 and 2 are used for simplicity. Usually, in a rank- $p$ , there are alternating layers of void and solid material, with layers of the ranks being orthogonal to each other. For example, in rank-1 material, there are only alternating layers of solid material and void in one direction. In rank-2 material, in addition to the initial alternating layers, there are orthogonal alternating layers of solid material. Figure 1.3 illustrates a rank-1 and rank-2 layered microstructure.

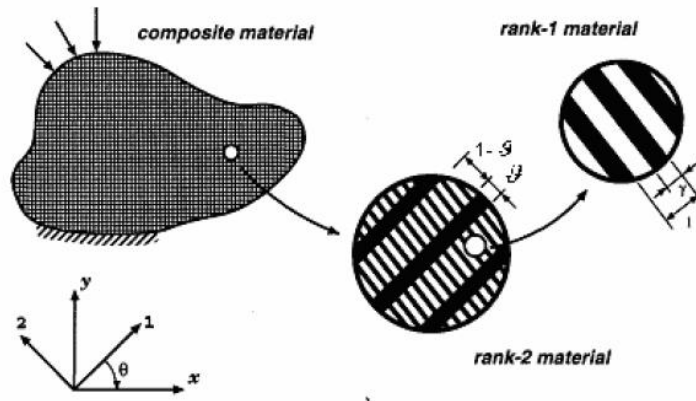


Figure 1.3 Example of Rank-1 and Rank-2 Microstructures [12]

In TO, rank-2 layers are most commonly used. In this case, the elements of the matrix of elasticity coefficients are functions of 3 parameters:  $\gamma$ ,  $\vartheta$  and  $\theta$  (as in Figure 1.3), where  $\vartheta$  and  $\gamma$  lie between 0 and 1, limits included. The parameter  $\gamma$  represents the width of the layers in rank-1 material, while  $\vartheta$  represents the width of the orthogonal layer in a rank-2 material. The parameter  $\theta$  gives the orientation of the layers. The volume  $\Omega_s$  occupied by the solid is given in (I-1):

$$\Omega_s = \int_{\Omega} (\vartheta + \gamma - \vartheta\gamma) d\Omega \quad (\text{I-1})$$

and the density of the composite can be written as in (I-2):

$$\rho = \rho(\vartheta, \gamma) = (\vartheta + \gamma - \vartheta\gamma)\rho_s \quad (\text{I-2})$$

where  $\rho_s$  is the density of the solid [12]. It must be noted that it is possible to vary the cell relative density from 0 to 1 by changing the value of  $\vartheta$  and  $\gamma$ .

The advantage of rank layered material is that the effective material properties can be derived analytically. The main weakness is that the material cells do not provide resistance to shear stress in between layers.

### *Rectangular Microstructure*

In this category, the microstructure is a square cell with a centrally placed rectangular hole in 2D, whereas in 3D, it is represented by a cubic cell with a rectangular parallelepiped hole, as in Figure 1.4.

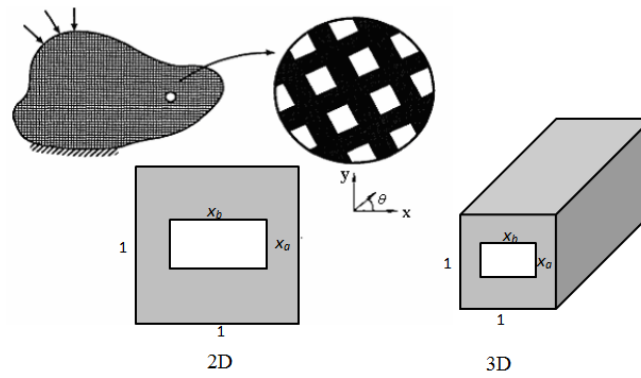


Figure 1.4 Rectangular Microstructure in 2D and 3D

Rectangular microstructure is one of the most commonly used for TO with HM. The area  $\Omega_c$  is occupied by the solid material in the base cell as given in (I-3), and the volume  $\Omega_s$  is occupied by the solid material in the design domain as given in (I-4).

$$\Omega_c = 1 - x_a \cdot x_b \quad (\text{I-3})$$

$$\Omega_s = \int_{\Omega} (1 - x_a \cdot x_b) d\Omega \quad (\text{I-4})$$

where  $x_a$  and  $x_b$  lie between 0 and 1, limits included. The angle of orientation is also  $\theta$ . For different orientations, the properties of elastic constitutive matrix are changed.

The main strength of rectangular microstructures making it popular in TO with HM is due to the smaller number of variables required if a square void is chosen. The main drawbacks are that, on one side the homogenisation equation has to be solved by numerical techniques, and on the other side the optimisation results often contain intermediate regions.

### *Triangular Microstructure*

Not very popular in TO, the triangular microstructure is a very complicated one, making it more tedious in numerical implementation and hence increasing computational cost. An example of the plate model setup for triangular microstructure is given in Figure 1.5. The main strength is that the true strain energy can be calculated numerically, which is not always the case with the other microstructures.

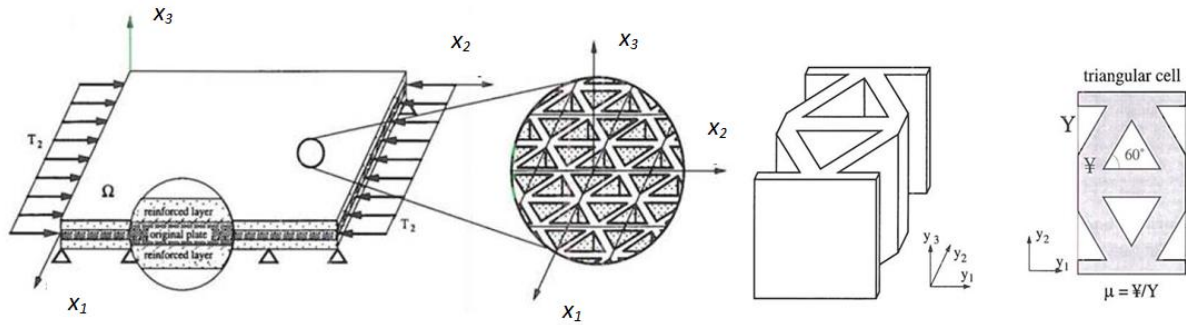


Figure 1.5 Plate Optimisation Model and its Microstructure [13]

### Hexagon Microstructure

Initially presented in [12], this type of microstructure is also called honeycomb based cell and is given in Figure 1.6(a), along with the dimensions. They have the same advantage and disadvantage as the triangular microstructure. Figure 1.6(b) depicts a FE mesh for a quarter of the honeycomb cell.

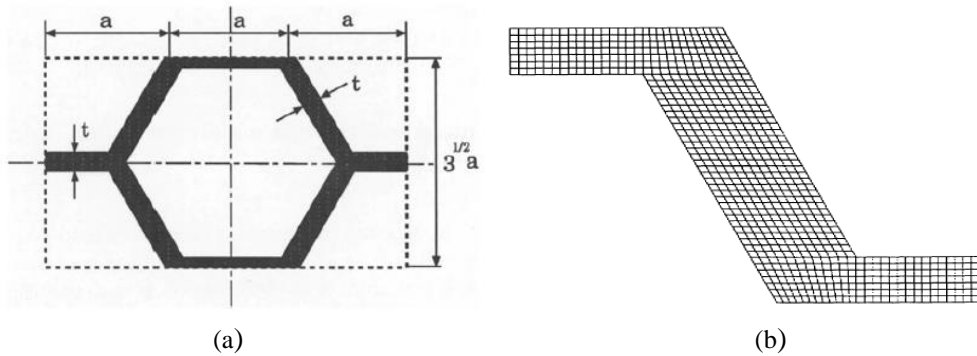


Figure 1.6 (a) Hexagonal Microstructure, (b) FE mesh of a Quarter of the Hexagonal Microstructure [10]

#### I.4.1.2 Bi-material Microstructure

Bi-material microcells involve two solid materials, whether voids are included or not. The geometry parameters of the hard materials, soft materials and voids are set as the design variables of the optimisation problem. As for the one-material microstructure, if a region consists of voids only, material is not placed there. Likewise, if a region has no porosity (no voids), a solid material is placed there. Rank layered microstructures are most commonly used for bi-material microstructures [10]. Figure 1.7 shows examples of bi-material microcell with rank layered microstructures. The black and blue areas represent different solid materials, while the white area represents void. In the case of Figure 1.7(a), optimisation is done only between two solids. The variables shown in the figure are allowed to vary between 0 and 1, limits included. The effective material properties can be derived analytically, and the method can be applied to both 2D and 3D models.

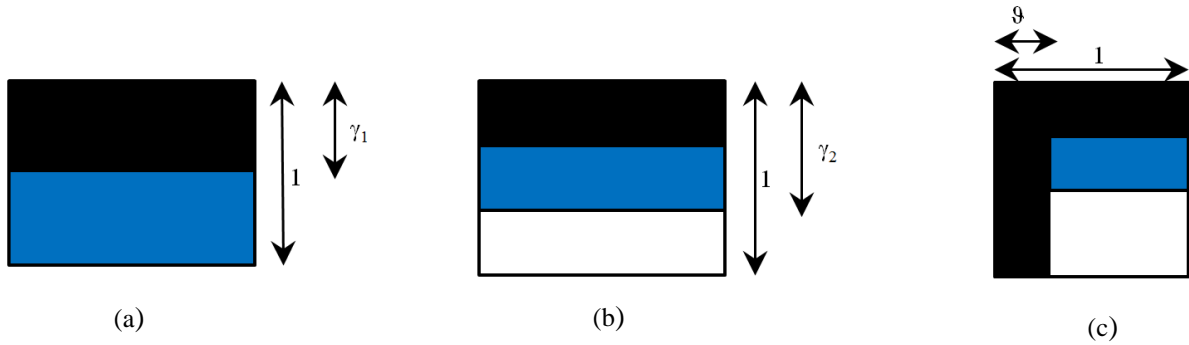


Figure 1.7 Rank Layered Bi-material Microstructures [10]

The volumes occupied by solid material  $\Omega_1$  (black) and solid material  $\Omega_2$  (blue) are given in (I-5) and (I-6) respectively [12].

$$\Omega_s = \int_{\Omega} (\vartheta + (1 - \vartheta) \cdot \gamma_1 \cdot \gamma_2) d\Omega \quad (\text{I-5})$$

$$\Omega_s = \int_{\Omega} ((1 - \vartheta) \cdot (1 - \gamma_1) \cdot \gamma_2) d\Omega \quad (\text{I-6})$$

Despite the numerous ways of formulating the optimisation domain using HM, it remains more popular in the mechanical field than in electromagnetism. The main reason would be the relative complexity of defining an optimisation problem with HM because of the various variables needed for one microstructure. Other methods, more adapted to electromagnetism were developed from HM, and will be seen in the later sections.

#### I.4.1.3 Optimisation Algorithms used with HM

Due to the high dimension of the optimisation problem using HM as described above with multiple variables per cell, it narrows the choice for algorithm classes. Most works with HM apply sensitivity-based approaches using analytical derivatives calculated directly from the definition of the homogenisation problem [14]. Amongst the popular algorithms are the Sequential Linear Programming (SLP), Method of Moving Asymptotes (MMA) or a variety of iterative update rules based on explicit optimality conditions.

#### I.4.1.4 Applications of HM to Electromagnetic Problems

The HM, being primarily derived for mechanical/structural designs has mostly been applied to the topology optimisation of cantilever beams, bridges and trusses. Its application to electromagnetic problems is quite rare and remains much dreaded due to the large number of variables. One of the few works that has been presented on TO using HM is [15], where the authors determine the optimal material distribution in a design domain by changing the inner

hole size and rotational angle of the unit cell. The objective is to maximise the magnetic mean compliance of an H-shaped magnet, which is the same as maximising the magnetic vector potential, and therefore improving the electromagnet performances, according to the authors. Different volume constraints are applied to the design domain to see the behaviour, and the materials used are assumed to be linear. Examples of the topologies obtained are given in Figure 1.8.

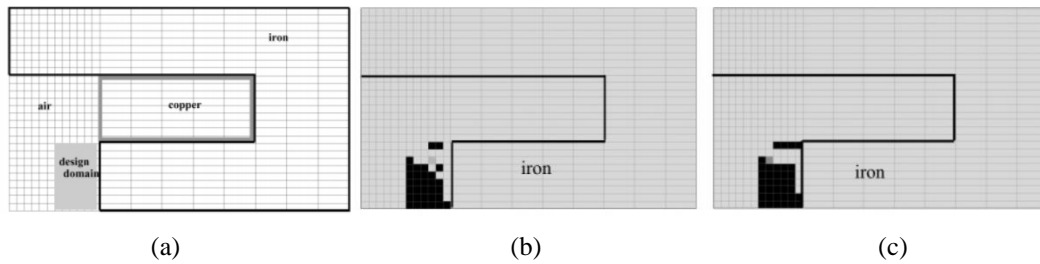


Figure 1.8 H-shaped Electromagnet (a) Initial Domain; Volume Constraint of (b) 60%, (c) 70% [15]

#### 1.4.2 Density-based Methods

Derived from the HM, the Density-based Method was elaborated to overcome some difficulties with the former. Firstly, the generation of areas with porosity were not quite desirable, due to their problematic tendency for manufacturing. An example of porosity would be during the use of rectangular microstructures in HM (Figure 1.2), where the cell would not completely be made of solid material or void. In the advent of many such microcells occurring adjacently, this would form a porous structure, which would be challenging to homogenise for any manufacturing purpose. Another issue could be the need for various design variables for one microcell. Since the process of topology optimisation is already known to be a long one, this would only add up to the lengthy calculation time. For instance, if the rectangular microstructure is again considered, there are 3 design variables in 2D namely  $x_a$ ,  $x_b$  and  $\theta$ , while there are additional ones in 3D. Regarding practicability, the HM is also known to be tedious in implementation, whether for mechanical or electromagnetic problems. To limit the aforementioned difficulties, the Density Method was introduced. It must be pointed out that Direct Approach, Engineer's Method or SIMP Method are the different names given to Density Method.

In [5], the Direct Approach was initiated and tested on a mechanical support structure. An artificial density function  $\rho_i$  was introduced, with  $0 \leq \rho_i \leq 1$ , and used to calculate the Young's Modulus  $E$  of cell  $i$  as in (I-7). The Young's Modulus of the solid material is given by  $E'$ , the penalisation coefficient by  $n$ , and  $i$  is an element of optimisation domain  $\Omega$ . Figure 1.9 depicts a typical 2D domain used in Density Method.



$$E_i = |\rho_i|^n \cdot E_i' \quad (\text{I-7})$$

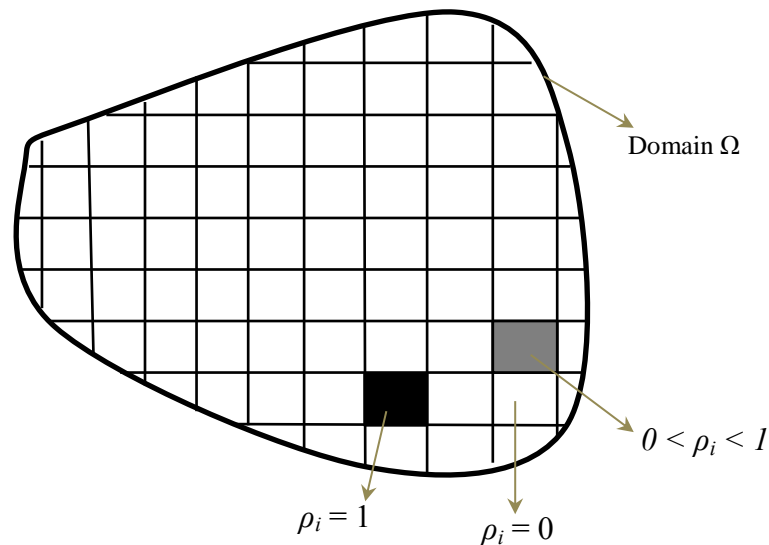


Figure 1.9 Example of 2D domain  $\Omega$  with Density Method

The artificial density values of  $\rho_i$  lying between 0 and 1 essentially represent a proportion of solid material or void. Of course, it is desired to have either solid material ( $\rho=1$ ), or void ( $\rho=0$ ) as final material in the cell, instead of having intermediates unless they are defined in the library of materials of the optimisation problem. The main interest here is that the material properties between the solid and void are interpolated with a smooth continuous function which depends on the material density  $\rho$ . The penalisation coefficient  $n$  is used to change the interpolation behaviour with  $n \geq 1$ , and actually apply a ‘penalty’ on the design variable  $\rho$  to transform it to either solid material or void. This part will be detailed in the following sections. The term SIMP (Solid Isotropic Material with Penalisation) was adopted in [16] by Rozvany et al. to refer to this same method and is today the most commonly used in literature. But the equation relating the various above mentioned parameters can differ in nature. Throughout time, many of these equations or so-called **Interpolation Schemes** have been introduced in literature, and the main ones are presented in the next section. All the equations will be given in terms of relative permeability.

#### 1.4.2.1 Interpolation Schemes

In [7], the Direct Method is revisited for application in the electromagnetic field. The authors propose a new philosophy of considering the method as a distribution of material in space, and called it OMD (Optimised Material Distribution). This point of view is still used today, as it is a more practical way of establishing the problem. In a domain to be optimised,

the material properties are defined at every point in space. Hence, for efficient distribution, the domain has to be discretised into cells. For magnetic devices, parameters such as permeability, permittivity and conductivity are used to represent the materials, where each cell can take these characteristics. For an optimisation, it is possible to consider many properties at the same time, or one at a time. The most common case is to consider only permeability as the material properties, as it is usually desired to optimise the topology of ferromagnetic materials. The relationship between the material density and the permeability was very much inspired from (I-7) and is given in (I-8), dubbed as **Geometric Mapping** in [7]. The main difference is that in the latter, the density is used as a power so that the minimum relative permeability (air) is always 1.

$$\mu r_i = \mu r_{air} \mu r_{iron}^{\rho_i} \quad (\text{I-8})$$

The relative permeability and material density in cell  $i$  are given by  $\mu r_i$  and  $\rho_i$  respectively, and the relative permeability of free space and the solid material are given by  $\mu r_{air}$  and  $\mu r_{iron}$  correspondingly. Following this work, other authors proposed different interpolation schemes between  $\mu r_i$  and  $\rho_i$ . For example in [17] and [18], the **Polynomial Mapping** is introduced, as given in (I-9), and is clearly inspired from (I-7) and (I-8):

$$\mu r_i = \mu r_{air} + (\mu r_{iron} - \mu r_{air}) \rho_i^n \quad (\text{I-9})$$

where  $0 \leq \rho_i \leq 1$  and  $n \geq 1$ . For  $n = 1$ , the function is a linear one, and normally referred to as **Permeability Mapping** in literature. The higher the value of  $n$ , the greater will be the variation of the gradient of the curve. This actually helps in the ‘penalisation’ of the intermediate density values to 0 and 1. The authors in [17] test the mapping using permittivity of a dielectric material instead of permeability, to be consistent with the nature of their problem. In [18], the authors test the interpolation scheme by optimising an electromagnet.

In [19] and [20], the authors initially propose an interpolation scheme with the inverse of the Young’s Modulus  $E$ , as given in (I-10), for  $i^{th}$  cell. In [9], the authors revisit the function and illustrate it as a **Rational Function**, or **RAMP** (Rational Approximation of Material Properties), as it might have been named in other circumstances. The RAMP Function is given in (I-11).

$$\frac{1}{E_i} = \frac{1}{E_{min}} + \rho_i \left( \frac{1}{E_0} - \frac{1}{E_{min}} \right) \quad (\text{I-10})$$

$$E_i = E_{min} + \frac{\rho_i}{1 + q(1 - \rho_i)} (E_0 - E_{min}) \quad (\text{I-11})$$

Of course, the function can also be adapted to electromagnetics by using permeability instead of Young's Modulus, as in (I-12). Usually  $q \geq 0$ , but the authors suggest that if  $E_{min}$  is much smaller than  $E_0$ , then it is wise to use a very large of  $q$  so that the final design is free of intermediate densities. It must be noted that, if  $q = 0$ , the interpolation scheme is linear.

$$\mu r_i = \mu r_{air} + \frac{\rho_i}{1 + q(1 - \rho_i)} (\mu r_{iron} - \mu r_{air}) \quad (\text{I-12})$$

In [21], the authors proposed the use of reluctivity instead of permeability, hence the **Reluctivity Mapping** as in (I-13). The topology optimisation of an electromagnet is treated in the same paper using this mapping. The resulting permeability when the cell  $i$  take the properties of iron or air should be the same when using reluctivity in the equation, except that the shape of the curve for intermediate materials (between 0 and 1) will be different. This is depicted in the next section.

$$\mu r_i = \frac{1}{\frac{1}{\mu r_{air}} + \left( \frac{1}{\mu r_{iron}} - \frac{1}{\mu r_{air}} \right) \rho_i} \quad (\text{I-13})$$

In [22], the authors propose mathematical sequences as interpolation schemes where the **Uniform Sequence**, **Geometric Sequence** and **Arithmetic-geometric Sequence** are evoked. An example of the Uniform Sequence adapted to the permeability is given (I-14).

$$\mu r_i = \mu r_{air} + \left( \frac{\mu r_{iron} - \mu r_{air}}{m} \right) \sum_{k=1}^m \rho_i^k, \forall \rho \in [0,1] \quad (\text{I-14})$$

The value of  $m$  can be varied according to the order of the summation terms desired.

Table 1.1 recaps the different interpolation schemes and Figure 1.10 illustrates the curves obtained with each, for  $\mu r_{air} = 1$ , and  $\mu r_{iron} = 2000$ . The next chapter will compare their efficiency with an academic test case.

Table 1.1 Recap of the Interpolation Schemes

Interpolation Scheme	Equation	Penalty Coefficient
Polynomial	$\mu r_i = \mu r_{air} + (\mu r_{iron} - \mu r_{air})\rho_i^n$	$n$
Geometric	$\mu r_i = \mu r_{air}\mu r_{iron}^{\rho_i}$	-
Reluctivity	$\mu r_i = \frac{1}{\frac{1}{\mu r_{air}} + \left(\frac{1}{\mu r_{iron}} - \frac{1}{\mu r_{air}}\right)\rho_i}$	-
RAMP	$\mu r_i = \mu r_{air} + \frac{\rho_i}{1 + q(1 - \rho_i)}(\mu r_{iron} - \mu r_{air})$	$q$
Uniform Sequence	$\mu r_i = \mu r_{air} + \left(\frac{\mu r_{iron} - \mu r_{air}}{m}\right) \sum_{k=1}^m \rho_i^k$ where $\forall \rho_i \in [0,1]$	$m$

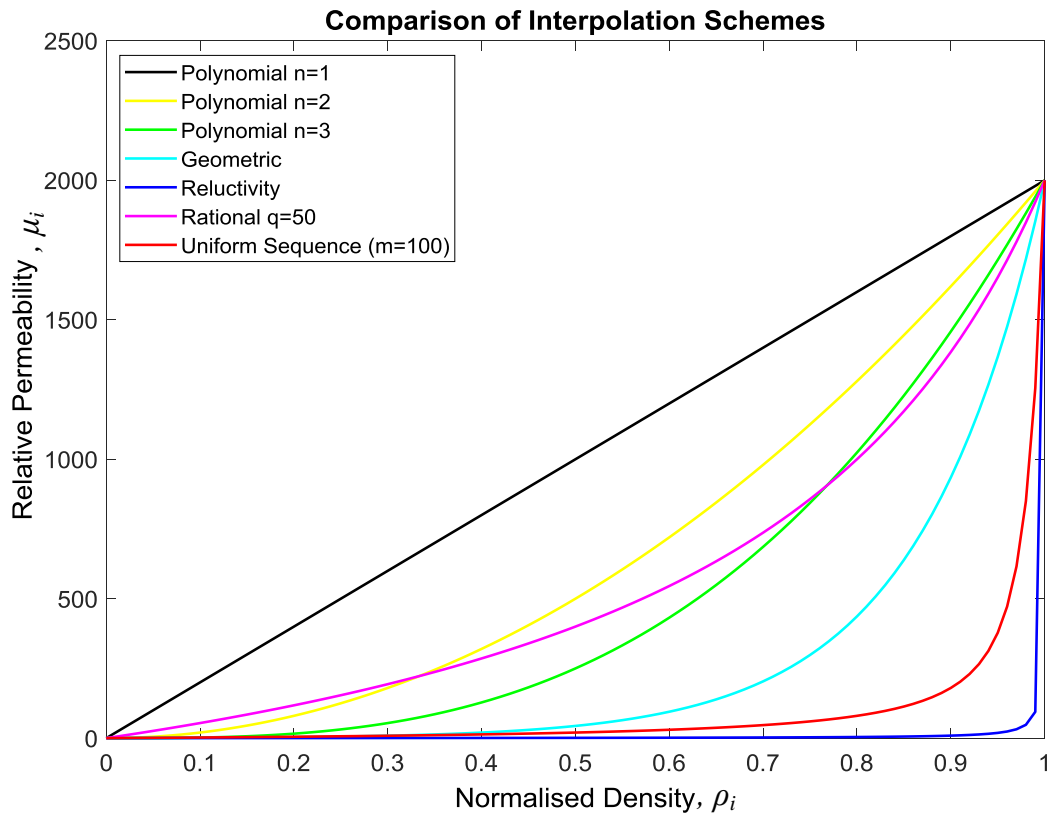


Figure 1.10 Comparison of Different Interpolation Schemes

These mapping equations represent a way of linking the artificial density  $\rho_i$  (variable) to the property of the cell  $i$  by showing their evolution over the range of  $\rho_i$ . These mappings are useful during optimisation as the density  $\rho$  is taken as variable instead of the permeability. Given the smaller range of  $0 \leq \rho_i \leq 1$ , it renders the optimisation process more efficient. Also, since the evolution of the materials during the optimisation process is represented by continuous values, the transition is smoother from one material to another.

#### I.4.2.2 Density Method for Bi-material

As for the HM, the Density Method can also consider the use of bi-material models, i.e. a hard and a soft material, and void. In mechanical structures, (I-15) can be used.

$$E(\rho^e) = (\rho_1^e)^n \cdot ((\rho_2^e)^n E^{(1)} + (1 - \rho_2^e)^n E^{(2)}) \quad (\text{I-15})$$

The elasticity matrix of element  $e$  is  $E$ , and those of material 1 and 2 are  $E^{(1)}$  and  $E^{(2)}$  respectively. The density  $\rho_1$  indicates the presence of material or void, while the density  $\rho_2$  indicates the presence of material 1 or 2. The penalisation coefficient  $n$  is common for both materials [10], [23]. The combinations of  $\rho$  values to indicate the different materials are given in Table 1.2.

Table 1.2 Combinations for Final Material

$\rho_1$	$\rho_2$	Final Material
0	0/1	Void
1	0	Material 1
	1	Material 2

In [23], the author proposes the use of Density Method for bi-material modelling, and suggests invoking each property independently, and writing them as constraints. This principle can also be replicated in electromagnetism to optimise the topology of a structure with hard and soft magnetic material, as given in (I-16). More details will not be provided here as it goes beyond the scope of this work.

$$\mu r(\rho^e) = (\rho_1^e)^n \cdot ((\rho_2^e)^n (\mu r^{(2)} - \mu r_{air}) + (1 - \rho_2^e)^n (\mu r^{(1)} - \mu r_{air})) + \mu r_{air} \quad (\text{I-16})$$

### **I.4.2.3 Optimisation Algorithms with Density Method**

With the Density method, the variables are made continuous, varying between 0 and 1. This allows the use of gradient-based optimisation algorithms, which are quite rapid as compared to discrete variable algorithms. Sequential Linear Programming (SLP), Sequential Quadratic Programming (SQP), or steepest descent are commonly used, as in [24] and [25]. Usually in the Density Method, since there is one variable per cell, the domain can be more finely discretised as compared to HM, with the same calculation time. The common practice is to use each finite element as a variable, hence having as much degree of freedom as the number of finite elements. Some authors [26], [27], [28] also use the analysis tools derived for the finite element formulation to obtain information about the design sensitivity, technique which is most commonly known as the Adjoint Variable Method (AVM). The sensitivity of the objective function to changes in the material properties at each element is calculated, at the expense of a single extra evaluation of the objective function.

### **I.4.2.4 Application of Density Method to Electromagnetic Problems**

Various applications have been inventoried from literature, with many proposing rather straightforward examples such as C-core electromagnets while others suggesting applications to more complex electro-technical structures such as electrical machines.

In [18], Wang & Kang propose to investigate the effect of nonlinearity of materials using a C-core electromagnet as example, for different volume constraints. Using the Polynomial Mapping as well, the authors propose their own code development for FE modelling and nonlinearity consideration. In [29], the same authors propose to optimise the topology of the C-core magnet with coil and magnet as materials as well. In [30], Choi and Yoo propose to use the SIMP Method with AVM and Sequential Linear Programming (SLP) to also optimise the topology of a C-core actuator. In [31], Okamoto et al. propose to revisit the nonlinearity of materials used with Stabilised SLP for a magnetic shield and a magnetic actuator (electromagnet). The energy stored in the systems are maximised, and the effect of taking nonlinearity into consideration is also investigated.

In [32], Byun et al. optimise the topology of an electrostatic actuator that can be manufactured by microelectromechanical system (MEMS) technology. The Polynomial Mapping is used, with the permittivity used as material characteristic in the optimisation process. It is desired to maximise the torque during operation of the actuator. An example of the initial design domain is given in

Figure 1.11(a). For torque maximisation, the difference of the system energy between rotor position A and position B is maximised. The variables coincide with the elements of the FE mesh.

Figure 1.11(b) shows one of the resulting topologies, depending strongly on the initial conditions as commented by the authors.

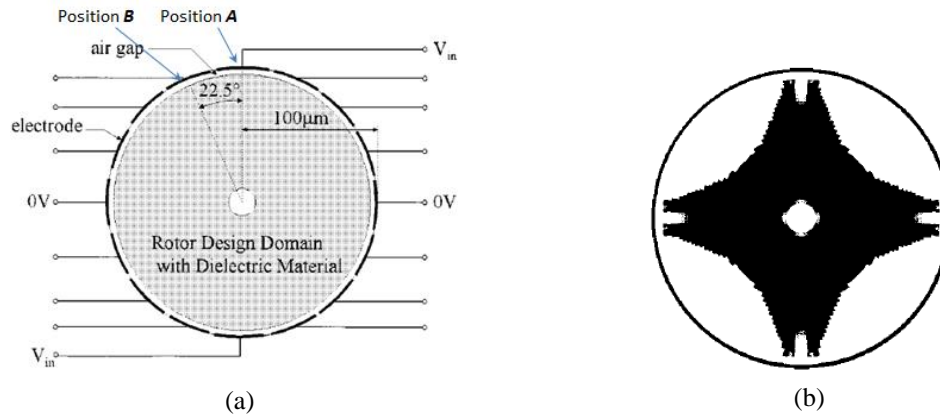


Figure 1.11 Electrostatic Actuator Design (a) Initial Design, (b) Final Design

In [33], the rotor topology of a single phase induction motor for a rotary compressor is optimised. The magnetic energy in the domain to be optimised is maximised, and the volume is also constrained. In [34], the use of Soft Material Composites (SMCs) for the topology optimisation of the outer rotor of a Brushless DC motor (BLDC) was investigated. SMCs are commonly described as ferromagnetic powder particles surrounded by an electrical insulating film offering advantages such as unique 3D isotropic ferromagnetic behaviour and very low eddy current, as compared to conventional laminated steel sheets [35]. The cogging torque was minimised for the BLDC by using a difference in co-energies between two specific positions. In [36], Labbé et al. propose to maximise the torque-to-weight ratio of a Permanent Magnet Synchronous Motor. Choi et al. [37] also attempted to minimise the cogging torque of an Internal Permanent Magnet Motor by using the Reluctivity Mapping. One of the latest applications found in literature is the topology optimisation of a Hall Effect Thruster using the Rational Mapping and Augmented Lagrangian Method to solve the problem [22].

Some other electromagnetic applications using Density Method can also be found such as design of a patch antenna [38] and piezoelectric multi-actuated microtools [39].

### 1.4.3 ON/OFF Method

The ON/OFF Method uses the same mode of discretisation of the domain as in Figure 1.9, except that the variable cells can only take binary/discrete values of 0 or 1, unlike with Density Method which allows continuous values. Consequently, every point within the design

space is filled with either material or void, without any intermediates. Among the first works using this method were [40] where the authors used discrete variables for the design of the structure, albeit the name ‘ON/OFF’ was not yet given.

This method has the advantage of not producing intermediate materials at the end of the optimisation process, and hence avoiding the ambiguity in choosing to place material or void in a grey region. On the other hand, such a method can yield topologies with checkerboard patterns, i.e. regions with a void surrounded by a solid material (or vice versa). These phenomena will be encompassed in the next sections with some examples. This problem can nevertheless be overcome with the use of filters or smoothing operators during or after optimisation. For example, in [41], the authors suggest the use of a topology smoother to enhance the final design, and eliminate the above described phenomena for 3D TO. On the other hand in [42], the blurring technique is introduced as shown in Figure 1.12, by creating giant structural clusters. The weights are allocated to the cells and their neighbourhood in the original structure. Then, the giant clusters are obtained by selecting elements according to the volume fraction constraint.

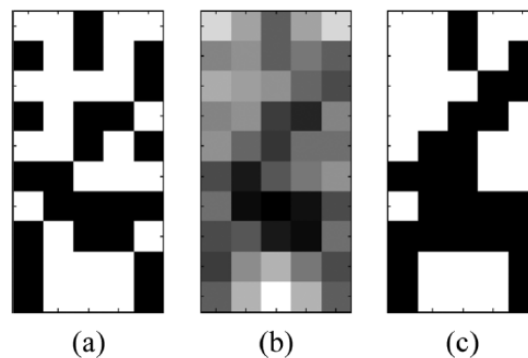


Figure 1.12 Blurring Technique (a) Original Structure, (b) Blurred Structure, (c) Topology Selected according to the Volume Fraction of 0.5 [42]

#### 1.4.3.1 Optimisation Algorithms with ON/OFF Method

Based on the previous works, evolutionary algorithms remain the most popular optimisation algorithms used with the ON/OFF Method. Genetic Algorithms (GA) are often used, whether directly or coupled with some local search procedures [43]. Other stochastic approaches such as Immune-based optimisation algorithms [44] [45] [46], Particle Swarm Optimisation [47], Branch & Bound [48] and Simulated Annealing [40] were used in TO of electromagnetic devices. The main advantage of these approaches is that the global optimum is more likely to be found, as compared to the use of gradient-based algorithms. Nonetheless, a higher number of generations/evaluations are generally needed, and this can increase the calculation time to a higher extent.



It is worth noting that a few works using sensitivity-based techniques with ON/OFF Method have been recorded. For instance in [49], the presence/absence of material in a particular cell is determined by the sign of the sensitivity of the performance function. In [41], Okamoto et al. use the Adjoint Variable Method (AVM) sensitivities to work out magnetic designs using ON/OFF.

#### **I.4.3.2 Application of ON/OFF Method to Electromagnetic Problems**

In [43], the authors propose to use a hybrid GA with the ON/OFF method to optimise the shape of a rotor pole so as to reduce the cogging torque. In [41], the authors use sensitivity analysis to optimise the Single-Pole-Type head having a magnetic shield so as to reduce the leakage flux in the adjacent component. In [50], Takahashi et al. also examine the optimal design of an electromagnetic shield using a Forward Difference method [51] to calculate the sensitivity, and an annealing at the end of the optimisation process to improve the objective function. In [42], the topology of a C-core asymmetric and symmetric magnetic actuator was optimised using GA and ON/OFF sensitivity Method. In [52], the authors derived a multistep GA and tested it on a magnetic shield system. In [53], the same authors applied the method to optimise the topology of a rotor core in an Interior Permanent Magnet (IPM) motor. The effective shape of the flux barrier is derived as it plays a major role in controlling torque characteristics. In the same paper, the effect on the current phase angle of the motor is also considered.

#### **I.4.4 Level Set Method**

Initially derived to track the motion of a front whose speed would depend on the local curvature, such as crystal growth and flame propagation, the Level Set Approach gained in popularity after the work by Osher and Sethian in 1987 [54]. Since then, many authors proposed to apply Level Set Method (LSM) to TO as in [55], [56], [57] and [58]. It is primarily a mathematical way of posing the problem, with equations representing the boundaries. The said boundaries are usually obtained from the contour when a surface intersects a plane, as in Figure 1.13.

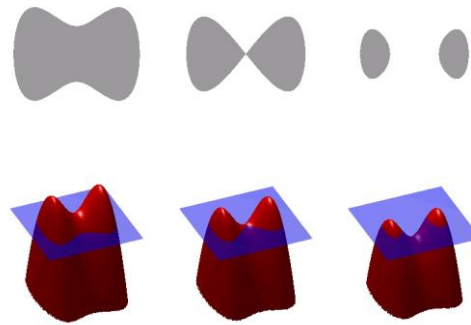


Figure 1.13 Contour Representation when a Surface Intersects a Plane [59]

The idea is to allow the surface to evolve so that the contours are changed, hence creating, merging or splitting the front. The front (or contour) is obtained where the surface has no height, i.e. at  $\phi = 0$ , defined as the zero level set. Figure 1.14 (a) shows an example of the square zero level set of a surface, while Figure 1.14 (b)-(d) shows the evolution of the surface over time, hence splitting the front.

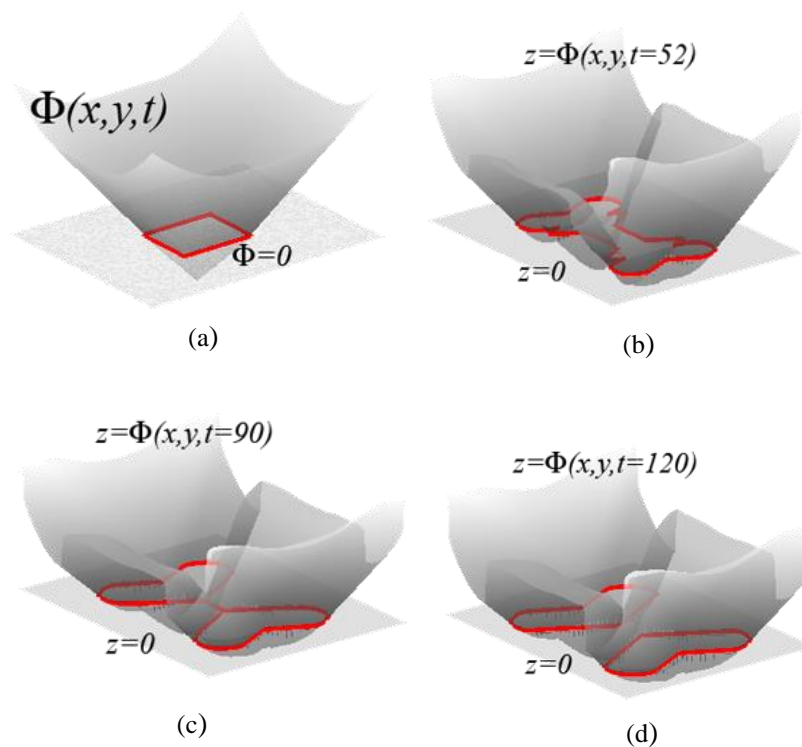


Figure 1.14 (a) Contour at Zero Level Set, (b)-(d) Evolution of a Contour by Splitting [60]

To differentiate the boundaries from their outside and inside regions, the rules in (I-17) are used. The working domain  $Q$  is given in Figure 1.15, in which the admissible shape  $\Omega$  is included, with  $\Omega \subset Q$  and level set function  $\phi$  defined on  $Q$ , and describing the boundary of  $\Omega$ . at any point  $(x,y)$  [55].

$$\phi(x, y) \begin{cases} < 0, & \text{if } (x, y) \in \Omega \\ = 0, & \text{if } (x, y) \in \partial\Omega \cap Q \\ > 0, & \text{if } (x, y) \in (Q \setminus \Omega) \end{cases} \quad (\text{I-17})$$

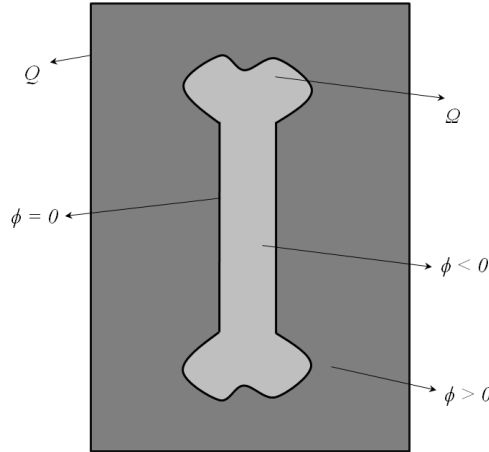


Figure 1.15 Representation of Domain  $\Omega$  and Boundary

To characterise the curve when the surface moves in the normal direction with speed  $v$ , the level set function  $\phi$  has to satisfy the “level set equation” given in (I-18), where  $|\cdot|$  is the Euclidean norm and  $t$  is time. This Hamilton-Jacobi equation can be solved numerically, for example by using finite differences on a Cartesian grid [61], [62]. To update the level set function, and hence the structure, (I-19) is used. It must be noted that the terms  $v(x,y)$  and  $g(x,y)$  are scalar fields over the design domain  $\Omega$ , and  $w$  is a positive parameter which determines the influence of the term involving  $g$ .

$$\frac{\partial \phi}{\partial t} = v|\nabla \phi| \quad (\text{I-18})$$

$$\frac{\partial \phi}{\partial t} = v|\nabla \phi| - wg \quad (\text{I-19})$$

The attractive aspect of splitting, merging and hole degeneration (but not hole generation) makes LSM popular with many authors for TO. It also provides a smooth geometrical description of the domain, and can also be extended to 3D structures.

But LSM remains a very mathematical method and hence complex in setting up. The calculation of the shape gradients often involve the implementation of Partial Differential Equation (PDE) systems, being known for their difficult implementation [14]. Another issue is the inability to generate new holes in the domain, and hence often leading to premature

convergence to sub-optimal topologies. To address this issue, the often used strategy is a highly perforated domain to allow the holes to later merge or disappear, or by including formulation terms in the level-set equations to allow for generation of new holes.

#### **I.4.4.1 Optimisation Algorithms with Level Set Approach**

The common practice is to use derivative-based optimisation methods with level-set formulations. In many cases, Lagrangian optimisation algorithms are coupled with Adjoint Variable Method to look for the topological/shape derivatives during the optimisation process [63] [64] [65]. The topological derivative is basically a function defined at every point  $x$  on the design domain  $\Omega$ , representing the information on the variation of the objective function if an infinitesimal hole is created at  $x \in \Omega$  [66]. Based on this information, holes can iteratively be created and grown at any point in the domain.

Conversely, a few works using derivative-free optimisation methods with Level-set have been recorded in literature. In [67], the authors introduced a spectral version of the level-set technique by using a combination of an initial random search with a posterior local search using a derivative-free trust region. In [68], the same methodology is used, but with an evolutionary algorithm instead. Unfortunately, these works did not fuel any further interest in the electromagnetic TO community.

#### **I.4.4.2 Application of Level Set Approach to Electromagnetic Problems**

Substantial works with level-set in the electromagnetic community started appearing essentially during the last decade. In [64], Shim et al. used the level-set with a topological derivative and a radial basis function to optimise the topology of a C-core actuator. The radial basis function is essentially a radial symmetric function centred at a specific position  $x_i$  in the domain and used with a multi-quadratic spline for interpolation. Afterwards, the Hamilton-Jacobi PDE is used to yield the level-set model.

In [56], the design of a dipole antenna is optimised by maximising the mean current density in the former. The Level-set with shape derivative is used, and is coupled with Method of Moment (MoM) model [69], which is a rather popular numerical method in electromagnetic wave propagation, using Maxwell's equations.

In [70], the rotor shape of an IPM motor is optimised. The results using LSM with a local search method are compared to results using ON/OFF Method with micro-genetic algorithm ( $\mu$ GA). The objective was to maximise the torque while minimising the torque ripple. An

example of the optimised shape and flux distribution of the motor is given in Figure 1.16(a) using the ON/OFF Method, and Figure 1.16(b) using the Level-set Method.

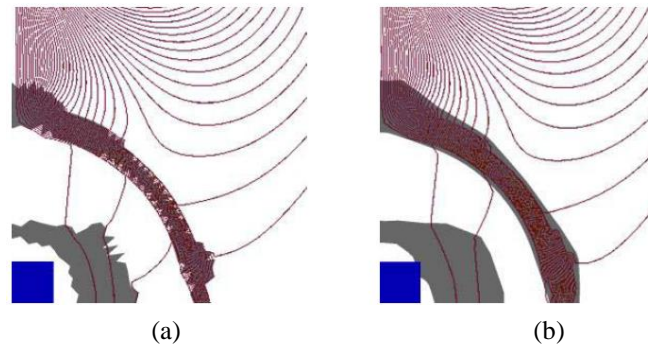


Figure 1.16 Optimised Shape and Flux Distribution (a) ON/OFF (b) Level-set Method [70]

Another interesting work using the Level-set method was conducted by Okamoto et al. [57] to solve 3D nonlinear magnetic field system with spatial symmetric condition. The topology of a magnetic shielding model is optimised, and results using linear and soft nonlinear materials are compared.

## I.5 General Complications with TO

Topology optimisation of a structure, whether mechanical or electromagnetic, is never a straightforward task. It is rather a very complex one as it involves common modelling (FE or others) and optimisation difficulties at the same time. Moreover, it also has to deal with complications related to the TO method itself. This section will encompass the most common obstacles encountered during TO, and the type of method in which it is prominent.

### I.5.1 Intermediate Material

Intermediate materials occur generally in Homogenisation and Density Methods due to the initial formulation of the problem. For the HM as shown in Figure 1.2, the occurrence of high porosity causes difficulties in deciding the boundaries for solid material or void. The use of different microstructures might help in avoiding these problems. Nevertheless, more efficient microstructures might be more complicated in terms of problem setup, and also increase calculation time.

As for the Density Method, due to the continuous nature of the density variables ( $0 \leq \rho \leq 1$ ), the densities very often end up in intermediate values instead of 0 (void) and 1 (solid material). These intermediate values, since not defined in the library of materials, do not have a physical meaning. Some propositions have been made in literature to overcome this problem, such as in (I-9) and (I-12), where the purpose of the coefficients  $n$  and  $q$  is to

‘penalise’ the intermediate values (hence the name penalisation coefficients), and turn them into integers of 0 and 1. But this method has not proved itself utmost efficient throughout the past works. For this reason, [9] proposed the **Continuation Method**. Here, the penalisation coefficient is gradually raised, starting from the lowest value. In the first optimisation with a value of  $n = 1$ , the density of the cells in the domain are allowed to take intermediate values. As  $n$  is increased in the following optimisations, the densities are naturally penalised to end up in a 0-1 design. This method works for any mapping dealing with a penalisation coefficient.

### I.5.2 Local Minima

One of the biggest difficulties of topology design remains the non-convexity of the optimisation problems. Non-convexity typically means that one can find several local minima to a single problem, and can therefore obtain different solutions/topologies depending on the initial conditions and parameters set. This non-uniqueness of solutions due to multiple optima is generally obtained with the HM, Density Method and Level-set Method as they make use of gradient-based and sensitivity based algorithms. Furthermore, according to literature, most global optimisation methods seem rather weak in handling problems of the size of a typical topology optimisation one [9]. The most efficient way of dealing with the local optima is to perform multiple optimisations from various initial points and parameters, and the best solution can be derived from there. Another approach might be the use of the above mentioned Continuation Method here as well to converge to a more reliable solution.

### I.5.3 Checkerboard Designs

Areas with checkerboard-like patterns are often generated in TO. These patterns occur mainly with the use of ON/OFF, Density and Homogenisation Methods. They can occur mainly due to the insufficient fineness of the domain discretisation, or mesh, depending on how the variables are treated. This phenomenon is mostly present in structural designs and less prominent in electromagnetic ones. The main reason for this is the way flux is distributed throughout a ferromagnetic structure, compelling the design to be compact enough for a more efficient flow of flux. Another type of checkerboard pattern that could occur in electromagnetism might be the advent of having a region with a solid material surrounded with air only, or vice-versa. This can happen mainly when considering linear ferromagnetic materials instead of nonlinear ones in electromagnetic structures; or due to an unfortunate mishap in the convergence of the algorithm when using the ON/OFF Method. Figure 1.17

gives an example of a checkerboard pattern in the topology design of a cantilever beam in Figure 1.17(a), and in an electromagnetic design in Figure 1.17(b).

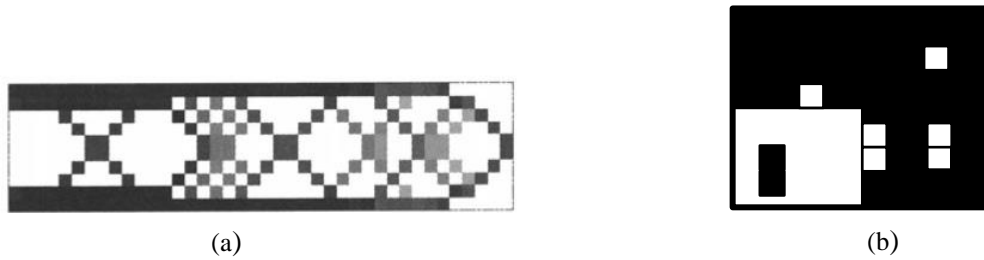


**Figure 1.17** Checkerboard Patterns with (a) Structural Design, (b) Electromagnetic Design

For electromagnetic problems, filters for checkerboard control can be used as optimisation constraints or in post-process of an optimisation to eliminate the undesired patches. A common example is the Neighbouring Method that consists of allocating a sensitivity to a specific element, and its direct 8 neighbours, as described in [9] and [71]. For example, a weight is applied to each element and its direct neighbours; if a void is surrounded by a certain percentage of solid material, the void is sensibly turned into a solid material. The same logic applies vice-versa.

#### 1.5.4 Mesh Dependencies

The problem of mesh dependency has been pointed out in various works, but it remains mainly a difficulty in structural topology design, despite its minor presence in magnetic designs. For instance, a coarse mesh might produce one topology, while a finer mesh might yield a pretty different one. An example for a structural design of a beam is shown in

Figure 1.18. This problem is less recurrent in electromagnetic designs due to the need for compactness of the structure for efficient flow flux. Nevertheless, the difference in topologies when using coarse and fine mesh is very noticeable if the mesh sizes are quite far apart. Of course, like in any other model, a coarse mesh cannot present very precise solutions.

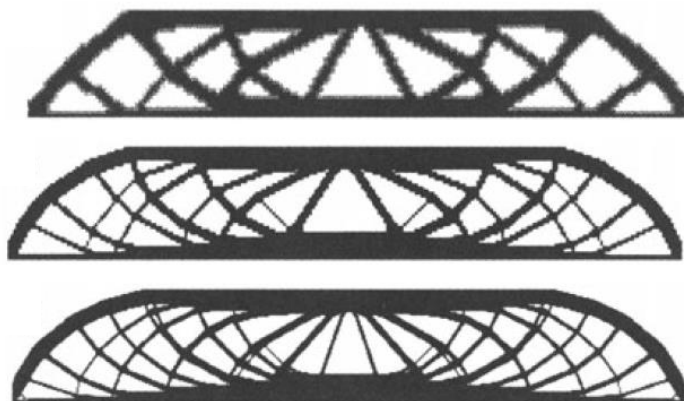


**Figure 1.18** Example of Mesh Dependency of the TO Design [9]

## I.6 Summary of TO Methods

The first part of this chapter has covered the main TO methods in literature, namely Homogenisation, Density, ON/OFF and Level-set Methods. Their modes of operation have been covered, alongside a few examples of application.

We have seen that for HM, different types of microstructures could be used to model the optimisation domain, and the microcells could have various design variables such as length, width, depth, rotation angle, and so on, where the latter are used in the optimisation problem. We have also seen that, depending how the microcells were filled, similar regions could be homogenised (hence the name Homogenisation Method) to produce the final structure. This method is among the first ones to have been devised for TO, but is rarely used in electromagnetism.

We have also elaborated on how the Density Method is used, i.e. how the discretisation of the domain is done, and how the various Interpolation Schemes could be used to model the variables and the properties of the domain to be optimised such as permeability. The variables are represented by artificial densities which are continuous in nature, varying between 0 and 1. The main advantage is the practical nature of the interpolation schemes, as they can easily be programmed for use. The main disadvantage would be the generation of local optima, which could bias final results.

The ON/OFF Method was introduced, and we have seen that the type of domain discretisation is the same when compared to the Density Method, except that the variables are discrete in nature, i.e. they can only take the values of 0 or 1. The main advantage is, as for Density Method, the relatively easy setup of the problem, and also the generation of global optima. On the other hand, the ON/OFF Method can produce checkerboard designs due to the discrete nature of variables, but also have a relatively high calculation for large amount of variables as compared to local methods.

We have also had a look at the Level-set Method, which is a completely different technique of tackling the TO problem. It is more mathematically challenging as compared to the other 3 methods. It does not require any discretisation of the domain, but rather a mathematical function to represent the domain. The boundaries of the function are allowed to evolve, until the final outline of the desired structure is obtained. The main advantage is that, since the boundaries are continuous functions, they can be more precise in topology as compared to the other methods using discretisations. However, the main disadvantage is the relative



mathematical difficulty of the problem setup, and also the generation of local optima as it uses gradient-based methods most of the time.

### *Choice of TO Method*

By taking into account the main advantages and disadvantages of each method, their ease of application, and their compatibility with the numerical tools already used at the L2EP, we retained the Density Method for further exploitation in the thesis work. The most attractive feature that led us to choose this method was the lucidity of the method for comprehension and application; for example the definition of the variables is simply the discretisation of the domain. As we project to use FE modelling, it would not be a problem to take into account the discretisation, and the model can be very well adapted. Moreover, the continuous nature of the variables would allow a smoother transition to a feasible structure. As for the optimisation part, various algorithms can be tested easily, without the need for a change in formulation of the problem.

On the other hand, despite having evoked the use of Adjoint Variable Method in TO and its various advantages, it will not be dealt with in this thesis due to its lengthy development in the 3D FE code used and our constrained time for the thesis completion.

The next part of this chapter will focus on the modelling and optimisation tools used during the thesis, and developed at the L2EP. The classical tools are presented in this chapter, but the tool dedicated to TO, based on the coupling of the classical ones, will be elaborated in the next chapter as it represents a substantial work of this thesis.

## **I.7 Numerical Tools**

Apart from the appropriate material distribution method, an adequate choice of the numerical tools is of utmost importance for the successful TO of any structure. The two main tools are: a performing optimisation algorithm, and a reliable modelling tool. Regarding the optimisation algorithm, it can be of any type, i.e. local search, global search or hybridised. As for the modelling tool, it can be with FE, Reluctance Network (RN), Moment's method and so on. For electromagnetic structures, FE method is the one usually preferred for precise modelling and accurate results.

Generally in literature, programs and codes are tailored exclusively for TO, i.e. the authors develop their own FE and optimisation programmes for a particular structure/model. The foremost advantages to this aspect is that the process is lighter in terms of calculation time and rather flexible, in the sense that modifications are easily brought to enhance the process.

On the other side, the chief drawback is that one has to go through the tedious process of redeveloping a whole code and, in numerous cases, it might not be a general one to all models. This has been the driving motivation for us to utilise a fully-fledged and independent FE and optimisation tool to benefit from all the functionalities of both.

Concerning the FE tool, our choice was directed towards *code\_Carmel* [72], a calculation code initially developed at the L2EP by the modelling team, but as from January 2006 onwards, co-developed with EDF (Électricité De France) R&D. A common laboratory, LAMEL (Laboratoire Avancé de Modélisation du Matériel Électrique) therefore regroups both teams for the continuous development of *code\_Carmel*. Regarding the optimisation tool, *Sophemis* (Superviseur d'optimisation de machines électriques dans leur environnement) was selected, being an optimisation platform also developed at the L2EP [73]. It can accommodate any programmed algorithm in *Matlab*<sup>®</sup> language.

For both to work complementarily towards optimising the topology of an electromagnetic structure, they have to be coupled so that the optimisation evaluations and FE calculations are performed alternately. This will be dealt with in the next chapter. The following sections will concisely cover the operating principle of each tool individually.

### **I.7.1 Code\_Carmel – A FE Calculation Code**

*code\_Carmel* is a Finite Element calculation code essentially based on the resolution of the Maxwell equations to solve electromagnetic problems in magnetostatic and magnetodynamic cases. For greater accuracy, the constitutive laws of materials that link the different fields are obviously considered. Indeed, since magnetic materials usually have a nonlinear magnetic behaviour, the latter must also be considered during calculations. Additionally, while solving electrical machine models, the consideration of specific moving parts is useful to model the corresponding phenomena. These aspects are taken into account by *code\_Carmel*, amongst others.

#### **I.7.1.1 Maxwell's Equations**

The theory of Electromagnetics (EM) was established based on the different findings of various scientists such as Ampere, Gauss, Faraday, Lenz, Coulomb, Lorentz and Laplace, amongst others. Later, Maxwell synthesised their consistent work into four equations, to establish a link between electric and magnetic quantities [74]. The four equations are given in (I-20) to (I-23).

*Gauss's Law for electric fields*

$$\nabla \cdot \mathbf{D} = \rho_v \quad (\text{I-20})$$

*Gauss's Law for magnetic fields*

$$\nabla \cdot \mathbf{B} = 0 \quad (\text{I-21})$$

*Faraday's Law*

$$\nabla \times \mathbf{E} = -\frac{\partial \mathbf{B}}{\partial t} \quad (\text{I-22})$$

*Ampere's Law*

$$\nabla \times \mathbf{H} = \mathbf{J} + \frac{\partial \mathbf{D}}{\partial t} \quad (\text{I-23})$$

With:

**D:** Electric Flux Density (C/m<sup>2</sup>)

**B:** Magnetic Flux Density (T)

**E:** Electric Field (V/m)

**H:** Magnetic Field (A/m)

**J:** Current Density (A/m<sup>2</sup>)

$\rho_v$ : Volume Charge Density (C/m<sup>3</sup>)

It must be noted that all Maxwell's equations are expressed in vectors forms. Figure 1.19 shows how the Maxwell's Equations can be divided into subgroups. For this work, our focus will be mainly on the magnetics subgroup.

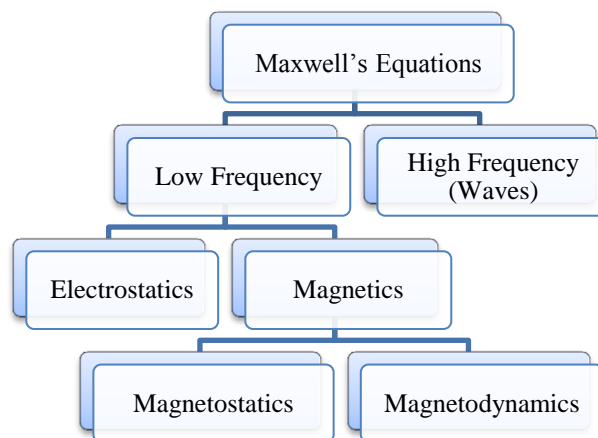


Figure 1.19 Subgroups of Maxwell's Equations

In the magnetostatic case, slow varying fields can be understood to be fields not leading to current redistributions, and therefore the eddy current effects are not considered. This is commonly called the *quasi-static* phenomenon. In the magnetodynamic case, fast varying time dependent fields are treated as *quasi-stationary*. In both cases, the term  $\frac{\partial D}{\partial t}$  is neglected in the Ampere's Law, and gives (I-24). This induces charge conservation, and therefore (I-25).

$$\nabla \times \mathbf{H} = \mathbf{J} \quad (\text{I-24})$$

$$\nabla \cdot \mathbf{J} = 0 \quad (\text{I-25})$$

To use Maxwell's equations to solve any electromagnetic problem, they must be completed with the constitutive laws, as briefed in the following section.

### I.7.1.2 Constitutive Laws of Materials

The field vectors  $\mathbf{D}$  and  $\mathbf{E}$ , and also  $\mathbf{B}$  and  $\mathbf{H}$  are related by the properties of the materials at any point in the field region. These relations are referred to as the constitutive properties of the material, and are given in (I-26), (I-27) and (I-28).

$$\mathbf{D} = \varepsilon \cdot \mathbf{E} \quad (\text{I-26})$$

$$\mathbf{B} = \mu \cdot \mathbf{H} \quad (\text{I-27})$$

$$\mathbf{J} = \sigma \cdot \mathbf{E} \quad (\text{I-28})$$

With:

$\varepsilon$ : Electrical Permittivity of the Material (F/m)

$\mu$ : Magnetic Permeability of the Material (H/m)

$\sigma$ : Electrical Conductivity of the Material (S/m)

The values of permittivity and permeability can also be expressed in relative form, as given in (I-29) and (I-30). The permittivity and permeability of free space are given by  $\varepsilon_0$  and  $\mu_0$ ; and the relative values for the material are given by  $\varepsilon_r$  and  $\mu_r$  respectively.

$$\varepsilon = \varepsilon_0 \cdot \varepsilon_r \quad (\text{I-29})$$

$$\mu = \mu_0 \cdot \mu_r \quad (\text{I-30})$$

It must be noted that (I-27) is a linear relationship, and is usually applicable to non-ferromagnetic materials only. For hard magnetic materials (permanent magnets), the relationship can be written as in (I-31), where  $B_r$  is the remnant induction in T, and  $\mu_r$  is the relative permeability for such materials, usually close to unity [75].

$$\mathbf{B} = \mathbf{B}_r + \mu_0 \mu_r \mathbf{H} \quad (\text{I-31})$$

For soft magnetic materials, such as iron alloys used in electromagnetic actuators (machine rotors and stators), the magnetic saturation must be considered. The new relationship is therefore as given in (I-32). Hysteresis is neglected in this case.

$$\mathbf{B} = \mu(\|H\|)\mathbf{H} \quad (\text{I-32})$$

It is worth noting that the constitutive laws chosen define largely the modelling quality of the electromagnetic phenomena.

### 1.7.1.3 Boundary Conditions

To solve the equations in the modelled domain, conditions on the fields are applied on its boundaries. Furthermore, the symmetries of the domain are also used to truncate it in order to limit the number of unknowns, and therefore the computation time. For a studied domain  $\Omega$ , the boundary is given by  $\Gamma = \partial\Omega$ .

Hence, the boundary condition given by  $\mathbf{B} \cdot \mathbf{n} = 0 |_{\Gamma_b}$  is applied at  $\Gamma_b$ , the boundary relative to the magnetic flux density, while the condition  $\mathbf{H} \times \mathbf{n} = 0 |_{\Gamma_h}$  is imposed, with  $\Gamma_h$  as the surface relative to magnetic field. Of course, both  $\Gamma_b$  and  $\Gamma_h$  are complementary in  $\Gamma$ , i.e.  $\Gamma = \Gamma_b \cup \Gamma_h$  and  $\Gamma_b \cap \Gamma_h = \emptyset$ .

For conductors, the studied domain is  $\Omega_c$ , and the boundary is given by  $\Gamma_c = \partial\Omega_c$ . Boundary conditions are also applied when using conducting materials, such as  $\mathbf{J} \cdot \mathbf{n} = 0 |_{\Gamma_j}$ , with  $\Gamma_j$  representing the envelope of the conducting domain. Furthermore, in many cases, the latter domain is also truncated. This leads to the condition  $\mathbf{E} \times \mathbf{n} = 0 |_{\Gamma_e}$ , where the surface  $\Gamma_e$  represents either a symmetry, or an equipotential surface with an imposed voltage. The two surfaces  $\Gamma_j$  and  $\Gamma_e$  are also complementary for the conductor boundary  $\Gamma_c$ , as in the case of magnetic materials previously. The schema of the domain in an electromagnetic system is depicted in Figure 1.20.

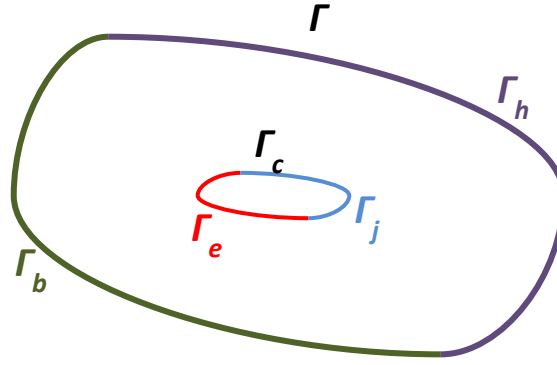


Figure 1.20 Schema of Electromagnetic Domain

#### I.7.1.4 Formulations

Generally, to solve Maxwell's Equations, scalar and vector potentials are introduced. This section will only deal with the formulations for electrostatic and magnetostatic fields. Magnetodynamic field will not be covered as it deals with induced currents, which is not covered in our TO study.

##### *Electrostatic Formulation*

Here, the studied space is limited to the domain  $\Omega_c$  for conductors. Only the electric field and current density are considered, and hence the term  $\frac{\partial B}{\partial t}$  representing the time variation of the magnetic flux density is neglected. The system in (I-33) is solved, along with the boundary conditions in (I-34).

$$\begin{cases} \nabla \times \mathbf{E} = \mathbf{0} \\ \nabla \cdot \mathbf{J} = 0 \\ \mathbf{J} = \sigma \mathbf{E} \end{cases} \quad (\text{I-33})$$

$$\begin{cases} \mathbf{E} \times \mathbf{n} = \mathbf{0} |_{\Gamma_e} \\ \mathbf{J} \cdot \mathbf{n} = 0 |_{\Gamma_j} \\ \Gamma_c = \Gamma_j \cup \Gamma_e \end{cases} \quad (\text{I-34})$$

To solve the system, the *Electric Scalar Potential*  $\varphi$  can be used, as given in (I-35). The latter is replaced in (I-33) so that (I-36) is to be solved.

$$\mathbf{E} = -\nabla \varphi \quad (\text{I-35})$$

$$\nabla \cdot (-\sigma \nabla \varphi) = 0 \quad (\text{I-36})$$

Another method is to use the *Electric Vector Potential*  $T$  as in (I-37), and therefore resulting in (I-38) to be solved.

$$\nabla \times \mathbf{T} = \mathbf{J} \quad (\text{I-37})$$

$$\nabla \times \left( \frac{1}{\sigma} (\nabla \times \mathbf{T}) \right) = 0 \quad (\text{I-38})$$

### *Magnetostatic Formulation*

In this case, the studied domain is limited to the non-conducting one, where there are no induced currents. Nevertheless, an imposed current  $J_s$  can be applied to the system to constitute the source term. Considering soft and linear magnetic materials, the magnetic quantities, i.e. magnetic field and magnetic flux density are determined by solving the system in (I-39), with the boundary conditions in (I-40).

$$\begin{cases} \nabla \times \mathbf{H} = \mathbf{J}_s \\ \nabla \cdot \mathbf{B} = 0 \\ \mathbf{B} = \mu \mathbf{H} \end{cases} \quad (\text{I-39})$$

$$\begin{cases} \mathbf{H} \times \mathbf{n} = \mathbf{0} |_{\Gamma_h} \\ \mathbf{B} \cdot \mathbf{n} = 0 |_{\Gamma_b} \\ \Gamma = \Gamma_b \cup \Gamma_h \end{cases} \quad (\text{I-40})$$

To solve this system, the *Magnetic Vector Potential*  $A$  can be introduced, as given in (I-41). By replacing in the system, (I-42) is obtained.

$$\nabla \times \mathbf{A} = \mathbf{B} \quad (\text{I-41})$$

$$\nabla \times \left( \frac{1}{\mu} (\nabla \times \mathbf{A}) \right) = \mathbf{J}_s \quad (\text{I-42})$$

Another way to solve the system is to use the *Magnetic Scalar Potential*  $\Omega$ . In this case, a source field  $H_s$  is introduced such as  $\nabla \times H_s = J_s$  and  $H_s \times n = 0 |_{\Gamma_h}$ . The new Maxwell-Ampère equation is then written as  $\nabla \times (\mathbf{H} - H_s) = 0$ , and  $\Omega$  is introduced as in (I-43).

$$\mathbf{H} = \mathbf{H}_s - \nabla \Omega \quad (\text{I-43})$$

The formulation for the Magnetic Scalar Potential to be solved is thus given in (I-44).

$$\nabla \cdot (\mu \nabla \Omega) = \nabla \cdot (\mu \mathbf{H}_s) \quad (\text{I-44})$$

Usually, an equation with ‘curl-curl’ as in (I-38) and (I-42) is rather difficult to solve, and thus less preferred than the other formulations. It is also worth noting that in the following chapters, the formulation  $\Omega$  will be mostly used, with only a few comparisons with formulation  $A$ .

To solve such a system of PDE to obtain a numerical solution, a spatial discretisation of the field equations is required. There are various discretisation approaches such as *Finite Differences*, *Boundary Elements*, *Moment’s Method*, *Monte Carlo Method* and *Finite Elements Method*. In our case, ***Finite Element Method***, which is more common in electromagnetism, is used.

### 1.7.1.5 Finite Elements Approach

Finite Elements (FE) approach, used for the discretisation in space, relies on approximation spaces for the physical quantities that possess locally supported basis/interpolation functions [76]. The principle of discretisation in the FE approach is to divide the studied domain into smaller (usually equal) elements. The nature of these elements depends on the dimension  $q$  of the studied domain. For example, in 1D the elements are segments, in 2D they are polygons, and in 3D they are polyhedra. The physical quantities are calculated in each of these elements. The solution can be found at the nodes, edges or faces using an interpolation function.

The general procedure for FE approach can be summarised in the following steps:

- a) The PDE, with the given boundary conditions, are multiplied by the appropriate test functions and integrated over the whole simulation domain
- b) A partial integration is done and a variational (weak) formulation is obtained
- c) At this point, the discretisation of the whole domain using FE is required
- d) An approximation method is applied to obtain the algebraic system of equations, i.e. the physical quantity of interest is approximated by functions, and the solution of the algebraic system of equations leads to the physical quantity in the discretisation points

Let’s consider the problem where the function  $u$  must be found, and the solution of the system is defined by (I-45).

$$A(\mathbf{u}) = \mathbf{f} \quad (\text{I-45})$$



Where  $\mathbf{A}$  is a derivative operator and  $\mathbf{f}$  is a function independent of  $\mathbf{u}$ . This system is the general form of FE approach used for any physical phenomenon. In our case, it is therefore replaced by the Scalar or Vector Potential equations presented before, depending on the formulation required.

This equation is transformed into the weak variational form. A functional space  $V$  must be defined, containing the exact solution  $u$  (continuous problem). The approximated solution  $u_h$  in the functional space  $V_h$  (discrete problem) must then be sought. The continuous problem is given by (I-46), where the solution  $u \in V$  must be found.

$$\mathbf{a}(\mathbf{u}, \mathbf{v}) = \mathbf{l}(\mathbf{v}), \forall \mathbf{v} \in V \quad (\text{I-46})$$

Where  $\mathbf{a}(\cdot, \cdot)$  is in bilinear form, and  $\mathbf{l}(\cdot)$  in linear.

The discrete problem is similar, and given in (I-47), where  $u_h \in V_h$  must be found.

$$\mathbf{a}(\mathbf{u}_h, \mathbf{v}_h) = \mathbf{l}(\mathbf{v}_h), \forall \mathbf{v}_h \in V_h \quad (\text{I-47})$$

The discrete problem takes complex geometries into account, where the latter are approximations of the structure of the system in the form of elements constituting the discrete domain [77].

#### 1.7.1.6 Nonlinearity

Due to the use of soft magnetic materials in the modelling of electrical devices, as mentioned previously, the consideration of the nonlinear behaviour of the ferromagnetic materials is very important, as in (I-31). Generally, the hysteresis cycle is neglected. Each material behaves differently under a certain  $B$  or  $H$ , and therefore a  $B(H)$  curve is usually established for each of them to give the true magnetic permeability  $\mu$ . To obtain the true values of the latter, the manufacturer usually carries out a series of tests on samples of the material, and provides the characterisation curve along with the material.

But this  $B(H)$  curve also has to be implemented in *code\_Carmel* so that the FE models (of machines) can be as close as possible to the actual ones. To do so, the **Marrocco Equation** [78] is used, as given in (I-48). The latter is suitable for mean-magnetization modelling of ferromagnetic materials, as in our case. Due to its continuous first derivative, the equation is also suitable for Newton-Raphson nonlinear iterative schemes, which are used in *code\_Carmel*.

$$H = \frac{B}{\mu_0} \left[ \frac{B^{2\alpha}}{B^{2\alpha} + \tau} (c - \varepsilon) + \varepsilon \right] \quad (\text{I-48})$$

where  $\alpha$ ,  $\tau$ ,  $\varepsilon$  and  $c$  are the coefficients to be adjusted in the equation.

From each  $B(H)$  curve supplied by the manufacturer, a regression function is used to find the correct values of the coefficients of the Marrocco equation, and the latter is used to model the desired system. An example of such a curve is given in Figure 1.21, showing the linear section before saturation, and nonlinear section after saturation.

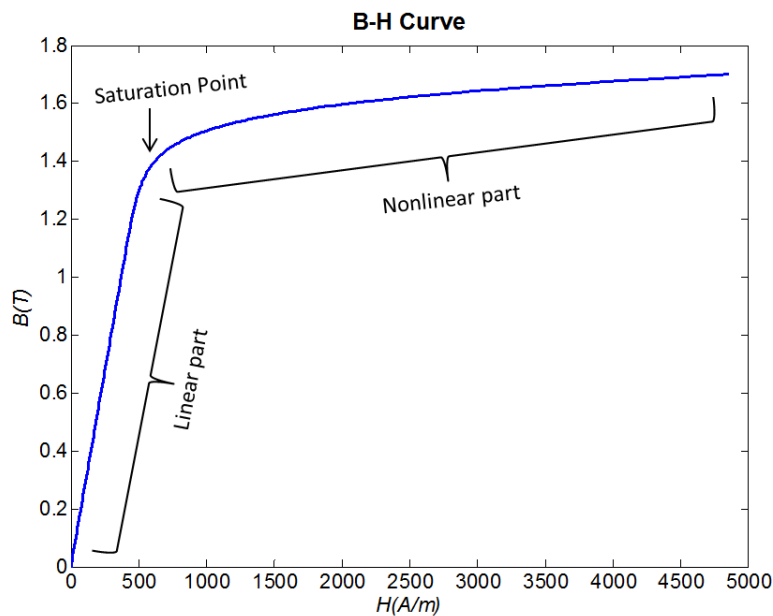


Figure 1.21 B(H) Curve using Marrocco Equation

Typically, most designs operate at, or near the saturation point. The permeability  $\mu$  is a function of the local magnetic field, which is unknown at the start of the problem. Therefore, an iterative process is used to keep correcting the permeability until it is consistent with the field solution. As mentioned before, the iterative method used in *code\_Carmel* is the Newton-Raphson Method, where it is also possible for the user to choose the number of iterations allowed for convergence, for more or less precise solutions.

### 1.7.1.7 Movements

Electrical machines are usually rotating ones, and therefore if a rigorous and accurate model simulation is desired, the movements must also be taken into account. In *code\_Carmel*, due to the rigidity of the machine materials, deformations are not considered. This hypothesis allows a fixed mesh to be used, i.e. no re-meshing of the model is needed at every step of the movement. To model the latter, in addition to the correct boundary conditions, the surface

where movement occurs must be defined. This is commonly called the ‘slipping surface’ in *code\_Carmel*, and considers the boundary/surface between the fixed and mobile domain.

This surface must be meshed in a regular way since the motion is simulated through a permutation of the unknowns of this surface. Therefore, this induces a link between the rotation speed and the simulation time step. Indeed, the rotation step is dependent on the mesh of this surface and can only be taken as an integer number of the angle between two successive nodes of the slipping surface. In general, the finer the mesh size, the higher will be the number of nodes on the slipping surface, and hence the smaller will be the time steps of the simulation.

#### 1.7.1.8 Energy

The magnetic energy calculated in *code\_Carmel* for a FE model returns a global value. The magnetic energy density  $w$  for a stationary magnetic field is calculated as in (I-49).

$$w = \int_0^b hdb \quad (\text{I-49})$$

#### 1.7.1.9 Force

The magnetic force calculated by *code\_Carmel* is done using the Virtual Work (VT) Method [79] [80], and was implemented based on the works of [81]. The VT method is based on the principle of transformation of the magnetic energy into mechanical energy. In a domain  $\mathcal{D}$ , the total force in a direction  $s$  can be calculated from the variation of the magnetic energy  $w$  of the system after a displacement in the same direction, as given in (I-50). This movement is done with a constant flux, i.e. with  $B$  constant.

$$F_s = -\partial_s w \Big|_{b=\text{const}}, \quad s = x, y, z \quad (\text{I-50})$$

A similar expression can be established using the variation of the magnetic co-energy  $w'$  when the current is constant, and hence  $h$  constant as given in (I-51).

$$F_s = \partial_s w' \Big|_{h=\text{const}}, \quad s = x, y, z \quad (\text{I-51})$$

Both calculations are done assuming no variation of  $b$  and  $h$  on the boundaries of the domain during the displacement, and only within the domain  $\mathcal{D}$ .

## I.7.2 *Sophemis* – An Optimisation Platform

*Sophemis* is essentially a Matlab<sup>®</sup> operated platform that provides a live interface for the user to supervise the optimisation process. It allows the execution of any Matlab<sup>®</sup> model, as long as the inputs and outputs are correctly defined. For an optimisation problem, the inputs include fixed parameters and variables, while the outputs comprise the objective functions and the constraints. It is possible to use Matlab-ready algorithms, but also user-programmed algorithms. Some of the algorithms already available in *Sophemis* are ***Particle Swarm Optimisation*** (PSO), mono/multi objective ***Genetic Algorithm*** (GA) and ***fmincon***. Design of Experiments (DoE) such as ***Full Factorial Design*** (FFD) and ***Latin Hypercube Square*** (LHS) are also available.

In the coming sections, the DoE and algorithms that will be used in the scope of this work will be described. This includes FFD, LHS, *fmincon* SQP and GA.

DoE is categorised by a series of tests conducted by changing the input variables so as to identify the reasons for the changes in output response. It is therefore necessary to define the problem and choose the *variables* (or input factors). A *design space* (or region of interest), being the range of variability of each variable, must also be defined.

### I.7.2.1 Full Factorial Design

Among the existing DoE, the FFD is probably the most common and intuitive strategy for experimental design [82]. Its aim is to cover all the possible combinations of input factors of a problem. The factors are assigned levels of variability  $L$  within which they can evolve. For example, if  $L = 2$ , the input factors can be *high* or *low*, i.e. +1 or -1. For  $k$  input factors of the problem, the sample size will be  $N = L^k$ , i.e.  $N$  experiments will be done to cover all the possible combinations of the problem. Therefore, the higher the number of factors and levels, the bigger will be the sample size, and hence more time will be required to cover all the combination possibilities. For this reason, the FFD is preferred for problems with low values of  $L$  and  $k$ . Table 1.3 gives an idea about how the sample size rapidly grows when input factors or levels are increased.

Table 1.3 Example of Full Factorial Design

Number of Levels $L$	Number of Factors $k$	Sample Size $N$
2	2	4
2	5	32
3	2	9
3	5	243

In TO, as the number of variables is usually high, this method cannot be used. On the other hand, it will be used in the next chapter for analysis of the behaviour of the test cases.

Nevertheless, it must be noted that **Fractional Factorial Designs** are also used in the event of larger number of  $L$  and  $k$ , so that the sample is downsized to half or quarter of the original size. This will not be dealt with in this thesis as it is beyond the scope of our work.

### 1.7.2.2 Latin Hypercube Square

LHS essentially aims at reducing the sample size for the factor combinations of a problem whilst keeping a resourceful sample distribution [82]. The level of variability for each factor is usually allowed to be higher than for FFD, i.e. 3 and over, as not all the levels are experienced in LHS. Instead, a choice of combinations to be investigated is made, hence reducing the sample size. The terms primary factors and nuisance factors are also introduced in LHS, respectively representing the main factor of interest and the other factors present in the problem. For example, if  $k = 3$ , where 2 of the 3 factors are nuisance factors, the sample size will be  $N = L^2$ . It must be pointed out that if:

- $k=3$ , the DoE is called Latin Square
- $k=4$ , the DoE is called Graeco-Latin Square
- $k \geq 5$ , the DoE is called Hyper-Graeco-Latin Square or Latin Hypercube Square

An example of how the Latin Square is combined is given in Figure 1.22, and the respective experimental design in Table 1.4 for  $k = 3$ ,  $L = 3$ , and  $N = 9$ , with  $X_1$  and  $X_2$  the nuisance factors, and  $X_3$  the primary factor.

A	B	C
C	A	B
B	C	A

Figure 1.22 Latin square Example

Table 1.4 Latin Square Experimental design

Experiment No.	Factor Level		
	X <sub>1</sub> (row)	X <sub>2</sub> (column)	X <sub>3</sub>
1	1	1	A
2	1	2	B
3	1	3	C
4	2	1	C
5	2	2	A
6	2	3	B
7	3	1	B
8	3	2	C
9	3	3	A

In each row and each column, the levels of factors must not be repeated, and each factor must follow a different letter/number pattern in the Latin Square. The advantage of the Latin Square is its ability to keep separated several nuisance factors in a relatively cheap way in terms of sample size. On the other hand, since the factors are never changed one at a time from sample to sample, their effect can be partially confounded. When using  $k \geq 5$ , the Hyper-Graeco-Latin Square is more difficult to be defined theoretically. In this case, in *Sophemis*, the sample size is specified, and the number of levels of variability required for the factors is calculated accordingly by the platform (see Appendix A).

### 1.7.2.3 *fmincon SQP*

For the optimisation algorithm used throughout this work, *fmincon SQP* was chosen due to its remarkable ability to handle nonlinear functions and satisfy constraints. The general nonlinear optimisation problem is usually as given in (I-52), and will be referred to as NLP in the following explanations. The functions in NLP must be continuously differentiable twice.

$$\left\{ \begin{array}{l} \min f(x) \\ \text{subject to: } \begin{cases} h(x) = 0 \\ g(x) \leq 0 \end{cases} \end{array} \right. \quad \text{(I-52)}$$

In *fmincon SQP* (Matlab<sup>®</sup>) used in our case, the gradient is calculated by finite difference and this information is used to advance towards the optimum. The problem can also include

as special cases, linear and quadratic programs in which the constraint functions  $h$  and  $g$  are affine, and  $f$  is linear or quadratic.

The basic idea of SQP is to model NLP at a given approximate solution, say  $x^k$ , by a quadratic programming subproblem, and then use the solution to this subproblem to construct a better approximation  $x^{k+1}$ . This process is iterated to create a sequence of approximations that is expected to converge to a solution  $x^*$ . If constraints are not considered, the SQP method reduces to the Newton's Method for finding the roots (zeroes) of a function. The presence of constraints makes the implementation of SQP more complex.

Two characteristics of the SQP Method must be pointed out. First, SQP Method is not a feasible-point method, i.e. neither the initial point nor any of the subsequent iterates need to be feasible (a feasible point satisfies all the constraints of NLP). This is a major advantage since finding a feasible point when there are nonlinear constraints may be nearly as hard as solving the NLP itself. SQP Methods can be easily modified so that linear constraints, including simple bounds, are always satisfied. Secondly, successful SQP Methods depend on the existence of rapid and accurate algorithms for solving quadratic programs. Fortunately, there are efficient algorithms to solve quadratic programs easily. In case of equality constraints, the problem reduces to a system of linear equations, while for inequality constraints, a sequence of systems may have to be solved.

It must also be pointed out that SQP Methods like Newton's Method and steepest descent are local algorithms. Therefore, to reach the global optimum, a *merit function* is used. It is a way of measuring the progress towards the true solution, which reduces while approaching the solution.

The Lagrangian for this NLP is given in (I-53).

$$\mathcal{L}(x, \lambda, \sigma) = f(x) - \lambda^T h(x) - \sigma^T g(x) \quad (\text{I-53})$$

where  $\lambda$  and  $\sigma$  are Lagrange multipliers. At an iterate  $x^k$ , a sequential programming algorithm defines an appropriate search direction  $d^k$  as a solution to the quadratic programming subproblem, as in (I-54).

$$\begin{cases} \min & f(x^k) + \nabla f(x^k)^T d + \frac{1}{2} d^T \nabla_{xx}^2 \mathcal{L}(x^k, \lambda^k, \sigma^k) d \\ \text{subject to} & h(x^k) + \nabla h(x^k)^T d = 0 \\ & g(x^k) + \nabla g(x^k)^T d \leq 0 \end{cases} \quad (\text{I-54})$$

### 1.7.2.4 Genetic Algorithm (GA)

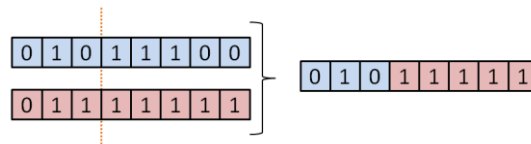
GA is an adaptive heuristic (metaheuristic) search algorithm based on the evolutionary ideas of natural selection and genetics. It represents an intelligent exploitation of an initially random generation to solve optimisation problems. It is considered as a global search method, unlike gradient-based methods which are local search methods. Both have their pros and cons, depending on the final purpose.

In the GA optimisation process, an initial random generation of individuals is generated called a **population**. Each individual in the population is attributed a unique **chromosome**. The chromosome is normally a string of binary digits {0,1} or characters, depending on how they are defined initially. An example of an individual's chromosome in binary digits is:

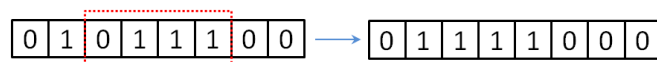
0	1	0	1	1	1	0	0
---	---	---	---	---	---	---	---

Each chromosome is made of genes, represented here by a binary digit. From this current population of individuals, a new population is generated. This new population is obtained based on different evolution processes:

- **Selection:** the fittest individuals (**parents**) from the population  $T$  are selected, based on their **fitness score**. The fitness score is usually the value of the objective being optimised; hence the individuals with the most optimal objectives are selected
- **Crossover:** the parents are mated with one another, creating better **children** of the next population  $T+1$ . A crossover point is chosen and portions of the chromosomes of the individuals are interchanged. An example of a type of crossover is:



- **Mutation:** some individuals of population  $T+1$  will have their bits flipped, but the probability of this is kept low. Its purpose is to maintain diversity within the population, and inhibit premature convergence, e.g.:



The fitness of the population  $T+1$  is evaluated, and the process is iterated until the best individual is found.



## I.8 Summary

After a deep insight into the various features of Topology Optimisation, i.e. the requirement of the material distribution methods, the tools for FE modelling and for optimisation, we can now proceed with tests of new methodologies and their application to electromagnetic devices to find new topologies. Table 1.5 summarises the tools chosen from the literature review for further use.

Table 1.5 Recap of Tool Chosen

Tool	Choice	Main Reason
FE analysis	<i>code_Carmel</i>	Fully functional FE code developed at the L2EP, and hence modifications accessible
Optimisation	<i>Sophemis</i>	Optimisation platform that can accommodate any algorithm, developed at the L2EP. Modifications accessible
Material Distribution Method	Density Method	Intuitive method, with lucid setting up. Compatible with our FE and optimisation tools

Regarding the optimisation algorithm, we will use *fmincon SQP* in most cases, but we will also use GA and the other presented DoEs for a few tests and comparisons.

We have seen that TO is quite a complex topic, and for this reason, we proceed gradually by starting with an academic electromagnetic test, which will be illustrated in Chapter II. Our awareness regarding the lengthy calculation times pointed out in literature for TO has also reinforced this choice. But despite the academic nature of the test case, it is a very useful one to lay the foundation stone of our work.

Once the methodology for TO is developed and tested, we will apply it to more tangible electromagnetic cases such as an electromagnet and a Salient Pole Synchronous Generator, presented in Chapter III and IV respectively. The various topologies obtained for different problem formulations will be discussed, as well as the major hindrances encountered during the TO process.

# Chapter II – Methodology and Tool Development

---

## II.1 Introduction

This chapter is dedicated to the development, testing and analysis of a methodology based on the Density Method for TO of electromagnetic structures. As stated earlier in this thesis, TO is a very complex process and requires attention of the user in various aspects of the topic, such as type of domain discretisation, mesh size, problem formulation, and so on. A change in one of the latter can change the optimal structure obtained. Additionally, the TO tool used throughout this work will also be covered in this chapter, as significant effort was invested in its development and testing. It involves the coupling of *code\_Carmel* and *Sophemis*, the two tools developed at the L2EP which have been introduced in the previous chapter. Since we are dealing with TO in electromagnetism, the consideration of the nonlinearity of the materials is also important. But it is nonetheless often overlooked in other works as it tends to encumber the process. Therefore, this chapter will also explain how the nonlinearity is taken into account in our case, w.r.t the methods already used in *code\_Carmel*.

Development of a tool and methodology is one part, but one should also be able to test it with a quick response so as to understand the behaviours for TO, and to further apply it to more complex electromagnetic cases. For this reason, this chapter will utilise an academic and relatively quick electromagnetic test case to explore the different angles of this subject and have a deeper insight of how the system functions as a whole. This will also help us to identify the main difficulties of TO in electromagnetism, and anticipate for future cases. Throughout this chapter, the test case will be fully exemplified, as well as its strengths and weaknesses. Furthermore, we will use the same test case to compare our methodology with some others to indicate where we stand, and why we have opted for this choice.

## II.2 Coupling of *code\_Carmel* and *Sophemis*

This section focuses on the coupling between *code\_Carmel* and *Sophemis*, explaining the overall process and how it functions. Since it is a ‘home-made’ tool, it has certain configurations in which it has to be used, and also certain restrictions. These points will be concisely presented here for the reader to have a wider overview of the system.

### II.2.1 Overall Process

To benefit from the functionalities of both tools, the software are coupled so that optimisation and FE solving of the model are done alternatively in a loop. Figure 2.1 shows a

simplified flowchart of the general process devised for this purpose. The latter is explained before detailing the coupling itself.

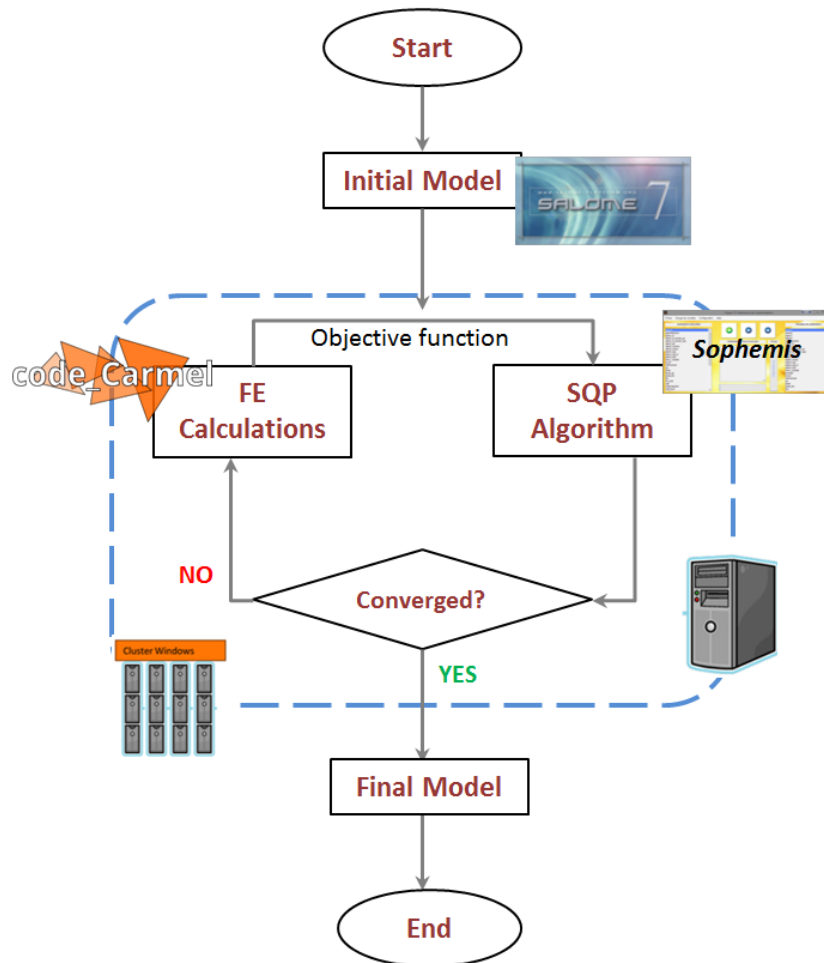


Figure 2.1 Flowchart for Overall TO Process

The initial structure is modelled using *Salome* [83], a FE software which allows 2D, extruded 2D and 3D modelling (creation of a geometry and its mesh). The structure is subjected to a TO method, for instance the Density Method here, and is fed to the *code\_Carmel-Sophemis* coupling for topology optimisation. At this step, the optimisation problem has normally already been defined, i.e. regarding the function to be maximised and constraints to be satisfied (see Appendix B). The optimisation process is started, and for every optimisation evaluation, the FE model is solved (see Appendix C). The latter feeds the optimisation algorithm with the output objective function which, in electromagnetics, is usually the energy, force, torque, magnetic field or magnetic flux density. The algorithm processes the information and evolves in the direction of convergence of the objective and iterates the loop until optimum is reached. Subsequently, for the optimum reached, the

corresponding structure is retained as the final optimal model. The latter is usually in the form of a vector of densities; hence a post process using *Salome* is done to extract the corresponding topology. Some other properties such as magnetic field and flux density can also be visualised with the latter. As for other outputs such as torque, force, energy, they can be obtained from *code\_Carmel* post process files (see Appendix D).

## II.2.2 Configurations of the Coupling

In general, *code\_Carmel* runs under any GNU/Linux compatible OS, and is installed on a server (Cleep) for academic use. It can also be installed on a PC, with the required authorisations. As for *Sophemis*, it operates under Windows and GNU/Linux, and is installed on a second server, but can also be installed on a PC. There are globally 3 configurations in which the coupled system can operate.

### 1. Local Utilisation

Here, both *code\_Carmel* and *Sophemis* are installed on the same computer/server system, and the OS must be GNU/Linux compatible (see Appendix E). Figure 2.2 shows the layout for this configuration. Its biggest strength is that the user can easily test and debug the models before launching any optimisation. Parameterisation of the model can also be rapidly adjusted in this case.

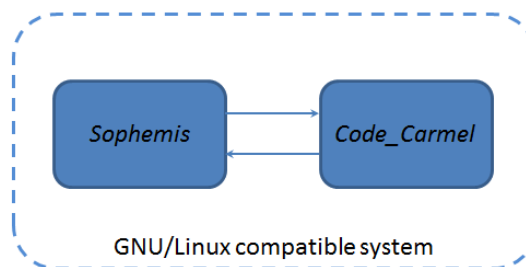


Figure 2.2 Local Utilisation Layout

### 2. Distant Utilisation

In this case, *Sophemis* runs on a computer/server system and *code\_Carmel* runs on a different GNU/Linux compatible server. Figure 2.3 shows how the systems interact. In this case, calculations can be more rapid due to the use of a different server, usually a more efficient one. Testing and debugging phase can be a little lengthier as compared to the previous case. On the other hand, it is rather inefficient for TO with short calculation time, as much of it is lost in communication between the servers.

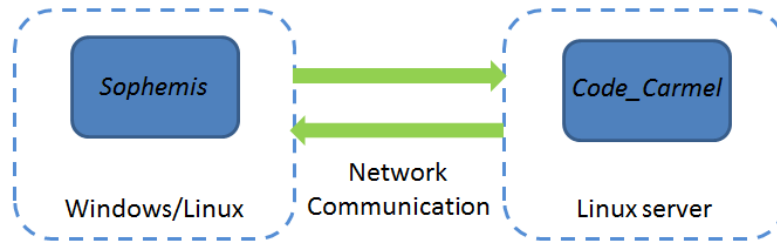


Figure 2.3 Distant Utilisation Layout

### 3. Distant and Distributed Utilisation

For this configuration, *Sophemis* runs on a computer/server system and *code\_Carmel* runs on the Cleep server, which in turn distributes calculations on a cluster. Figure 2.4 shows the layout in this case. The biggest advantage here is that for lengthy calculations, time is saved during execution as evaluations can be parallelised. This makes it efficient for the exploitation of fine models. Also, there are no constraints w.r.t the user's OS. The main drawbacks would be a cumbersome testing and debugging of the model, and not efficient for rapid models due to communication delays.

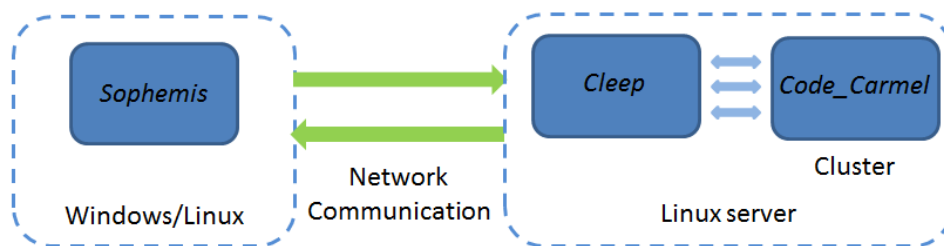


Figure 2.4 Distant and Distributed Utilisation Layout

## II.3 Choice of TO Method – Density Method

As evoked in Chapter II, the Density Method is retained for this thesis work, for a number of reasons:

- a) It is easier to implement, from an engineering point of view, as compared to the others (Homogenisation and Level-set Methods)
- b) Various Interpolation Schemes can be used and compared when using Density Method
- c) It is compatible with our present tools
- d) It is rather intuitive, especially regarding the ways of considering the variables

On the other hand, as for all other methods, it might present some difficulties. These are mainly in:

- a) The ability of producing composite-free structures

- b) The ability of producing a global optimum instead of a local one, relative to the optimisation algorithms normally used with this method (e.g. gradient based, SQP)
- c) A long calculation time, which is nevertheless a common problem to all the other methods

The *Polynomial Mapping*, as introduced in Chapter I - Section I.4.2.1, is chosen as Interpolation Scheme, and is recapped in (II-1).

$$\mu r_i = \mu r_{air} + (\mu r_{iron} - \mu r_{air})\rho_i^n \quad (\text{II-1})$$

where  $\mu r_{air}$ ,  $\mu r_{iron}$  and  $\mu r_i$  are respectively the relative permeability of air, iron and the final material in the structure for every discretisation  $i$  of the domain. The normalised density is given by  $\rho_i$  with  $0 \leq \rho_i \leq 1$ , and the penalisation coefficient to remove composites is  $n$ .

It must be noted that the mapping as presented here is meant to optimise the topology of a structure made of iron and air. If two other materials with different permeability were to be optimised, such as two different types of iron, the  $\mu r_{air}$  and  $\mu r_{iron}$  could be replaced by  $\mu r_{min}$  and  $\mu r_{max}$  respectively. Similarly, if other materials such as copper coils and magnets are used, the permeability is replaced by electrical conductivity or remanence respectively to represent the former's characteristics. For this thesis work, we will stick to structures made of iron and air. The method by which the mapping is applied to the optimisation domain for a general case is also recapitulated here. Figure 2.5(a) shows the initial domain to be optimised, where each discretisation represents a variable of the problem, and Figure 2.5(b) presents the colour legend for the materials, with the corresponding  $\rho$  and  $\mu r$ . Since the final structure should be composed of iron and air, each variable is allowed to take the relative magnetic permeability of either iron ( $\mu r_{iron}$ ) or air ( $\mu r_{air}$ ) so as to maximise an objective function  $f$ . The algorithm uses the interpolated value of  $\rho$  (from the Polynomial Mapping) during the optimisation, as given in Figure 2.6 for different values of penalisation coefficient  $n$ , and  $\mu r_{iron} = 2000$ . The purpose of  $n$  is to prevent intermediate (composite) materials from occurring in the final optimised structure by increasing its value. Some authors such as in [84] suggest that setting  $n = 3$  produces no intermediate values. But this strongly depends on the size and nature of the model.

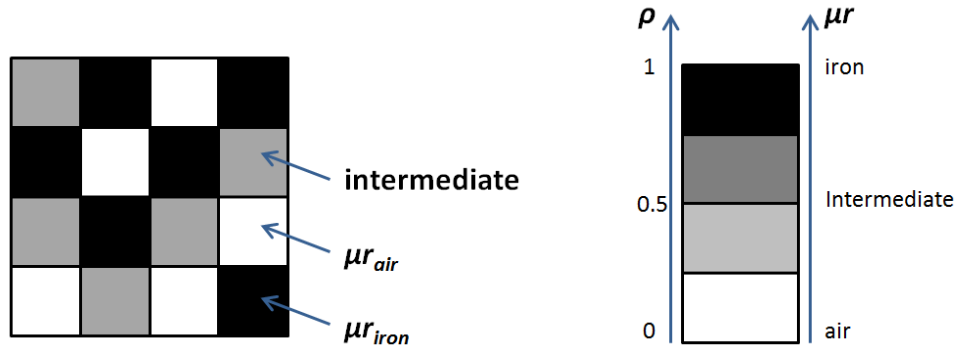


Figure 2.5 (a) Example of Initial Domain, (b) Colour Legend for  $\rho$  and  $\mu_r$

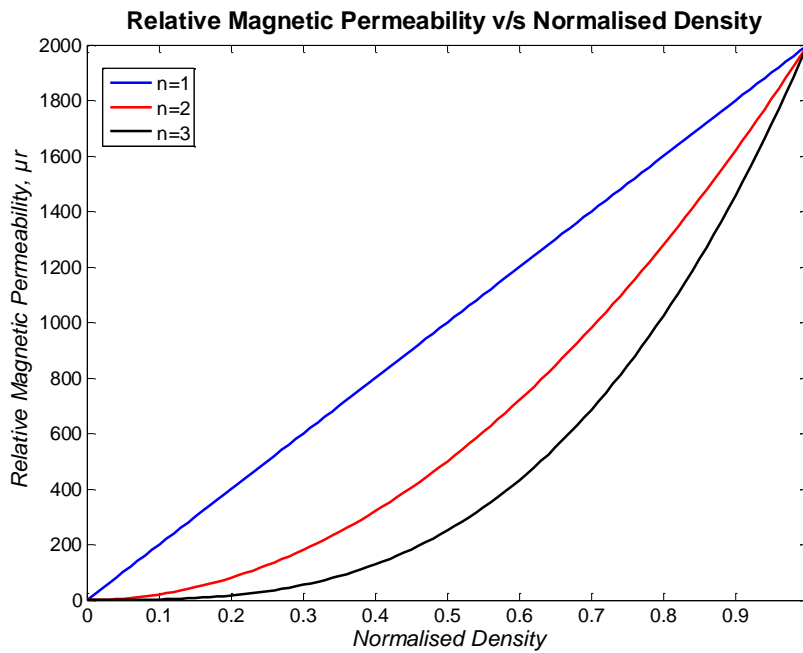


Figure 2.6 Polynomial Mapping for different Penalisation Coefficients  $n$

Figure 2.6 depicts the relationship between the relative permeability  $\mu_r$  and the variable of the problem, i.e. density  $\rho$ . When penalisation coefficient  $n = 1$ , the function between  $\mu_r$  and  $\rho$  is linear. As  $n$  is increased, the function becomes a nonlinear one. A small value of  $\rho$  gives a small value of  $\mu_r$ , and a high value of  $\rho$  gives a higher value of  $\mu_r$ . We can see that for  $n \geq 1$ , the derivative of the function is nil at zero. This particularity of the mapping presents a problem in the evolution of gradient-based algorithms. Therefore, to counteract this problem, we use a minimum density slightly higher than 0, such as 0.05.

#### *Global TO Process with Density Method*

Figure 2.7 shows the TO process globally in the form of a block diagram while using Density Method. The Polynomial Mapping is taken as example here, but the diagram is valid for any interpolation scheme. After discretisation of the domain to be optimised, an initial



value of  $\rho$  is allocated to each discretisation. The interpolation scheme of the Density Method is used to convert the  $\rho$  into  $\mu_r$  to be applied to the initial FE model. This step is essential as *code\_Carmel* can evaluate the FE model only if the appropriate ferromagnetic materials are described. The value of the objective function is sent to the optimisation algorithm for evaluation. In the case of a first evaluation, or cases when the objective function has not yet converged to an optimal value according to the stopping criteria of the algorithm, the process is iterated. A new vector of  $\rho$  representing the values of the variables is allocated to the discretisations, and the process is repeated. If the objective values converge to an optimal value, the optimisation process is stopped, and the topology of the final structure is derived from the values of  $\rho$ .

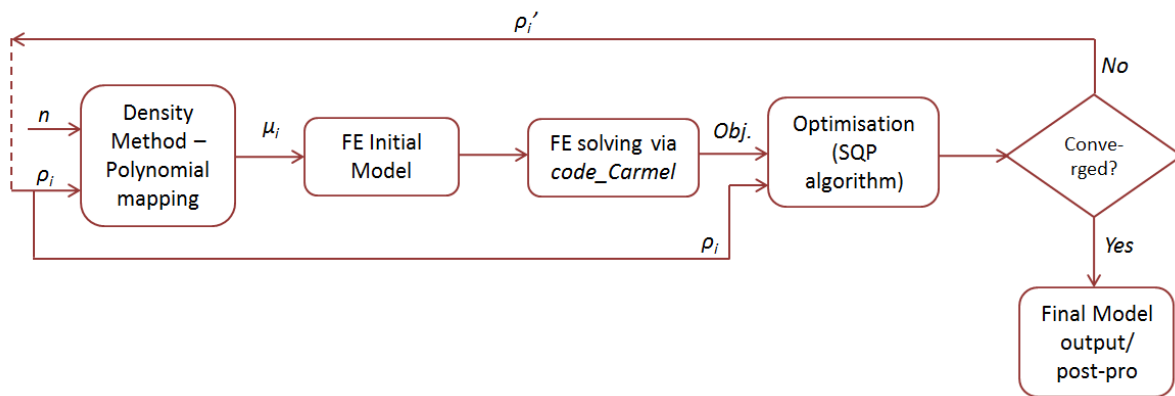


Figure 2.7 Block Diagram of TO Process with Polynomial Mapping

The interpolation process is straightforward when linear materials are used, as shown here. However, when using nonlinear materials, some changes must be brought. The next section encompasses the different modifications.

## II.4 Nonlinear Behaviour of Materials for TO using *code\_Carmel-Sophemis*

The nonlinear behaviour of ferromagnetic materials is considered in *code\_Carmel* using the Newton-Raphson method with  $A-\varphi$  formulation, and Fixed-point method with  $T-\Omega$  formulation. Both are iterative methods, where the system to be solved is linearized at each iteration. It is important to define an initial solution of the system for the iterative process, and in the case of *code\_Carmel*, the initial solution is zero. The system to be solved is given in (II-2).

$$A(X).Y = b(X) \quad (\text{II-2})$$

In this thesis work, the use of  $T$ - $\Omega$  formulation is favoured since the FE models are in 3D. The latter formulation is more adapted to 3D models because it involves a div-div resolution of the problem (Chapter I Section I.7.1.4), which is easier than a curl-curl resolution. Since 3D models have a higher number of unknowns than 2D, the calculation time can be higher. Therefore, the use of a div-div resolution can contribute to facilitate calculation time.

Therefore, we will exemplify the resolution of the problem in this section using  $T$ - $\Omega$  formulation and Fixed point Method. Moreover, since our FE calculations are in magnetostatics, the formulation reduces to  $\Omega$  only.

At each step, the state of the equation is as given in (II-3), where  $X^{N+1}$  must be found, with a certain tolerance defined by the user. The criterion  $\xi$  for the convergence of the solution is given in (II-4), where  $\epsilon$  is the admitted tolerance.

$$A(X^N).X^{N+1} = b(X^N) \quad (\text{II-3})$$

$$\xi = \left| \frac{X^{N+1} - X^N}{X^N} \right| \leq \epsilon \quad (\text{II-4})$$

The value of  $H$  is derived directly from the system solution in (II-3). If a wound inductor is used as magnetic source,  $H = 0$  initially. On the other hand, if a Magnetic Potential Difference (MPD) is used as magnetic source, the initial  $H$  will depend on the value imposed by the MPD. It must be noted that the first iteration is linear. Then, the corresponding initial value of  $\mu$  is calculated from  $\mu(H)$  curve, as in Figure 2.8.

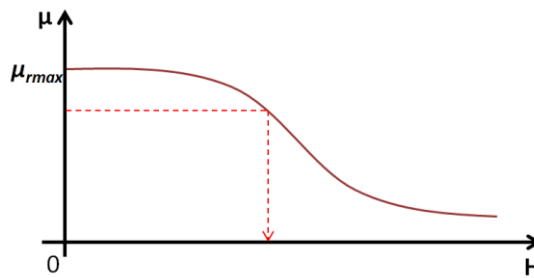


Figure 2.8  $\mu(H)$  Curve

Subsequently, the value of  $B$  can be calculated from the  $H(B)$  curve obtained from the Marrocco equation [78], given in Figure 2.9. Since the Marrocco equation in (I-48) is given as  $H$  in terms of  $B$ , finding the corresponding value of  $B$  is not straightforward. In *code\_Carmel*, the Bisection Method [85] [86] is used as iterative scheme to compute  $B$  by numerical inversion of the  $H(B)$  equation. The whole process is iterated until the stopping criterion is met, and the solution found.

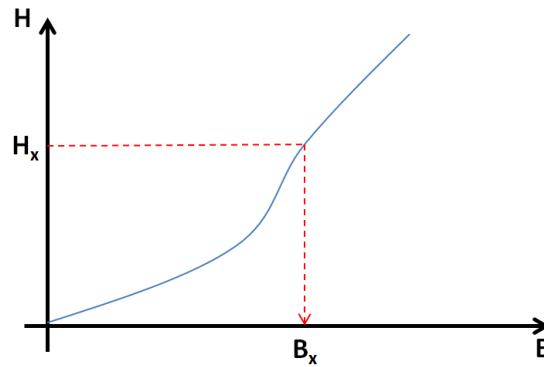


Figure 2.9 H(B) Curve

As for the  $A-\varphi$  formulation, the overall process is comparable, but with some key variances. The main variance is the calculation of  $B$  first, which is derived from the system equation in (II-3). The initial value is taken as  $B = 0$ , and therefore the permeability is derived from the  $\mu(B)$  curve; initially  $\mu = \frac{1}{\varepsilon}$ , where  $\varepsilon$  is one of the coefficients of the Marrocco equation as in (I-48). Therefore, with the value of  $B$  and  $\mu$  found, the value of  $H$  can directly be obtained from the Marrocco equation, without the need for an iterative process using the Bisection Method.

#### *Integrating the Nonlinear Calculation in the TO process*

The above method infers that the value of  $\mu$  cannot be fixed for the nonlinear calculation and must be found during the iterative process. However, this poses a problem in the sense that during TO, a fixed value of permeability should be fed to *code\_Carmel* for evaluation of the FE model. Since this is not possible, the code is directly modified to use the value of density  $\rho$  as input (variable), instead of the  $\mu$ , as in the linear case. The density represents a mixture of air and iron for a variable, and can therefore be fixed for a FE evaluation. This suggests that every time the permeability  $\mu$  is calculated, a new  $\mu'$  is deduced corresponding to the density  $\rho$  initially fixed for this FE evaluation. This new value of permeability  $\mu'$  is obtained by combining the Marrocco equation with the Polynomial Mapping, and is as given in (II-5). The equation is given in terms of absolute values here for consistency with the above explanations. The whole process is then iterated as above to find the solution.

$$\mu_i' = \mu_0 + \left( \frac{B(H_i)}{H_i} - \mu_0 \right) \rho_i^n \quad \text{(II-5)}$$

Similar to the linear case, a block diagram can also be drawn to illustrate the steps for the nonlinear case, as shown in Figure 2.10. The main differences are in red.

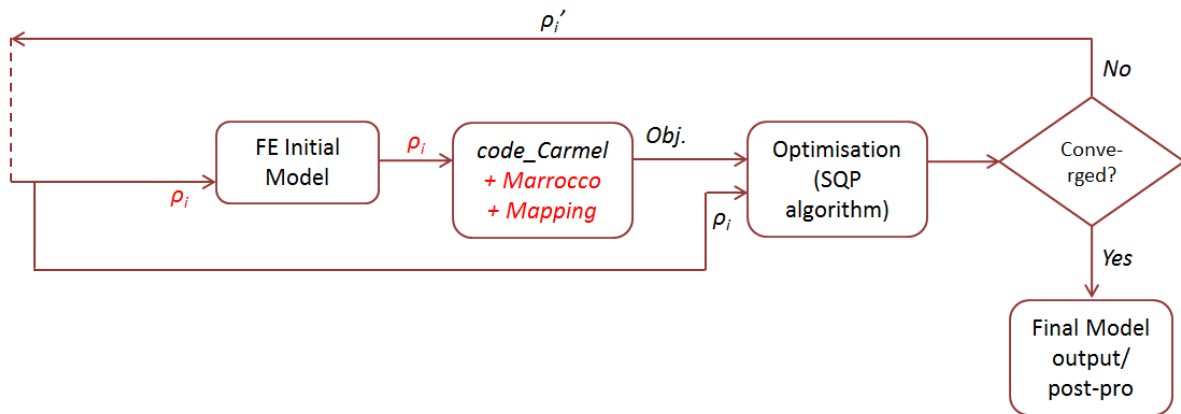


Figure 2.10 Block Diagram to Highlight Main Differences using Nonlinear Materials

Following the discretisation of the initial FE model, each discretisation is allocated a density of  $\rho$ . These densities are used directly in *code\_Carmel* for calculation of  $\mu$  and other parameters as described in the previous section. The rest of the process is carried out as for the linear case.

## II.5 3D Electromagnetic Test Case

After having had a deeper look into the tools developed for TO, they can now be used on any electromagnetic structure. Nevertheless, for a successful TO, it is essential to understand how the global process behaves. To accomplish this part, we will introduce in this section, an electromagnetic test case to analyse the behaviour of the TO process. Since the latter is a long and tedious process, especially when a large number of variables are involved, an academic and rapid test case is favoured. The chosen test case constitutes a 3D cube, with a Magnetic Potential Difference (MPD) applied to a portion of two opposite faces. The interests of such an example lie, on one hand, in the predictability and verification of the physical optimal structure and on the other hand, in the flexibility of the discretisation of the model. Figure 2.11 shows an example of two test cases, with 8 and 64 variables, with the left hand side depicting the geometry, and the right hand side the FE model. In the latter, the blue squares represent the hexahedral finite elements of the mesh. For example, the test case with 8 variables in Figure 2.11(a) has 64 hexahedra per variable.

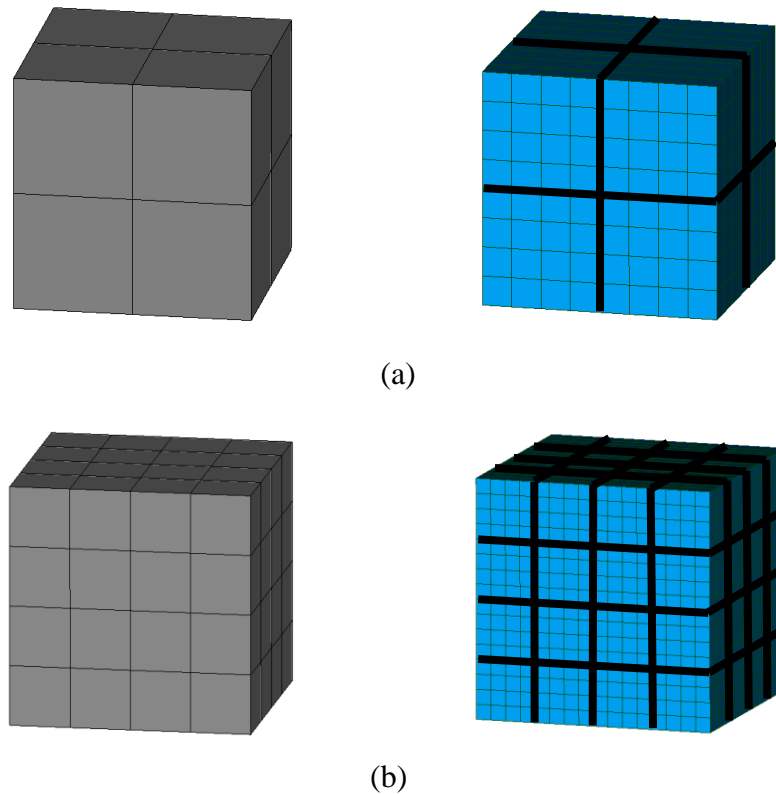


Figure 2.11 Test Cases with respective number of variables (a) 8, (b) 64

As stated above, a MPD is applied to the test case via a part of two opposite faces of the cube. Figure 2.12 shows the nodes on which are imposed the MPD for the 8 variables cube.

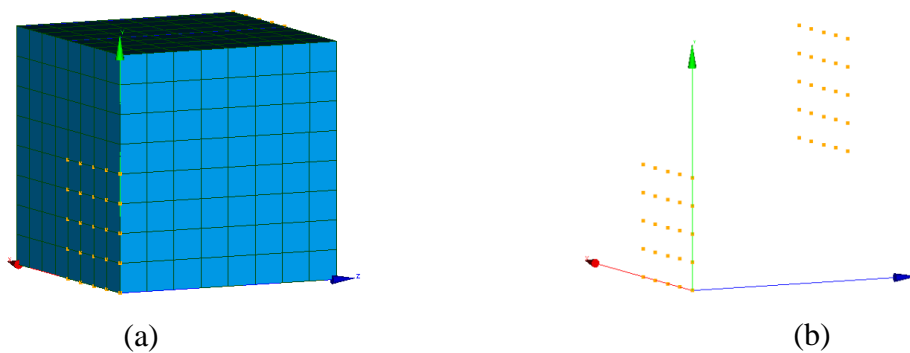


Figure 2.12 Magnetic Potential Difference Applied to Nodes

Generally, there are two ways of considering the optimisation variables for the FE model. The first method is to consider each spatial discretisation, as shown on the left hand side of Figure 2.11, as a variable of the test case; they will be referred to as “zones” henceforward. The second method is to consider each finite hexahedral element of the model as a variable. If the same mesh is used, the optimisation model will be finer and more precise as there will be more variables, but at the expense of having a lengthier calculation time. If this method is chosen, a coarser mesh will have to be used to compensate for the calculation time. This

aspect will be investigated later in this chapter. For the moment, the first method will be used for analysis.

## II.6 Behaviour Analysis of TO using Design of Experiments

In this section, we will focus on the analysis of the behaviour of the model before engaging into any topology optimisation using the cubic test case. This step is vital to have a deeper insight on how the variables of the model behave, and also about the level of complexity of the TO problem itself. The cubic test case with 8 variables was chosen in this section, and will also be concisely presented. All calculations will be done using linear behaviour of the ferromagnetic materials.

In a first phase, investigation will be done using Full Factorial Design (FFD) and Latin Hypercube Square (LHS), introduced earlier in Chapter I. Since FFD and LHS are both DoE, it will help us see a large portion, if not all of the possible combinations of the final structure of the test case. This justifies the small number of variables chosen here, as DoE would be impossible with a larger number of variables such as 64 or more due to the never-ending calculation time.

Secondly, we will use the DoE to analyse the behaviour of the variables individually. This will allow us to see if the problem is multi-modal or mono-modal (i.e. has many local optima or a global optimum). This step will enable us to better formulate and parameterise the optimisation problem in the later sections.

### II.6.1 Cubic\_Case\_8

The model used in this section will be called '*Cubic\_Case\_8*', as it represents a cube with 8 variables, where each variable is represented by a zone of  $1\text{ cm} \times 1\text{ cm} \times 1\text{ cm}$ , as shown in Figure 2.13(a). Therefore, each zone contains 64 hexahedral mesh elements. A MPD of 10 AT is applied to the faces, as shown in Figure 2.12 and Figure 2.13(b), with the higher magnetic potential on the bottom left face, and lower magnetic potential on the upper right face.

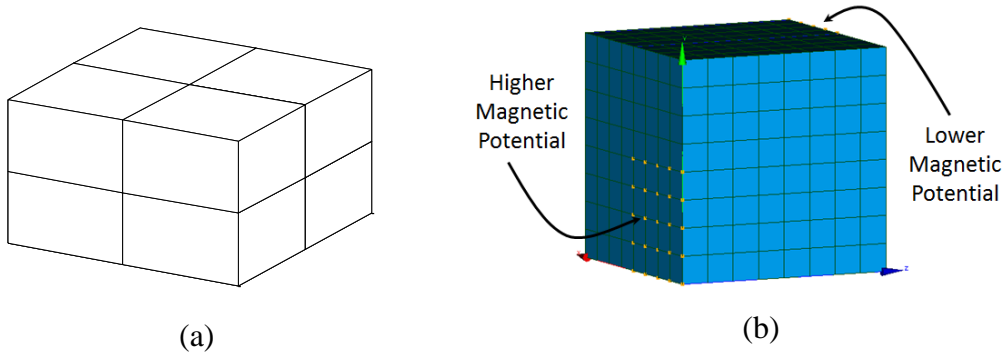


Figure 2.13 Cubic\_Case\_8 (a) showing 8 zones (variables), (b) showing MPD

The energy of this structure is investigated. The ferromagnetic materials allowed to constitute the structure are iron and air. Obviously, if the whole structure is made of iron, the energy will be maximum. But if one wants to limit the amount of iron constituting the structure, and still have a relatively good energy, an optimal structure needs to be found. This is, by the way, the key purpose of TO which produces the optimal structure while respecting the objective functions and constraints.

Hence, in this section, we will investigate the energy of the structure w.r.t the amount of material in it. The amount of material will henceforward be addressed as **Material Quantity** (MQ), which represents the amount of iron in the final structure. In other words, it represents the sum of all the discretisations having taken iron properties over the total number of discretisations; and is therefore a fraction. A representation of the MQ equation is given in (II-6). The purpose of considering MQ in this example is because the energy will always be maximum when the whole cube is made of iron. Hence, we have to somehow constrain the problem to see a variation in the energy of the cube, where the MQ is the most obvious parameter.

In case of optimisation, one would want to maximise the energy in the structure while constraining the MQ. The maximisation of energy will be formulated in the following texts as minimisation of the negative of energy, which is numerically equivalent. The latter is done mostly for optimisation reasons. The general problem formulation for the test case is given in (II-6). Optimisation will be dealt with in other sections of this chapter.

$$\begin{cases} \min (-Energy(\boldsymbol{\rho})) \\ s. t. \quad MQ(\boldsymbol{\rho}) = \frac{\sum_{i=1}^m \rho_i}{m} \leq \beta \end{cases} \quad (\text{II-6})$$

The normalised density for each variable is given by  $\rho_i$ , with a total number of  $m$  variables, and  $\beta$  is the parameter to which the MQ is constrained. Its value will be specified later in this manuscript depending on the optimisation problem to be solved. The relative permeability

of iron is taken as  $\mu r_{iron} = 2000$  here, and a linear behaviour of iron is considered. It is also worth mentioning that the energy is normalised w.r.t the maximum energy (when the structure is made of iron only), and the MQ is normalised w.r.t the total number of variables  $m$ .

## II.6.2 Design of Experiments

As evoked earlier, FFD and LHS can only handle a limited number of variables, justifying the use of the *Cubic\_Case\_8*. The main aim of this section is to expose the difficulty of the TO problem in general by showing the numerous combinations possible for such a simple example. To do so, a FFD is first launched with 2 levels for each variable, i.e. they can either be 0 or 1. For the 8 variables, we will have  $2^8$  possible combinations, and hence 256 possible design topologies. Figure 2.14 plots the MQ v/s the Energy for each of the 256 topology combinations for FFD, represented by red circles. In the present case, the negative of energy is rather shown to put forward the Pareto Front obtained.

A similar DoE is now performed using LHS to see how the test case behaves if the zones are allowed to take continuous values. A set of 1000 sample points are taken, and the number of levels used for each variable is calculated directly by *Sophemis*. The resulting combinations are shown in Figure 2.14, represented by the blue crosses.

It can be seen that the combinations with FFD coincide with those obtained with LHS. This demonstrates the coherence of both DoE. But with FFD, we can also see many points for different MQ at zero energy. This is because these topology combinations might not include the zones where the entry/exit of the MPD is present. This nullifies the energy through it as no magnetic path is created. On the other hand, for same MQ in various cases, the combinations with LHS have greater energy than with FFD. This is because with LHS, the combinations have continuous values, thereby pointing out one of the main difficulties of TO: structures are usually more optimal with intermediate values rather than discrete values, but these structures are physically infeasible. Moreover, if a Pareto Front is drawn as in the figure, it can be seen that most intermediate combinations lie on it.



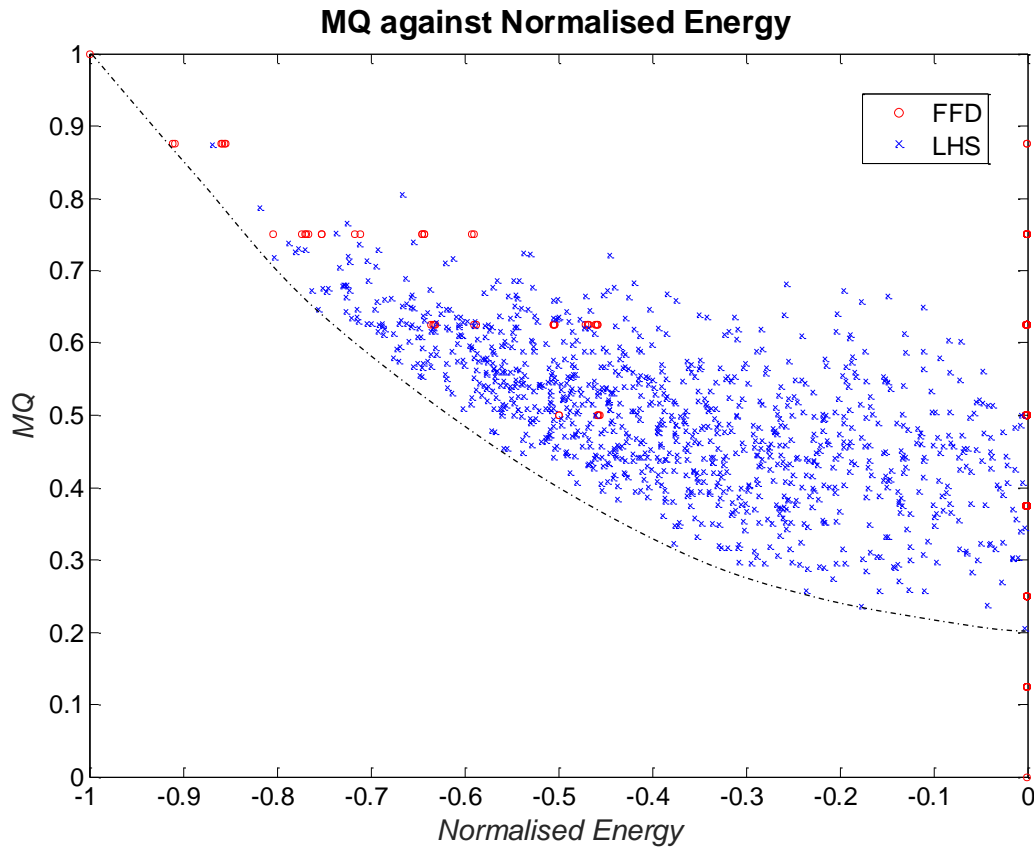


Figure 2.14 MQ v/s Energy for FFD and LHS

The next section will analyse the convexity behaviour of the variables to see why intermediate variables are prominent in TO. The same *Cubic\_Case\_8* will be used, as well as FFD as design of experiment.

### II.6.3 Analysis of the Convexity of the Variables

Following the DoE analysis to get an idea of how numerous the combinations are, the next step is to analyse how the variables behave during an optimisation process. This will help us comprehend the convexity of the variables, i.e. where the maxima and minima are located. To understand why a certain behaviour is preferred rather than another one, let us first have a look at the typical ones. Figure 2.15 shows a concave, convex and desired shape [87].

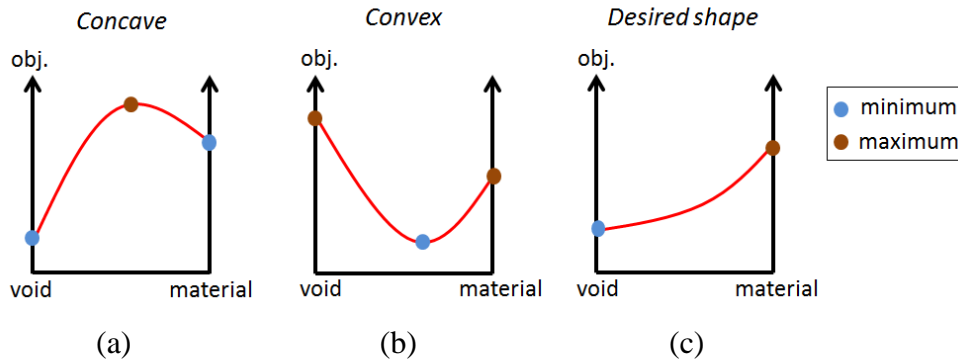


Figure 2.15 (a) Concave, (b) Convex, (c) Desired Shape

Let's assume the objective is to maximise the energy. For the concave shape, we can see that the maximum lies at an intermediate point between void and material. This means that the optimum value will always be with composite materials, and hence the final structure would be physically infeasible.

On the other hand, if we take the convex shape, we can see that there are 2 maxima, depending on the initial point chosen to start the optimisation. In that case, multi-start optimisation must be used to solve the problem.

In either case, there is a difficulty in solving the problem. The ideal desired shape is one with no turning point, i.e. where the gradient is always positive or negative as in Figure 2.15(c). This produces only one maximum, hence easing the task of the optimisation algorithm in finding the optimum.

With these points in mind, we can analyse the behaviour of the variables. The *Cubic\_Case\_8* is used again here for this purpose, but with some slight changes in the definition of the problem. Two cases are analysed. Firstly, we will vary the density of only one zone of the test case between 0 and 1 while all the others are kept constant. The behaviour of the objective function is then analysed. Secondly, the densities of two zones are varied and the new behaviour is analysed.

### II.6.3.1 One zone is varied

A topology combination is chosen here, corresponding to the structure depicted in Figure 2.16. The black regions represent the iron zones, the white represent the air zones, and the grey zone is allowed to vary between 0 and 1. Hence the MQ of the topology will vary between  $4/8$  and  $5/8$ .

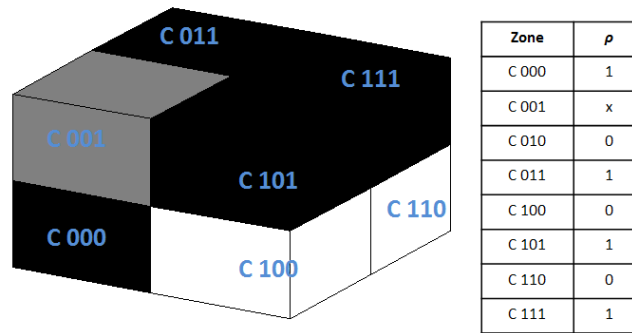


Figure 2.16 Initial Structure with one zone varying

We can afford to use a multilevel FFD in this case, as there is only 1 variable. The number of levels between 0 and 1 is 101. Hence, for each level of variation, the energy of the structure is obtained.

Thereafter, the same experiment is done while varying the density of the other zones, one at a time. Figure 2.17 illustrates the behaviour of the total energy in the structure w.r.t the density for each zone varied one at a time. The energy and density are both normalised.

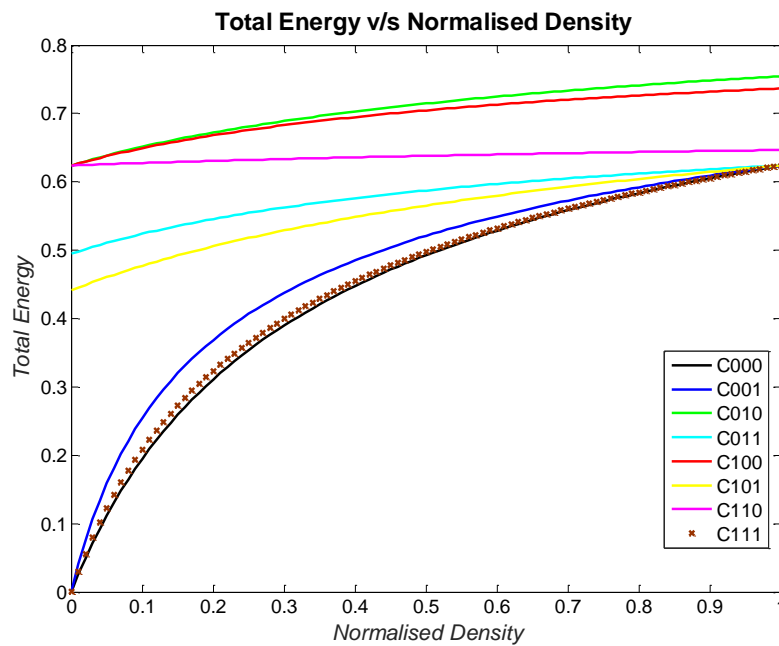


Figure 2.17 Energy v/s Density for each zone varied

It can be seen that the evolutions of the variables have only positive derivatives, hence always having a global maximum, easing the search of the algorithm. The difference in the variation of energy changes greatly according to the zone modified. For example, if a particular zone is crucial in the magnetic path (say C000) and is given a small density value, it affects largely the total energy; and vice-versa. Unfortunately, this problem does not take any constraints into consideration, such as the MQ. Also, in TO all the zones are varied

simultaneously instead of one at a time. This renders the behaviour even more complex. The following example will take into account a constraint, and vary the density of two zones at the same time for a better analysis.

### II.6.3.2 Two zones are varied

The initial structure is as shown in Figure 2.18. The grey zones are varied between 0 and 1, and the rest is kept constant. The variables are named  $\rho_1$  and  $\rho_2$  respectively as indicated in the figure and their sum is constrained to 1, as given in (II-7). A multilevel FFD is also used here, and is achievable because we have only 2 variables. It must also be pointed out that due to the constraint imposed,  $\rho_1$  will be dependent on  $\rho_2$  (or vice-versa).

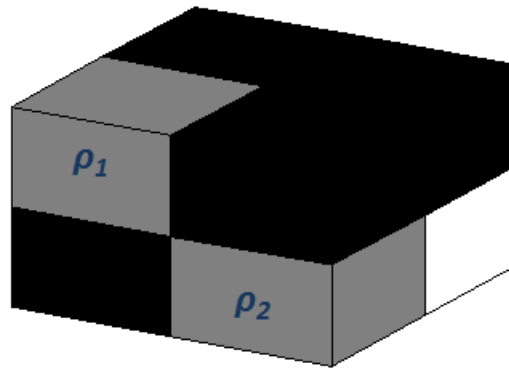


Figure 2.18 Initial Structure for Two Zones Varied

$$\rho_1 + \rho_2 = 1 \quad (\text{II-7})$$

The evolution of the Energy in the structure w.r.t the variation in density of  $\rho_1$  is given in Figure 2.19, for different values of penalisation  $n$  of the Polynomial Mapping. The evolution for  $\rho_2$  is not given here as it is complementary of  $\rho_1$ .

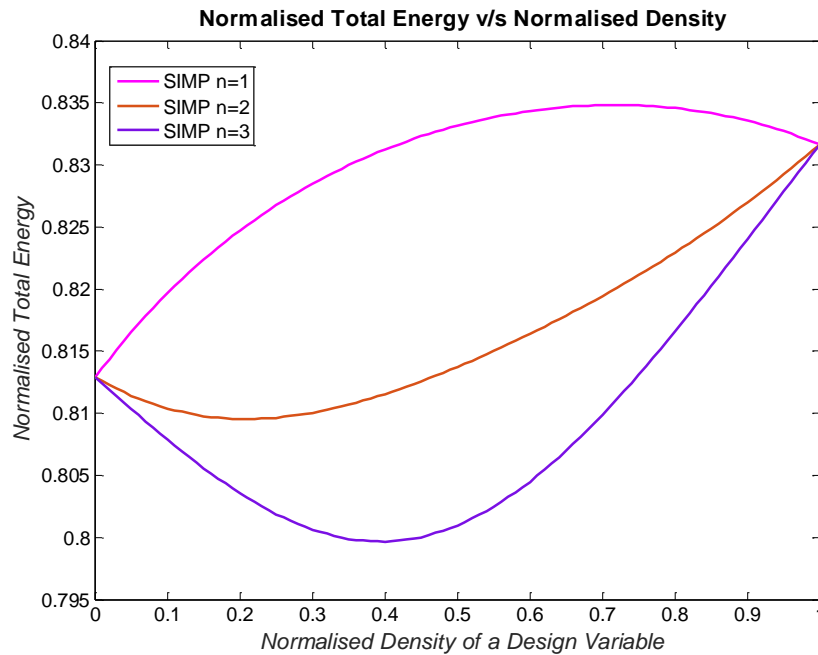


Figure 2.19 Energy v/s Density for Two Zones Varied

We notice that for each penalisation  $n$ , either the concave or the convex shape is obtained as behaviour. For instance, at  $n = 1$  we notice that the maximum point is around  $\rho = 0.7$  due to the concave shape. Hence, the final structure is bound to have intermediate values of density for an optimum energy. As for  $n = 2$  and  $n = 3$ , the behaviour has a convex shape, and therefore the true maxima will depend on the initial values of  $\rho$ . This would necessitate a multi-start optimisation as mentioned earlier, therefore further increasing the calculation time.

It might be tempting to use a continuous value of penalisation coefficient  $n$  between 1 and 2 so that the behaviour follows the desired shape as in Figure 2.15(c). But the main problem remains that this behaviour analysis is for a simplified case of TO with constraints where only two zones are varied; when in fact the true behaviour (when all zones are varied) might just have many more local optima than that. The latter is not exemplified here as a multilevel FFD with 8 variables would be too lengthy.

Some authors, as in [24] and [22], propose to use an equivalent of the Continuation Method [9], which can be described as the sequential continuous increase of the penalisation during the optimisation until the solution converges to an optimum, based on the predefined stopping criteria. The latter can be in terms of no further improvements in the objective function, eradication of all intermediate densities, respect of the constraints, and so on. A simplified block diagram of how the Continuation Method works is given in Figure 2.20.

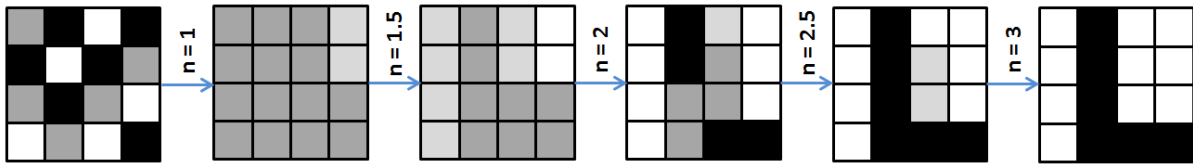


Figure 2.20 Example of Continuation Method

But this method remains cumbersome as the optimisations have to be continuously sequenced, where each optimisation already has a long calculation time. In literature, the use of these types of strategies is mainly to eliminate the intermediate variables, which is one of the greatest challenges of the Density Method, as mentioned in the previous chapter. Nevertheless, it must also be reminded that the optimal solution dwells in composite structures as depicted in Figure 2.14; but due to the infeasibility of the latter, the final solution must imperatively be free of intermediates. For this reason, the next section proposes another method of solving TO problems.

## II.7 Development of a Methodology for TO

In this section, we will focus on the development of a methodology for TO. The test case used to perform the optimisations will be detailed, which is a cubic case of 64 variables. Thereafter, the methodology to be used is explained, and tested on the cubic case. The former will be compared to the other interpolation schemes of the Density Method to allow us to position our work w.r.t the existing ones. Comparison will also be done with the ON/OFF method as it uses the same method of modelling and discretisation of the domain. On the other hand, comparisons with Homogenisation Method and Level-set Method will not be done as the modelling of the structure is different.

### II.7.1 Cubic\_Case\_64

The test case chosen for this section is a cube of 64 variables (zones), where each zone of  $1\text{cm} \times 1\text{cm} \times 1\text{cm}$  is meshed with 64 hexahedral elements, as shown in Figure 2.21(a). The numerical case will henceforward be called *Cubic\_Case\_64*. The green outlined cube on the latter represents one zone, and a MPD of 10 AT is applied to the nodes as shown. The outline of the test case with the 64 variables is pictured in Figure 2.21(b).

The objective is to maximise the energy within the test case made of iron and air, while constraining the MQ. The relative permeability of iron is  $\mu_{iron} = 2000$ , and all the FE calculations will consider a linear behaviour of the ferromagnetic materials for this study. The

energy is also normalised w.r.t the maximum energy of the structure, which occurs when all the variables are iron. Figure 2.22 depicts the magnetic flux density distribution in that case.

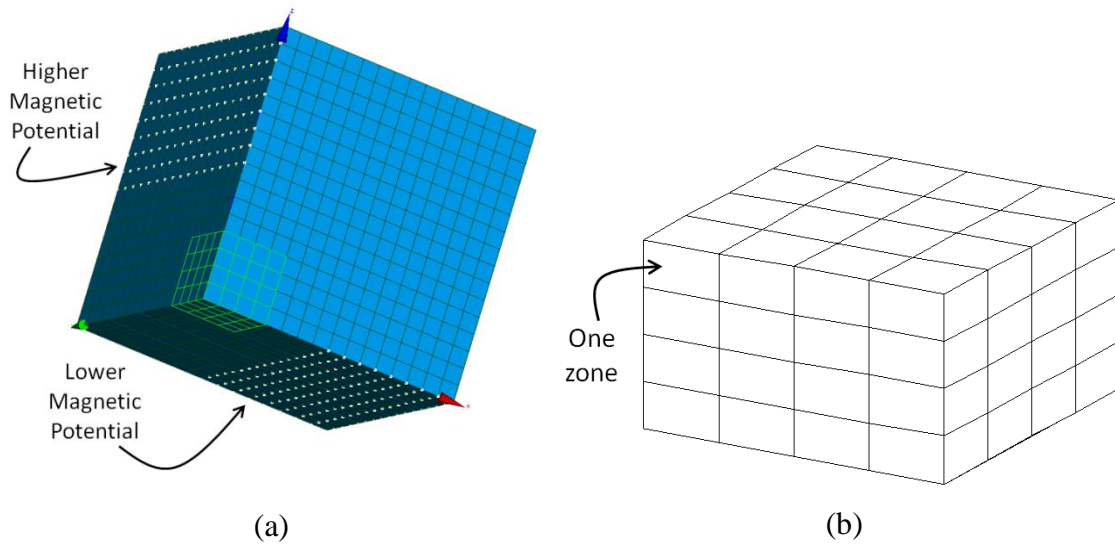


Figure 2.21 Cubic\_Case\_64 (a) FE Model, (b) Model showing only zones

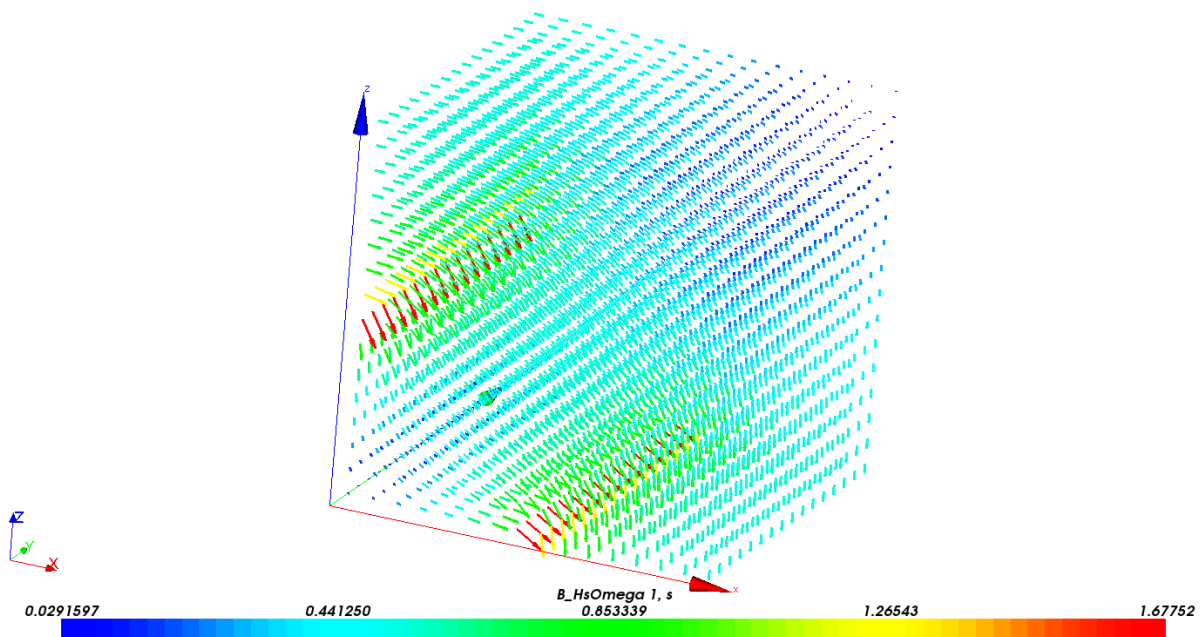


Figure 2.22 Magnetic Flux Density Distribution for Maximum Energy (Linear Case)

The mesh size chosen was based on a study of the energy for different mesh sizes so that a good precision is kept, with an appropriate number of finite elements. This investigation was not done for the *Cubic\_Case\_8* as the case was quite simple, and the number of variables was quite low. As the variables increase in number, more care is required when defining the model and the problem.

## II.7.2 Mesh Size Investigation

In FE analysis, the mesh size used is considered an important factor for a precise solution. Usually for FE calculations, given a fairly accurate FE model, a fine mesh is desired for best calculation approximations. On the other hand, we cannot naturally go for the finest mesh as it would infer a very high calculation time, which is a hindrance to TO. Therefore, to have the best compromise between mesh size and precision, we investigated the energy precision against various mesh sizes for *Cubic\_Case\_64*. Calculations were done using both  $A$  and  $\Omega$  formulations, and the maximum energy is analysed (structure completely made of iron). Figure 2.23 displays the resulting energy for different mesh sizes of the *Cubic\_Case\_64*, with hexahedral mesh elements shown on the x-axis. The mesh size chosen for the test case contains 4096 hexahedra, and from the figure it can be seen that it is adequate as it falls within 0.2 % of the finest mesh investigated for both formulations. Table 2.1 also recapitulates the various information relevant to this investigation, with the different mesh sizes. The true energy in Joules is given in this study.

One can conclude that care must be taken when choosing the right mesh size for the FE model being used, both in  $A$  and  $\Omega$  formulations. Also, refining the mesh size to a great extent does not necessarily yield a much better solution, and it would only add up to the calculation time.

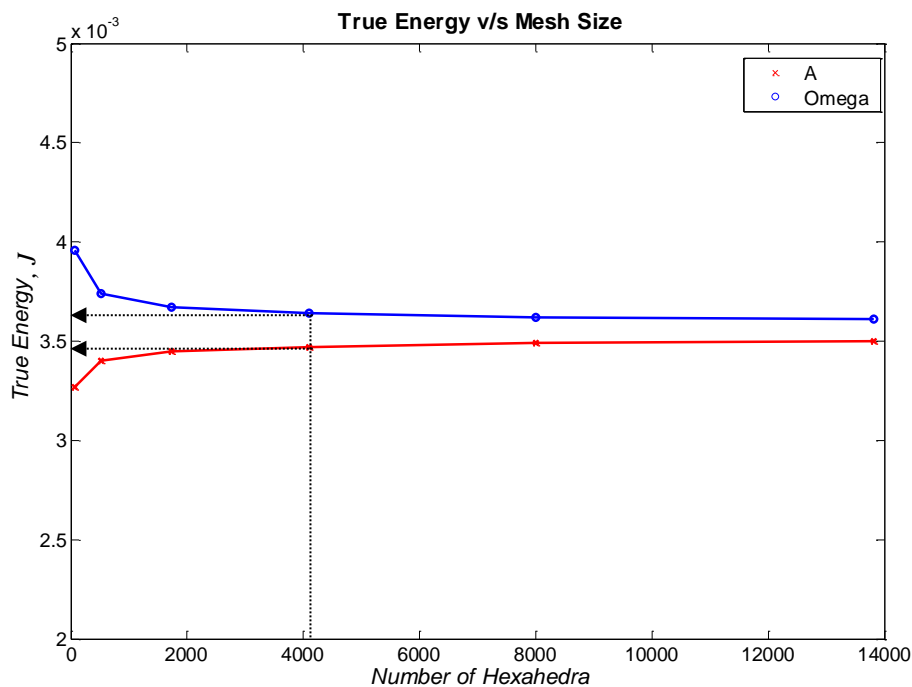
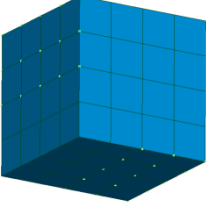
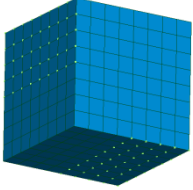
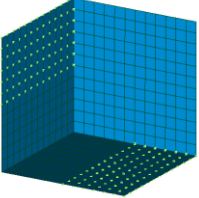
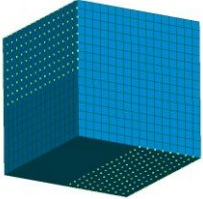
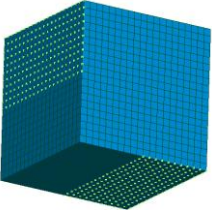
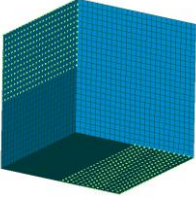


Figure 2.23 True Energy v/s Mesh Size of *Cubic\_Case\_64*



Table 2.1 Recap of Mesh Size Investigation Information

Mesh Size	Number of Hexahedra	Energy ( $A$ formulation) $\times 10^{-3}$	Energy ( $\Omega$ formulation) $\times 10^{-3}$
	64	3.27	3.96
	512	3.40	3.74
	1728	3.45	3.67
	4096	3.47	3.64
	8000	3.49	3.62
	13824	3.50	3.61

### II.7.3 Introduction of the Feasibility Factor (FF) in the Methodology

The *Permeability Mapping* via the Density Method is used in the development of a new TO strategy with the introduction a new function, called the *Feasibility Factor* (FF) as given in (II-8). The FF serves mainly as a means to eliminate all the intermediate variables, while finding an optimal solution. The behaviour of this function w.r.t the density  $\rho_i$  is shown in Figure 2.24. The value of FF is always normalised w.r.t the maximum value it would have if all the variables were composites.

$$FF(\rho) = \frac{\sum_{i=1}^m \rho_i(1 - \rho_i)}{0.25 \times m} \quad (\text{II-8})$$

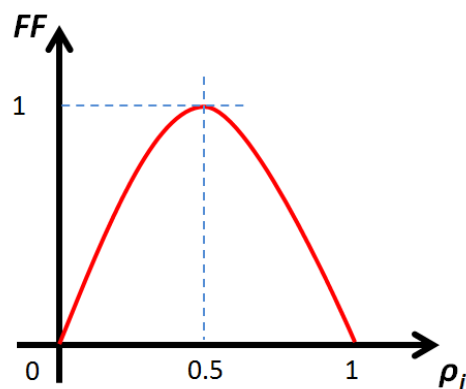


Figure 2.24 Feasibility Factor (FF) w.r.t  $\rho_i$

If the function is equal to zero, from the Figure 2.24 we can see that the density  $\rho_i$  must be either 0 or 1. Otherwise, if  $\rho_i$  is an intermediate value, the FF can rise up to 1. We can deduce that FF must always be minimised. The way the function is used in the methodology is detailed in the next section.

The reason for using Permeability Mapping instead of Polynomial Mapping with the varying  $n$  is because the latter normally has the same goal of penalising the intermediate densities, as for the FF. So, in order not to mix both methods, only one should be kept.

### II.7.4 Using FF in the Optimisation Problem Formulation

With *fmincon SQP* (and most other algorithms), it is possible to use the Feasibility Factor as a constraint, or objective; choosing which one is used is very important for the final solution. This section reviews both choices, and concludes on which should be adopted for the final methodology.

### II.7.4.1 FF as Constraint

The use of FF as a constraint is very tempting, especially when using *fmincon SQP*, known to rigorously respect constraints. The problem is defined as in (II-9). All the outputs, i.e. Energy, MQ and FF are normalised, as in (II-6) and (II-8), and the initial points for the variables are 0.5.

$$\begin{cases} \min(-Energy) \\ s. t. \begin{cases} FF = 0 \\ MQ \leq \beta \end{cases} \end{cases} \quad (\text{II-9})$$

But the problem in this case is that the constraint can too rigidly be taken into account, and produces an invalid solution. The latter consists of randomly allocated density values of 0 and 1 in the structure so that the algorithm respects the constraints first, and then optimises the energy according to that. An example of a biased final solution is obtained when the MQ is constrained to a value of  $\beta = 0.3$ . In this case, all the variables are driven to zero, and the final structure is shown in Figure 2.25, with only air in the latter. Table 2.2 recaps the solution's information and Figure 2.26 shows the evolution of the Energy as objective, the MQ and FF constraints w.r.t the number of evaluations.

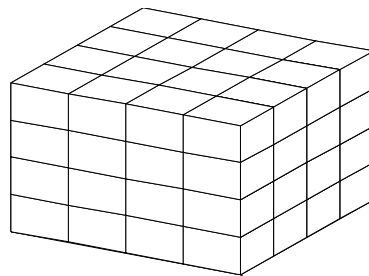
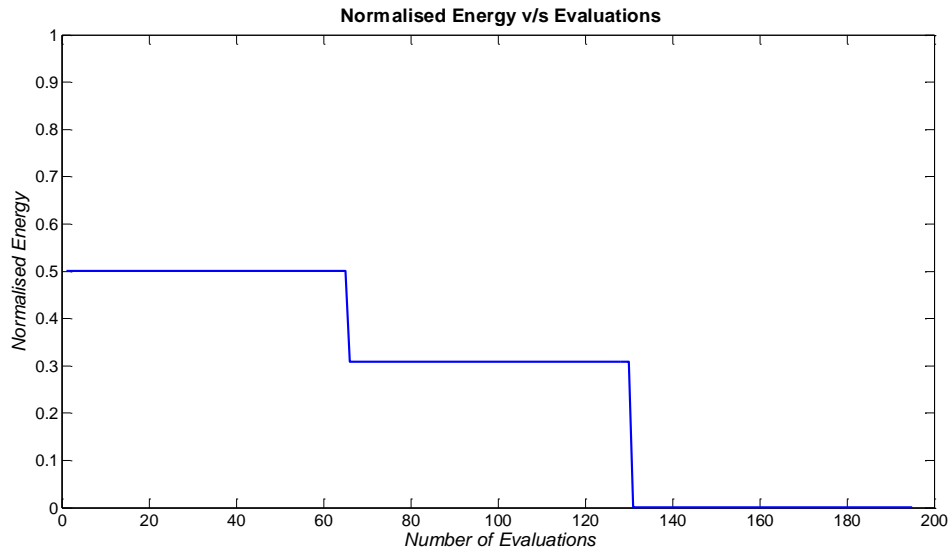


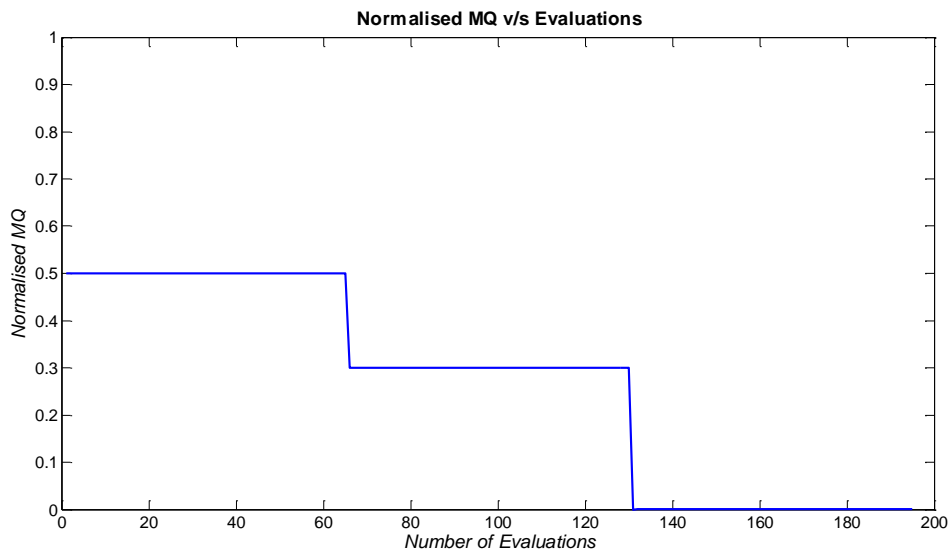
Figure 2.25 Example of biased solution with *FF* as constraint

Table 2.2 Biased Solution's Information

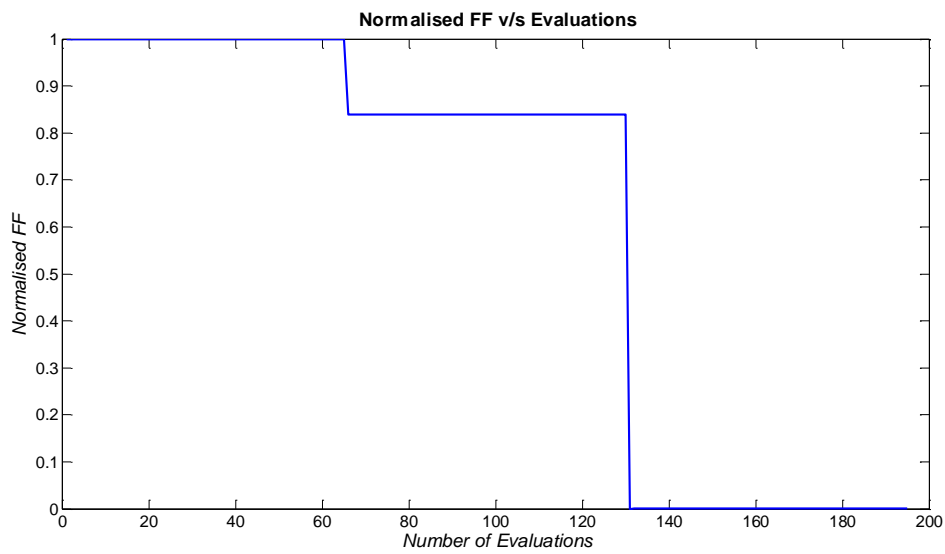
$\beta$	MQ Reached	FF reached	No. of Evaluations	Calc. time (min)
0.3	0	0	195	2.6



(a)



(b)



(c)

Figure 2.26 Evolution of (a) Energy, (b) MQ, (c) FF w.r.t the Number of Evaluations

From the graphs, we can see that a solution is converged to (Figure 2.26 (a)), as there is no further improvement in the final solution. The constraints (Figure 2.26 (b) & (c)) are also respected as we reach  $MQ = 0$  (with  $MQ \leq 0.3$  formulated in the problem) and  $FF = 0$ , which is correct according to the problem definition in (II-9). But the optimum is a local one as the final energy is zero. Only 3 iterations are done (195 evaluations), and a good solution cannot be found with such a premature convergence. This method is hence discarded due to the rigidity of the constraints, and the FF is used in the objective function as a weighted function, as detailed in the next section.

#### II.7.4.2 Proposed Formulation with FF

The FF is used as a weighted function in the objective term, with a weightage coefficient of  $\lambda$ , which can be changed depending on the models used. The weightage coefficient for the main objective, which is the energy here, is given by  $\gamma$ . An example of the problem definition is given in (II-10).

$$\begin{cases} \min\{-\gamma \cdot Energy(\boldsymbol{\rho}) + \lambda \cdot FF(\boldsymbol{\rho})\} \\ \text{s. t. } MQ \leq \beta \end{cases} \quad \text{(II-10)}$$

Defining the problem with the weightages allows a smoother convergence to the optimal solution as the impact of the FF function is more progressive. The weightage coefficients are chosen from a series of optimisations of the same model with different values of  $\lambda$ . It must be noted that the  $\lambda$  found is usually valid for one model, irrespective of the definition of the problem. Furthermore, the value of  $\gamma$  is usually taken as 1 for this study. An example of the behaviour of the objective w.r.t the value of  $\lambda$  and FF for *Cubic\_Case\_64* is given in Figure 2.27. The value of  $\lambda$  is varied, and the resulting values for FF and Normalised Energy are shown.

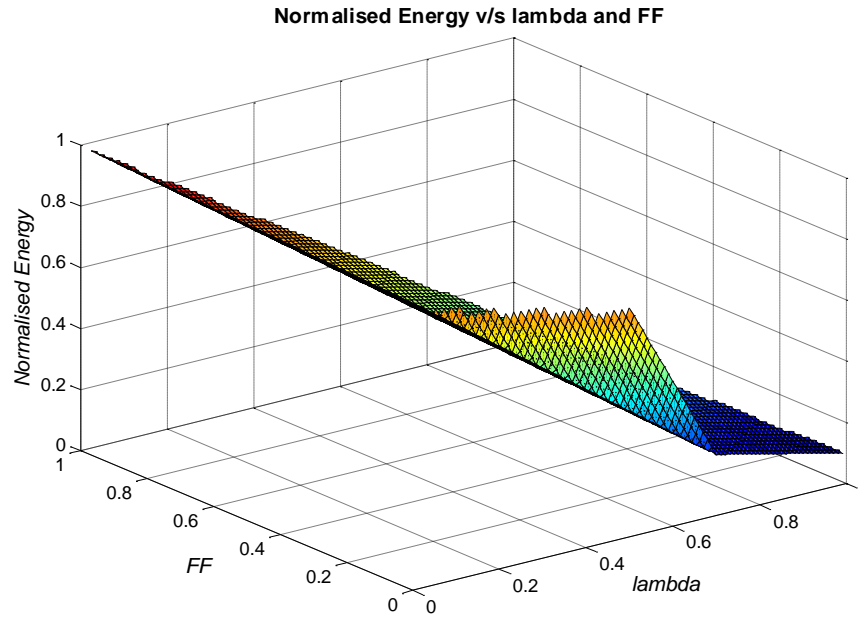
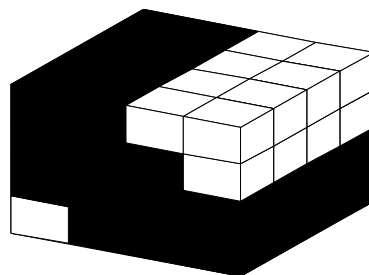


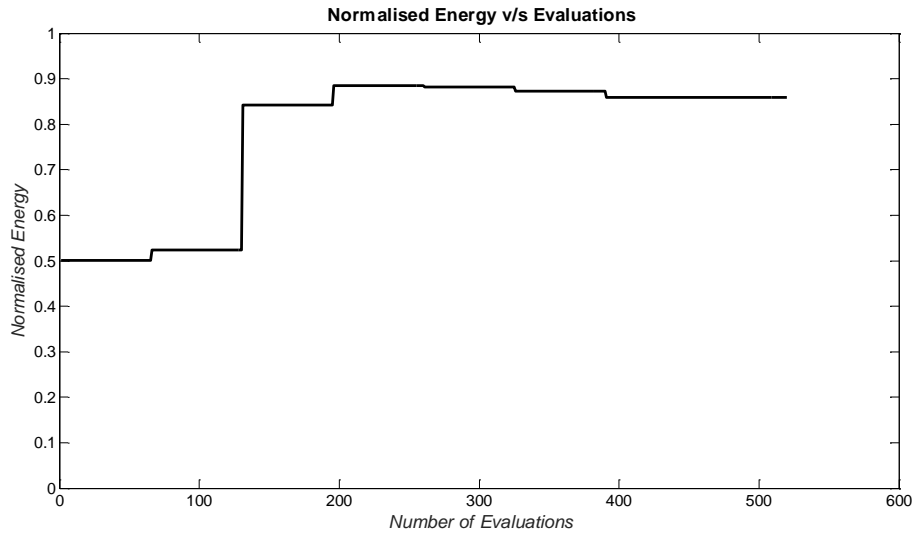
Figure 2.27 Energy and FF against Weightage Coefficient  $\lambda$

The normalised energy of the whole structure is investigated when the value of  $\lambda$  is varied. At each value, the FF obtained is different, representing the amount of composites in the final structure. In the present case, we are looking for a value of  $\lambda$  which yields maximum energy with zero composites. This, according to Figure 2.27, occurs around  $\lambda = 0.5$ . Hence this value is retained for the test in the following sections.

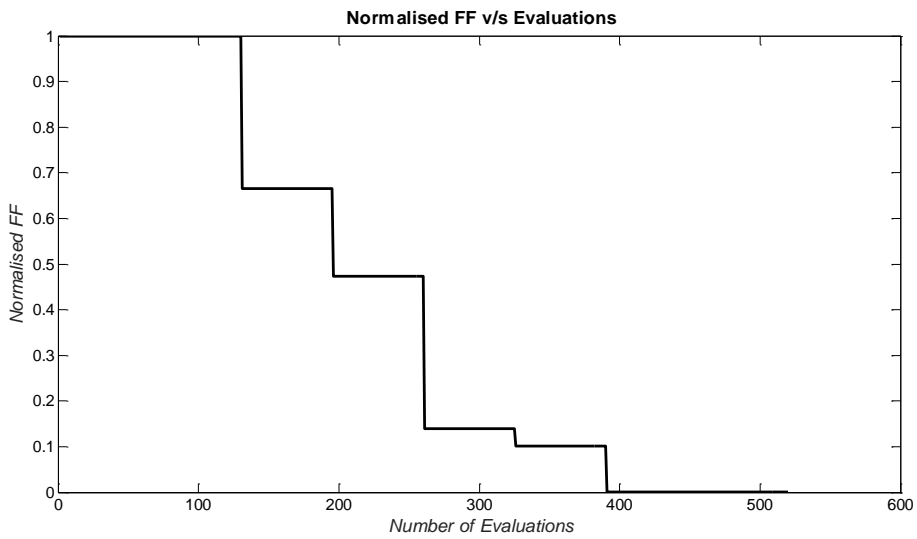
To prove the convergence to a good solution with this formulation, the problem is defined as in (II-10), with  $\beta = 0.75$ . The initial points for the variables are 0.5. The results are given in Figure 2.28. The final structure is given in Figure 2.28(a). Figure 2.28(b), (c) and (d) depict the convergence of energy, FF and MQ respectively, while (e) gives the convergence for the sum of objectives. To be consistent with the positive axes and the real aspect, the positive normalised energy is shown.



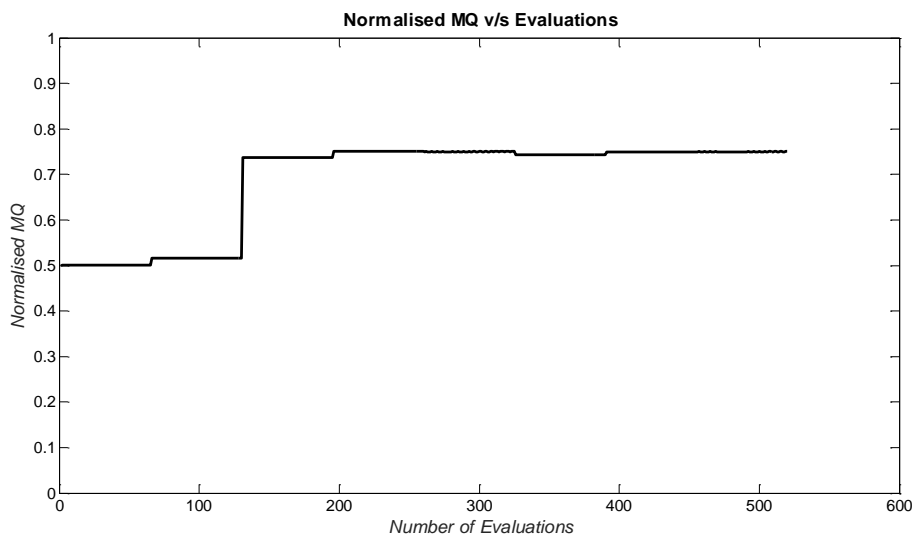
(a)



(b)



(c)



(d)

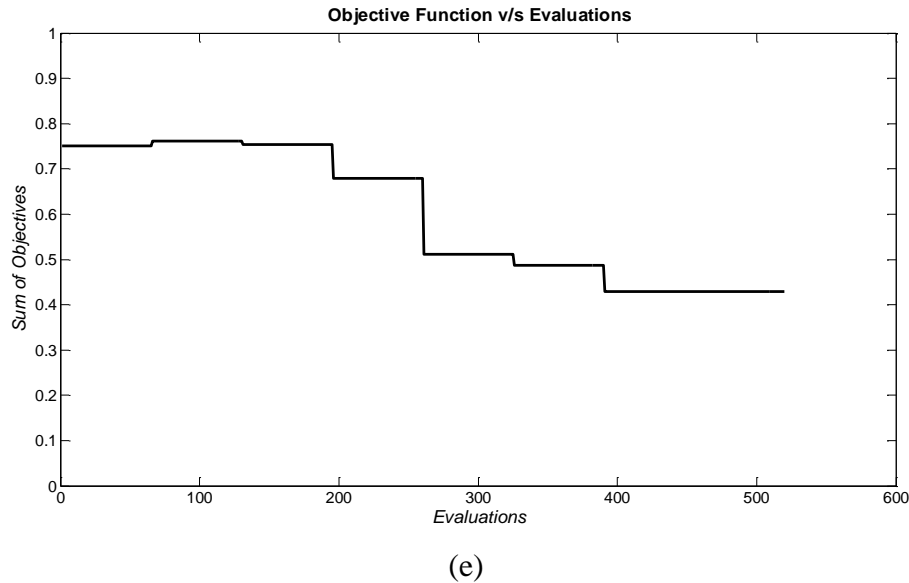


Figure 2.28 (a) Final Topology, (b) Energy, (c) FF, (d) MQ, (e) Sum of Objectives

In Figure 2.28(b), we see that the energy converges to an optimum solution in around 200 evaluations, but the algorithm keeps iterating. This is because the FF (Figure 2.28(c)) has not converged yet to its minimum, and does so for the rest of the evaluations. This shows that a higher importance is given to the Energy objective, and then the FF is considered once a high energy value is reached. In this way, the algorithm does not get trapped in a local optimum, as for the previous case (section II.7.4.1). As for the MQ in (d), we can see that it rises at quite an early stage to reach the upper limit of the constraint, and oscillate around this value throughout. In Figure 2.28(e), we can see that the overall objective keeps converging to the solution throughout the evaluations until the optimum is reached.

## II.7.5 Comparison of Proposed Methodology with other Density Mappings

To evaluate the strengths and weaknesses of the proposed methodology, it is important to compare it to other existing Interpolation Schemes commonly used in literature for the Density Method. The most common ones, namely the Polynomial, Reluctivity, Geometric and Rational (RAMP) Mappings as presented in Chapter I (Section I.4.2.1) will be used for the comparison. The main aspects of the optimisation will be considered, i.e. the final topology, the convergence of the objective, the respect of the constraints, the number of evaluations, the calculation time, and the amount of intermediate densities in the final structure. The *Cubic\_Case\_64* is used, and the problem is formulated as in (II-11), with  $\lambda = 0.5$  and  $\gamma = 1$ . The amount of iron allowed in the final structure is 75% of the optimisation domain, with  $\beta = 0.75$ . The initial points for the variables in each case are 0.5.

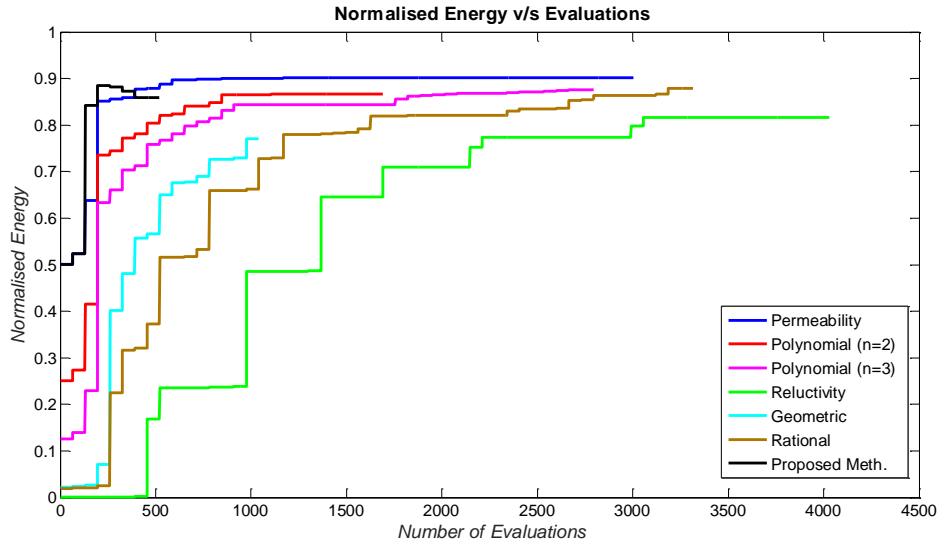


$$\begin{cases} \min \left\{ (-Energy(\boldsymbol{\rho})) + \frac{1}{2} \cdot FF(\boldsymbol{\rho}) \right\} \\ \text{s. t. } MQ \leq 0.75 \end{cases} \quad (\text{II-11})$$

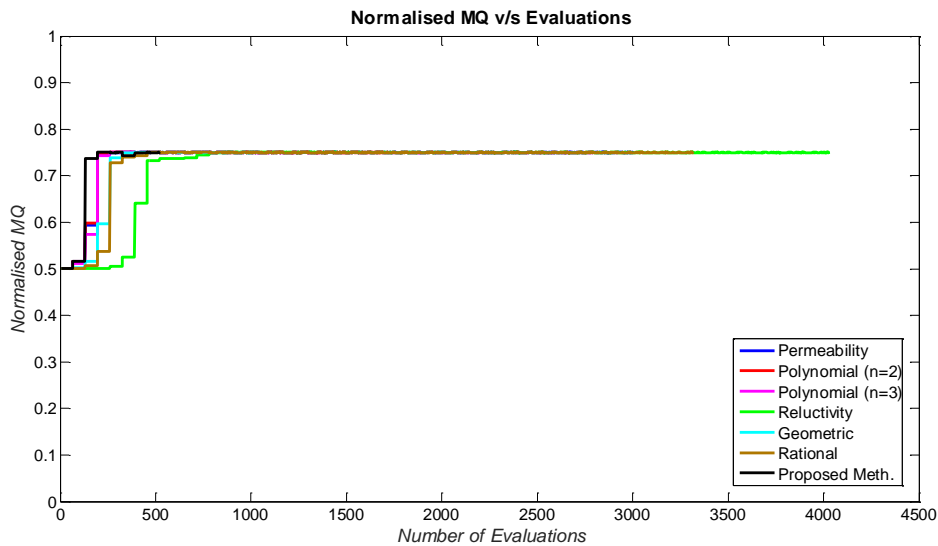
Figure 2.29 shows the evolution of the positive energy, MQ and FF w.r.t the number of evaluations. For the Polynomial Mapping, different values of  $n$  are also tested.

From a first glance at Figure 2.29(a), we notice that the energy has converged normally for all mappings, except the Geometric one. The choice of the latter can therefore be eliminated at this stage. On the other hand, the quality of the resulting topologies is not the same for all the other mappings. Before discussing this point, we should also make sure that the constraint, which is the MQ here, is well respected.

From Figure 2.29(b), we can see that all the mappings, despite the overlapping of one another, have not crossed the constraint limit. Therefore, this aspect will not be prominent in choosing the best mapping.



(a)



(b)

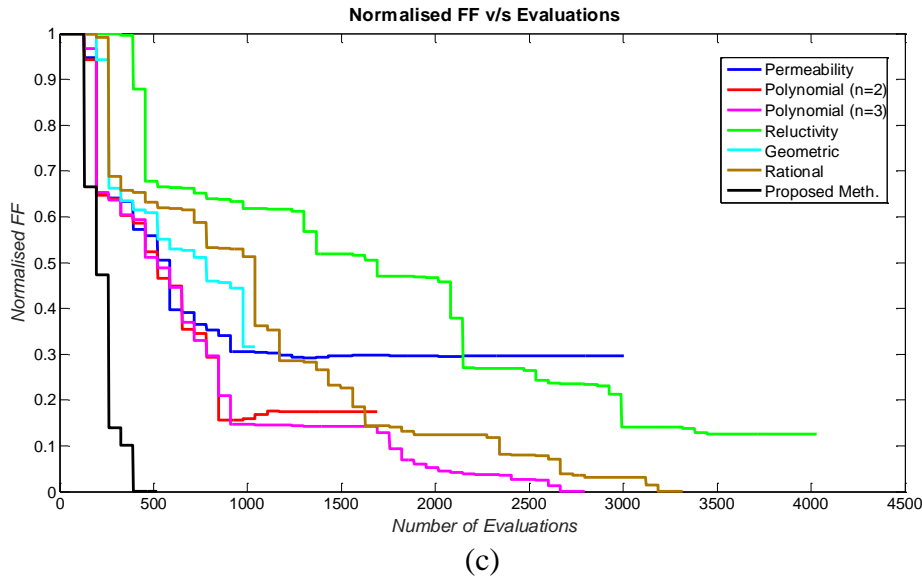


Figure 2.29 Comparison of Density Methods with Proposed Methodology for (a) Energy, (b) MQ, (c) FF, against the Number of Evaluations

From Figure 2.29(c), we notice that only the Polynomial with  $n = 3$ , Rational and Proposed Methodology reach a composite-free structure. As for the Reluctivity, Polynomial with  $n = 2$  and Permeability mappings, despite a good convergence of the energy, the final structures obtained are physically infeasible as they still have a high amount of composites. This comforts the logic of Figure 2.14 which shows that structures made of composites are most of the time more performant than composite-free ones for the same MQ, which can be in reality translated as weight of the structure. But their manufacturability remains a main obstacle, therefore discarding their use. From the 3 mappings without composites, and having converged, the Rational and Polynomial ( $n = 3$ ) respectively have around 5 and 6 times more evaluations than the proposed methodology. Therefore, the latter would also allow us to gain the same amount of calculation time, which is generally a big hindrance in TO.

Table 2.3 summarises the results for each of the above mentioned methods, and the proposed method. The variation of the outputs for different mappings can more precisely be observed here. For example, the percentage discrepancy between the energy found by the Rational Mapping (which yields the highest value) and the proposed method is merely 2%, while the number of evaluations for the former is around 6 times. Moreover, there is no big difference for both topologies, and there are only 4 variables placed differently. As for the Permeability Mapping, Polynomial Mapping ( $n = 2$ ), Reluctivity Mapping and Geometric Mapping, the intermediate materials generated are clearly visible in the topologies. Polynomial Mapping ( $n = 3$ ) works out for this example here, but not for larger number of variables ( $> 100$ ). Subsequently, one can conclude that the best compromise in terms of

optimum results and time would be the proposed method. It is hence retained for further tests and application to more real cases in the next chapter. Figure 2.30 also depicts the magnetic flux density distribution with the proposed methodology to verify the magnetic viability of the model.

Following the comparison of the proposed methodology with other interpolation schemes, we can also compare the former with a discrete TO method such as the ON/OFF method. The next section presents some results with the latter.

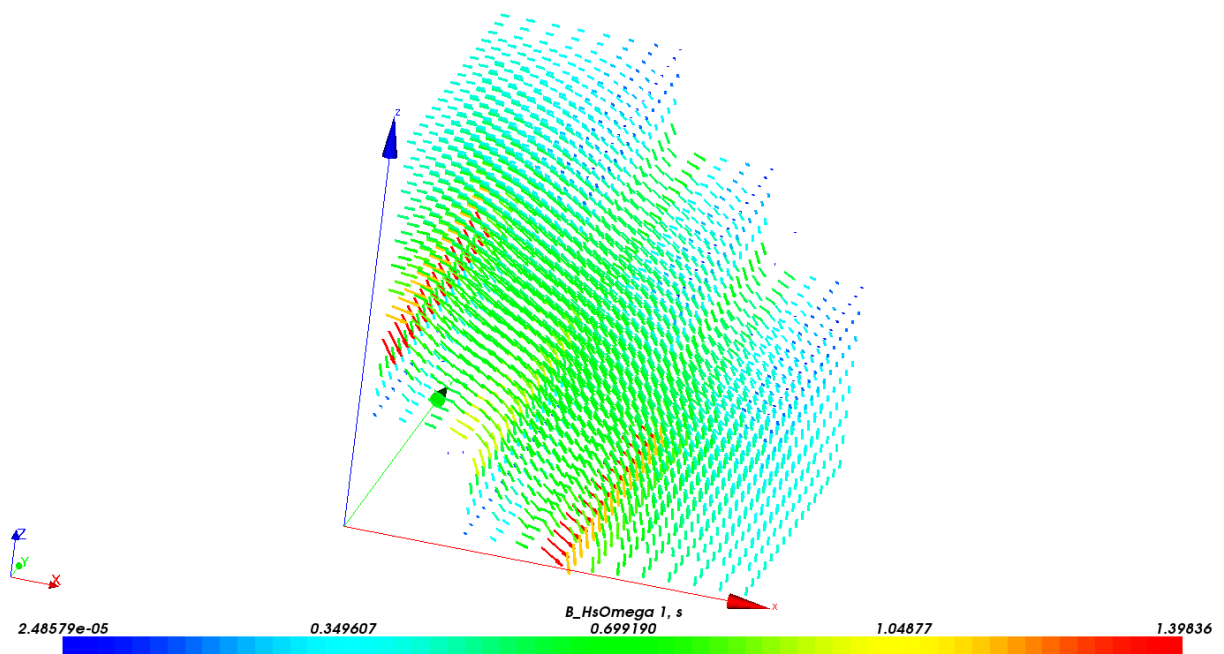
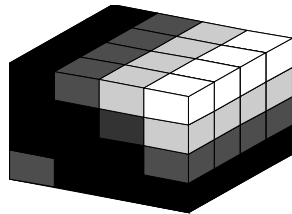
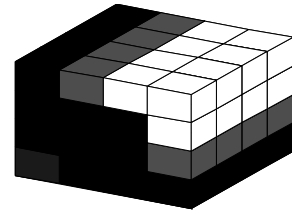
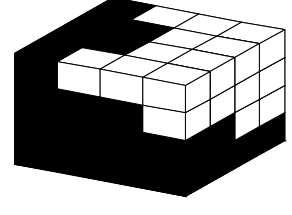
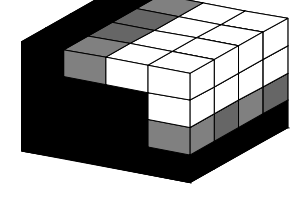
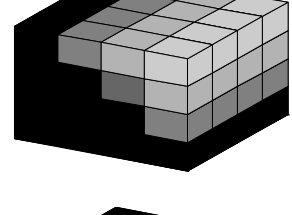
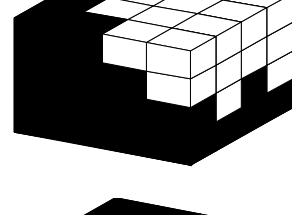
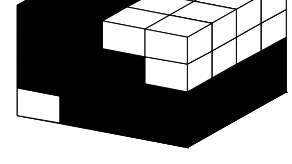


Figure 2.30 Magnetic Flux Density Distribution for Topology with Proposed Methodology (Linear Case)

Table 2.3 Comparison of Different Mappings with Proposed Method

Method	Energy	FF	No. of evaluations	Calculation time (min)	Topology
Permeability	0.9010	0.2960	3004	39	
Polynomial (n=2)	0.8663	0.1752	1692	22	
Polynomial (n=3)	0.8755	0	2795	37	
Reluctivity	0.8159	0.1251	4030	64	
Geometric	0.7709	0.3167	1040	17	
Rational	0.8788	0	3315	43	
Proposed Meth.	0.8593	0	520	7	

## II.7.6 Comparison with ON/OFF Method

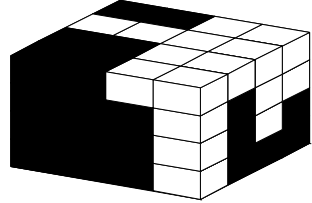
The ON/OFF method is a discrete TO method where the variables can only take the values of 0 or 1, as seen in Chapter I. Therefore, global evolutionary algorithms can be used instead of local gradient-based methods. In this thesis work, the ON/OFF Method is easily compared with the Density Method as the modelling and discretisation of the optimisation domain is the same, as evoked earlier. The main advantage over the Density Method is the yielding of composite-free structures, but the weakness is the checkerboards that could be present in the topologies, as seen in Chapter I.

In this comparison, we choose the Genetic Algorithm (GA). The purpose is to explore other possibilities of TO with our numerical tools, and conclude as to why this possibility is discarded for future optimisation of other devices in the subsequent chapters.

The problem is formulated as in (II-12) and the results are given in Table 2.4. The *Population Size* is 200, the number of *Generations* is 50, the *Crossover Fraction* is 0.8, and the *Penalty Factor* is 100.

$$\begin{cases} \min(-Energy(\boldsymbol{\rho})) \\ \text{s. t. } MQ \leq 0.75 \end{cases} \quad \text{(II-12)}$$

Table 2.4 Results with GA

Method	Energy	MQ	FF	No. of evaluations	Calculation time (min)	Topology
GA	0.8788	0.75	0	4011	56	

It can be seen that the normalised energy is similar to what was obtained with the Rational Mapping, but with a different topology. This leads us to say that TO models have many local optima, thus making it a rather tedious type of optimisation. On the other hand, the number of evaluations is much higher than all the mappings of Table 2.3, and so is the calculation time. Thus, if GA were to be used for much larger number of variables, it would probably give optimal results, but at the expense of a much higher number of evaluations. Nevertheless, the FF function does not need to be used in the optimisation process as discrete GA, by nature, yields only 0s and 1s for the variables.

Despite all the attractive strengths regarding this method, the proposed methodology is still retained as it represents the best compromise amongst the different methods presented.

### II.7.7 Repeatability of Solutions

Repeatability of the results with the methodology used is very important to evaluate the stability of the solution. One can have a converging algorithm, but the latter has to be effective when launched multiple times. A way to investigate this aspect would be to carry out the same optimisation with various initial points. Figure 2.31 graphically depicts the results obtained with various initial points while using the proposed method. The initial points in the previous cases were 0.5 for each variable. For this particular study, initial points from 0 to 1 with an interval of 0.1 are utilised. All the variables are given same initial value.

From Figure 2.31, it can be seen that the optimum is found for initial points from 0.5 to 1, but the solution is erroneous for the other values. Also, for the values of 0.6 to 1, the number of evaluations are greater than for initial point at 0.5 despite reaching the same results. Therefore, it can be concluded that care must always be taken when defining the initial points for a particular optimisation, as solutions can be local or worse, invalid.

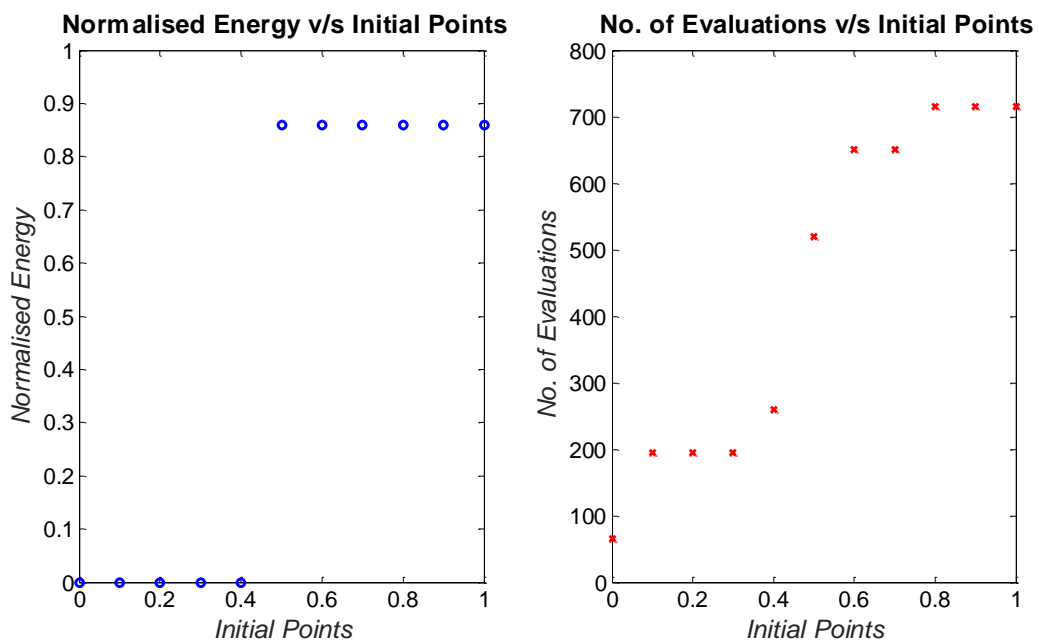


Figure 2.31 Effect of Initial Points on Optimal Results

### II.7.8 Using Mesh Elements as Variables

Until now in this thesis work, the variables used were zones of the FE model, as illustrated in Section II.4. But in this section, we will consider a different way of defining the variables in the FE model: here each finite hexahedral element is used as a variable, instead of a group

as hexahedra, as previously. The model is as given in Figure 2.32, with the geometry in (a) and FE model in (b). The number of variables and hexahedra are both 64, and hence a coarser mesh size than *Cubic\_Case\_64*. A MPD of 10 AT is applied to the nodes shown, which are less numerous than for *Cubic\_Case\_64*. The optimisation problem is defined as in (II-11), with the proposed method, and calculations are done in  $\Omega$  formulation.

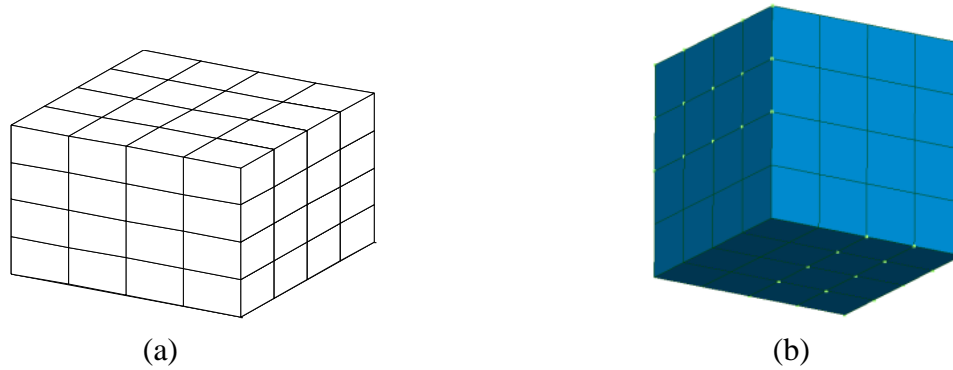


Figure 2.32 Model using Mesh Element as Variable with (a) Geometry, (b) FE Model

The resulting topology is the same as that presented in Table 2.3 for the proposed methodology, but the true maximum energy is obviously higher, if we refer to Figure 2.23. The calculation time is 3 minutes in contrast with the 7 minutes when using zones. This is because the number of unknowns in the FE problem is smaller, and therefore this speeds up the time of resolution of the FE model, which is 0.35 s instead of the 0.8 s earlier. We can also note that despite the use of a coarser mesh size, the final topology is still correct. This is because the objective function is normalised, and the mesh does not change throughout the TO. This would mainly apply for TO in electromagnetic cases where no movements of the devices are required. This technique will be used in the next chapter for one of the presented applications.

## II.8 Nonlinear Behaviour of the Ferromagnetic Materials

As presented in the earlier sections of this chapter, the consideration of the nonlinear behaviour of the ferromagnetic materials used is important in electromagnetism to account for saturation. For the calculations until now, only the linear behaviour of the ferromagnetic materials has been considered.

Hence, in this section, the nonlinear behaviour will be considered while using the proposed methodology in Section II.7.4.2. The problem is formulated as in (II-11). The energy is also normalised here w.r.t the maximum energy in a complete iron structure. The magnetic flux

density distribution is given in Figure 2.33, where the peak value of B is smaller than for the linear case, as expected.

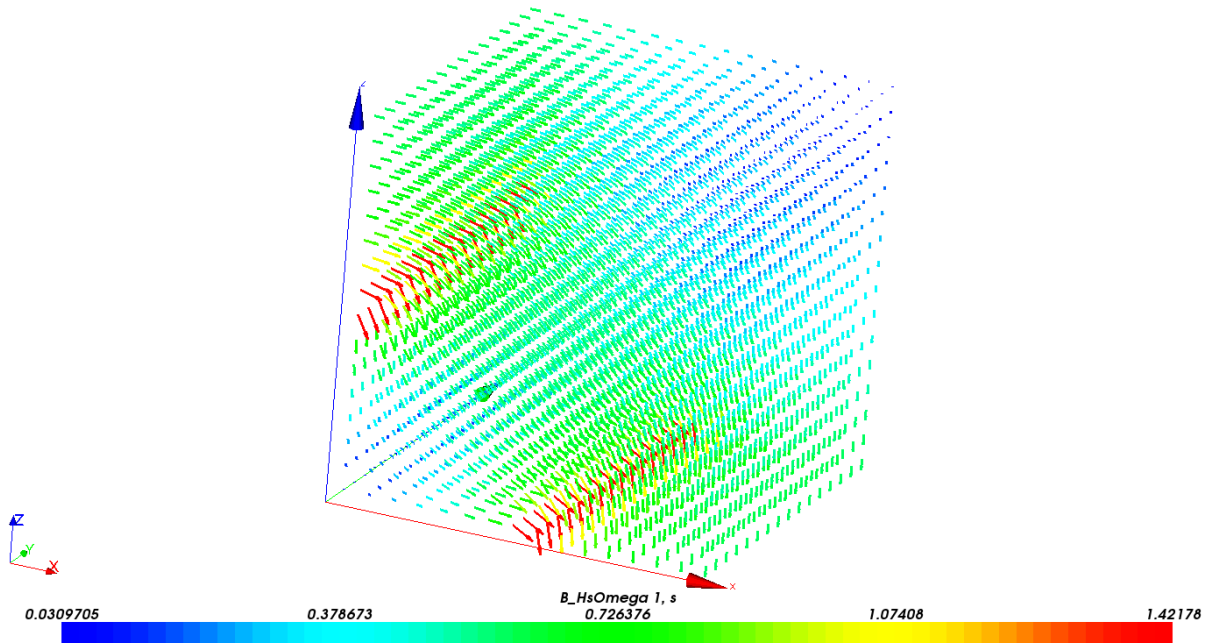


Figure 2.33 Magnetic Flux Density Distribution with Maximum Energy (Nonlinear Case)

The results are shown in Table 2.5. It can be seen that the final topology is the same as for the linear case, despite a smaller number of evaluations. But the calculation time is around 3 times higher than for the linear case, owing to the iterative process for considering the nonlinear behaviour of the materials. The magnetic flux density distribution is depicted in Figure 2.34. The normalised energy is higher than for the linear case, but comparison is not very judicious here as the maximum values are not the same.

Table 2.5 Results with Nonlinear Behaviour of Materials

Method	Energy	MQ	FF	No. of Evaluations	Calculation Time (min)	Topology
Proposed Meth.	0.8937	0.75	0	456	22	



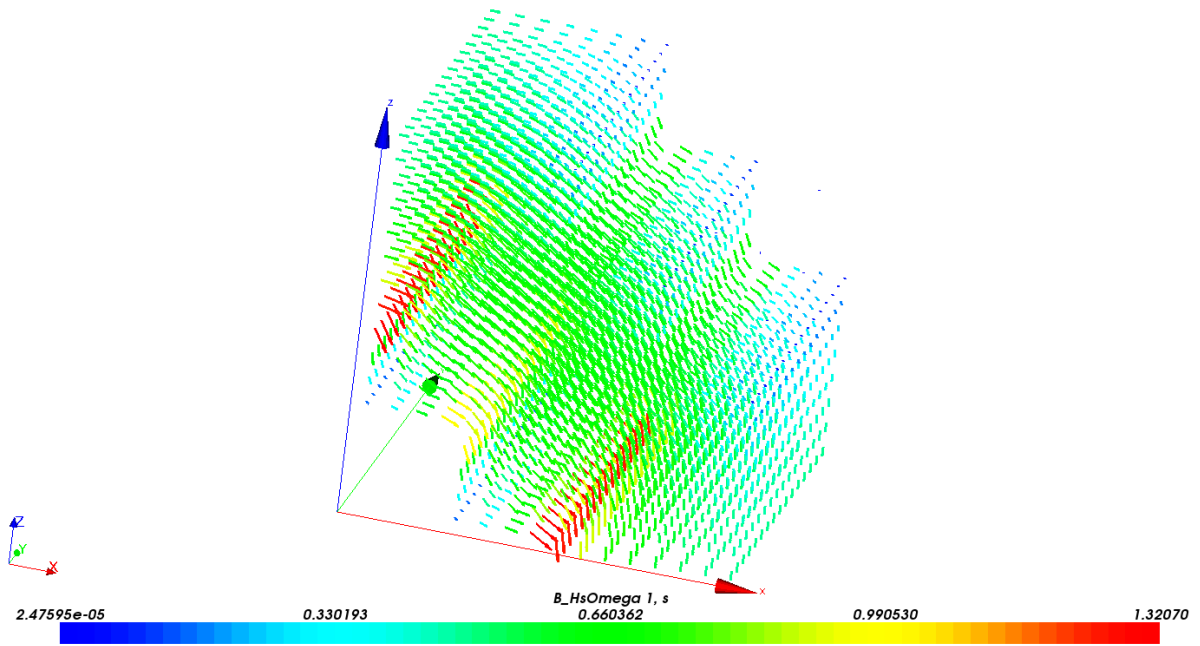


Figure 2.34 Magnetic Flux Density Distribution of Optimal Topology (Nonlinear Case)

This example is pretty efficient when investigating the behaviour of various methods for TO, but less revealing when it comes to the analysis of the behaviour while considering nonlinearity. Another optimisation problem will be studied in the next section to demonstrate the importance of considering the nonlinear behaviour of the materials.

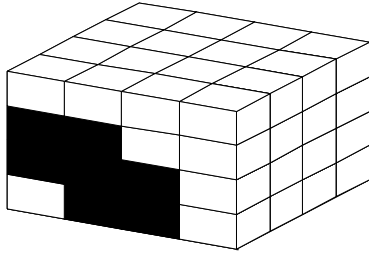
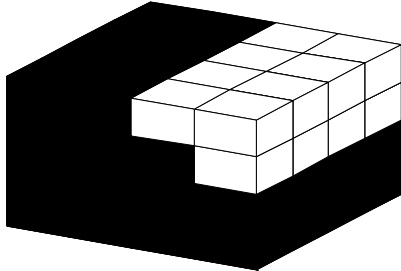
## II.9 Other Problem Formulations

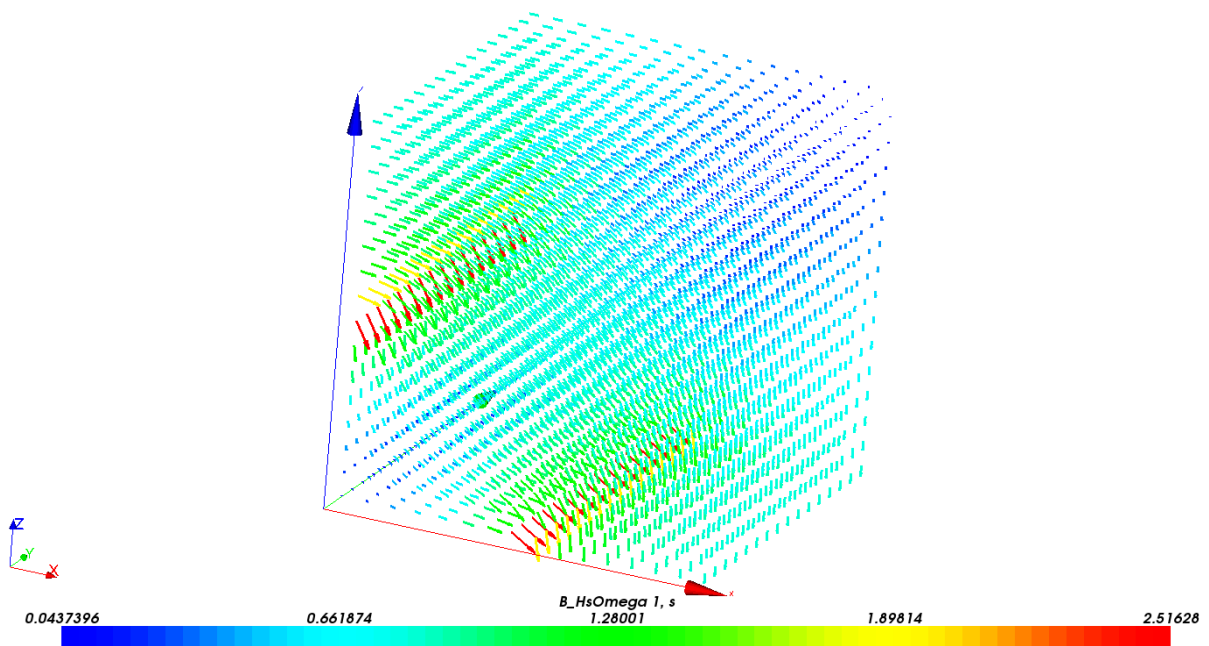
Owing to the academic nature of the test cases used in this chapter, the study of various objective functions is rather limited. In this section, we will investigate the optimisation of the energy per unit volume, as formulated in (II-13). This provides a higher degree of freedom as no constraints are imposed on the optimisation. The coefficients  $\gamma = 1$  and  $\lambda = 0.5$ , as for the previous case.

$$\min \left\{ - \left( \frac{Energy(\boldsymbol{\rho})}{Volume(\boldsymbol{\rho})} \right) + \frac{1}{2} FF(\boldsymbol{\rho}) \right\} \quad (\text{II-13})$$

For the same MPD as in the previous cases, i.e.  $MPD = 10AT$ , and using *Cubic\_Case\_64*, the results are given in Table 2.6. The same topologies are obtained using linear and nonlinear behaviour of the materials. Therefore, the MPD is increased to 15 AT for the saturation effect to be more visible. Figure 2.35 shows the magnetic flux density distribution for the linear and nonlinear cases when the structure is made of iron only so that the level of saturation in this case is emphasised.

Table 2.6 Comparison of Linear and Nonlinear Cases

Case	$\frac{Energy}{Volume}$	FF	No. of Evaluations	Calculation Time (min)	Topology
Linear, <i>MPD=10</i> <i>AT</i>	1.4756	0	2080	35	
Nonlinear, <i>MPD=10</i> <i>AT</i>	1.5032	0	4615	182	
Linear, <i>MPD=15</i> <i>AT</i>	1.4756	0	2080	35	
Nonlinear, <i>MPD=15</i> <i>AT</i>	1.1599	0	520	39	



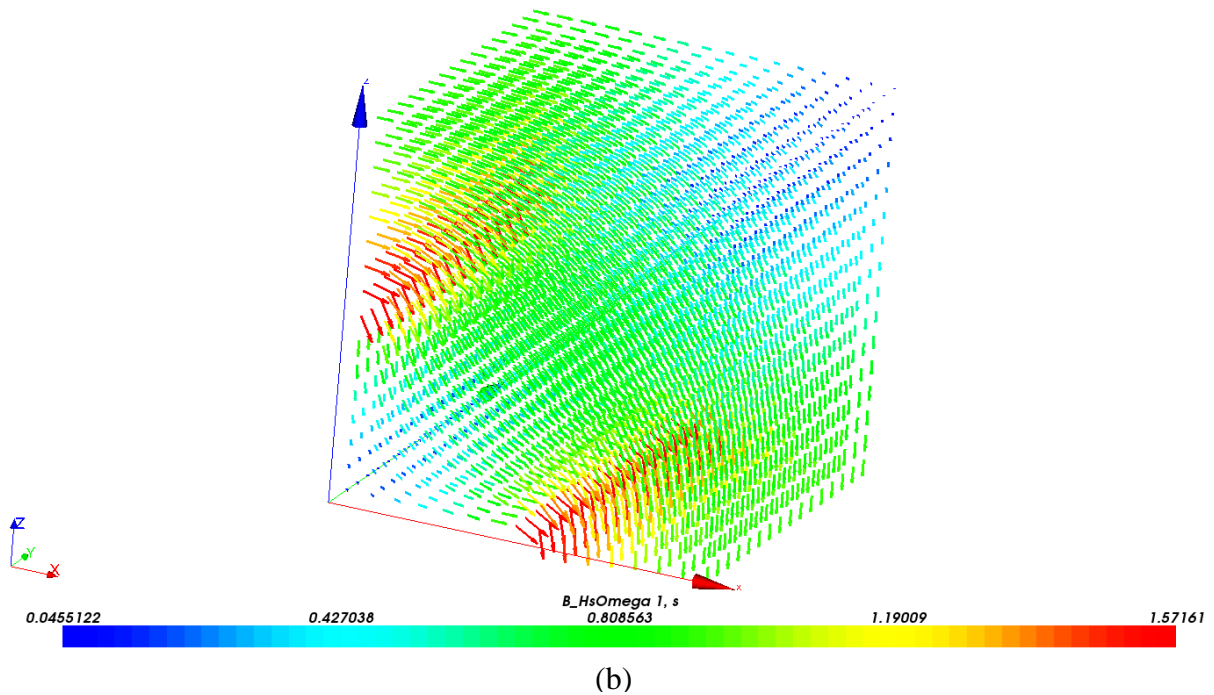


Figure 2.35 Magnetic Flux Distribution with MPD=15 AT (a) Linear Case, (b) Nonlinear Case

From Table 2.6, it can be seen that the topology for the linear case is the same, whereas in the nonlinear case, more iron is added during the optimisation process to compensate for the saturation in the ferromagnetic materials. From these findings, we can deduce that if a structure is not saturated, one does not need to consider nonlinearity for TO, as results will be the similar. But if saturation is high, then nonlinearity definitely affects TO and must be considered. The effect of saturation on the topologies found during optimisation will be further detailed in the coming chapters.

## II.10 Summary and Contributions

This chapter has encompassed different aspects of TO, from the types of tools used to the various difficulties of TO, through the comparison of different methods. This step was essential in grasping the behaviour of the TO process as a whole, as it is a rather complex one due to the various factors involved.

Some of the factors covered in this chapter were the analysis of the FE model used, i.e. its precision, fineness of the mesh, definition of the variables in the optimisation domain (whether to use zones or mesh elements), consideration of linear or nonlinear behaviour of materials, and so on. Other optimisation difficulties have also been investigated, such as the multi-modality of the problem, the optimisation algorithms to be used, and so forth.

Having an upper hand on all of the above aspects has provided us with sufficient information to devise our methodology and understand its behaviour so that it can be applied to more complex electromagnetic devices. The proposed methodology, based on the Density Method, has been compared with other Interpolation Schemes found in literature, and we have seen that it is the best compromise for TO. It has mainly allowed us to converge to an optimum solution, with a reduced number of evaluations, and elimination of intermediate materials.

Based on what has been explored here, i.e. the tools, the proposed methodology and the behaviour of the models, the following chapters will apply the same reasoning to optimise the topology of more real electromagnetic examples to validate our methodology. Chapter III will study a 3D electromagnet, and will explore the different possible optimised topologies. Since the latter example is closer to a real electromagnetic device, the potential of analysing the effect of saturation will also be interesting.

# Chapter III – Application of TO Methodology to a 3D Electromagnet

---

### III.1 Introduction

After exploring the different angles of the TO in electromagnetism in the previous chapter, we now have enough information and know-how to apply the proposed methodology to a more tangible electromagnetic example. In this chapter, we have chosen the topology of a 3D electromagnet to be optimised. The motivation behind this choice is because it illustrates the basic laws of electromagnetism in a rather lucid manner, and the assessment of the results is rather logical from an engineering point of view.

The main aim of this chapter is to assess and validate the proposed TO methodology on a moderately challenging electromagnetic case, and analyse the behaviour of the former when optimising different features of the model, and when saturation of the materials is taken into account. Since we are using a fully functional FE code (*code\_Carmel*), we benefit from all its features and therefore can more precisely analyse meaningful characteristics such as magnetic force, instead of energy. On the other hand, focus will not be on the use of very fine mesh for visually perfect structures, but we will nevertheless choose models with correct mesh viability to avoid unnecessarily long calculation times.

In a first place, a concise literature review of the works using electromagnets as numerical applications will be decomposed, irrespective of the TO methods used, with the objective being to see the different results obtained. Subsequently, the FE model used in this thesis is detailed, with a short mesh analysis to verify its correctness. Afterwards, the results for different optimisation problem formulations are discussed, as well as for linear and nonlinear behaviours of the ferromagnetic materials used. The various strengths and limitations of the methodology and model will be elaborated, and how they can be perfected for future optimisations.

### III.2 State of the Art

Works on TO using Homogenisation Method in electromagnetism have not been very expansive as they were mostly mechanical/structural oriented. One of the sparse works includes [15] where the authors optimise the shape of an H-shaped magnet to maximise the Mean Magnetic Compliance (MMC) while constraining the volume to a certain percentage. Figure 3.1(a) shows the H-shaped magnet to be optimised, and (b) shows the optimisation domain. The materials used in the TO are iron and air, and the optimisation is carried out on a 2D cross-section. Figure 3.1(c) and (d) illustrate the optimisation results for the volume constrained to 60% and 70% respectively. The overall tendency of the shape is approached,

but a finer final structure could be interesting. The optimisations were done using linear ferromagnetic materials.

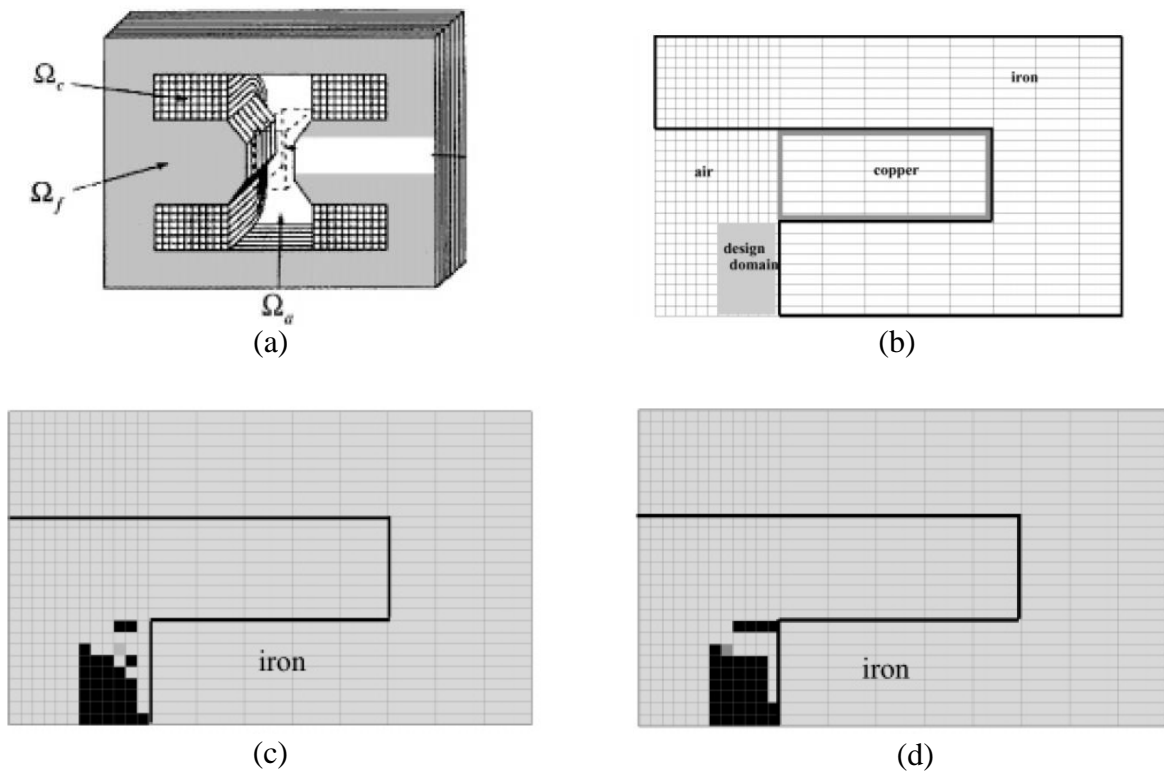
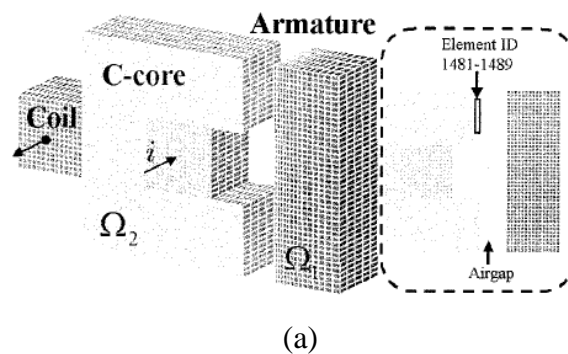


Figure 3.1 (a) H-Shaped Electromagnet, (b) Design Domain, Optimised Shape with Volume Constraint (c) 60%, (d) 70% [15]

In [18], the topology of a C-core actuator is optimised so as to maximise the magnetic force. The density method is used, with the polynomial mapping, and all the calculations are performed using a 2D model. Comparison of the optimised topologies when the materials are considered to behave linearly and nonlinearly is also done. Figure 3.2 shows the initial core actuator and the results obtained for the linear and nonlinear cases.



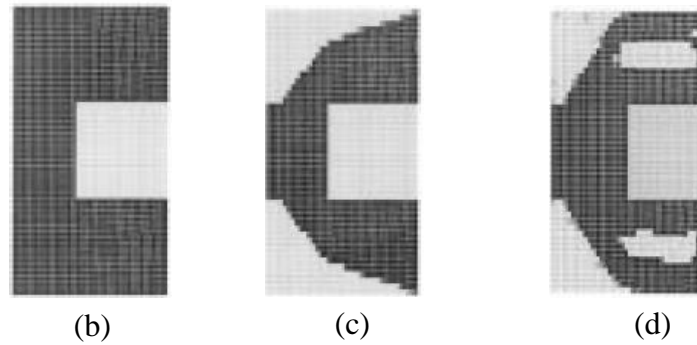


Figure 3.2 (a) C-core Actuator, (b) Initial Domain, Results in (c) Linear Case, (d) Nonlinear Case [18]

Some other examples of TO of electromagnets with the Density Method include the works presented in [29], [30] and [31], where different algorithms or methodologies are tested. Furthermore, TO of a C-core electromagnet is performed using the Level-set Method (LSM) in [64], where the results are compared with the Density Method. Figure 3.3 shows the initial 2D design domain and the results obtained with both SIMP and LSM. The magnetic energy stored in the system is maximised, and the nonlinearity of the materials is not considered.

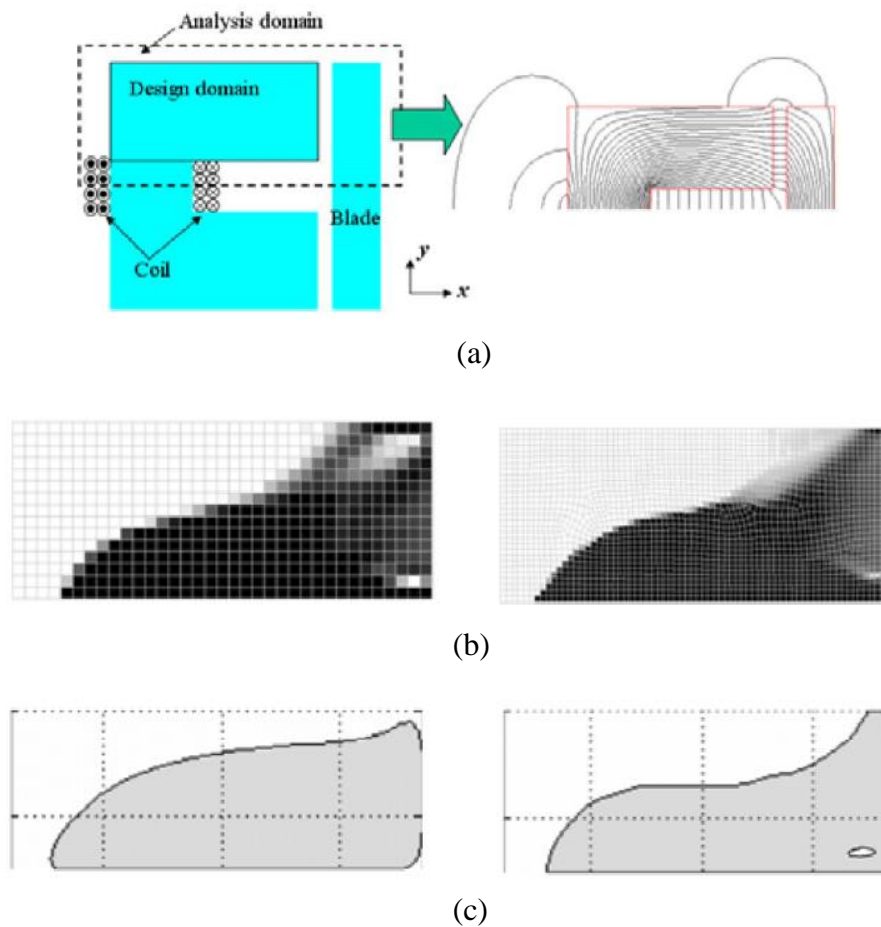


Figure 3.3(a) Initial Domain, (b) Density Method Results (coarse mesh on left & fine on right), (c) LSM (conventional on left and advanced on right) [64]



As for the ON/OFF Method, among the ones inventoried is the TO of the yoke of a magnetic actuator in [42] where the authors use GA as algorithm, and the nonlinearity of the materials is disregarded. Figure 3.4 shows the design domain and the results obtained with this method. The objective is to maximise the magnetic force by Maxwell Stress Tensor.

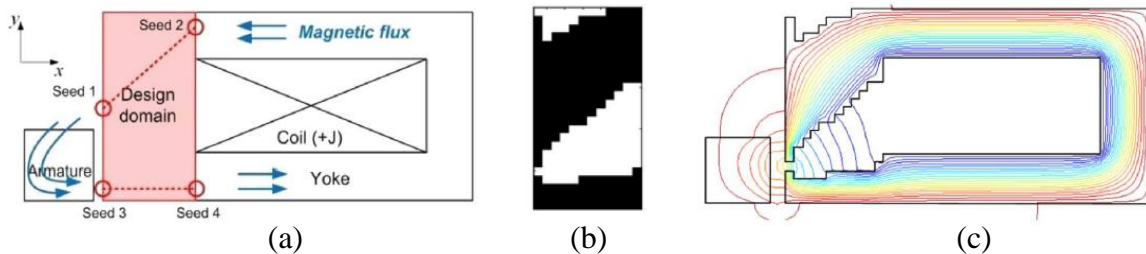


Figure 3.4 TO of Magnetic Yoke (a) Design Domain, (b) Optimised Yoke shape, (c) Magnetic Flux Line Plot

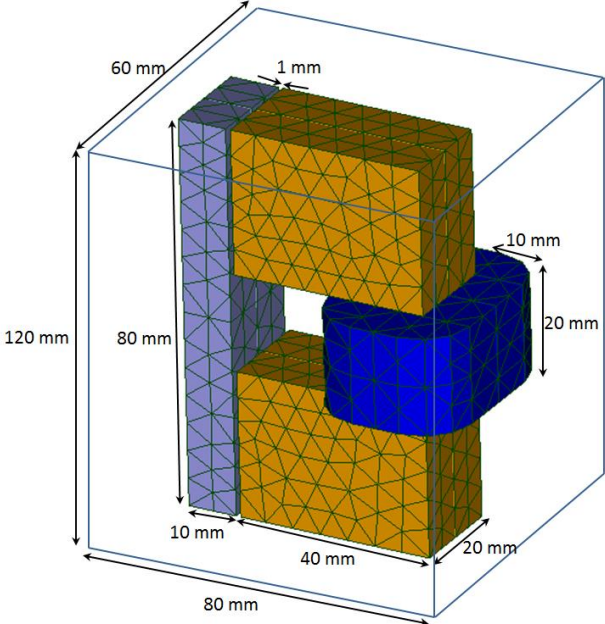
We have seen that various authors utilise different shapes of the electromagnet for TO such as H-shaped, C-shaped or magnetic yoke. Our choice will be oriented towards the C-core electromagnet, with the iron core to be optimised. The FE model will be in 3D, and the materials allowed are iron and air. Since literature suggests the use of magnetic energy and magnetic force as objective function, we will investigate both, and discuss the pertinence of each. We will also compare the results obtained when considering linear and nonlinear behaviour of the materials, which is not very often seen in TO of electromagnetic devices despite being a turning point.

### III.3 3D FE Electromagnet Model

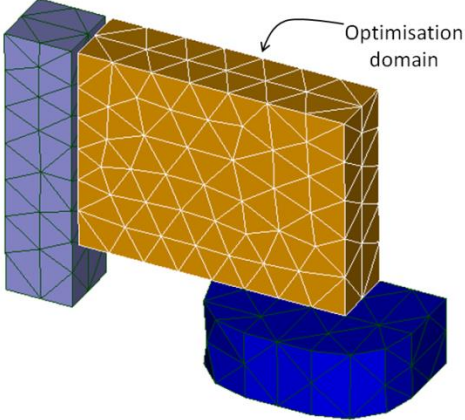
Before conducting any optimisation, we will first detail the FE model of the 3D electromagnet, with the respective dimensions, symmetries and boundary conditions. The accuracy of the mesh chosen is verified through a mesh size investigation before validating the model to be optimised. Subsequently, the core of the electromagnet is optimised with different objectives, and the results are discussed. The more pertinent one is retained, and the results for the case of linear and nonlinear materials are compared. The convergence of the results is also examined to make sure the latter are of appropriate relevance.

#### III.3.1 Finite Element Model

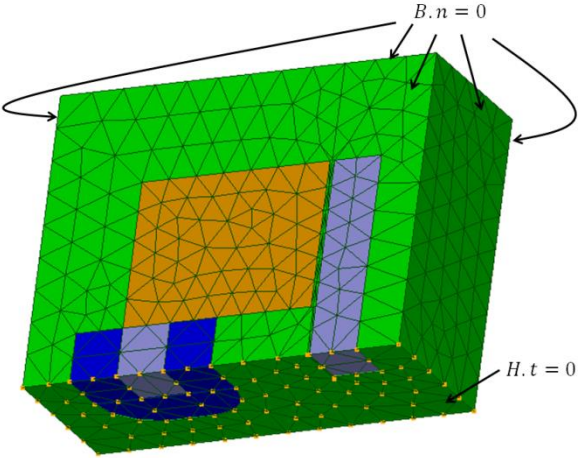
The electromagnet model is made up of current-carrying copper coils surrounding an iron core, which in turn attracts an iron bar; all enclosed by an air box to allow flux leakage and hence mimic real conditions as much as possible. Figure 3.5(a) shows the electromagnet system as a whole, with the respective dimensions.



(a)



(b)



(c)

Figure 3.5 (a) Electromagnet Model with Dimensions, (b) Quarter Model, (c) Model with Boundary Conditions

Due to the symmetry of the system along the XY and XZ planes, only one quarter of the electromagnet can be modelled, as given in Figure 3.5(b). This offers a gain in calculation time, and also allows a finer discretisation of the model, with more variables in the optimisation domain. The domain to be optimised is represented by the cuboid-shaped brown region in Figure 3.5(b), which makes up the iron core. To be close to a ‘physical’ model, it is also necessary to properly define the boundary conditions, as illustrated in Figure 3.5(c). The lower side of the FE model is allocated the boundary condition of  $H.t = 0$  to allow normal flow of flux through the surface, while all the other sides of the model are allocated the boundary condition of  $B.n = 0$  to favour tangential flow of the flux w.r.t the surface.

### *Optimisation Variables*

In Chapter II, we have chosen the variables of the cubic test case to be zones of the FE model. But we have also seen in Section II.7.8 of the same chapter that it is possible to use the finite elements of the model to represent the variables. The results obtained with the latter were similar to those with zones of the model. Therefore, in the case of the electromagnet, we will use the finite elements of the mesh to represent the variables. Since the model is meshed using tetrahedra, the variables will take the form of tetrahedra, and will correspond to those lying in the brown area of Figure 3.5(b). Care must be taken to normalise the values of the objective functions so that the solutions are not biased. This flexibility of our TO tool could be interesting for refining optimisation models without intervention on the geometry itself. Also, the use of tetrahedral elements was chosen for an easy generation of the mesh. But any other type of mesh is possible such as hexahedral elements.

Nonetheless, the size of the mesh has to be verified for consistency, despite the normalisation of the objectives of the optimisation problem. The next section will be dedicated to this matter, and investigations will be done using both  $A$  and  $\Omega$  formulations, although only the last one will be used for optimisation.

### **III.3.2 Mesh Size Investigation**

Verifying the coherence of the mesh size is an important step in FE modelling, more so when it comes to TO. To do so, various mesh sizes will be studied with the  $A$  and  $\Omega$  formulations, for the energy and attractive force in the air gap. The aim is to determine the most compromising one between calculation time and fineness of mesh leading towards an unbiased solution. Investigating both energy and force is useful as one is a global value of the model (energy), and the other a local one (force). Hence, it will allow us to see if refining the

mesh only in the zone where force is calculated still produces acceptable results. The current density used here is 3.0 A/mm<sup>2</sup>.

### Computation of Energy

The mesh sizes investigated in this section have tetrahedral elements in the model varying between 2400 and 17500, for both  $A$  and  $\Omega$  formulations (see Appendix F). Figure 3.6 pictures the energy of the system against the number of finite elements. The true energy in Joules is given in the figure to avoid any confusion or bias.

We note that both formulations converge towards a solution, but the solutions do not coincide despite a fine mesh size. This is normal due to the underestimation of energy with formulation  $A$ , and overestimation with  $\Omega$ . Hence the real solution lies in between the two (but not necessarily mid-way). In  $A$  formulation, the discrepancy between the energy obtained with the coarsest and the finest mesh is 20%, while with  $\Omega$  formulation, it is 13%.

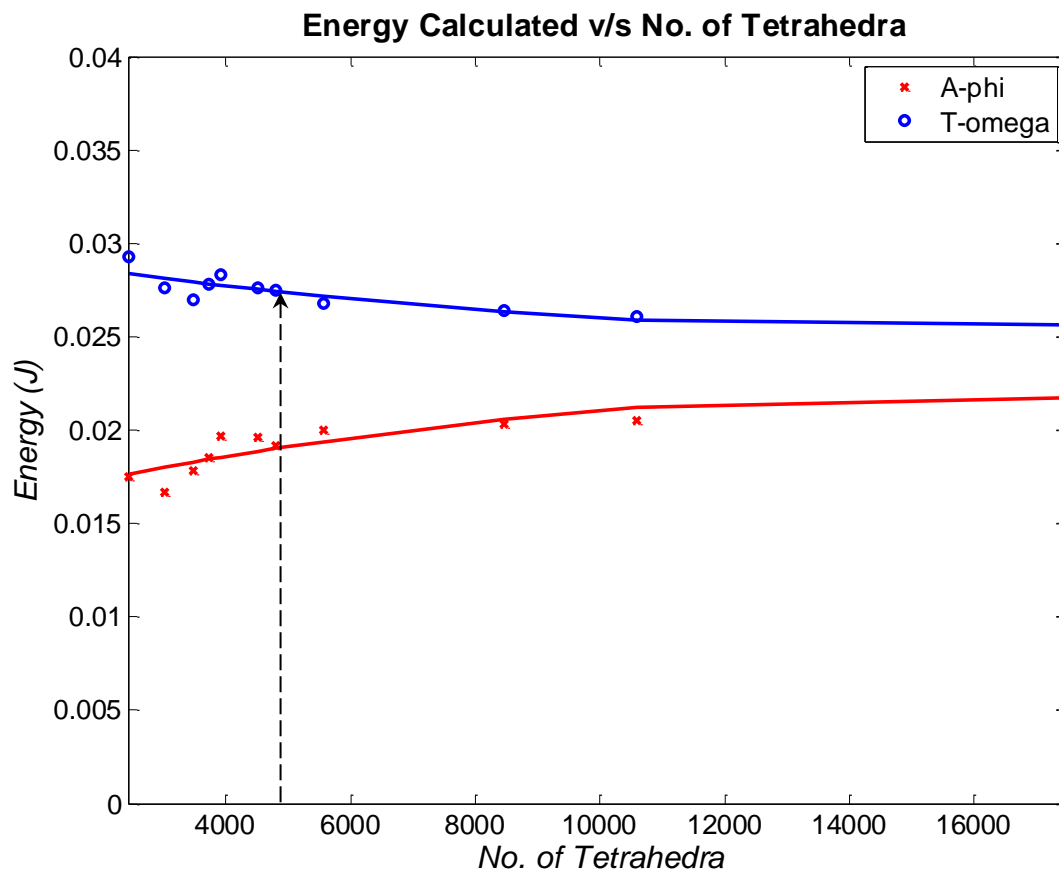


Figure 3.6 Energy for Different Mesh Sizes

From the above information, we can choose a reasonable mesh size for the model. The goal is to keep the number of tetrahedra in the optimisation domain high enough for a good

precision, and low enough for an affordable calculation time. Therefore, we choose the mesh with a total of 4800 finite elements, as pointed in Figure 3.6. For the  $A$  formulation, the percentage deviation of energy between the chosen mesh and the finest mesh is around 12%, while for  $\Omega$ , it is around 7%. As evoked earlier, the  $\Omega$  formulation is preferred in our case since we are dealing with a 3D FE model, where the number of unknowns is greater than in 2D. This is due to the divergence-divergence nature of the problem to be solved, which is easier than the curl-curl nature of the problem in the  $A$  formulation, as seen in Chapter I.

Now that the energy has been explored, it is also important to investigate the behaviour of the force with the mesh size. This will help us forge the suggestion made in this section.

### *Computation of force*

In this section, the same type of analysis as for energy is carried out, except that the force is a local value, and therefore has to be calculated at a particular position. The magnetic force is calculated on the nodes of a specific surface where desired, and the Virtual Work Method is used. Figure 3.7 shows the surface and nodes on which the force is calculated, lying between the optimisation domain and the iron bar (shown in the earlier figures).

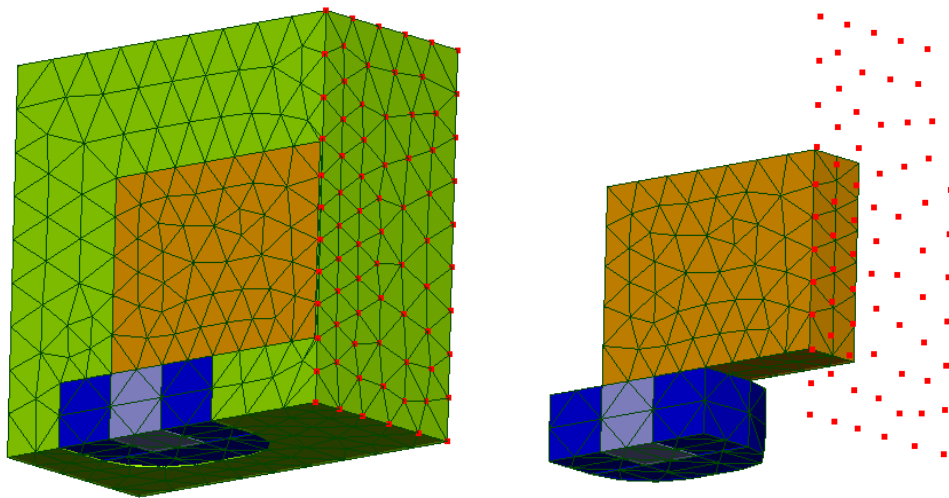


**Figure 3.7 Nodes on which Force is Calculated**

To see how the number of nodes on the surface affects the force calculation, we will vary the former while keeping the mesh size of the same size range. Figure 3.8 shows the variation of the true force in N for different number of nodes on the surface, for both  $A$  and  $\Omega$  formulations. We can see that for  $A$  formulation, the deviation of force from the lowest to the highest number of nodes is steeper than for  $\Omega$ . We choose a number of nodes of 75 from the figure, which is a good trade-off between calculation time and precision. Moreover, as we will carry all our optimisation using  $\Omega$  formulation, we can see from the graph that the difference

between the lowest and highest number of nodes is not very big (14.2%), as compared to the A formulation (54%).

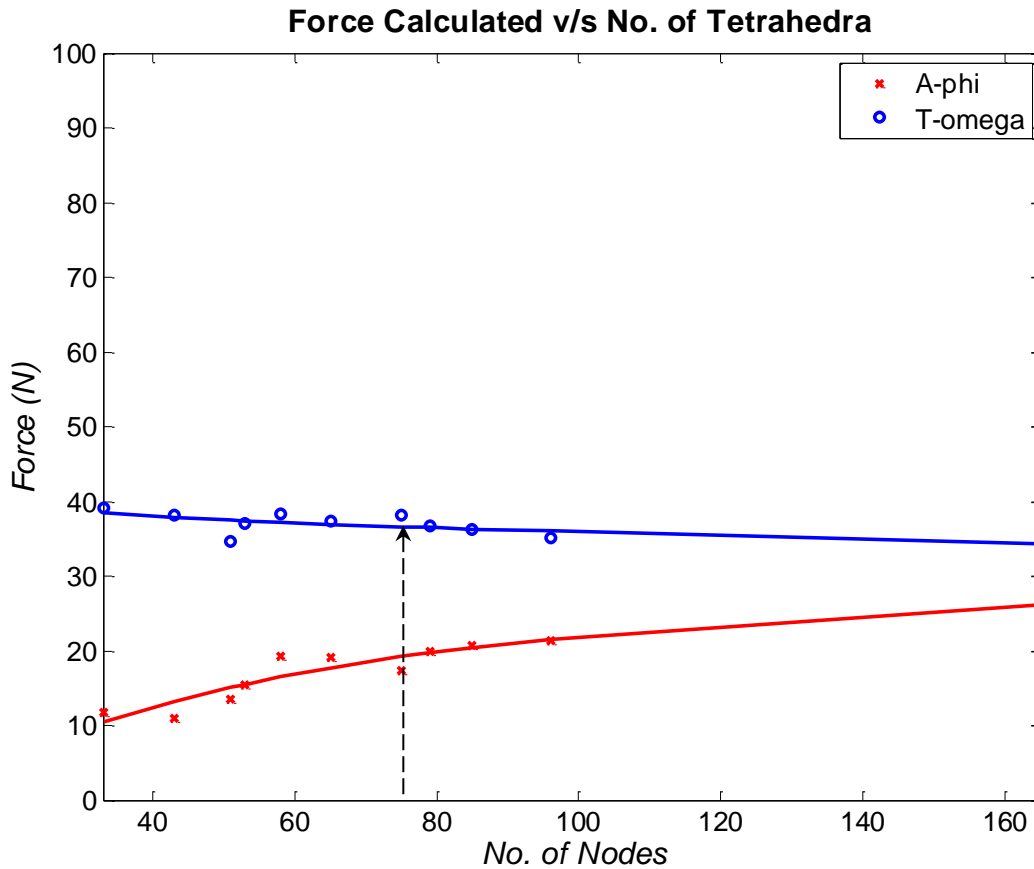


Figure 3.8 Attractive Force v/s Number of Nodes

Consequently, the number of nodes and mesh size (in terms of finite tetrahedral elements) to be used in our FE model is 75 and 4800 respectively. This sets the number of tetrahedra in the optimisation domain to be 342. The finite elements in the latter are of the same size, and hence the calculation of the Material Quantity (MQ) is not biased. The maximum energy is  $2.75 \cdot 10^{-2} J$  for 3.0 A/mm<sup>2</sup>, which occurs when the domain to be optimised is completely made of iron, with a relative magnetic permeability of 2000. To cross check the validity of this information, a calculation with Reluctance Network (RN) is done.

#### *Cross verification with Reluctance Network*

The same dimensions, current density and relative permeability as above are used to calculate the maximum energy with RN, and hence cross verify the value with the FE model. The RN is constructed as in Figure 3.9, and the mean energy is calculated as in (III-1). The mean reluctance for each element is found using  $\mathfrak{R} = \frac{l}{\mu_0 \mu_r \text{iron} \times A}$ , and the flux by  $\varphi = \frac{ni}{\mathfrak{R}}$ . The calculated values of  $\mathfrak{R}$  are given on the figure, with  $\mathfrak{R}_{core1}$  and  $\mathfrak{R}_{core2}$  representing the

reluctances for the iron core,  $\mathfrak{R}_{airgap}$  for the reluctance of the air gap and  $\mathfrak{R}_{bar1}$  and  $\mathfrak{R}_{bar2}$  for the reluctance of the iron bar. The flux obtained is  $\varphi = 1.49 \cdot 10^{-4} \text{ Wb}$ . The magnetomotive force is calculated by  $\varepsilon = ni$ , where the source has a cross section of  $1 \text{ cm}^2$ .

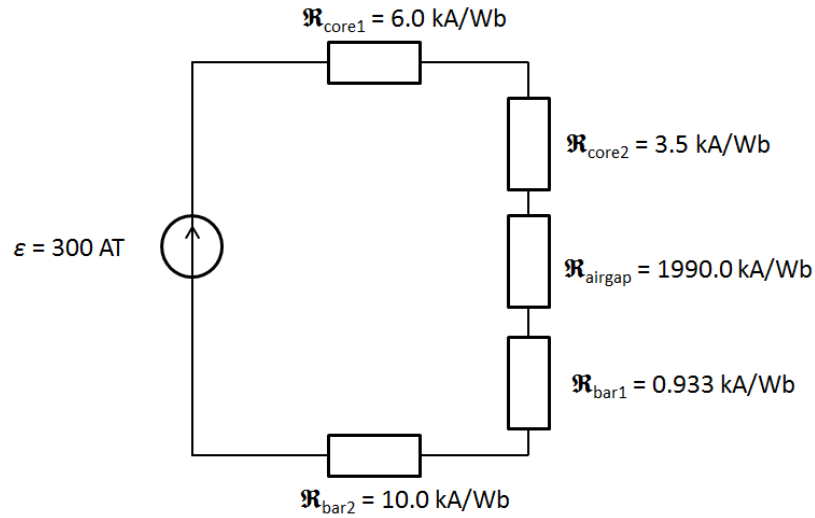


Figure 3.9 Reluctance Network for Electromagnet

$$Energy = \frac{1}{2} \mathfrak{R} \varphi^2 \quad (\text{III-1})$$

The maximum mean energy obtained with the RN is  $2.22 \cdot 10^{-2} \text{ J}$ , which is of the same range as the energy calculated from the FE model with the chosen mesh size ( $2.75 \cdot 10^{-2} \text{ J}$ ). We can thus validate the model before optimisation.

### III.4 TO of the Electromagnet

As seen in the brief literature review of this chapter, the topology optimisation of the electromagnet can be done by considering different objective functions. In this section, energy and force will both be considered, and the amount of material allowed in the optimisation domain is also constrained, as for the cubic test case in the previous chapter. Furthermore, we will also investigate the use of linear and nonlinear behaviour of materials in TO. A current density of  $3.0 \text{ A/mm}^2$  and a relative magnetic permeability of 2000 for iron will be used for calculations in this section.

#### III.4.1 Maximising Energy

The maximisation of the energy to optimise the topology of the electromagnet is one way of formulating the problem, as seen in literature. In our case, the optimisation problem is defined as in (III-2).

$$\begin{cases} \min\{-\gamma \cdot \text{Energy}(\boldsymbol{\rho}) + \lambda \cdot \text{FF}(\boldsymbol{\rho})\} \\ \text{s. t. } \text{MQ}(\boldsymbol{\rho}) \leq \beta \end{cases} \quad (\text{III-2})$$

It must be noted that the energy, FF and MQ are all normalised, as for the cubic test case in Chapter II. For the energy, the normalisation is done w.r.t the maximum energy (optimisation block as iron only). Figure 3.10 shows the magnetic flux density when the energy is maximum, in case of linear materials. The energy is  $2.75 \cdot 10^{-2} \text{ J}$  for  $3.0 \text{ A/mm}^2$ , and  $\mu_{r_{\text{iron}}} = 2000$ . The values of  $B$  are quite high (above 2 T) due to the linear behaviour. The coefficients used here are  $\gamma = 1$  and  $\lambda = 0.5$ , following a similar study as in Chapter II (Section II.7.4.2).

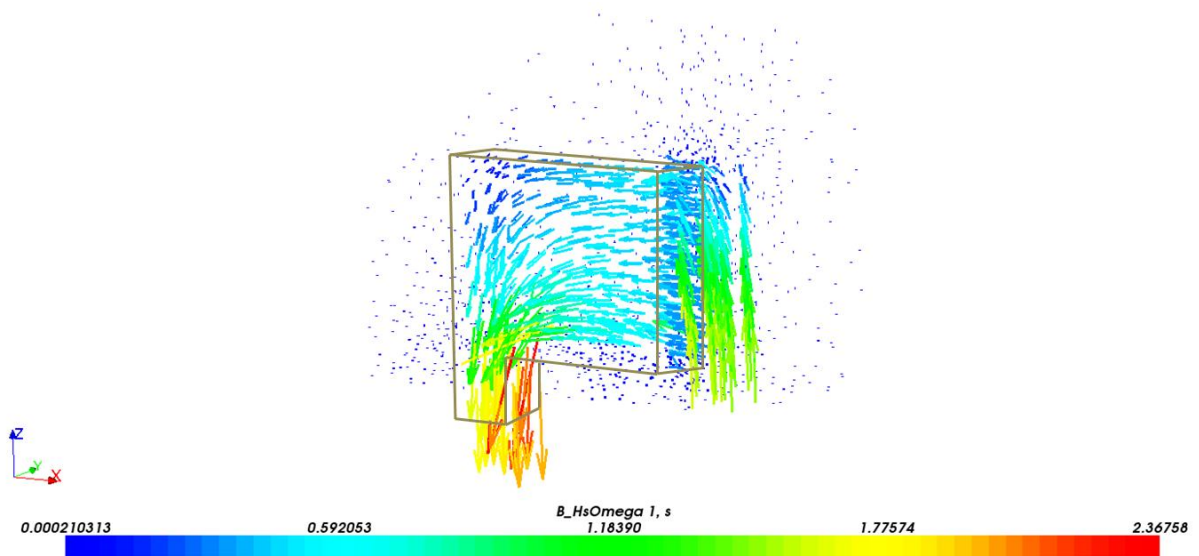


Figure 3.10 Case of Maximum Energy in the Electromagnet for Linear Material Behaviour

### Results

The energy calculated by *code\_Carmel* is a global value, and therefore obtained for the whole system. Figure 3.11 shows the resulting topology for  $\beta = 0.8$ , and Table 3.1 gives the information respective to the computation. The optimal topologies presented in this chapter will be displayed as vertical cross sections of the electromagnet in Figure 3.5(a).



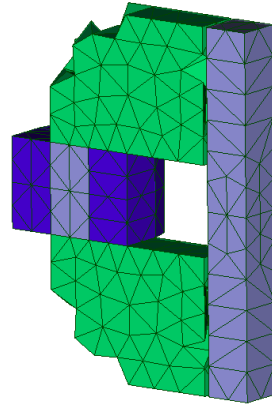


Figure 3.11 Optimal Topology while Maximising Energy with MQ = 0.8

Table 3.1 Information about the TO Results with Energy

$\beta$	Normalised Energy	MQ Reached	FF	No. of Evaluations	Time Taken (h)
0.8	0.9956	0.7929	0.002	35329	20.1

It can be seen that the final shape obtained is quite similar to what is usually observed in literature for C-core actuators. Despite calculating the global value, we can see that it does not greatly affect the quality of the results as the energy in the air gap is usually high as compared to the other areas. Hence, the higher the energy in the air gap, the most optimal will be the topology.

Nevertheless, it would be interesting to compare the results with the maximisation of force instead, which is a local value, and might be more pertinent to the optimisation problem.

### III.4.2 Maximising Attractive Force

We will now investigate the maximisation of the attractive force to optimise the topology of the electromagnet. The effect of the linear and nonlinear behaviours of the ferromagnetic materials is also discussed. Results will be presented for various cases of Material Quantity, and the convergence of the solutions will also be encompassed. The problem is defined as in (III-3).

$$\begin{cases} \min\{-\gamma \cdot \text{Force}(\boldsymbol{\rho}) + \lambda \cdot \text{FF}(\boldsymbol{\rho})\} \\ \text{s. t. } \text{MQ}(\boldsymbol{\rho}) \leq \beta \end{cases} \quad \text{(III-3)}$$

All the objectives and constraints are normalised. For the force, which is done w.r.t the case where the domain is made of iron, the magnetic flux density distribution is the same as given in Figure 3.10, for a current density of 3.0 A/mm<sup>2</sup> in the coil, and the maximum attractive

force is  $38.1\text{ N}$ . The relative magnetic permeability used for iron is  $\mu_{r_{iron}} = 2000$  here as well, and all the calculations are done in the  $\Omega$  formulation only. The coefficients used here are  $\gamma = 1$  and  $\lambda = 0.5$ , as for the case of maximisation of energy.

### III.4.2.1 Linear Behaviour of Ferromagnetic Materials

The different constraints imposed on the MQ are:  $\beta=0.8, 0.6, 0.4$  and  $0.2$ . The resulting topologies are given in Figure 3.12 and the information w.r.t the optimisation process is given in Table 3.2. It must be noted that the optimal topologies presented in this chapter will be shown as vertical cross sections of the electromagnet depicted in Figure 3.5(a).

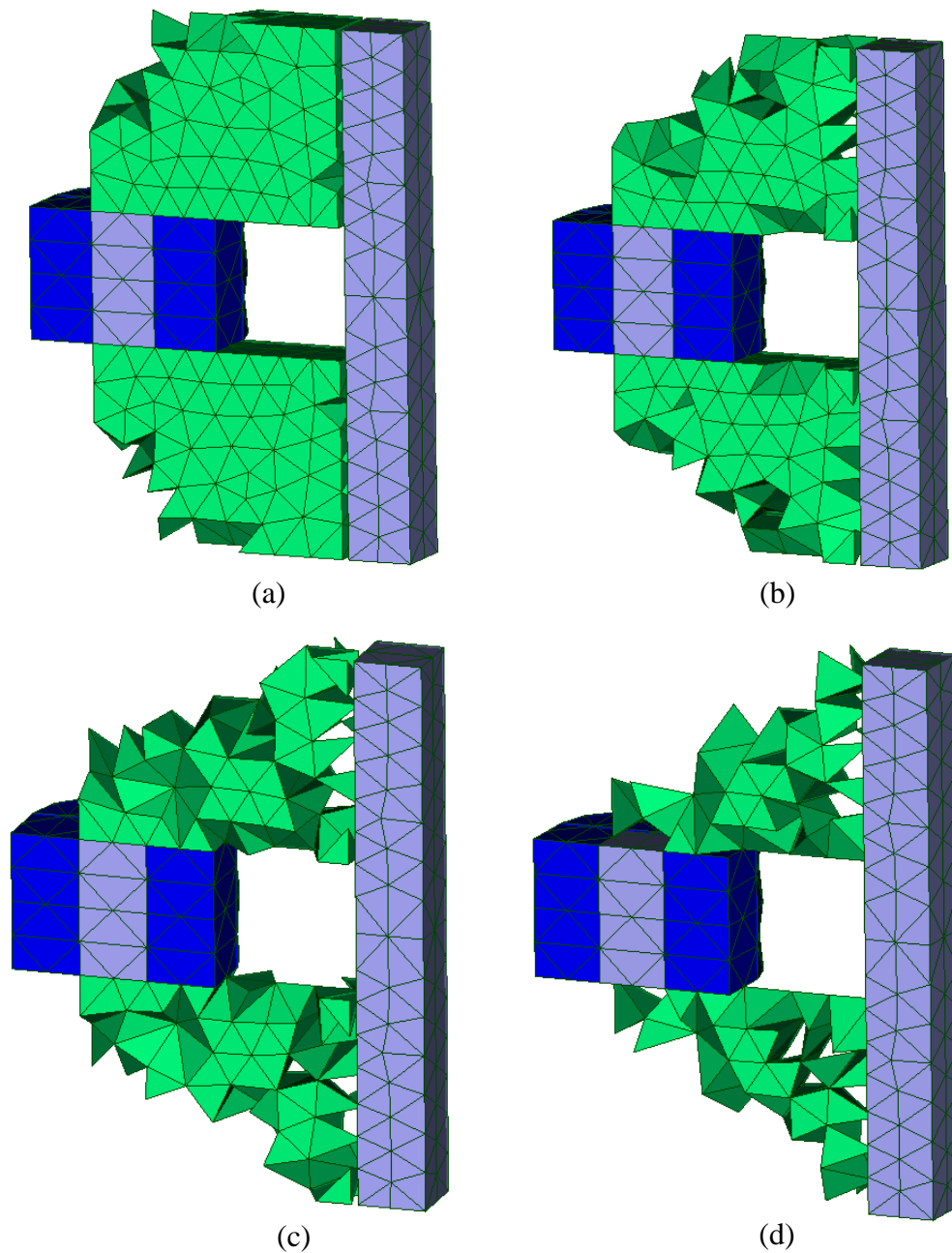


Figure 3.12 (a)  $\beta=0.8$ , (b)  $\beta=0.6$ , (c)  $\beta=0.4$ , (d)  $\beta=0.2$

Table 3.2 Additional Information about the TO Results

$\beta$	Normalised Force	MQ Reached	FF	No. of Evaluations	Time Taken (h)
0.8	0.996	0.795	$1.74 \cdot 10^{-10}$	27440	16
0.6	0.973	0.563	0.0064	30185	17
0.4	0.933	0.353	0.0066	39445	22
0.2	0.841	0.175	0.0166	28127	16

From Figure 3.12(a) with  $\beta = 0.8$ , it can be seen that the upper left corner of the iron core is removed as the magnetic flux density in this part is the lowest. This can be seen from Figure 3.10 where the magnetic flux density in the corner is dark blue, which can be assimilated as nearly 0 T. From the table, we can see that the force barely drops. From Figure 3.12(b) with  $\beta = 0.6$ , we note that more material from the corner is removed, as well as material from the lower part of the iron core. Furthermore, some material near the air gap is also removed. This occurs mainly as we are in linear case, where the saturation doesn't occur and hence magnetic flux density in the surrounding variables can be increased largely without any constraints. This effect is even more pronounced in Figure 3.12(c) with  $\beta = 0.4$  and (d) with  $\beta = 0.2$ . However, it must be noted that until  $MQ = 0.4$ , the force is still above 0.9, while for  $MQ = 0.2$ , the force drops by approximately 10%. In the latter case, as the MQ is quite small, the main idea is to see if a magnetic path is nevertheless created by the optimisation process for an attractive force to occur. In all cases, the materials near the 'neck' of the core are retained. This is because, according to Figure 3.10, B at this level is around 1.4 T. Despite the presence of many 'holes' in the magnetic path due to lack of materials, the magnetic path is valid. This effect should be less visible in the nonlinear cases.

Figure 3.13(a) shows the magnetic flux density distribution for the topology in the case of  $\beta = 0.2$ , and Figure 3.13(b) for the case of  $\beta = 0.6$  for a brief comparison. The boundaries shown in the figures represent the outline of the topologies obtained for each case. In Figure 3.13(a), it can be seen that the magnetic path is correct despite the low amount of materials present in the topology. For this reason, B is quite high in the path, and since magnetic saturation is not taken into account here, B is allowed to take values over 1.8 T. On the other hand, in Figure 3.13(b), for  $\beta = 0.6$ , we note that B is much lower as there are more materials present in the magnetic path, and hence a more uniform distribution  $B(T)$  with less saturation.

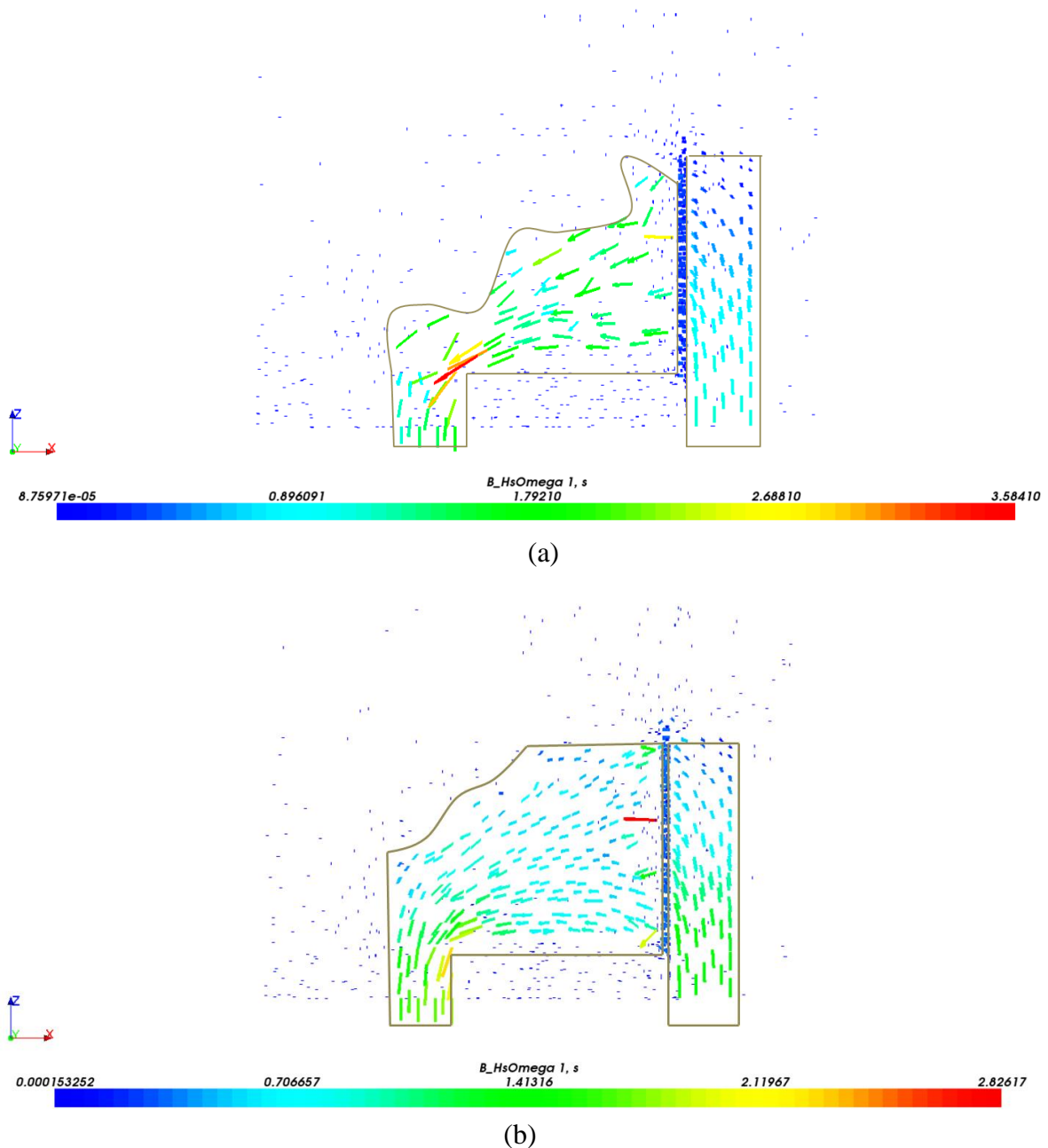
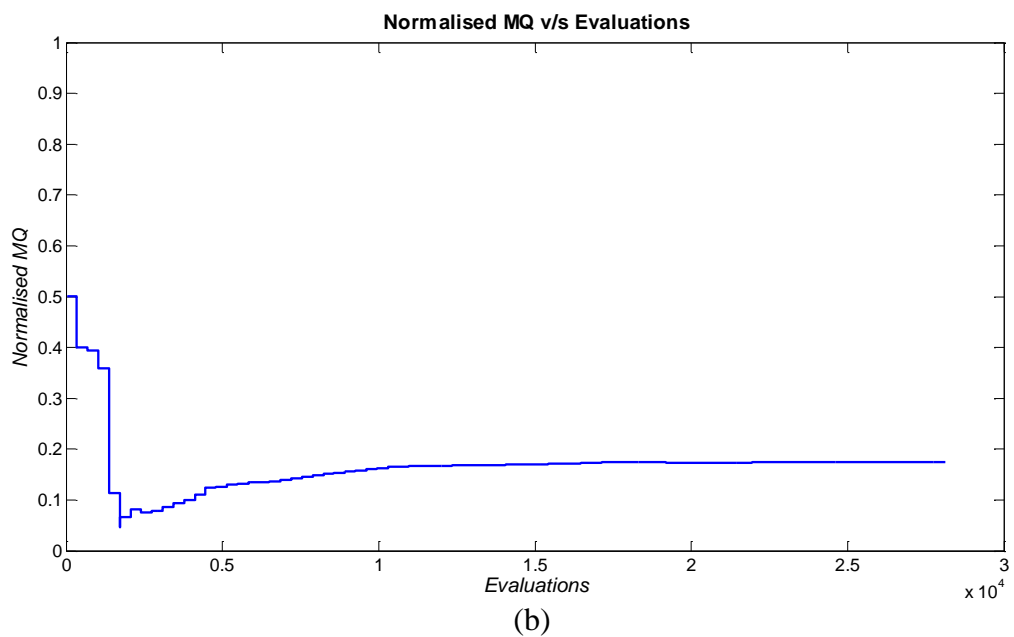
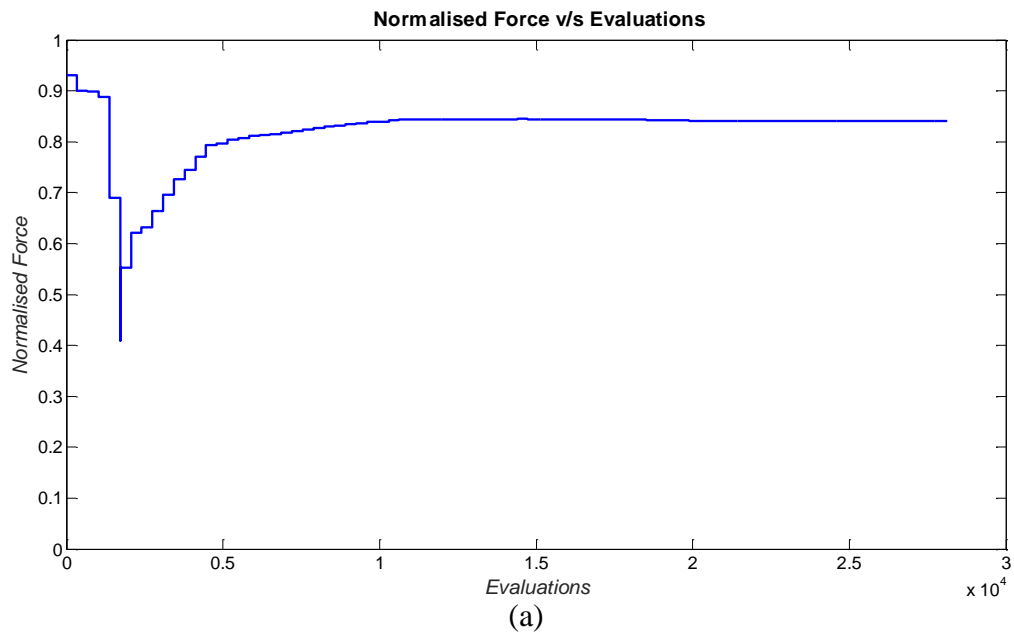


Figure 3.13 Magnetic Flux Density Distribution for (a)  $\beta = 0.2$ , (b)  $\beta = 0.6$

To verify the convergence to a correct solution, we examine the evolution of the parameters w.r.t the evaluations. The stopping criterion for the algorithm in our case is when no further evolution is found in the objective function. Figure 3.14 respectively shows the evolution of the normalised force, MQ, FF, overall objective function and the final value of the variables for the case of  $MQ = 0.2$ .

From Figure 3.14(a), it can be seen that the force converges to its final value at a quite early stage of the optimisation process (around  $1.5 \cdot 10^4$  evaluations), as well as the MQ which reaches a fixed value (Figure 3.14(b)). Nevertheless, the algorithm adds more iterations to the process as the FF has not yet reached the minimum value (Figure 3.14(c)). When all the

objectives and constraints are satisfied and no further evolution is seen, the optimisation process stops. From Figure 3.14(d), we can see the trend of the overall objective function. It keeps iterating until the algorithm converges. As for the final value reached by the variables, 97.7% in this case have converged to 0 or 1 (Figure 3.14(e)), which is the worst case as compared to the other higher MQ cases. Moreover, the values of the non-converged variables are all below 0.2; hence they can be assimilated as 0 (or absence of material). It is also interesting to note that those non-converged variables occur adjacent to the air gap, as shown in Figure 3.15. This could justify the presence of multiple ‘holes’ near the gap.



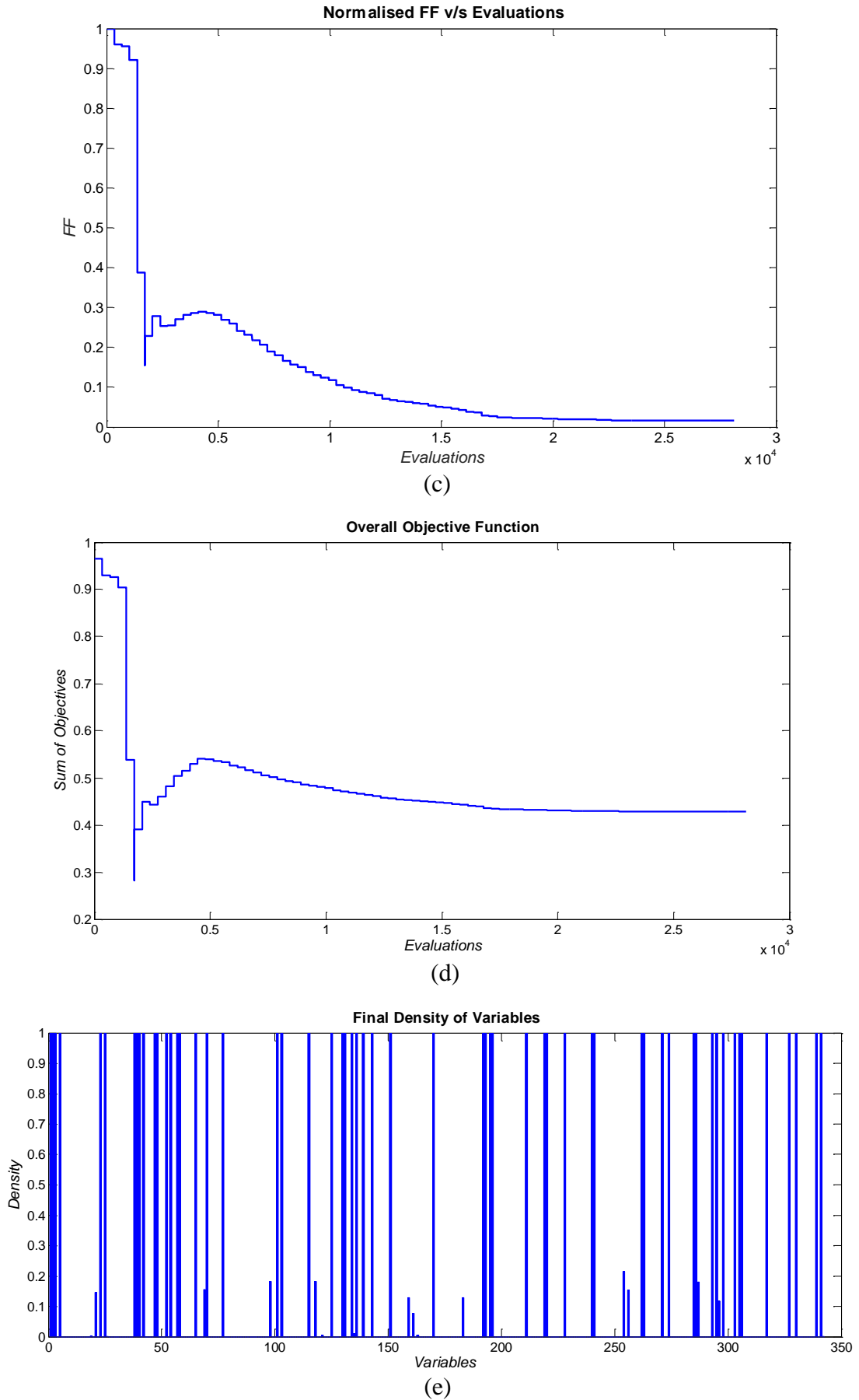


Figure 3.14 Convergence Graphs for Linear Case with  $\beta = 0.2$

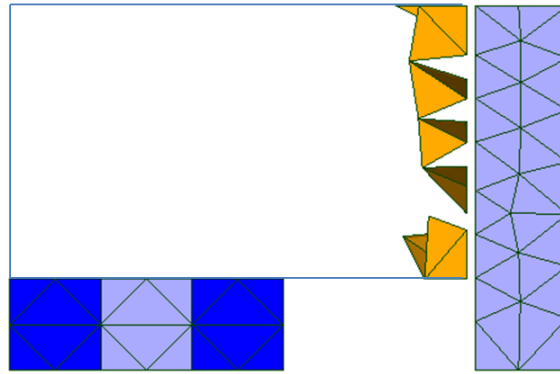


Figure 3.15 Position of Non-converged Variables

We can see from Table 3.1 and Table 3.2 that the number of evaluations and amount of time taken to optimise the force in the air gap is lower. Furthermore, the calculation with linear characteristics of materials is correct in terms of magnetic path, force and topology, but lacks the saturation aspect. For this reason,  $B$  is sometimes allowed to rise up to more than 2 T when the MQ is very low. As the behaviour is linear, some individual elements can have a very high  $B$ . This suggests that the investigation of the nonlinear behaviour of the materials is essential to be closer to a real case.

#### III.4.2.2 Nonlinear Case

The same problem as in the previous section is now optimised while taking into consideration the nonlinearity of the materials used. The magnetic flux density distribution when the optimisation domain is made of iron only and 3.0 A/mm<sup>2</sup> is applied to the coils is given in Figure 3.16, and the saturation curve used is shown in Figure 3.17, taken from a manufacturer's ferromagnetic material characterisation already available at the laboratory. A regression function was used to find the correct values of the coefficients in the Marrocco equation, which are in this case:

$$\varepsilon = 4.67 \cdot 10^{-4}$$

$$c = 0.0119$$

$$\alpha = 9.98$$

$$\tau = 1.06 \times 10^5$$

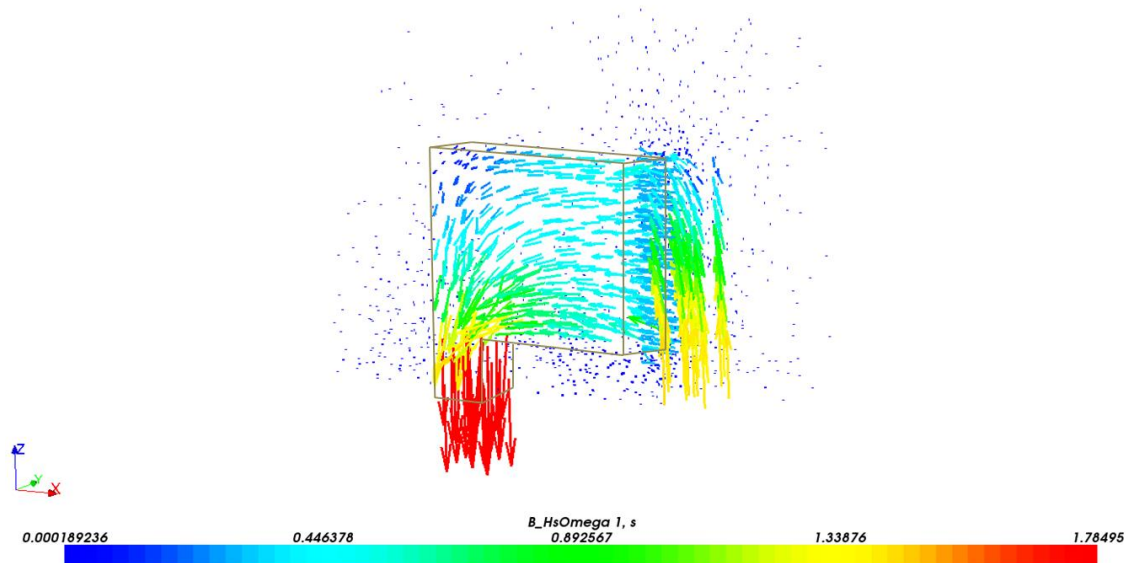


Figure 3.16 Magnetic Flux Density Distribution in Nonlinear Case with Variables as Iron

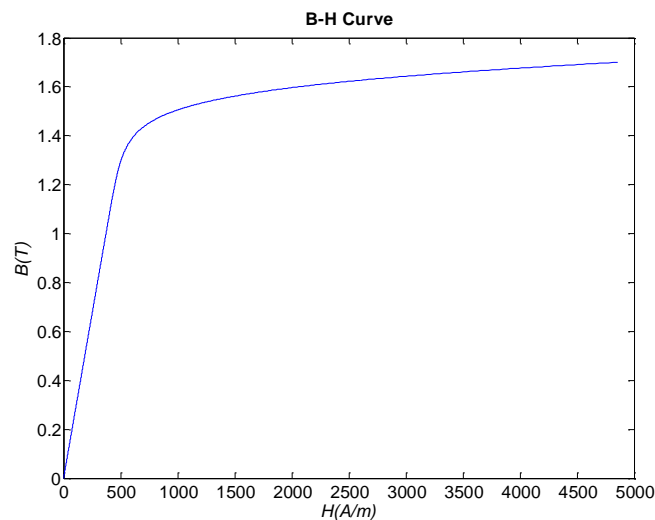


Figure 3.17 Marrocco Saturation Curve

The ferromagnetic material situated at the core of the coils is highly saturated as compared to the other regions due the concentration of flux there. The maximum attractive force in this case is 31.2 N and the global energy is  $2.26 \cdot 10^{-2} J$ . This presents a decrease by 18.1 % for the force, and 17.8 % for the energy w.r.t the linear case.

We will now analyse the results for different MQ cases while considering the nonlinear behaviour of the ferromagnetic materials for the electromagnet. In Chapter II, the outcome of the analysis of the nonlinearity and comparison with linearity of the materials was not very appealing as the cubic test case was a rather straightforward electromagnetic one. The effects of saturation and behaviour of the optimisation process in this case could not be clearly discussed. But the electromagnet, being a more ‘real’ electromagnetic case, could be more pertinent.



The topologies obtained while constraining the MQ at different values, namely 0.8, 0.6, 0.4 and 0.2 are pictured in Figure 3.18, and the additional information w.r.t the optimisation process of the nonlinear case is given in Table 3.3.

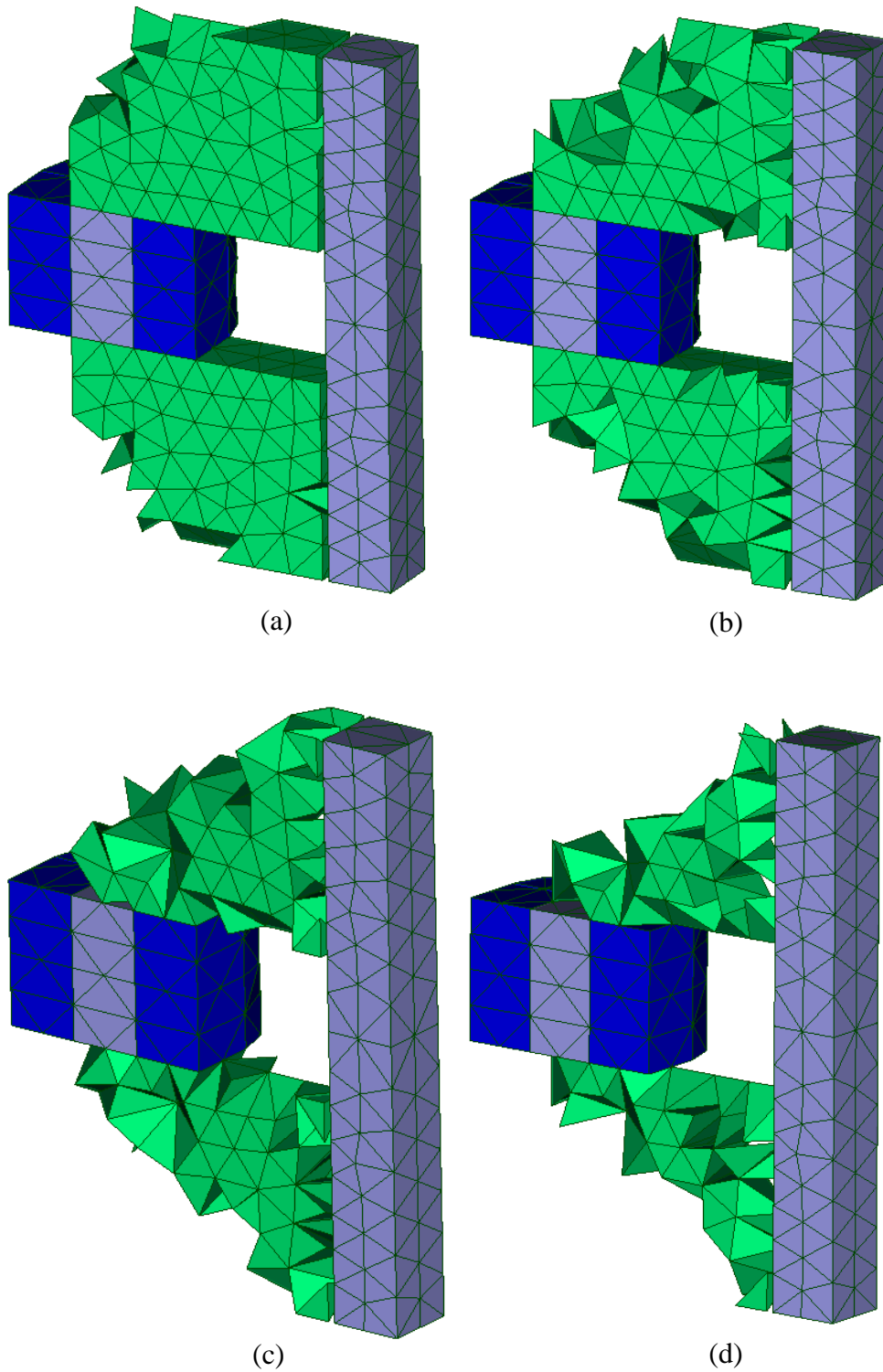


Figure 3.18 (a)  $\beta=0.8$ , (b)  $\beta=0.6$ , (c)  $\beta=0.4$ , (d)  $\beta=0.2$

Table 3.3 Additional Information for Nonlinear Case

$\beta$	Normalised Force	MQ Reached	FF	No. of Evaluations	Time Taken (h)
0.8	0.9963	0.7982	$1.79 \cdot 10^{-7}$	19563	13
0.6	0.9654	0.5994	$1.32 \cdot 10^{-5}$	20254	13
0.4	0.9480	0.3713	$1.17 \cdot 10^{-5}$	23667	17
0.2	0.8656	0.2	0.0192	27008	25

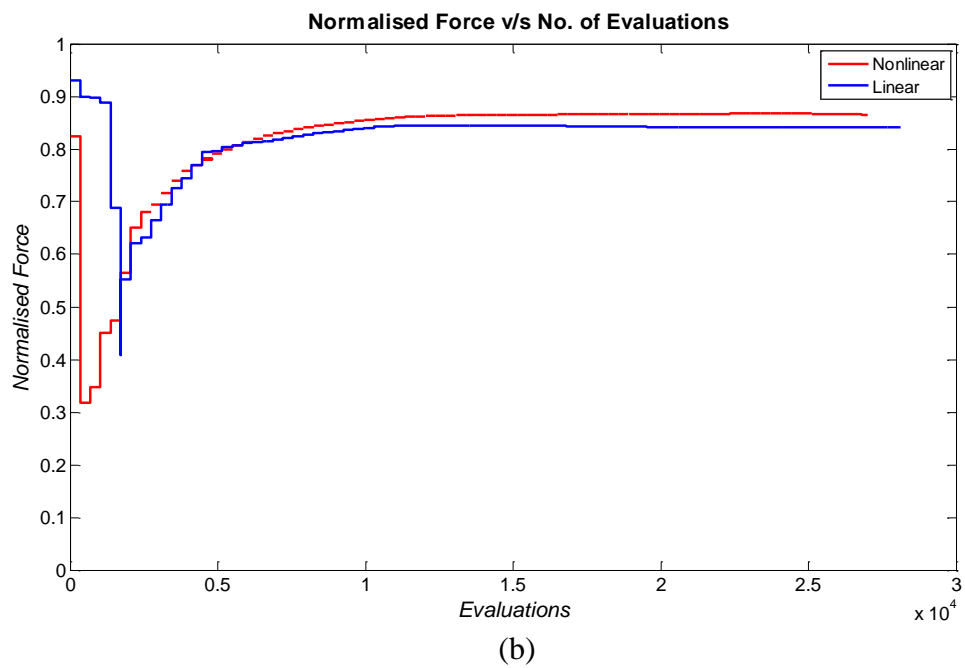
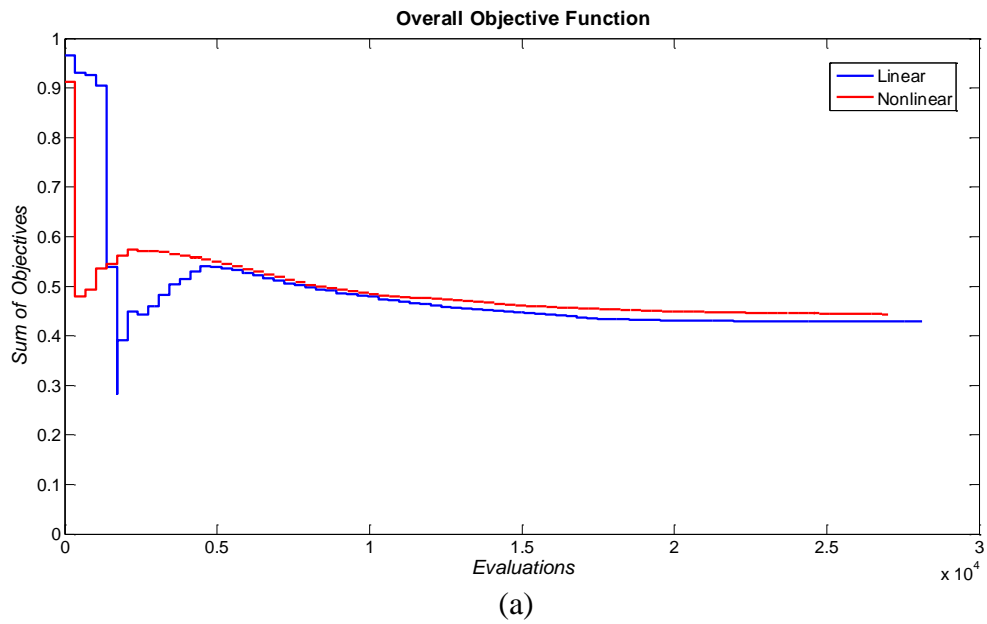
From Figure 3.18, it can be seen that the materials are distributed in the optimisation domain with the same trend as for the linear case. On the other hand, the nonlinear case presents a higher ‘compactness’ of the topologies as compared to the linear case. This translates by the fact that less ‘holes’ are found in the optimal topologies, as well as a more uniform distribution of materials near the air gap.

As for the normalised forces, the MQ reached and the FF, they are in the same range as for the linear case despite the difference in topology. On the other hand, the problem converges more rapidly into a solution as less evaluations are observed. Also, the time taken for one evaluation is more than the linear case due to the nonlinearity loop, as explained in the previous chapters. But due to the lower number of total evaluations, the overall time taken for the optimisation is lower. The stopping criteria defined for the optimisation algorithm are the same for both linear and nonlinear cases for a more judicious comparison.

The convergence graphs are shown in Figure 3.19. It can be seen from Figure 3.19(a) that the overall objective converges correctly in 27008 evaluations. For the normalised force, a solution is reached in approximately 15000 evaluations, as in Figure 3.19(b), and the FF is minimised for the rest of the evaluations, allowing the variables to converge to 0 or 1 at the end of the optimisation (Figure 3.19(c)). As for the MQ, the optimisation process makes sure to satisfy it first before proceeding, as in Figure 3.19(d). It must nevertheless be pointed out that 98.5% of the variables have converged to 0 and 1, from Figure 3.19(e), which also represents the worst case of convergence if Table 3.3 is considered. Those intermediate variables also appear adjacent to the air gap, as for the linear case.

The purpose of having the curves for the linear and nonlinear material behaviour on the same plot is to see how they evolve for the same problem formulation. We can see that the overall trend is the same, but with fewer evaluations for the nonlinear case. Also, the force

appears higher for the nonlinear case because the normalisation is not w.r.t the same values for both.



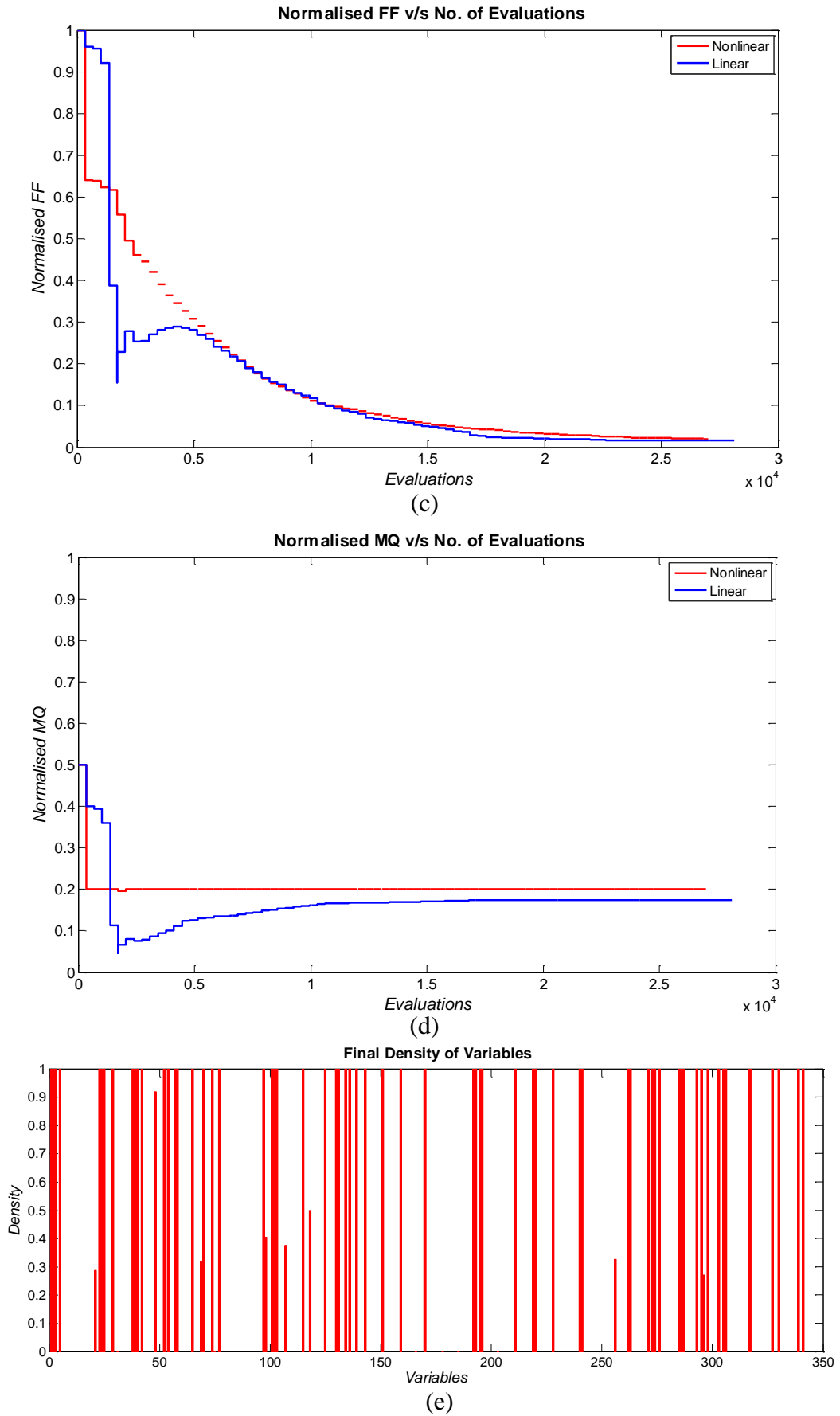


Figure 3.19 Nonlinear Case  $\beta = 0.2$  (a) Overall Objective, (b) Force, (c) FF, (d) MQ, (e) Density of Variables

### III.5 Summary and Contributions

The objective of this chapter was to apply the methodology devised for TO in Chapter II on a real electromagnetic device for further in-depth analysis. It was successfully applied on a 3D C-core electromagnet, often used in literature for their practical nature and simplicity of functioning. The FE model of the electromagnet was also detailed and the different limitations were explained. A concise but useful study on the choice of the mesh size was also performed to verify the coherence of the mesh used. The objective was to maximise the attractive force of the electromagnet by finding an optimum shape of the iron core. The TO was done for various cases where the MQ was constrained at different values, and the resulting structures were discussed. Moreover, a comparison when using the linear and nonlinear behaviour of the ferromagnetic materials was done, and the convergence of the solutions were elaborated.

From our observations, we have seen that TO with linear and nonlinear materials do not produce the same results, despite the overall topology being similar at a certain level. The magnetic path created to allow the flow of flux was similar, but the way the materials were disposed differs. The nonlinearity produced more efficient results as the topologies appeared more feasible, and manufacturing friendly. Furthermore, despite a longer calculation time per evaluation, the convergence to a proper solution was seen to be reached in fewer evaluations.

The main contribution of this chapter to already existing works in literature lies in the comparison of topologies obtained with linear and nonlinear ferromagnetic materials in TO for a 3D model. We could readily see how the second one is very important in electromagnetic modelling and can affect the efficiency of the results. The next chapter will further emphasise on this characteristic to present the topology optimisation of an electrical machine.

# Chapter IV – TO of a Salient Pole Synchronous Generator

---

## IV.1 Introduction

After exploring the various angles of TO, and applied it to two 3D test cases, namely an academic cubic case (Chapter II) and an electromagnet (Chapter III), the proposed methodology is now used towards the topology optimisation of a more complex electromagnetic case. In this chapter, the rotor top of a Salient Pole Synchronous Generator (SPSG) will be optimised for a more optimal magnetic flux density distribution in the machine. Apart from the fact that electrical engineers are always in quest of new topologies of machines for higher efficiency, the choice of a SPSG was backed by the already existing industrial prototype at Jeumont Electric. This prototype has a rated power of 1MVA and is designed to generate electricity from wind turbines. The aim of this chapter is to look for new topologies of the rotor of the machine w.r.t the desired objective, and discuss their viability in practical. As evoked in earlier chapters, accounting for the nonlinear behaviour of the ferromagnetic materials is also very important in such electromagnetic examples, and will thus be encompassed. To achieve this, we will investigate the original machine for a paramount positioning of its characteristics, and subsequently decide on the domain to be optimised. With the help of the TO tool previously presented, we benefit from the full functionality of the FE tool to create a precise model of the machine, and the use of a robust optimisation algorithm.

Primarily, this chapter will concisely present a few electrical machine-oriented TO applications found in literature alongside their methods and results. Afterwards, the model of the original SPSG will be detailed, while focusing on the parameters to be optimised. Finally, we will present some topologies of the machine obtained as optimisation results using both linear and nonlinear behaviour of the ferromagnetic materials, and analyse their feasibility and coherence from a numerical and electromagnetic point of view.

## IV.2 State of the Art

In this section, a few examples of the topology optimisation of electrical machines found in literature are presented. Some examples have already been presented in Chapter I, and hence will not be repeated here. The scope of this section will be very large as various authors often choose machines that are already accessible at their respective laboratories (whether FE models or prototypes), and for many cases, on which they already have previous experience. Nevertheless, the objective of this state of the art is to get a more extensive sight of the works carried out in this particular topic.

In [88], the topology of a Permanent Magnet Synchronous Generator (PMSG) is optimised with the aim of reaching a higher output power characteristic with less permanent magnet volume than an existing PMSG (as reference). The rotor structure is designed from empty space, and the TO method used is based on a concept of cluster and cleaning with Genetic Algorithm. They allow iron, air and permanent magnet regions in the domain to be optimised. The design region and results are depicted in Figure 4.1.

The authors found that the designed machine had a larger output power per stator current than the reference model, and for a stator current of less than 200A they both had same torque ripple. Despite a good optimisation convergence of the objectives, the main weakness in this type of optimisation is the use of a linear behaviour of the ferromagnetic materials. It is therefore hard to tell whether the resulting topology would be adapted to a practical model.

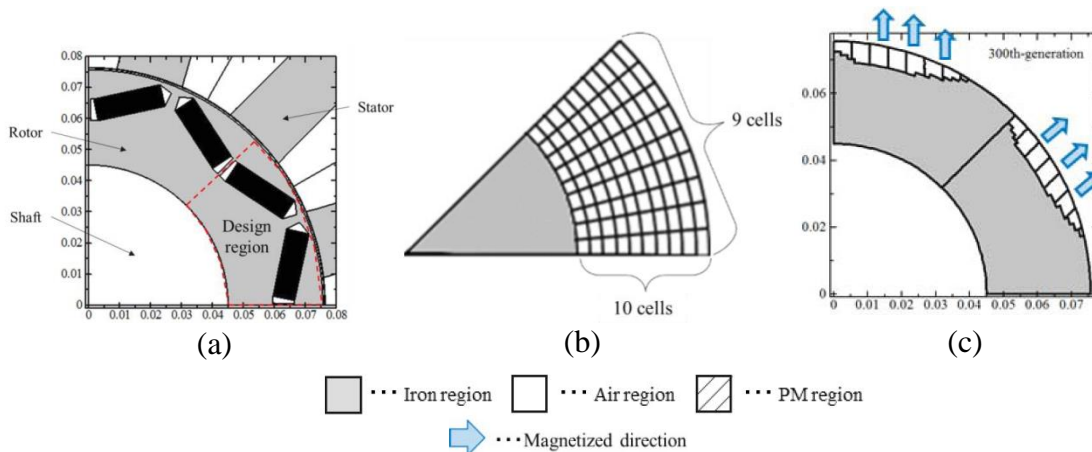


Figure 4.1(a) Design Region of Machine, (b) Cell Division for TO, (c) Final Results

In [89], the authors optimise the topology of an Interior Permanent Magnet (IPM) brushless electric motor by using a sensitivity analysis method of topological derivatives with the ON/OFF method, based on the works of Ohtake et al. [90]. The objective is to optimise the radial component of the magnetic flux density  $B$  in the air gap by approaching its behaviour to a sine curve. The rotor is considered to be in a fixed position without considering any induced current. The ferromagnetic materials used were assumed to behave linearly. Figure 4.2(a) shows the initial machine with magnets in orange, coils in light blue, ferromagnetic material in brown and air in dark blue, and (b) shows the area to be optimised in red, i.e. to be replaced by iron or air. Figure 4.2(c) shows the amount of iron removed during the optimisation process (in green) and (d) illustrates the final optimised shape. The optimised radial component as compared to the initial one is shown in Figure 4.2(e), with a visible improvement.



Once again, in terms of TO, the method converged correctly to a good solution. But from an engineering point of view it lacked the investigation of the nonlinear behaviour of the materials to approach practical issues.

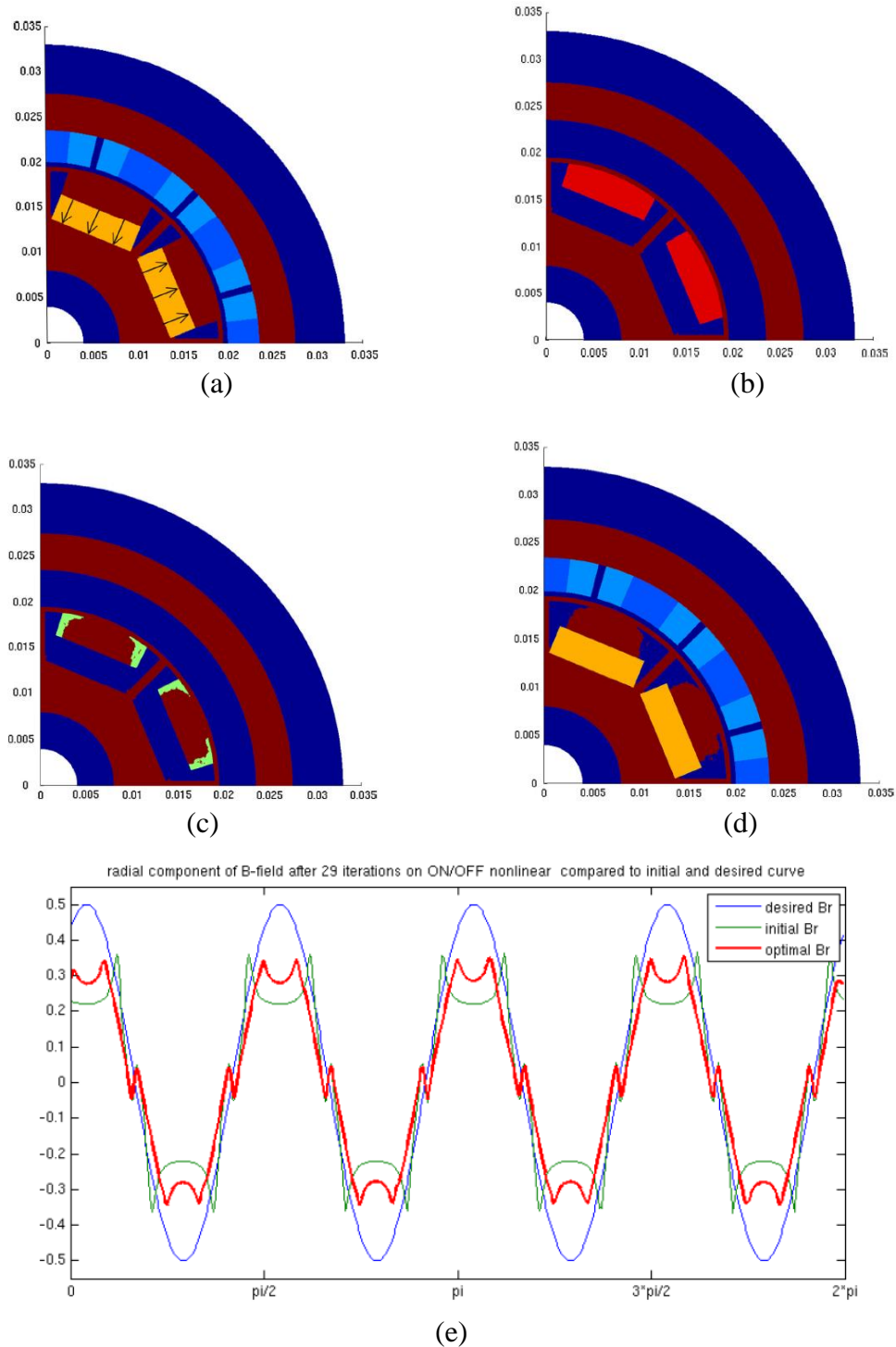


Figure 4.2 (a) Initial IPM Motor, (b) TO Domain in Red, (c) Material Removed in the Optimisation process (Green), (d) Optimised Shape, (e) Optimised Radial Component

In [53], the authors propose an effective shape of the flux barrier in an IPM motor, important in controlling the torque characteristics of the latter. The topology of the rotor core

is optimised using a multistep genetic algorithm (MSGGA) to determine the effective flux barrier. The effect on the current phase angle is also considered by using combinatorial optimisation. The initial domain of the machine considered is given in Figure 4.3(a), and the optimised shape with phase angle change using MSGGA in (b).

The work was rather methodology oriented, i.e. it served to compare the efficiency of MSGGA with standard GA. Torque characteristics were found to be higher with MSGGA. But the topology obtained in Figure 4.3 (b) presents some manufacturing difficulty due to the two lines of material in the middle, and will also be inefficient if saturation is considered.

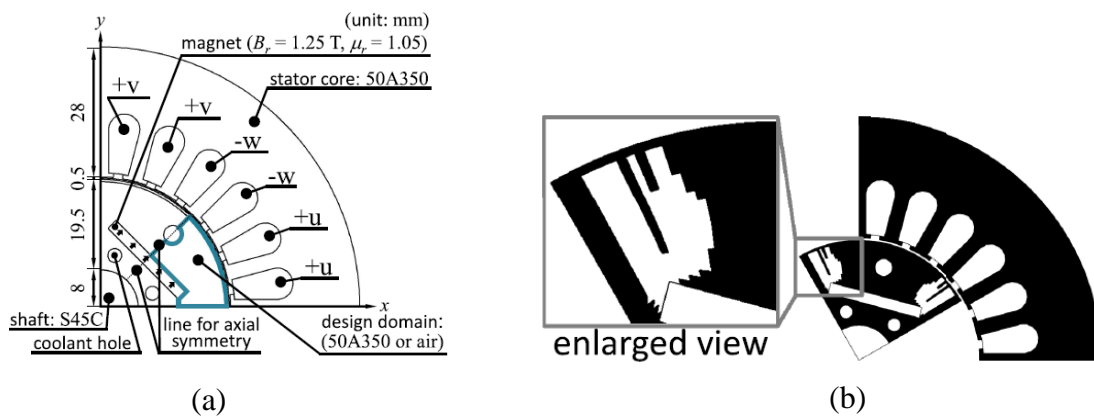
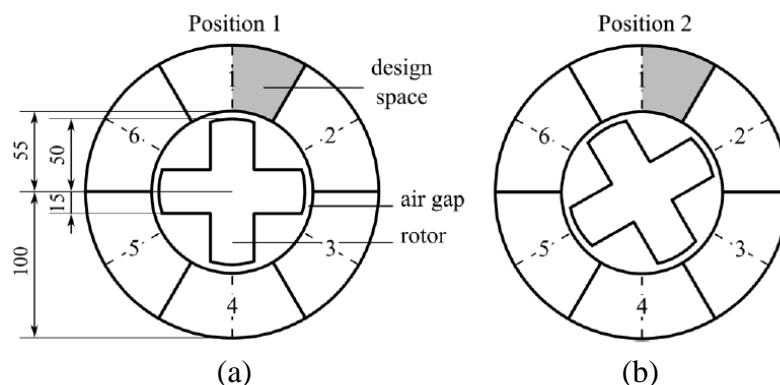


Figure 4.3 (a) Initial Domain of IPM, (b) Optimised Topology

In [24], the authors propose to use a combination of the geometric mapping and a convexity-oriented mapping to optimise the topology of a switched reluctance motor. The shape of the stator is optimised by considering iron and coils so that the torque is maximised. The average torque is calculated from the magnetic energy between two different positions, as shown in Figure 4.4(a) and (b). The design space is also shown on the same figure. Some of the solutions obtained with specific penalisation speeds are given in Figure 4.4(c) and (d) for 5 and 8 iterations respectively.

In this work, the switched reluctance motor was used as a means to validate the methodology proposed by the authors, but the saturation was not considered.



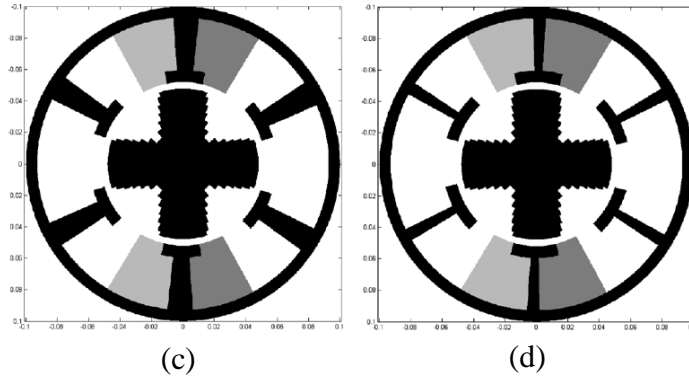


Figure 4.4 (a)&(b) Initial Design Space and Positions, Optimised Topologies for (c) 5 Iterations (d) 8 Iterations

After a concise but broad overview of the actual status of TO of electrical machines in literature, we can note that most of the works that have been carried out tend to put forward the TO methodology rather than the viability of the applications. Very often, the electromagnetic saturation of the machines is overlooked, resulting sometimes into structures that are difficult to explore in practical.

The works accomplished in this chapter will be oriented towards the TO of the rotor top of a SPSG while considering the nonlinear behaviour of the materials. A comparison of topologies and convergence of solutions will be done with cases where linear behaviour of the materials is used. The same TO methodology as proposed in the Chapter II & III will be used. The FE model of the SPSG is an extruded 2D one, and its magnetic flux density distribution will be used as optimisation objective. The following sections will elaborate on how the latter will be used as objective function.

### IV.3 Salient Pole Synchronous Generator (SPSG) Model

The SPSG used in this study was very much inspired from the existing prototype of a Doubly Excited Synchronous Generator at Jeumont Electric, designed for wind turbines [91] [92]. Nevertheless, in our work we will not consider the double excitation with permanent magnets, but only the excitation with rotor windings. Salient pole rotors are usually very popular due to its ease of manufacturing, especially in case of high number of pair of poles.

The original SPSG is illustrated first, relative to its main ratings, FE model and electromagnetic characteristics. Thereafter, the design space will be detailed, as well as the properties we want to optimise.

#### IV.3.1 FE Model of the Original SPSG

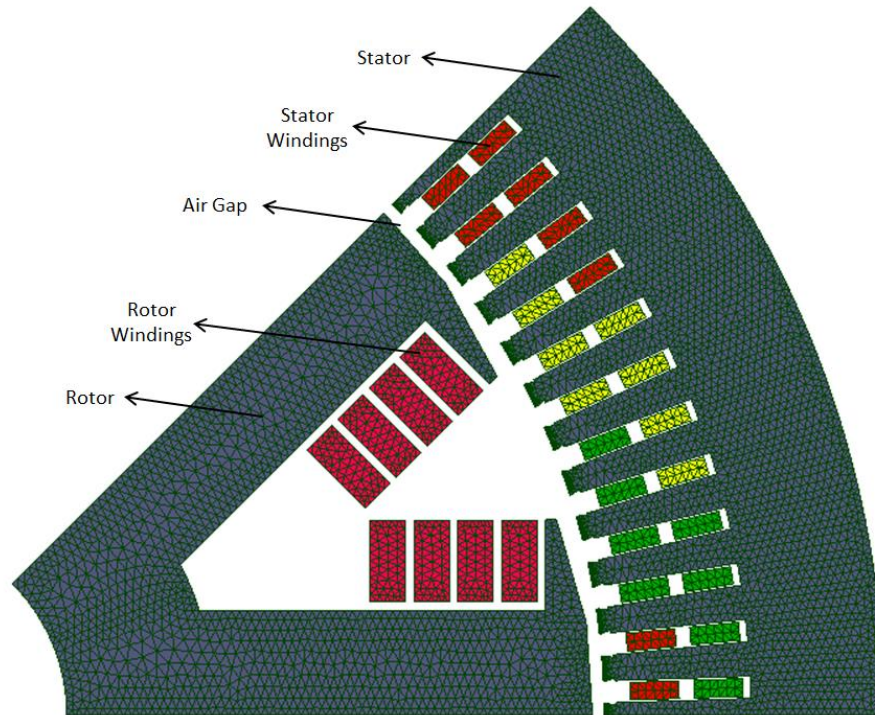
The original SPSG is illustrated in Figure 4.5(a), with the different parts of the machine labelled. Considering an antiperiodic symmetry, one eighth of the machine is modelled. The

FE model is an extruded 2D one, as shown in Figure 4.5(b), and the number of finite elements in the mesh is 20838. A relatively fine mesh size is chosen on purpose for a correct FE modelling. The parameters of the machine are given in Table 4.1.

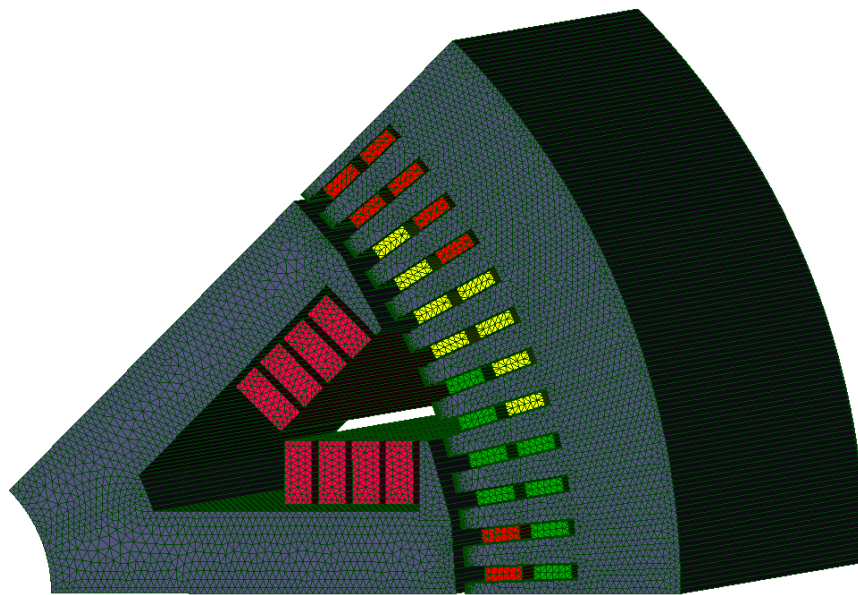
**Table 4.1 SPSG Parameters**

<b>Parameter</b>	<b>Value</b>
Rated Power	1 MVA
Phases	3
Rated Excitation Current	192 A
Rated Output Voltage	3 kV
Power Factor	0.8
Rated Speed	750 rpm
Frequency	50 Hz
Overspeed	900 rpm
Depth of Machine	750 mm
No. of Poles	8
Air Gap Size	5 mm

The optimal topology of the rotor will be sought so that the magnetic flux density distribution in the machine is optimised. There are different ways of considering  $B$  in the objective function of the problem. In this chapter, we will investigate the distribution of the  $B$  throughout the machine, and also the shape of  $B$  in the air gap. Hence, no-load simulations of the machine will be performed. As a starting point, we will study the spatial flux distribution in the original machine, as well as the  $B$  in the air gap.



(a)



(b)

Figure 4.5 SPSG (a) Geometry, (b) Mesh

### *Magnetic Flux Density in the Air Gap and Spatial Distribution*

A current density of  $3.0 \text{ A/mm}^2$  will be used for the excitation windings to stay within the range of what is used in the prototype for no-load tests. The spatial distribution of  $B$  in the machine is pictured in Figure 4.6(a) with linear behaviour of the materials, and in Figure 4.6(b) with nonlinear behaviour. All calculations are done in magnetostatics, using  $\Omega$  formulation. The  $B(H)$  curve for the nonlinear ferromagnetic materials are obtained from the

manufacturer, and the coefficients for the Marrocco equation are obtained by a regression function. The coefficients are:

$$\varepsilon = 1.23 \cdot 10^{-3}$$

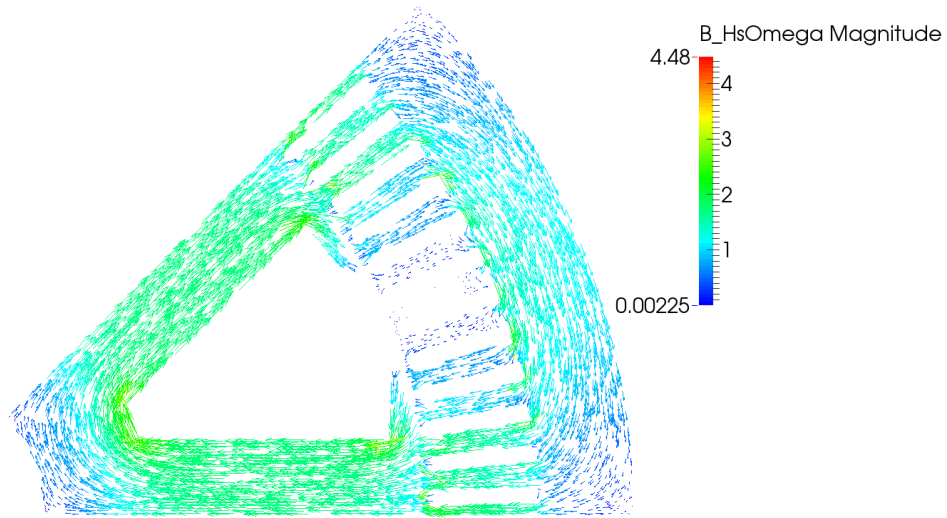
$$c = 0.261$$

$$\alpha = 6.81$$

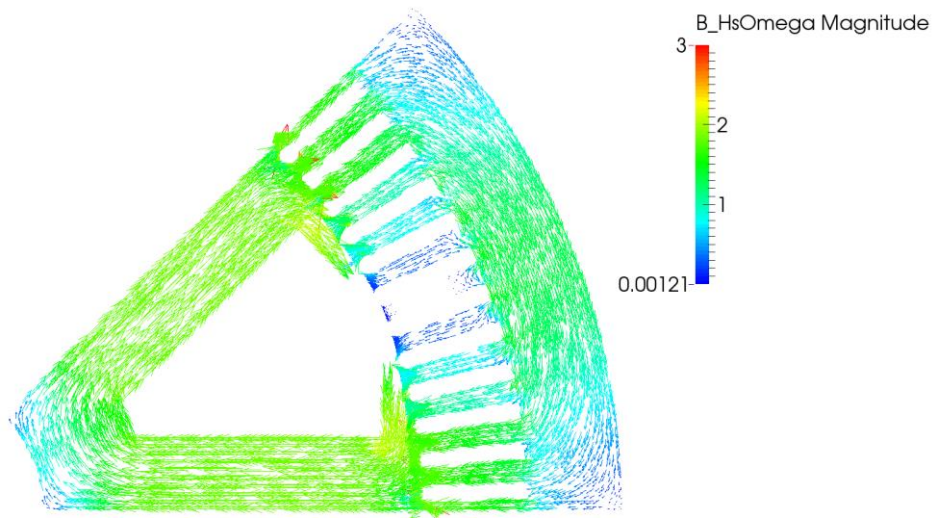
$$\tau = 68.7$$

The magnetic pole of the SPSG can clearly be seen, despite some leakage flux in the stator teeth in the middle of the machine. It must be noted that for the linear case, the magnetic flux density is quite high throughout the machine, with approximately 3.5 T in the rotor, and slightly less in the stator. However, when the nonlinear behaviour is considered, B is around 1.5 T in the rotor and the stator. This obviously reflects a practically more feasible working point than the linear case. The reason for which nonlinearity is often overlooked is because it is more tedious in setting up, especially for TO and also it increases the computation time.

As for the magnetic flux density in the air gap, Figure 4.7(a) illustrates the shape for a linear material behaviour, and Figure 4.7(b) for nonlinear. The radial B is considered in this case because the flow of flux through the air gap should be parallel to the radius of the machine. It can be seen that the peaks of B in the air gap for the nonlinear case are lower (1.2 T) than the linear case (1.6 T). But both have the same overall shape. The slot effect can be noted due to the presence of slots in the stator to accommodate the stator windings. This produces a drop in B at each slot, and a peak at each tooth. Due to this manufacturing constraint, the shape of the B in the air gap can never reach a perfect cosine curve. However, if the latter's shape must be optimised, it is judicious to consider the fundamental only, which should approach a cosine curve.



(a)



(b)

Figure 4.6 Spatial Distribution of B in the Machine with (a) Linear, (b) Nonlinear Material Behaviour

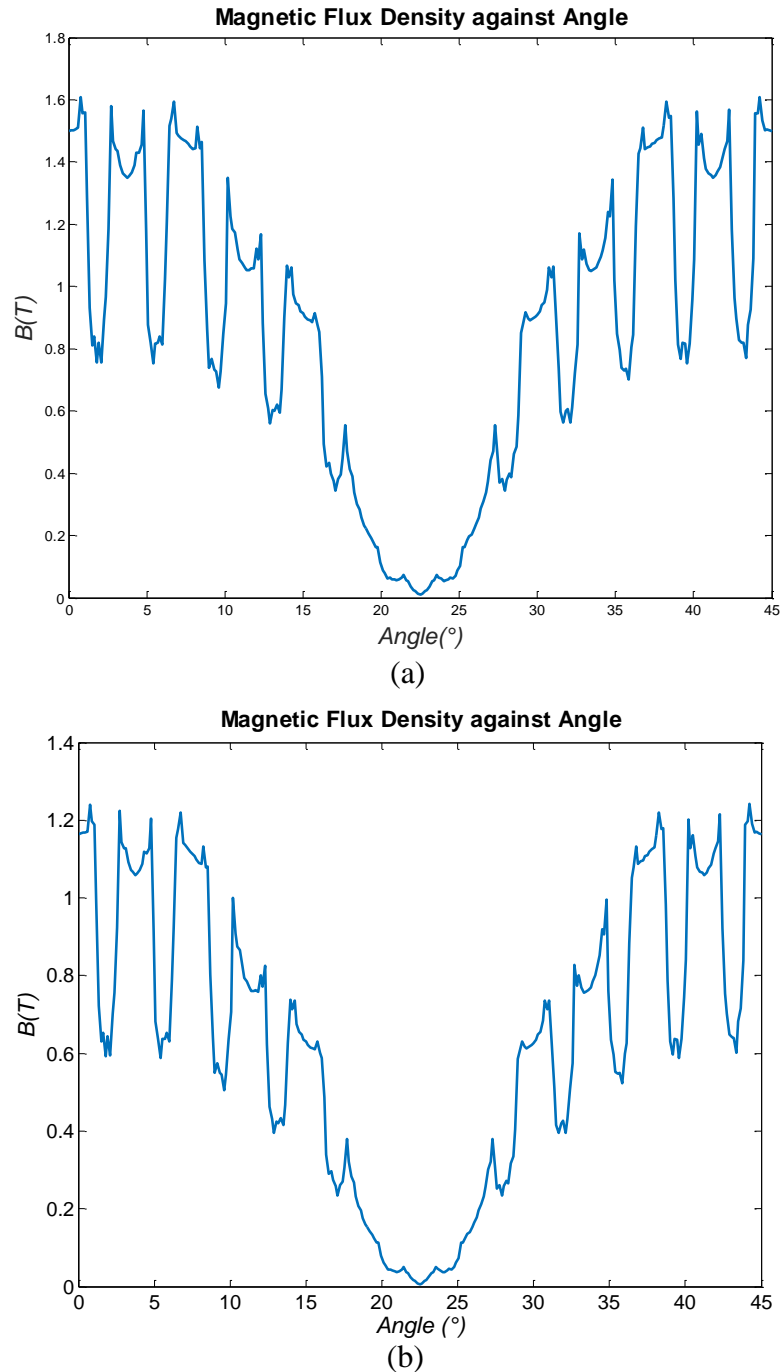


Figure 4.7 Magnetic Flux Density in Air Gap with (a) Linear, (b) Nonlinear Material Behaviour

After exploring the magnetic flux density in the original machine, the following section will now define the design space to be used for the TO of the rotor top.

### IV.3.2 TO of the Machine

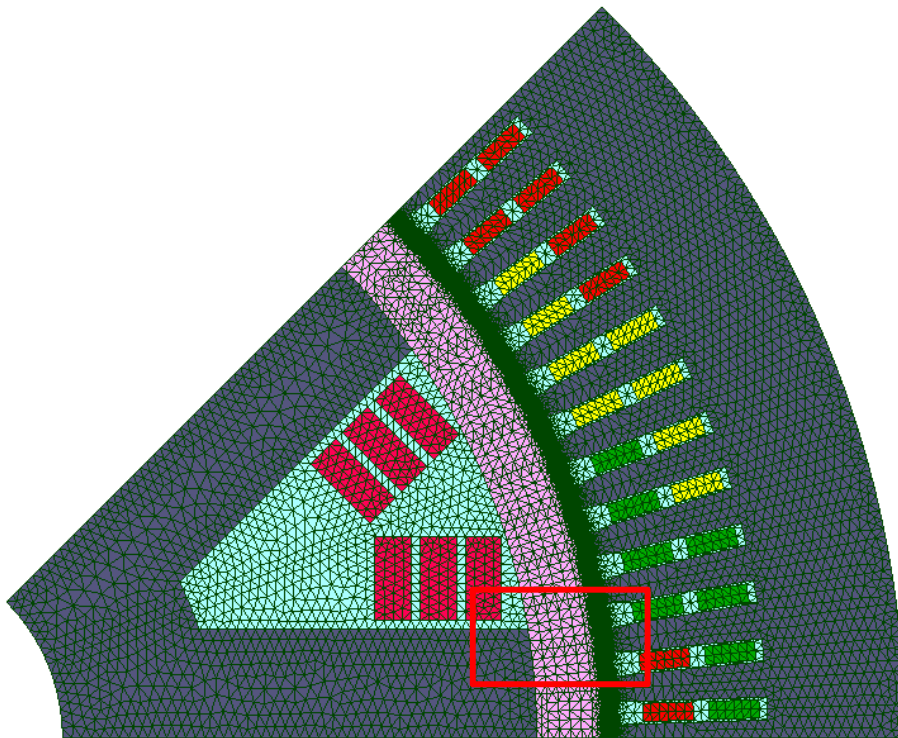
Following the concept of TO, it suggests that the optimal structure should be found from an unbiased empty design space. An optimised shape of the rotor top is sought, and hence the design area is as shown in Figure 4.8(a), shaded in pink. To keep a higher degree of freedom in the design space, the latter is allowed to span from one rotor pole top to the other. The



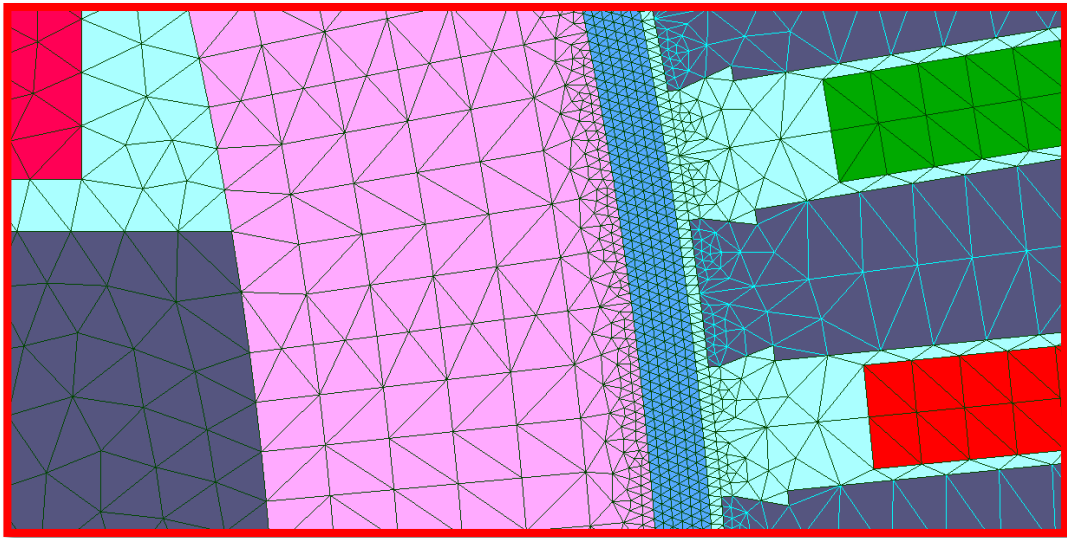
mesh size chosen here is similar to that of the original model for coherence. A fine mesh size is also used in the air gap, as in Figure 4.8(b) showing a zoom, since we will investigate B in the latter.

As for the discretisation of the optimisation domain, it is characterised by rectangular-shaped zones, as in Figure 4.8(c), where each zone is finely meshed. These zones are, in reality, curved bands but they do not appear so because of the slight curvature. The higher the discretisation, the more precise will be the results, but the lengthier will be the computation time. For this study, we will use 60 zones, which will correspond to the variables of the optimisation problem.

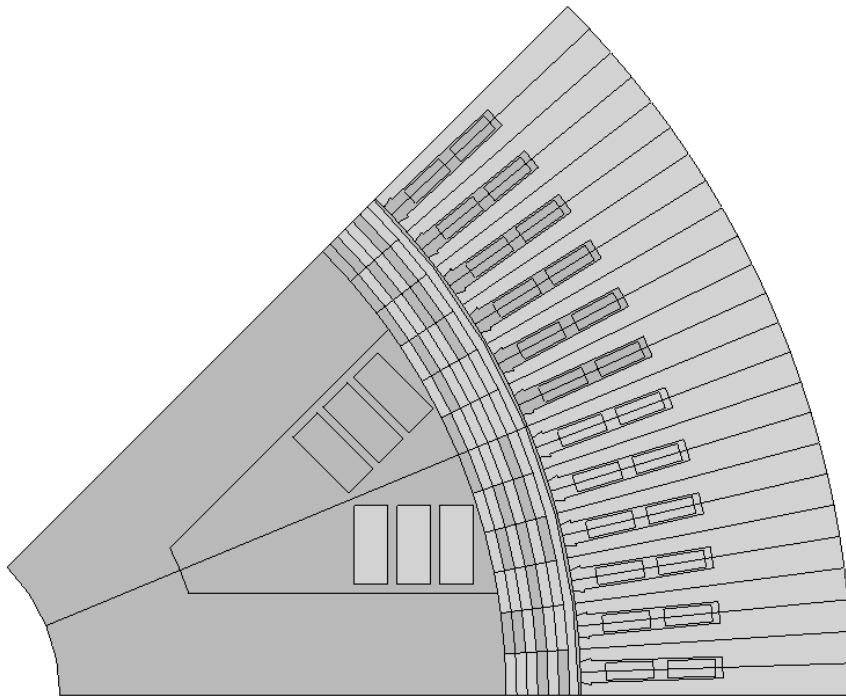
The advantage of using zones as variables (as in cubic test case of Chapter II) instead of finite elements (as in electromagnet of Chapter III) is to maintain an appropriate mesh size and accurate model, even when a low number of variables is used. This is useful for modelling of machines as a fine mesh is usually required, unlike other electromagnetic devices.



(a)



(b)



(c)

Figure 4.8 Domain to be Optimised (a) FE model, (b) Zoom, (c) Geometry

As for the original SPSG model, we will investigate some properties of the FE model with TO domain before engaging in any optimisation.

#### *Magnetic Flux Density in the Air Gap and Spatial Distribution*

It is interesting to investigate the magnetic flux density in the machine when the design space is made up of iron only. As for the original model, no-load simulations are performed, and the same magnetomotive force (excitation)  $n.i$  is used. All calculations are done in magnetostatics, using  $\Omega$  formulation. Figure 4.9(a) depicts the spatial distribution of B in the

machine linear materials behaviour, and Figure 4.9(b) for nonlinear behaviour. It can be seen that the values are excessively high, especially in the linear case where values of 100 T are attained in the design space. For the nonlinear case, smaller values are obtained (3 T), but they are nevertheless aberrant for physical feasibility.

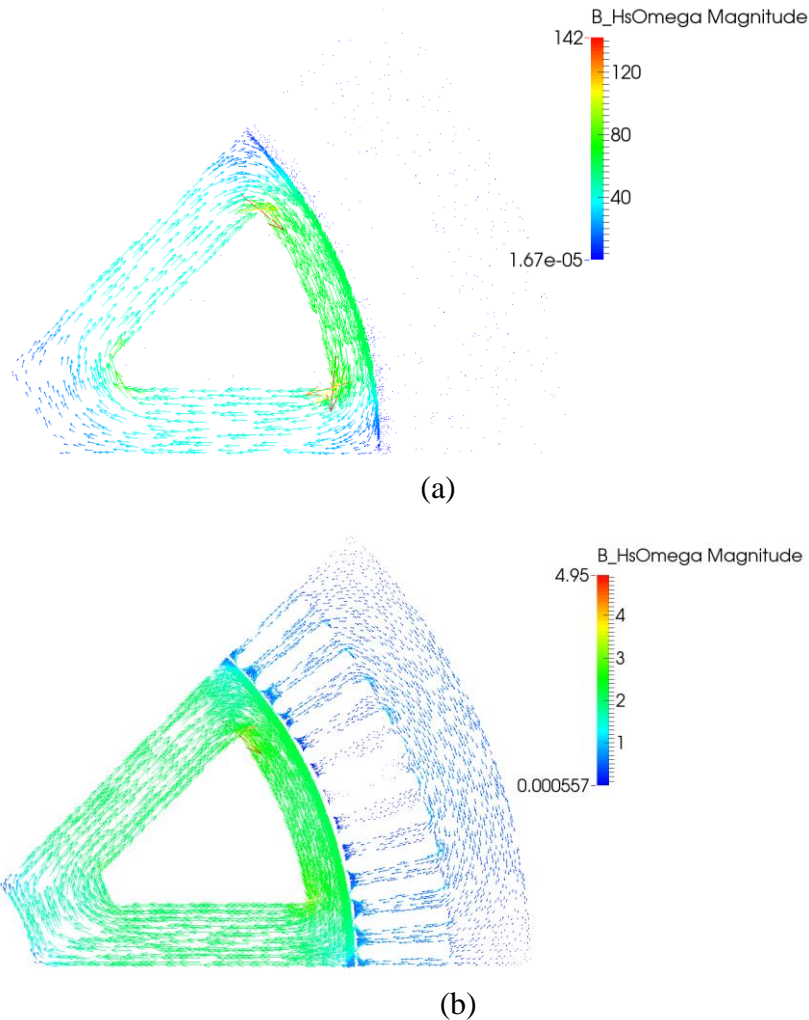


**Figure 4.9 Spatial Distribution of B in the Machine for (a) Linear, (b) Nonlinear Behaviour of Materials**

Figure 4.10 displays the shape of B in the air gap for both linear and nonlinear behaviours of the materials. We note that for both cases, we still obtain a sinusoidal shape of B, which very much resembles those of the original machine. But here, B is much lower, with peaks of around 0.5 T at the teeth for both linear and nonlinear cases. This occurs due to leakage flux passing through the air gap towards the stator. Therefore, care must be taken in avoiding such magnetic short circuit during TO so that erroneous topologies are not obtained, especially with linear behaviour of materials.

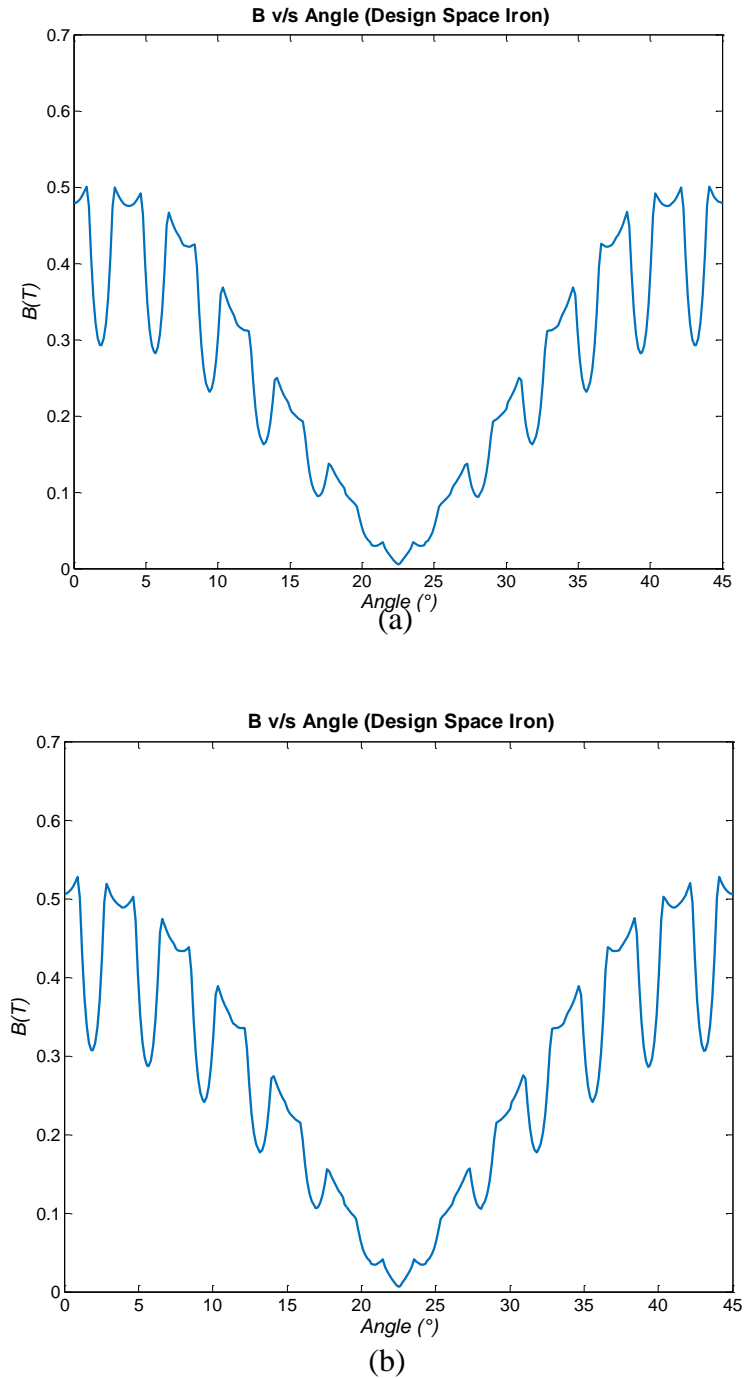


Figure 4.10 Magnetic Flux Density in Air Gap for (a) Linear, (b) Nonlinear Behaviour of Materials

After studying the characteristics to be optimised in the model, TO of the rotor top can now be undertaken, for both linear and nonlinear material behaviours. Two ways of formulating the objectives will be considered to generate new rotor shapes. Firstly, we will maximise the flux in the stator. And secondly, we will optimise the shape of B in the air gap.

## IV.4 Optimisation of SPSG

As a quick recap, the TO process will be concisely presented in this section, based on what has already been seen in Chapter II. Nonetheless, an additional step will be added to the process in this case, which is detailed as well.

Subsequently, the TO of the rotor top will be detailed, using two different objectives. For each, the formulation of the problem will be explained, as well as the reason why this particular setting is considered. Afterwards, an analysis of the TO results obtained will be made, with both linear and nonlinear materials. All calculations are done in magnetostatics, using  $\Omega$  formulation.

In a first phase, the flux in the stator will be maximised. This amounts to acting on a global value of the model during optimisation. The topologies and spatial distributions of B will be presented and analysed.

Secondly, the magnetic flux density in the air gap will be optimised. This corresponds to acting on local values of the model during optimisation. The shape of B and the corresponding topologies will be examined.

This will allow us to have a wider overview of how the system behaves depending on the type of optimisation problem defined. Acting on local and global values can produce totally different results, and this aspect will also be discussed.

### IV.4.1 Recap of TO Process

The overall process has already been seen in Chapter II, but for the SPSG model, an additional step is added. The block diagram summarising the process is given in Figure 4.11. The methodology proposed with the density mapping and the FF is used, and the FE model is subjected to the TO using the tools. After the optimisation process, a TO filter is used to smooth out the model obtained. This goes towards the explanation of filters in Chapter I to eliminate some undesired effects such as checkerboard, intermediates, and so on. The use of filters is optional in the process, and will be pointed out whenever it is used. Thereafter, the final model is obtained.

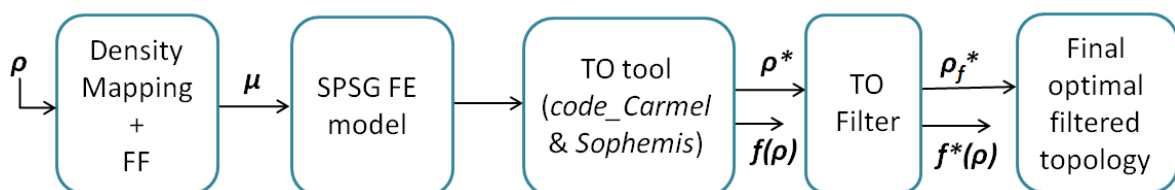


Figure 4.11 Block Diagram for Overall TO Process

### TO Filter

The TO filter in our case will serve to eliminate the isolated materials that can sometimes occur in a topology after optimisation, and hence smooth out the topology. It is mainly based on the Neighbourhood Filter explained in [9], and the works of [71]. It acts on the densities of the structure obtained after optimisation, and uses the sum of each zone's 'neighbours' to determine whether it is isolated or not. To understand how the neighbours of each zone are considered, we shall first consider their numbering, as in Figure 4.12. To consider the neighbours of a zone, we will use zone 5 as example. The 8 zones surrounding it are considered as its neighbours, with the directly adjacent ones being zones 2, 4, 6 and 8, and the diagonal ones being zones 1, 3, 7 and 9. When considering the zones lying on the edges, the number of neighbours might be 3 or 5, depending on the position of the former.

3	6	9	12	15
2	5	8	11	14
1	4	7	10	13

Figure 4.12 Zones Numbering

For each zone  $\rho_z$ , the density sum  $\rho_{sum}$  is calculated from its neighbours, as in (IV-1).

$$\rho_{sum} = \frac{1}{(r + t)} \left( \kappa \sum_{i=1}^r \rho_{adj_i} + \sigma \sum_{j=1}^t \rho_{diag_j} \right) \quad (IV-1)$$

Where  $r$  and  $t$  represent the number of adjacent and diagonal neighbours respectively, and  $\rho_{adj}$  and  $\rho_{diag}$  represent their respective densities. The coefficients  $\kappa$  and  $\sigma$  correspond to the weightage given to each type of neighbour. The adjacent zones are given a high weight, and the diagonal ones, a lower weight. The values retained in our case are  $\kappa = 1$  and  $\sigma = 0.8$ . These coefficients are kept high so that only very isolated densities are changed. We will see later in this section how the choice of coefficients can affect the overall topology. To determine whether the density of a zone  $\rho_z$  is isolated, and therefore must be changed, we apply the conditions in (IV-2).

$$\rho_z = \begin{cases} 0, & \text{if } \rho_{sum} \leq v \\ 1, & \text{if } \rho_{sum} \geq w \\ \rho_z, & \text{Otherwise} \end{cases} \quad (\text{IV-2})$$

The values of  $v$  and  $w$  should be close to zero and 1 respectively so that it doesn't largely alter the topology obtained after filtering.

To give an example of how the TO filter is applied, we will use the topology in Figure 4.13(a), obtained after optimisation. The  $\rho_{sum}$  for each zone are given in Figure 4.13(b), and the values of  $v = 0.05$  and  $w = 0.95$  are applied to the conditions in (IV-2) to give the filtered topology of Figure 4.13(c). The latter eliminates only the isolated zone on the middle right hand side, but does not alter much the actual topology. A case of altered topology would be in Figure 4.13(d), if the limiting conditions of the filter were relieved further by setting  $v = 0.1$  and  $w = 0.9$ , for instance. This could be desirable in some cases, depending on the problem. Hence, care must be taken when defining the coefficients of the filter.

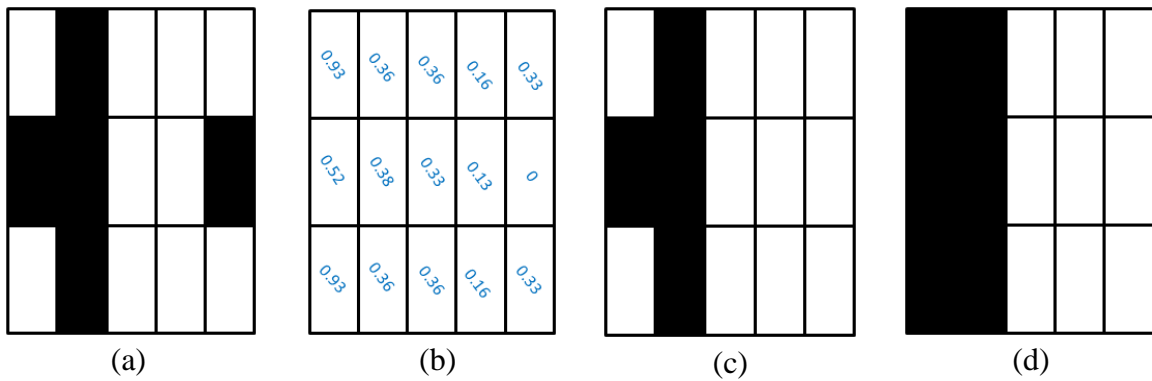


Figure 4.13 (a) Topology Before Filter, (b)  $\rho_{sum}$  for each zone, (c) Filtered topology with  $v = 0.05$  and  $w = 0.95$ , (d) Filtered Topology with  $v = 0.1$  and  $w = 0.9$

#### IV.4.2 Maximisation of B in the Stator

The point in maximising B in the stator is to keep a good conservation of flux in the magnetic pole, i.e. from the rotor through the stator teeth, to the yoke, and back to the rotor. An optimal distribution of B in the machine is therefore sought through this optimisation. This can be assimilated as optimising a global characteristic of the structure. The problem is formulated as in (IV-3). The value of  $n$  represents the number of points at which B is calculated, used in the optimisation. Dividing the summation term by  $n$  allows one to stay within the same range as FF. The values for the coefficients used are  $\gamma = 1$  and  $\lambda = 0.5$ . The latter were chosen following some optimisations with different values of the coefficients, and those ones seemed to work best for our model.

$$\min_{\rho} \left( -\frac{\gamma}{n} \sum_{i=1}^n B_i(\rho) + \lambda \cdot FF(\rho) \right) \quad (\text{IV-3})$$

The magnitudes of B are considered at the yoke as shown in Figure 4.14. The resulting topologies obtained with linear and nonlinear material behaviour are given in Figure 4.15(a) and (b) respectively, as well as their corresponding spatial distribution of B in (c) and (d). No filter was used in this case.

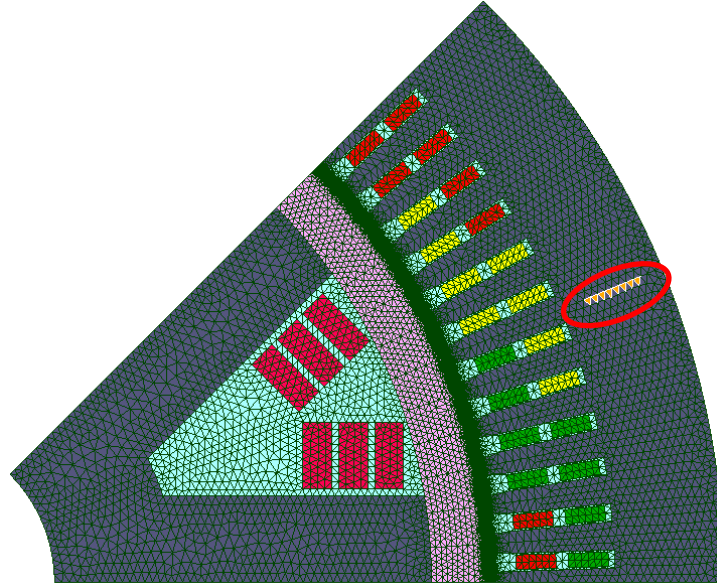
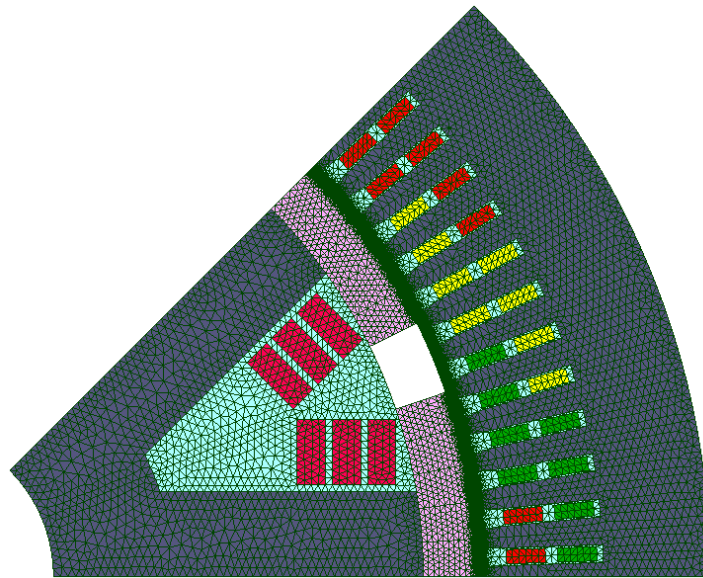
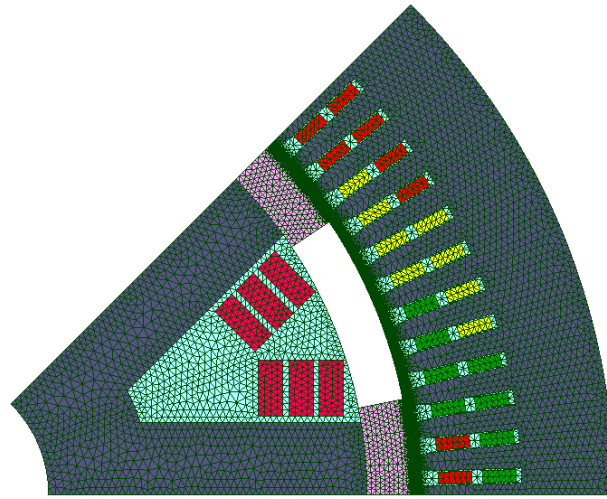


Figure 4.14 Maximisation of B in the Stator Yoke

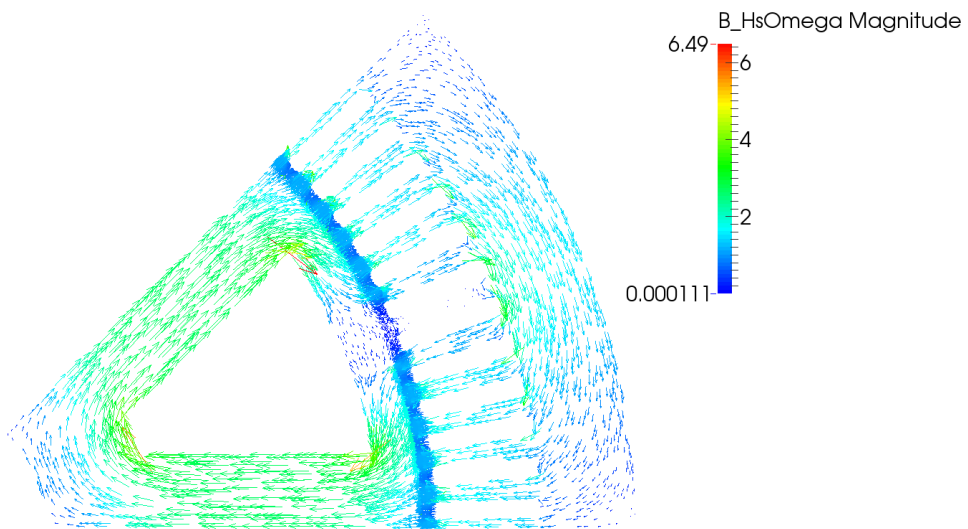


(a)

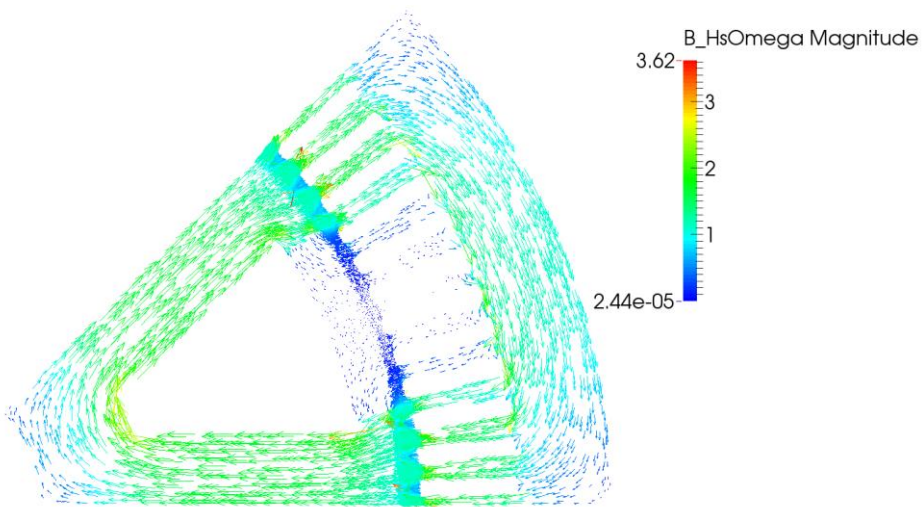




(b)



(c)



(d)

Figure 4.15 Topologies in (a) Linear, (b) Nonlinear, B Distribution in (c) Linear, (d) Nonlinear

We can see that both topologies are coherent, w.r.t the type of materials considered. In both cases the magnetic flux flows through the stator yoke and back to the rotor to create a magnetic pole. On the other hand, with linear materials we can see that the values of  $B$  can rise up to above 4 T while for the nonlinear case, the values are around 2 T.

This analysis puts forward, in a first round, the fact that topologies can be obtained with linear materials but are not necessarily a good choice for an electromagnetically feasible one. Furthermore, the maximisation of flux in the yoke does not yield a detailed topology of the rotor top, but rather a block approximation of what should be obtained. Therefore, a different optimisation problem should be formulated if one wants to have a better topology. Hence, we will investigate the optimisation of the magnetic flux density in the air gap.

#### IV.4.3 Optimisation of Magnetic Flux Density in Air Gap

The desired shape of the magnetic flux density in the air gap of a rotating machine is usually sinusoidal. But due to the slot effect as evoked earlier, only the first harmonic of the shape of  $B$  can be close to a sinusoid. In this study, we will impose a sinusoidal shape of  $B$  in the air gap as optimisation target. Figure 4.16 shows the sine curve imposed, where the modulus of the values is considered.

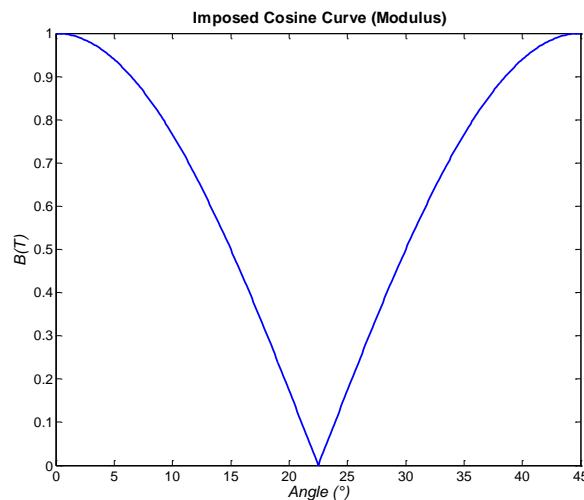


Figure 4.16 Modulus of Sine Curve Imposed

The optimisation problem is defined as in (IV-4). For the results to be as accurate as possible, the difference between the desired and obtained values is normalised w.r.t the desired values, and the square of the normalised difference is calculated. The latter's sum is calculated for all the desired spatial points.

$$\min_{\rho} \left( \frac{\gamma}{n} \sum_{i=1}^n \left( \frac{B_i(\rho) - B_{obj_i}}{B_{obj_i}} \right)^2 + \lambda \cdot FF(\rho) \right) \quad (\text{IV-4})$$

The optimisation of the rotor top for the linear material behaviour is presented first for a few cases, and subsequently the results for the nonlinear behaviour are shown.

#### IV.4.3.1 Linear behaviour of Materials

In this section, we will perform the optimisation with 2 different numbers of spatial points in the air gap: 73 and 13. The reason for the 73 points is to take into consideration the slot effect during optimisation, while the 13 points is to filter the first harmonic, hence avoiding the slot effect. The aim of this section is to see how the model behaves in different cases when the problem is posed differently. Some results can be very appealing in terms of topology but less in terms of convergence, or vice versa.

##### A. Case 1 – 73 Spatial Points

We want to optimise  $B$  in the air gap at 73 spatial points, as shown in Figure 4.17(a). The convergence of the main objective (sum of  $B$ ) is given in Figure 4.17(b). The unfiltered results are given in Figure 4.18, and the filtered ones in Figure 4.19. The number of evaluations done to reach this solution is 2350, and the time taken is 3.36 h. The final value of  $FF = 0.04$ , which is close to zero, and therefore means that all the densities have converged to 0 or 1. Also, the convergence of the objective function is coherent. But the values do not lie between 0 and 1 here despite normalisation of the  $B$  in the optimisation problem. This occurs if the values of  $B(\rho)$  obtained in the optimisation process is much greater than the objective value of  $B_{obj}$ , say by more than twice. By calculation, we can see that the squared normalised difference can go beyond 1. But this does not affect the optimisation process as long as it stays within the same range as the  $FF$ .

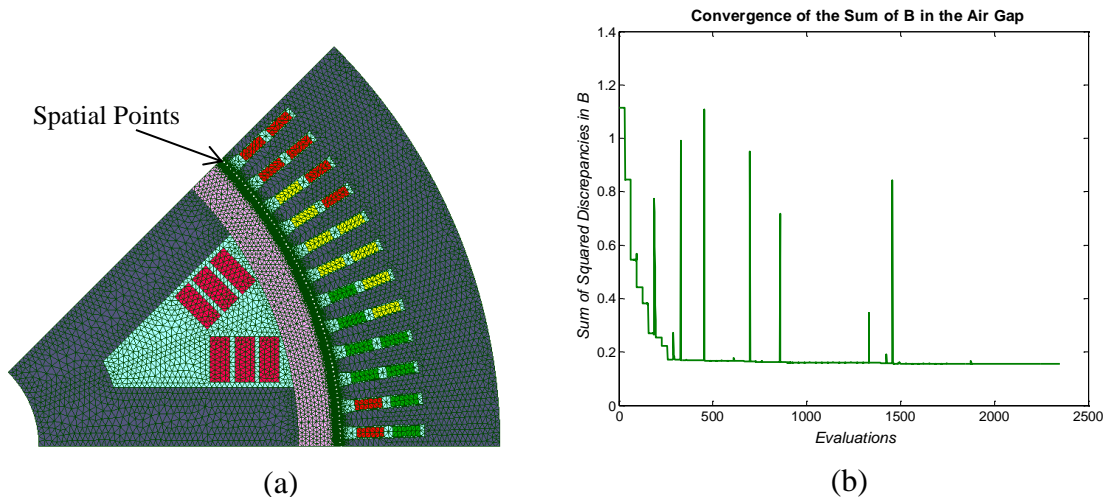


Figure 4.17 (a) Spatial Points, (b) Convergence of Objective

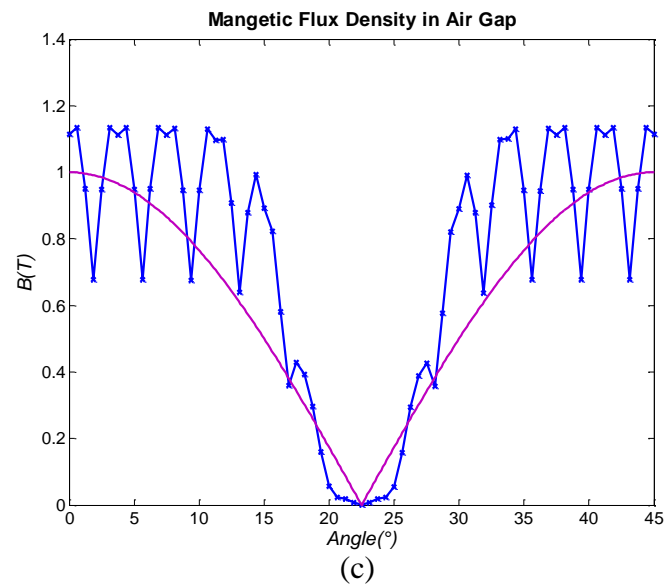
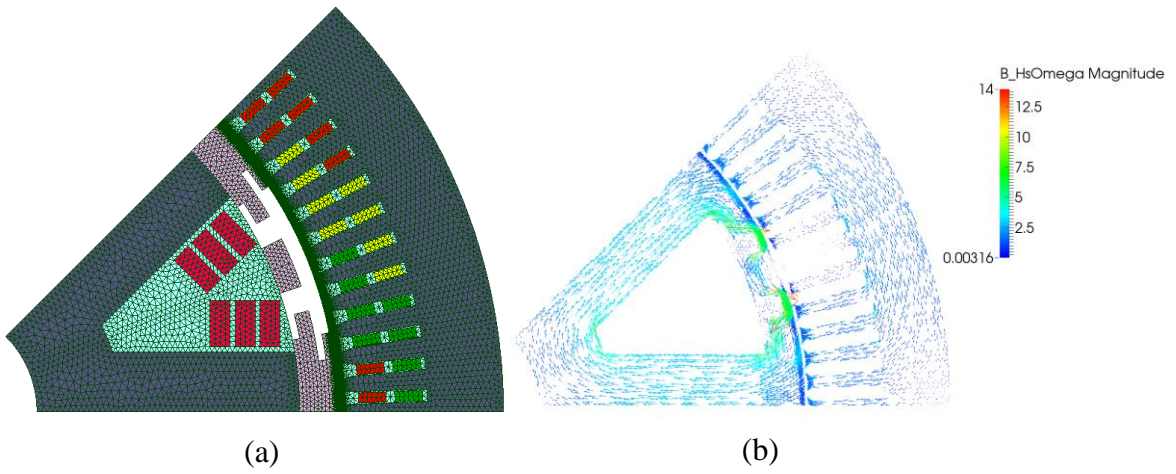
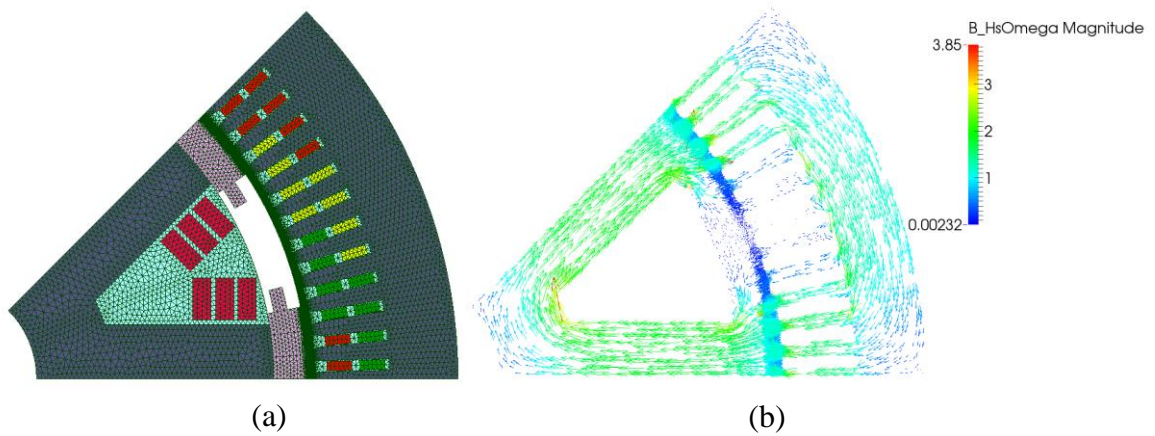


Figure 4.18 Unfiltered Results (a) Topology, (b) B Distribution, (c) B in Air Gap



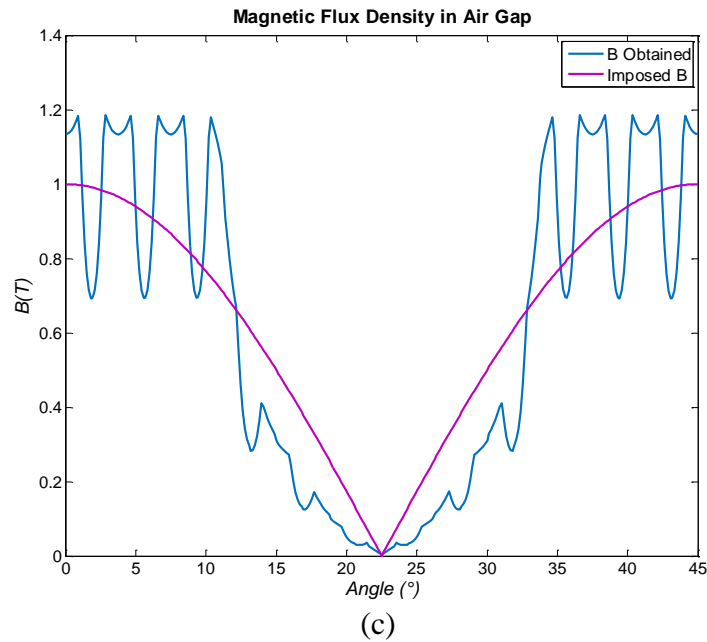


Figure 4.19 Filtered Results (a) Topology, (b) B Distribution, (c) B in Air Gap

The unfiltered topology contains a block of iron in the middle which, according to the algorithm, contributes in bringing the values of  $B$  in the air gap near this block to zero. We note that many points of  $B$  obtained lie on the sine curve imposed. The results are numerically correct, but are questionable from an engineer's point of view. Therefore, when the topology is filtered, we also take into account the manufacturing difficulty of the block in the middle. It is hence removed to get the new topology. We can see that the overall curve still follows the sine curve, but the results are blurred by the slot effect. This makes it quite hard to assess the values obtained for  $B$ . Hence, to undermine this obstacle we will use only 13 spatial points in the air gap, where one is taken opposite each tooth, so that the slots are avoided.

### B. Case 2 – 13 Spatial Points

With the slot effect avoided in the optimisation, some topology results are presented with the same problem formulation as above. Here again, the efficiency of the results can differ largely. For example, an optimisation can converge very nicely to a good solution, but the topology obtained can be totally irrelevant, or vice versa. Case B will present one example for each.

#### Example 1 – Average Convergence with Relevant Topology

The 13 spatial points in the air gap are shown in Figure 4.20(a), and the convergence the main objective (sum of  $B$ ) is given in Figure 4.20(b). Note that the spatial points on the figure are enlarged for visibility, but they are actually the same size as in Figure 4.17(a). The

unfiltered results are given in Figure 4.21, and the filtered ones in Figure 4.22. The number of evaluations is 964, with  $FF = 0.01$ , and the calculation time is 1.4 h.

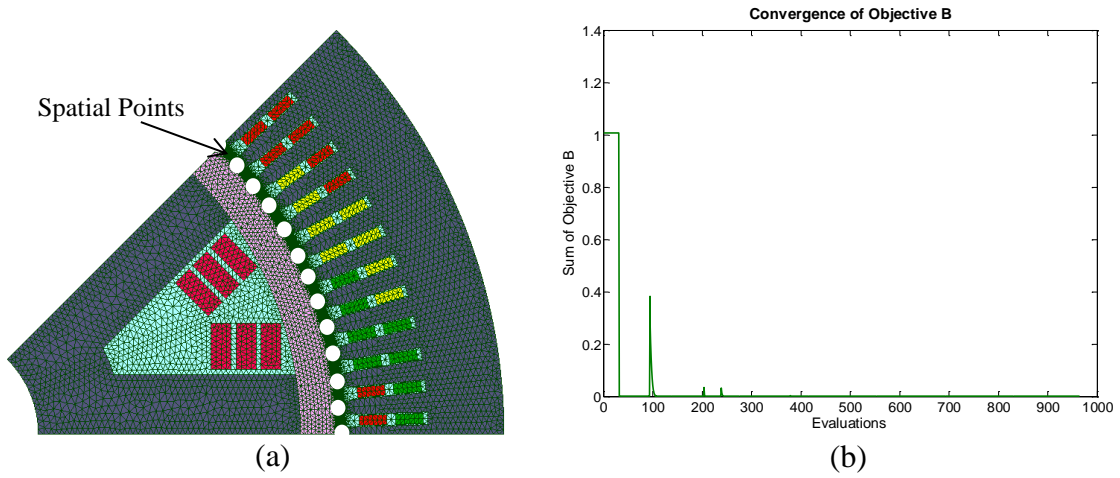


Figure 4.20 (a) Spatial Points, (b) Convergence of Objective

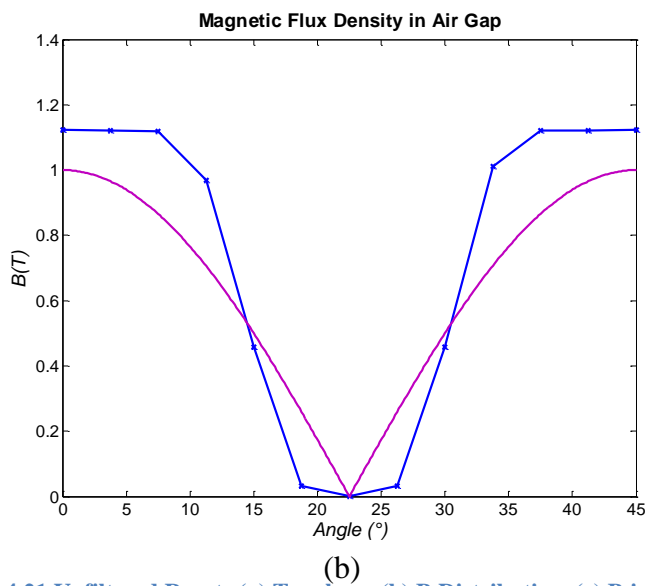
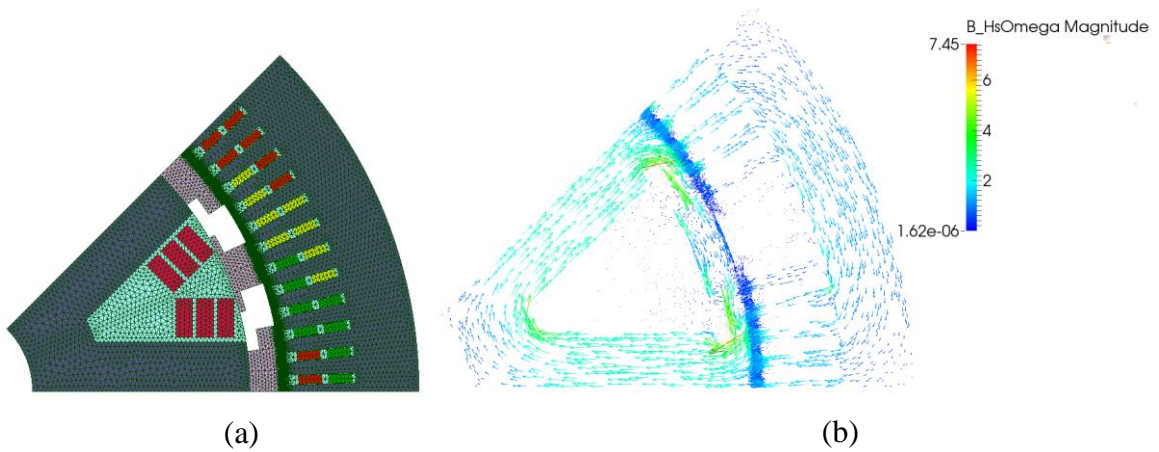


Figure 4.21 Unfiltered Results (a) Topology, (b) B Distribution, (c) B in Air Gap

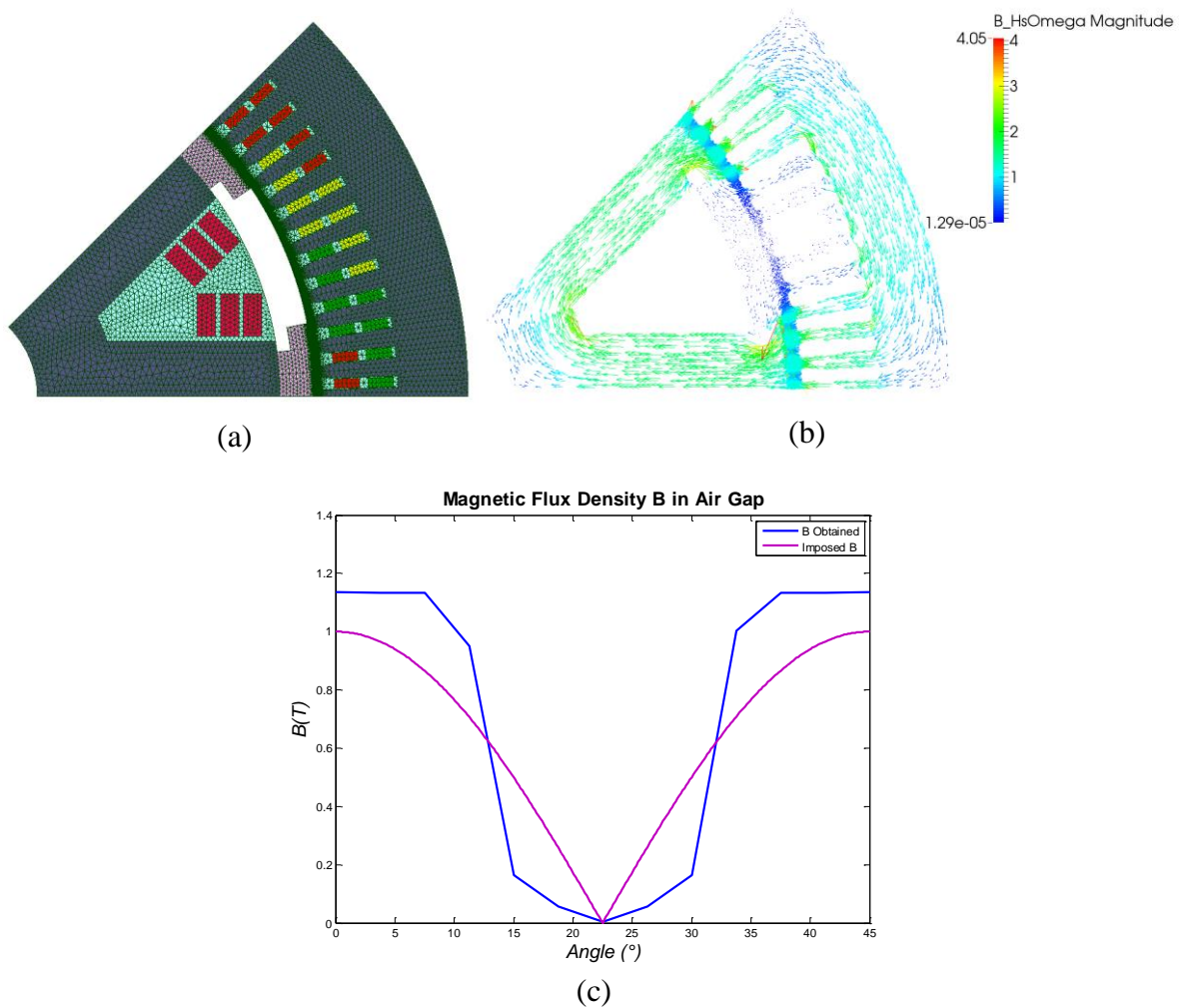


Figure 4.22 Filtered Results (a) Topology, (b) B Distribution, (c) B in Air Gap

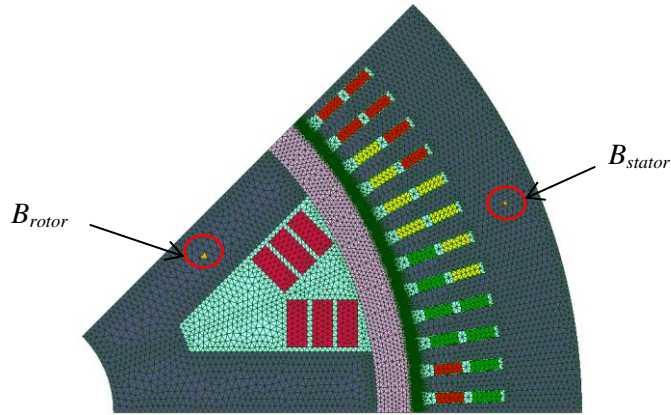
We note that for the unfiltered results, an iron block is again placed in the middle of the rotor tops to prevent leakage flux in the air gap in this region. The numerical results follow a sine curve trend. On the other hand for the filtered results, we eliminate the material in the middle, but there are no extreme changes in the values of  $B$  obtained. Nonetheless, it contributes to reducing the magnetic flux density in the machine as they drop from 4 T to 2.5 T. These values are normal for a linear behaviour, but would be rather infeasible for a nonlinear behaviour of materials, as in reality.

#### Example 2 – Good Convergence with Poor Topology

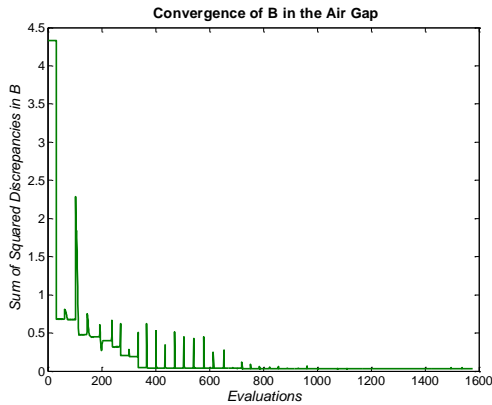
In this example, we subject the problem to a constraint on  $B$ , as given in (IV-5). It suggests that the flux flowing in the stator should be at least 90% of that flowing in the rotor. The points in the stator yoke and rotor are shown in Figure 4.23(a). The idea is to prevent leakage flux in the design space. The results are given in Figure 4.23, where (b) gives the convergence

of the objective, (c) plots the values obtained on the sine curve, (d) depicts the topology obtained, and (e) the B distribution. The results are not filtered in this case. The number of evaluations is 1577, with  $FF = 0.1$ , and the computation time is 2.27 h.

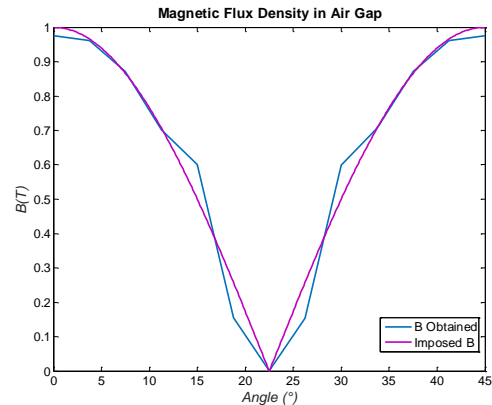
$$\begin{cases} \min_{\rho} \left( \frac{\gamma}{n} \sum_{i=1}^n \left( \frac{B_i(\rho) - B_{obj_i}}{B_{obj_i}} \right)^2 + \lambda \cdot FF(\rho) \right) \\ \text{s. t. } \mathbf{B}_{stator} \geq 0.9 \times \mathbf{B}_{rotor} \end{cases} \quad \text{(IV-5)}$$



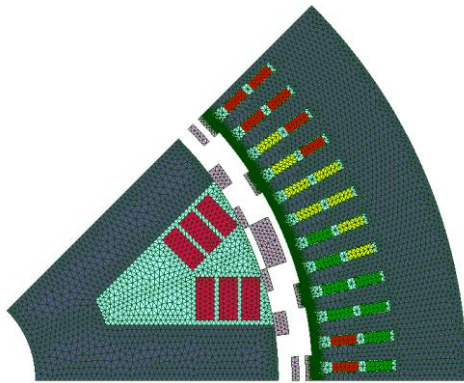
(a)



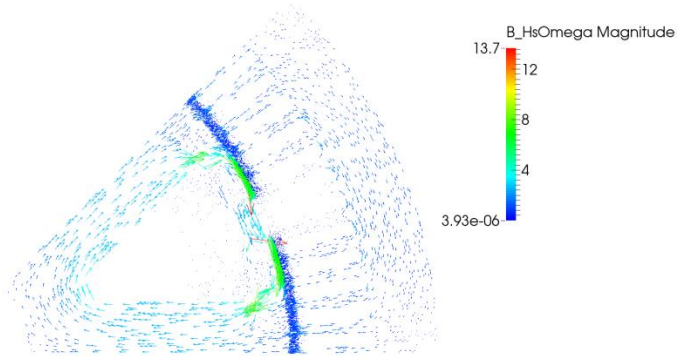
(b)



(c)



(d)



(e)

Figure 4.23 For 13 Spatial Points (a) B in Stator and in Rotor Used in Constraint (b) Objective Convergence, (c) B in Air Gap with 13 points, (d) B in Air Gap with 73 points, (e) Optimal Topology



The values of  $B$  obtained correspond to the imposed sine curve, as in Figure 4.23(c). The numerical optimisation results are correct, but the topology obtained is quite unfeasible from an engineering viewpoint (Figure 4.23(d)), despite a coherent distribution of the magnetic flux density in (e). The reason behind this type of behaviour is due to the linearity of the materials. It is therefore interesting to see what a nonlinear material behaviour could change in the results.

#### IV.4.3.2 Nonlinear Behaviour of Materials

The same optimisation problem as in (IV-4) is used. The initial conditions are the same, and the number of spatial points on the air gap is 13. The results are given in Figure 4.24. The number of evaluations 765, for a total time of 5.21h, and with  $FF = 0.09$ . Figure 4.25(a) shows that the objective converges to a good solution, and (b) shows the magnetic flux density  $B$  in the air gap for the 13 spatial points optimised. We can see that the curve imposed is respected. Also, we can see that the unfiltered topology has a block of iron in the middle but the distribution of  $B$  is coherent. The values of  $B$  are around 2 T, which corresponds to a real case example.

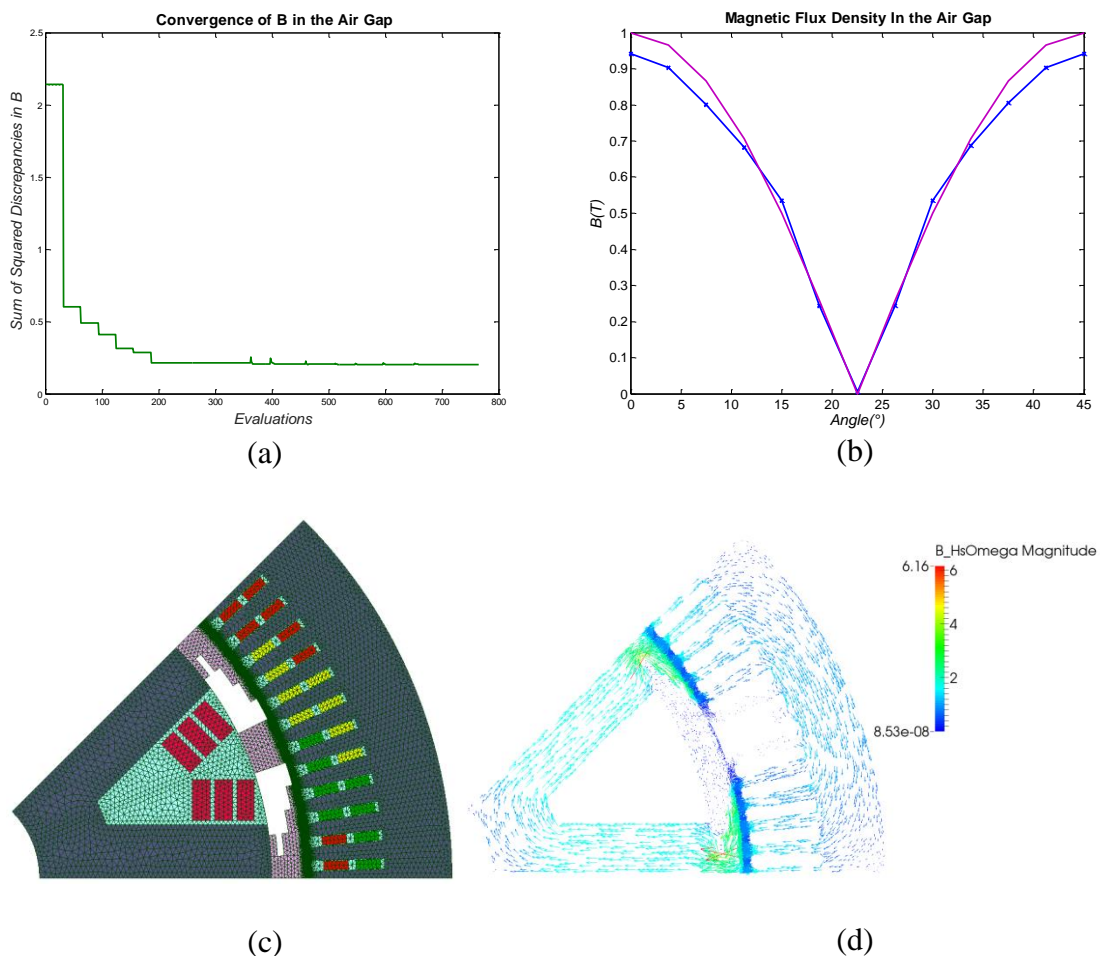


Figure 4.24 (a) Convergence of Objective, (b)  $B$  in the Air Gap, (c) Unfiltered Topology, (d)  $B$  Distribution

The results for the filtered topology are depicted in Figure 4.25. The topology corresponds to a feasible one, as well as the magnetic flux density distribution. Some high values of  $B$  are reached during the simulation, but the values in the air gap are still coherent with the imposed sine curve.

If we consider the percentage of flux that is conserved from the rotor to the stator, for the unfiltered case it is 65%, while for the filtered case it is 72%. On the other hand, the sum of the objective term involving  $B$  at the end of the convergence is 0.20 for the unfiltered case (Figure 4.24(a)), but if the results are filtered, the value of the objective would be 0.51. This shows that the optimisation results are good, but the filtering is sometimes necessary to have a feasible final structure.

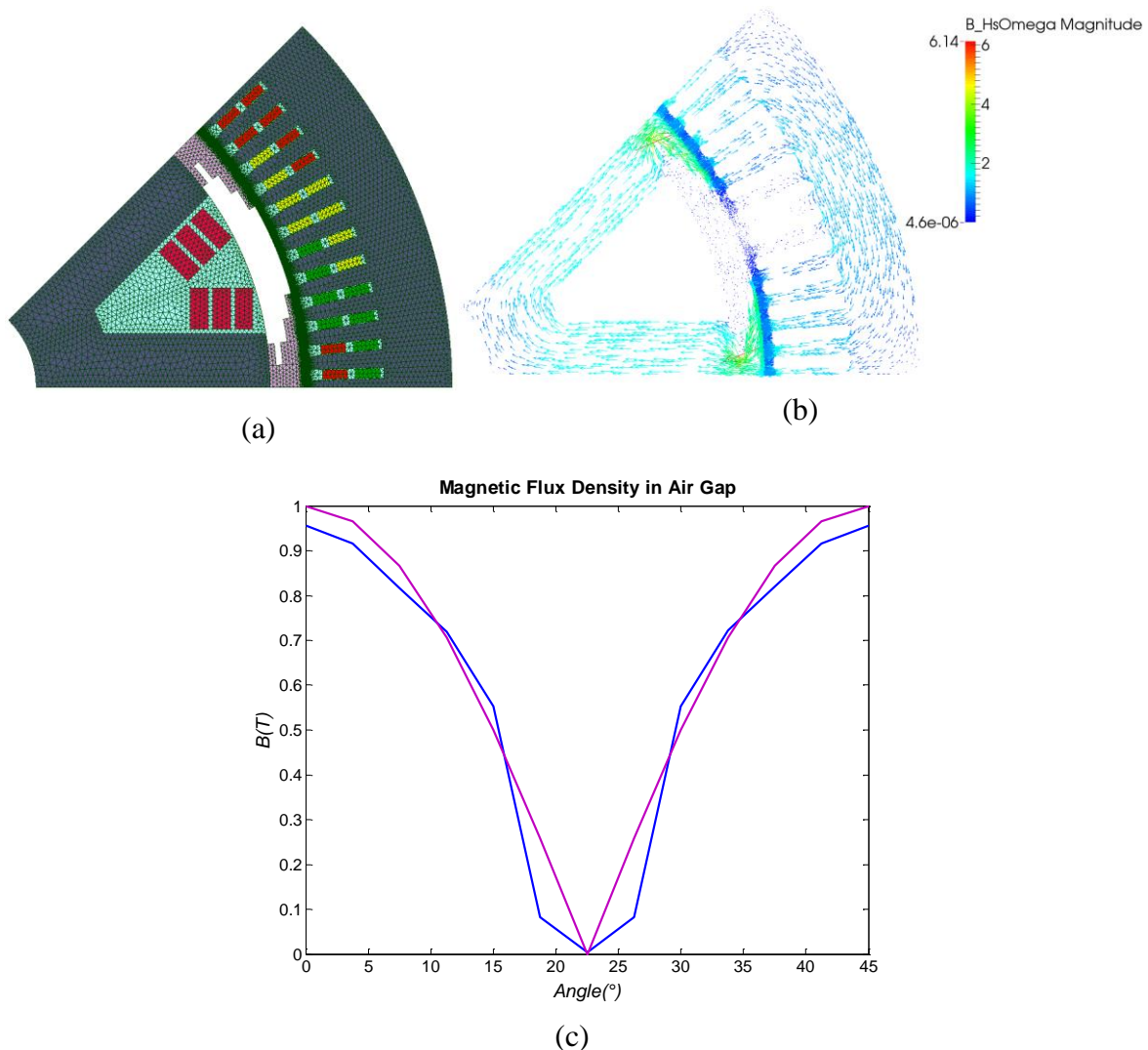


Figure 4.25 (a) Filtered Topology, (b)  $B$  Distribution, (c)  $B$  in the Air Gap

From our findings, we can conclude that the TO of complex structure such as electrical machines are not straightforward due to different factors characterising the latter. This infers

that, to optimise a particular region of a machine, many aspects can be considered but the results will vary depending on the former. As for the SPSG, one shape of the rotor top was obtained when we maximised the flow of flux in the stator, but a different was obtained when the shape of B was optimised in the air gap. We have also seen cases where the numerical solutions had correctly converged to an optimal solution, but the topologies were completely infeasible from an engineer's point of view.

To add another level of complexity to the problem, the topologies also varied when nonlinear material behaviour was used. This demonstrates that optimality of a single parameter cannot be considered in the case of machines to optimise the structure. This means that the problem should be highly multi-objective for a truly optimal structure. And if a fine discretisation is also desired, this adds up in the computation time. All these factors render the TO problem even more complex, and should invoke greater attention during the formulation of the problem. We have nevertheless presented some of the interesting results obtained during this thesis work, which are correct for the objectives chosen. But a more varied number of objectives should be taken into account to confirm or alter the topologies obtained.

## IV.5 Summary and Contributions

In this chapter, we have put forward the application of the TO methodology to a Salient Pole Synchronous Generator to yield various rotor topologies while optimising the magnetic flux density distribution in the machine. The original SPSG was primarily investigated for its various characteristics, and the design space chosen to perform TO was detailed. The calculations were performed for both linear and nonlinear behaviour of the ferromagnetic materials. Different formulations of the optimisation problem were investigated.

We have seen that the TO is very dependent on how the problem is posed. It can yield very good convergences to solutions, but with infeasible topologies from an engineer's point of view, but it can also yield the complete opposite. This was the first strength of this chapter as it served to demonstrate how topologies can differ from objective to objective. None is wrong, but for utmost optimality, all should be considered at once. Obviously, this is impossible in practical for an optimisation process, which present the greatest limitation of TO.

Furthermore, we have shown how the nonlinear materials behaviour can produce drastic changes in the results when compared to the linear case for the same problem, especially for machines. This aspect has often been overlooked in numerous works on TO in electromagnetism, as it might be more mathematically challenging, requiring a longer computation time. But it remains a turning point in this type of problem as seen in the results presented. This was the second strength of this chapter as it has emphasised on this matter, with various examples. Interesting topologies of a rotor top have also emerged from our calculations, and it would be interesting to further investigate the behaviour of other characteristics of the machine with such a topology.

Consequently, a more careful framing of the problem is essential to assume coherence of the results. Obviously, one cannot have absolute success during the first trials, but the latter should serve to direct the user towards a better solution while understanding the behaviour of the process.

# Conclusion

---

## Summary and Contributions

The objectives set at the beginning of this thesis work have been met, albeit not without various obstacles. The foremost task, which was to develop a functional TO tool from the 'home-made' FE and optimisation tools, has been completed and tested with a parameterised academic test case. In the same process, a TO methodology was developed, based on the existing TO methods in literature, and the latter's weak points such as the occurrence of intermediate variables in the final structures and lengthy computation times were mitigated. This represents our first contribution to the complex subject that characterises TO.

Furthermore, we have also introduced the nonlinear behaviour of the ferromagnetic materials in the TO process, which is not very common in TO literature. It was tested and compared with the case where a linear material behaviour is used for 2 cases: the 3D electromagnet, and the Salient Pole Synchronous Generator. Despite increasing the computation time of the model, the results obtained were better and represented a more feasible electromagnetic structure as real material characteristics were taken. This constitutes a second major contribution of our work to yield more realistic topologies.

Finally, the rotor top of the SPSG was optimised w.r.t various problem formulations, and various topologies were presented. It enabled us to see how an ill-posed problem in TO could produce correct solutions in terms of optimisation calculations, but incoherent topologies in terms of feasibility of the structures. This work can serve to direct other topology optimisers in taking the necessary actions when posing a TO problem to inhibit unwanted structures from occurring.

To show the other side of the coin, it is also interesting to evoke the many obstacles met throughout the course of this work. The main difficulty was in the setting up of the TO tool, as it involved the coupling of two different software, programmed in different languages. Their compatibility was not obvious, and many runs were required before coming up with a functional tool. Moreover, since it was the work on the subject within the laboratory, we could not benefit from past experiences, and hence kick-starting the project and acquiring necessary skills was rather long. Additionally, we were confronted with the high computation times for TO simulations, and this was also a major burden to the subject. Despite all these hurdles, the main goal of the work was accomplished. But as in any other work, there is always scope for more, and therefore a few perspectives can be suggested.

## Perspectives

It would be interesting to further explore the works that have been carried out during this thesis. This includes the methodology, the tools, the electromagnet, and the SPSG.

### *Methodology*

Regarding the TO methodology, new strategies for convergence to a global optimum could be tested. For example, we could favour a hybrid algorithm, starting from a Genetic Algorithm to find a global optimum, but limiting the number of generations so that a rough solution is approached. In a second phase, a local algorithm such as *fmincon* SQP could be applied to approach a better solution. Other strategies such as more developed filters in the TO process could be implemented when complex devices are optimised.

Relative to the management of the variables, we could test further techniques. For instance, we could use a two-step approach: in a first phase, the variables are considered as zones (as for cubic case and SPSG), and in a second phase, we could consider only regions that need fine-tuning and therefore use the finite elements in those regions as variables. This two-step process would allow us to keep the same mesh size, but still refine the results with a smaller discretisation.

### *Tool*

As for the TO tool, an effort could be invested rendering it more user friendly so that any non-expert user could test his own strategies. We are already currently working towards point at the L2EP with a new local platform (*SophemisTopo*) with a few FE test cases available, such as the cubic case, the electromagnet, the SPSG and a rectangular reluctance network. A user can submit a TO algorithm to the platform, and choose any of the models for testing. A classification is done with the various results, with the strategy producing the best topology in terms of convergence of objective, no intermediates, computation time, feasibility and robustness ranked first.

### *Applications*

About some perspectives related to the numerical examples, suggestions would mostly be directed towards the TO of the SPSG, or other rotating machines. The movements of the rotor could be considered in TO to allow investigation of other characteristics of the machine, such as emf, torque, torque ripple, and so on. Also, at-load machine functioning could also be thought-provoking as it could find new structures that are more optimal for at-load runs, but

not as optimal for off-load runs. These aspects are rarely seen in literature, and thus could be a novel way of attacking the problem.

All these ideas can be realised with the presently developed TO tool, but again, a stepwise testing is always necessary to prevent ill-posed problems, and thus generation of incoherent structures.



# References

---

- [1] A. G. M. Michell, 'LVIII. *The limits of economy of material in frame-structures*', *Philos. Mag. Ser. 6*, vol. 8, no. 47, pp. 589–597, Nov. 1904.
- [2] G. I. N. Rozvany, 'Grillages of maximum strength and maximum stiffness', *Int. J. Mech. Sci.*, vol. 14, no. 10, pp. 651–666, Oct. 1972.
- [3] G. I. N. Rozvany and W. Prager, 'Optimal design of partially discretized grillages', *J. Mech. Phys. Solids*, vol. 24, no. 2–3, pp. 125–136, Jun. 1976.
- [4] M. P. Bendsøe and N. Kikuchi, 'Generating optimal topologies in structural design using a homogenization method', *Comput. Methods Appl. Mech. Eng.*, vol. 71, no. 2, pp. 197–224, Nov. 1988.
- [5] M. P. Bendsøe, 'Optimal shape design as a material distribution problem', *Struct. Optim.*, vol. 1, no. 4, pp. 193–202, Dec. 1989.
- [6] G. I. N. Rozvany and M. Zhou, 'The COC algorithm, part I: Cross-section optimization or sizing', *Comput. Methods Appl. Mech. Eng.*, vol. 89, no. 1–3, pp. 281–308, Aug. 1991.
- [7] D. N. Dyck and D. A. Lowther, 'Automated design of magnetic devices by optimizing material distribution', *IEEE Trans. Magn.*, vol. 32, no. 3, pp. 1188–1193, May 1996.
- [8] 'Scopus - Document search'. [Online]. Available: <http://www.scopus.com/>. [Accessed: 12-Jun-2014].
- [9] M. P. Bendsøe and O. Sigmund, *Topology Optimization - Theory, Methods and Applications*. Berlin, Heidelberg: Springer Berlin Heidelberg, 2004.
- [10] Y. Wang, 'A Study on Microstructures of Homogenization for Topology Optimization', Victoria University of Technology, Melbourne, Australia, 2003.
- [11] F. Belblidia and S. Bulman, 'A hybrid topology optimization algorithm for static and vibrating shell structures', *Int. J. Numer. Methods Eng.*, vol. 54, no. 6, pp. 835–852, Jun. 2002.
- [12] B. Hassani and E. Hinton, *Homogenization and Structural Topology Optimization*. London: Springer London, 1999.
- [13] J. Folgado, H. Rodrigues, and J. M. Guedes, 'Layout Design of Plate Reinforcement with a Buckling Load Criterion.', Goslar, Germany, 1995.
- [14] F. Campelo, J. A. Ramírez, and H. Igarashi, 'A survey of topology optimization in electromagnetics: considerations and current trends', *Academia.edu*, p. 46, 2010.
- [15] J. Yoo and N. Kikuchi, 'Topology optimization in magnetic fields using the homogenization design method', *Int. J. Numer. Methods Eng.*, vol. 48, no. 10, pp. 1463–1479, Aug. 2000.
- [16] G. I. N. Rozvany, M. Zhou, and T. Birker, 'Generalized shape optimization without homogenization', *Struct. Optim.*, vol. 4, no. 3–4, pp. 250–252, Sep. 1992.
- [17] Song-Yop Hahn, Kyung Choi, Hyang-Beom Lee, Il-Han Park, Ju-Hyun Lee, and Jin-Kyu Byun, 'Inverse problem application of topology optimization method with mutual energy concept and design sensitivity', *IEEE Trans. Magn.*, vol. 36, no. 4, pp. 1144–1147, Jul. 2000.
- [18] S. Wang and J. Kang, 'Topology optimization of nonlinear magnetostatics', *IEEE Trans. Magn.*, vol. 38, no. 2, pp. 1029–1032, Mar. 2002.
- [19] M. Stolpe and K. Svanberg, 'On the trajectories of penalization methods for topology optimization', *Struct. Multidiscip. Optim.*, vol. 21, no. 2, pp. 128–139, Apr. 2001.
- [20] A. Rietz, 'Sufficiency of a finite exponent in SIMP (power law) methods', *Struct. Multidiscip. Optim.*, vol. 21, no. 2, pp. 159–163, Apr. 2001.
- [21] J. S. Choi and J. Yoo, 'Structural optimization of ferromagnetic materials based on the magnetic reluctivity for magnetic field problems', *Comput. Methods Appl. Mech. Eng.*, vol. 197, no. 49–50, pp. 4193–4206, Sep. 2008.

- [22] S. Sanogo, ‘Conception Optimale de Circuits Magnétiques dédiés à la Propulsion Spatiale Electrique par des Méthodes d’Optimisation Topologique’, Université Toulouse 3 Paul Sabatier, Toulouse, 2016.
- [23] O. Sigmund, ‘Design of multiphysics actuators using topology optimization – Part II: Two-material structures’, *Comput. Methods Appl. Mech. Eng.*, vol. 190, no. 49–50, pp. 6605–6627, Oct. 2001.
- [24] T. Labbe and B. Dehez, ‘Convexity-Oriented Mapping Method for the Topology Optimization of Electromagnetic Devices Composed of Iron and Coils’, *IEEE Trans. Magn.*, vol. 46, no. 5, pp. 1177–1185, May 2010.
- [25] S. Sanogo, F. Messine, C. Henaux, and R. Vilamot, ‘Topology Optimization for Magnetic Circuits Dedicated to Electric Propulsion’, *IEEE Trans. Magn.*, vol. 50, no. 12, pp. 1–13, Dec. 2014.
- [26] H. Igarashi and K. Watanabe, ‘Complex Adjoint Variable Method for Finite-Element Analysis of Eddy Current Problems’, *IEEE Trans. Magn.*, vol. 46, no. 8, pp. 2739–2742, Aug. 2010.
- [27] G. Allaire, ‘A review of adjoint methods for sensitivity analysis, uncertainty quantification and optimization in numerical codes’. 2015.
- [28] S. Jameson and A. Jameson, ‘Adjoint Formulations for Topology, Shape and Discrete Optimization’, 2007.
- [29] S. Wang, S. Park, and J. Kang, ‘Multi-domain topology optimization of electromagnetic systems’, *COMPEL - Int. J. Comput. Math. Electr. Electron. Eng.*, vol. 23, no. 4, pp. 1036–1044, Dec. 2004.
- [30] J. S. Choi and J. Yoo, ‘Simultaneous structural topology optimization of electromagnetic sources and ferromagnetic materials’, *Comput. Methods Appl. Mech. Eng.*, vol. 198, no. 27–29, pp. 2111–2121, May 2009.
- [31] Y. Okamoto, Y. Matsubayashi, S. Wakao, and S. Sato, ‘Material-Density-Based Topology Optimization With Magnetic Nonlinearity by Means of Stabilized Sequential Linear Programming: SLPSTAB’, *IEEE Trans. Magn.*, vol. 51, no. 3, pp. 1–4, Mar. 2015.
- [32] Jin-kyu Byun, Il-han Park, and Song-yop Hahn, ‘Topology optimization of electrostatic actuator using design sensitivity’, *IEEE Trans. Magn.*, vol. 38, no. 2, pp. 1053–1056, Mar. 2002.
- [33] S. Wang, J. Kang, and J. Noh, ‘Topology Optimization of a Single-Phase Induction Motor for Rotary Compressor’, *IEEE Trans. Magn.*, vol. 40, no. 3, pp. 1591–1596, May 2004.
- [34] D.-H. Kim, J. K. Sykulski, and D. A. Lowther, ‘The Implications of the Use of Composite Materials in Electromagnetic Device Topology and Shape Optimization’, *IEEE Trans. Magn.*, vol. 45, no. 3, pp. 1154–1157, Mar. 2009.
- [35] H. Shokrollahi and K. Janghorban, ‘Soft magnetic composite materials (SMCs)’, *J. Mater. Process. Technol.*, vol. 189, no. 1–3, pp. 1–12, Jul. 2007.
- [36] T. Labbe, B. Dehez, M. Markovic, and Y. Perriard, ‘Torque-to-weight ratio maximization in PMSM using topology optimization’, 2010, pp. 1–5.
- [37] J. S. Choi, K. Izui, S. Nishiwaki, A. Kawamoto, and T. Nomura, ‘Topology Optimization of the Stator for Minimizing Cogging Torque of IPM Motors’, *IEEE Trans. Magn.*, vol. 47, no. 10, pp. 3024–3027, Oct. 2011.
- [38] G. Kiziltas, ‘Automated Topology Design for Electromagnetic Devices’, 2004, vol. 712, pp. 2155–2160.
- [39] R. C. Carbonari, E. C. N. Silva, and S. Nishiwaki, ‘Design of piezoelectric multi-actuated microtools using topology optimization’, *Smart Mater. Struct.*, vol. 14, no. 6, pp. 1431–1447, Dec. 2005.

- [40] G. Anagnostou, E. M. Rønquist, and A. T. Patera, 'A computational procedure for part design', *Comput. Methods Appl. Mech. Eng.*, vol. 97, no. 1, pp. 33–48, May 1992.
- [41] Y. Okamoto, K. Akiyama, and N. Takahashi, '3-D topology optimization of single-pole-type head by using design sensitivity analysis', *IEEE Trans. Magn.*, vol. 42, no. 4, pp. 1087–1090, Apr. 2006.
- [42] Jae Seok Choi and Jeonghoon Yoo, 'Structural Topology Optimization of Magnetic Actuators Using Genetic Algorithms and ON/OFF Sensitivity', *IEEE Trans. Magn.*, vol. 45, no. 5, pp. 2276–2279, May 2009.
- [43] Chang-Hwan Im, Hyun-Kyo Jung, and Yong-Joo Kim, 'Hybrid genetic algorithm for electromagnetic topology optimization', *IEEE Trans. Magn.*, vol. 39, no. 5, pp. 2163–2169, Sep. 2003.
- [44] K. Watanabe, F. Campelo, and H. Igarashi, 'Topology Optimization Based on Immune Algorithm and Multigrid Method', *IEEE Trans. Magn.*, vol. 43, no. 4, pp. 1637–1640, Apr. 2007.
- [45] F. Campelo, K. Watanabe, and H. Igarashi, '3D topology optimization using an immune algorithm', *COMPEL - Int. J. Comput. Math. Electr. Electron. Eng.*, vol. 26, no. 3, pp. 677–688, Jun. 2007.
- [46] F. Campelo, S. Ota, K. Watanabe, and H. Igarashi, 'Generating Parametric Design Models Using Information From Topology Optimization', *IEEE Trans. Magn.*, vol. 44, no. 6, pp. 986–989, Jun. 2008.
- [47] Wen Wang, Yilong Lu, J. S. Fu, and Yong Zhong Xiong, 'Particle swarm optimization and finite-element based approach for microwave filter design', *IEEE Trans. Magn.*, vol. 41, no. 5, pp. 1800–1803, May 2005.
- [48] S. Sanogo and F. Messine, 'Design of space thrusters: a topology optimization problem solved via a Branch and Bound method', *J. Glob. Optim.*, vol. 64, no. 2, pp. 273–288, Feb. 2016.
- [49] K. Akiyama, D. Miyagi, and N. Takahashi, 'Design of CF-SPT Head Having Large Recording Field and Small Stray Field Using 3-D ON/OFF Method', *IEEE Trans. Magn.*, vol. 42, no. 10, pp. 2431–2433, Oct. 2006.
- [50] N. Takahashi, Takaya Yamada, and D. Miyagi, 'Optimization of rotor of actual IPM motor using ON/OFF method', 2010, pp. 1–1.
- [51] M. Alexe and A. Sandu, 'Forward and adjoint sensitivity analysis with continuous explicit Runge–Kutta schemes', *Appl. Math. Comput.*, vol. 208, no. 2, pp. 328–346, Feb. 2009.
- [52] Y. Okamoto, Y. Tominaga, and S. Sato, 'Topological Design for 3-D Optimization Using the Combination of Multistep Genetic Algorithm with Design Space Reduction and Nonconforming Mesh Connection', *IEEE Trans. Magn.*, vol. 48, no. 2, pp. 515–518, Feb. 2012.
- [53] Y. Okamoto, Y. Tominaga, S. Wakao, and S. Sato, 'Topology Optimization of Rotor Core Combined With Identification of Current Phase Angle in IPM Motor Using Multistep Genetic Algorithm', *IEEE Trans. Magn.*, vol. 50, no. 2, pp. 725–728, Feb. 2014.
- [54] S. Osher and J. A. Sethian, 'Fronts propagating with curvature-dependent speed: Algorithms based on Hamilton-Jacobi formulations', *J. Comput. Phys.*, vol. 79, no. 1, pp. 12–49, Nov. 1988.
- [55] G. Allaire, F. Jouve, and A.-M. Toader, 'A level-set method for shape optimization', *Comptes Rendus Math.*, vol. 334, no. 12, pp. 1125–1130, Jan. 2002.
- [56] S. Zhou, W. Li, and Q. Li, 'Level-set based topology optimization for electromagnetic dipole antenna design', *J. Comput. Phys.*, vol. 229, no. 19, pp. 6915–6930, Sep. 2010.

- [57] Y. Okamoto, S. Wakao, and S. Sato, 'Topology Optimization Based on Regularized Level-Set Function for Solving 3-D Nonlinear Magnetic Field System With Spatial Symmetric Condition', *IEEE Trans. Magn.*, vol. 52, no. 3, pp. 1–4, Mar. 2016.
- [58] Y. Hidaka, T. Sato, K. Watanabe, and H. Igarashi, 'Stochastic topology optimization based on level-set method', *COMPEL - Int. J. Comput. Math. Electr. Electron. Eng.*, vol. 33, no. 6, pp. 1904–1919, Oct. 2014.
- [59] 'Level Set Method', *Wikipedia*. [Online]. Available: [https://en.wikipedia.org/wiki/Level-set\\_method](https://en.wikipedia.org/wiki/Level-set_method).
- [60] H. Lombaert, 'Level set method: Explanation'. 2006.
- [61] S. Osher and R. P. Fedkiw, *Level set methods and dynamic implicit surfaces*. New York: Springer, 2003.
- [62] J. A. Sethian and J. A. Sethian, *Level set methods and fast marching methods: evolving interfaces in computational geometry, fluid mechanics, computer vision, and materials science*, 2nd ed. Cambridge, U.K.; New York: Cambridge University Press, 1999.
- [63] Sang-In Park and Seungjae Min, 'Magnetic Actuator Design for Maximizing Force Using Level Set Based Topology Optimization', *IEEE Trans. Magn.*, vol. 45, no. 5, pp. 2336–2339, May 2009.
- [64] Hokyung Shim, Vinh Thuy Tran Ho, Semyung Wang, and D. A. Tortorelli, 'Level Set-Based Topology Optimization for Electromagnetic Systems', *IEEE Trans. Magn.*, vol. 45, no. 3, pp. 1582–1585, Mar. 2009.
- [65] Sang-in Park and Seungjae Min, 'Optimal Topology Design of Magnetic Devices Using Level-Set Method', *IEEE Trans. Magn.*, vol. 45, no. 3, pp. 1610–1613, Mar. 2009.
- [66] M. Masmoudi, J. Pommier, and B. Samet, 'The topological asymptotic expansion for the Maxwell equations and some applications', *Inverse Probl.*, vol. 21, no. 2, pp. 547–564, Apr. 2005.
- [67] A. A. Gomes and A. Suleman, 'Application of spectral level set methodology in topology optimization', *Struct. Multidiscip. Optim.*, vol. 31, no. 6, pp. 430–443, Jun. 2006.
- [68] F. Campelo, K. Watanabe, and H. Igarashi, 'A spectral topology optimization approach to the design of magnetic devices', presented at the 13th IEEE conference on Electromagnetic Field Computation (CEFC), Athens, Greece, 2008.
- [69] E. Arvas and L. Sevgi, 'A Tutorial on the Method of Moments [Testing Ourselves]', *IEEE Antennas Propag. Mag.*, vol. 54, no. 3, pp. 260–275, Jun. 2012.
- [70] Y. Hidaka, T. Sato, and H. Igarashi, 'Topology Optimization Method Based on On-Off Method and Level Set Approach', *IEEE Trans. Magn.*, vol. 50, no. 2, pp. 617–620, Feb. 2014.
- [71] T. A. Poulsen, 'A simple scheme to prevent checkerboard patterns and one-node connected hinges in topology optimization', *Struct. Multidiscip. Optim.*, vol. 24, no. 5, pp. 396–399, Nov. 2002.
- [72] 'Présentation générale | code\_Carmel'. [Online]. Available: <http://code-carmel.univ-lille1.fr/>. [Accessed: 11-Apr-2017].
- [73] 'Sophemis by L2EP'. [Online]. Available: <http://optimisation.l2ep.ec-lille.fr/>. [Accessed: 11-Apr-2017].
- [74] R. Bargallo, 'Finite Elements For Electrical Engineering'. 2006.
- [75] Y. Le Menach, 'Contribution à la modélisation numérique des phénomènes électromagnétiques 3D en basse fréquence', Université de Lille1, Lille, 2012.
- [76] E. Delgado da Carvalho, 'Finite Element Method for Maxwell's Equations'. 2007.
- [77] A. Bacchus, 'Représentativité de la modélisation aux éléments finis pour le diagnostic de machines synchrones de grande puissance', Université de Lille 1, Lille, 2016.

- [78] A. Marrocco, ‘Analyse Numérique des Problèmes d’Électrotechniques’, *Ann. Sci. Math. Québec*, vol. Vol. 1, no. 2, pp. 217–296, 1977.
- [79] Z. Ren and A. Razek, ‘Local force computation in deformable bodies using edge elements’, *IEEE Trans. Magn.*, vol. 28, no. 2, pp. 1212–1215, Mar. 1992.
- [80] J. Coulomb, ‘A methodology for the determination of global electromechanical quantities from a finite element analysis and its application to the evaluation of magnetic forces, torques and stiffness’, *IEEE Trans. Magn.*, vol. 19, no. 6, pp. 2514–2519, Nov. 1983.
- [81] B. Boualem, ‘Contribution à la modélisation des systèmes électrotechniques à l’aide des formulations en potentiels: application à la machine asynchrone’, Université de Lille 1, 1997.
- [82] M. Cavazzuti, ‘Design of Experiments’, in *Optimization Methods*, Berlin, Heidelberg: Springer Berlin Heidelberg, 2013, pp. 13–42.
- [83] ‘SALOME’. [Online]. Available: <http://www.salome-platform.org/>.
- [84] O. Sigmund and K. Maute, ‘Topology optimization approaches: A comparative review’, *Struct. Multidiscip. Optim.*, Aug. 2013.
- [85] P. Venkataraman, *Applied optimization with MATLAB programming*, 2nd ed. Hoboken, N.J: John Wiley & Sons, 2009.
- [86] T. Young and M. J. Mohlenkamp, ‘Introduction to Numerical Methods and Matlab Programming for Engineers’, Department of Mathematics, Ohio University.
- [87] T. Labbe, ‘Topology optimization methods for the design of electromagnetic actuators’, Université Catholique de Louvain (UCL), 2011.
- [88] T. ishikawa, T. Watanabe, S. Mizuno, and N. Kurita, ‘Effect of Cleaning Level on Topology Optimization of Permanent Magnet Synchronous Generator’, presented at the 19th International Conference on Electrical Machines and Systems (ICEMS), 2016, Chiba, Japan, 2016.
- [89] P. Gangl and U. Langer, ‘Topology optimization of electric machines based on topological sensitivity analysis’, *Comput. Vis. Sci.*, vol. 15, no. 6, pp. 345–354, Dec. 2012.
- [90] Y. Okamoto, M. Ohtake, and N. Takahashi, ‘Magnetic shield design of perpendicular magnetic recording head by using topology optimization technique’, *IEEE Trans. Magn.*, vol. 41, no. 5, pp. 1788–1791, May 2005.
- [91] A. Ammar, ‘Modélisation et Optimisation d’un Générateur Synchrone à Double Excitation de Forte Puissance’, Ecole Centrale de Lille, Lille, 2013.
- [92] M. Ployard, ‘Efficacité énergétique des machines de production d’électricité’, Centrale Lille, Lille, 2017.

# APPENDICES

---

## Appendix A

### Calculation of LHS with Sophemis

```

function out = lhsSangka(var, sample, maxiter, option)

% Latin Hypercube Sampling
% Maximin criteria
%
% output = lhs(var, sample, maxiter)
%
% var      = variable number
% sample   = sample point number
% maxiter  = maximum iteration (default = 100)
% option   = 'lhs' point at random space in cube
%           'mod' point at cube edges
%           'lattice' centered point
% -----
% by Sangkla Kreuawan
% 20 may 2006
%
% Rev. 10/06/2007 --- do not compute distance if maxiter =1
% Rev. 23/06/2007 --- add option
% Rev. 31/05/2011 --- AlexB, the calculation of I and J is done
only once
% Rev. 31/05/2011 --- AlexB, best_x is only initialized at the
first iteration

if nargin < 3 || isempty(maxiter)
    maxiter = 100;
end

if nargin < 4
    option = 'lhs';
end

%                               x                               =
lhsdesign(sample, var, 'iterations', maxiter, 'criterion', 'maximin');

best = 0;
x = zeros(sample, var);

% AlexB, 31/05/2011 -- code extracted from "if maxiter ~=1" loop
% Distant cal. code taken from latin hypercube matlab
% Maximize the minimum point-to-point difference
% Get I and J indexing each pair of points
[m, p] = size(x);
pp = (m-1):-1:2;
I = zeros(m*(m-1)/2, 1);
I(cumsum([1 pp])) = 1;
I = cumsum(I);
J = ones(m*(m-1)/2, 1);
J(cumsum(pp)+1) = 2-pp;
J(1)=2;
J = cumsum(J);

```



```

% AlexB

for iter = 1:maxiter
    % if isempty(input_latin)
    switch option
        case 'mod' % point at cube edges
            for i = 1:var
                x(:,i) = (randperm(sample)-1)/(sample-1);
            end
        case 'lattice' % point at cube center --- lattice sample
            % Ref. Computer experiments - J.R. Koehler and A.B.
Owen
            for i = 1:var
                x(:,i) = (0.5 + (randperm(sample)' - 1)) / sample;
            end
        otherwise % normal LHS --- point at random space in cube
            for i = 1:var
                x(:,i) = (rand(sample,1) + (randperm(sample)' - 1))
/ sample;
                % latin_rand = (inputmax - inputmin).*latin_rand +
inputmin;
            end
        end
    end

    % AlexB, 31/05/2011
    % Initialize best_x only at the first iteration
    if iter==1, best_x = x; end
    % AlexB

    if maxiter ~=1
        % To save space, loop over dimensions
        d = zeros(size(I));
        for j=1:p
            d = d + (x(I,j)-x(J,j)).^2;
        end
        s = sqrt(min(d));

        if s > best
            best = s;
            best_x = x;
        end
    end
end
% best
out = best_x;

% subplot(2,2,1); plot(x(:,1), x(:,2), 'o');
% subplot(2,2,2); hist(x(:,2));
% subplot(2,2,3); hist(x(:,1));

```

## Appendix B

### Example of Sophemis Model on Matlab for TO

```

classdef TopologicTemporalModel < TemporalCarmelModel
    % Topologic model temporal
    % @author : Bilquis Mohamodhosen && Florent Delhaye<florent.delhaye@ec-lille.fr>

    methods

        function obj = TopologicTemporalModel()
            obj@TemporalCarmelModel('topo', 'topo', 'T', 'topo.med', 'configuration.xml', ...
                false, 1, 'localhost', '8080');
            % false -ECL
            % true - P2
            % 1 - Time step
            % localhost - calculations launched on pc
            % scheduler - calculations launched on linux server @ ECL

            % for parallel pooling - configure on Sophemis--> configurer
            % plateforme --> Nombre de coeurs (4)

%% Outputs from Carmel

%     obj.setH();
%     obj.setK();
%     obj.setRotK();
%     obj.setN();
%     obj.setB();
%     obj.setEnergie();
%     obj.setForce();

%% Declaration of inputs & outputs

% Inputs

% Constant inputs
obj.addInput(Input('mu_r', 'Permeability of material (iron)', '_', InputType.constant, [], 2000));
obj.addInput(Input('mu_o', 'Permeability of free space', '_', InputType.constant, [], 1));
obj.addInput(Input('n', 'penalisation coefficient', '_', InputType.constant, [], 1));
obj.addInput(Input('dimension', 'dimension', '_', InputType.constant, [], 64));

% Variables
obj.addInput(Input('d', 'density', '_', InputType.continuous, 'dimension', [0 1]));
%     obj.addInput(Input('d', 'density', '_', InputType.discrete, 'dimension', 1));

% Outputs

% carmel outputs
obj.addOutput(Output('energie', 'energie', '_')); % scalar

% Calculated Outputs
obj.addOutput(Output('MQ', 'MQ', '_')); % scalar

% Constraints to force density to 0 and 1

obj.addOutput(Output('FF_sum', 'FF_sum', '_'));

```

```

end

function result = compute(obj, input)

%% Mappings

%      % Polynomial Mapping (SIMP)
input.mu_i = input.mu_o*(1+(input.mu_r - 1)*input.d.^input.n);

%% Outputs
carmelResult = compute@TemporalCarmelModel(obj, input);

% Using the outputs
result.energie = -carmelResult.energie/3.64131033081171963e-3 ; % (result.X - X must be defined in
outputs above)
result.MQ = sum(input.d) / input.dimension;

%% Constraints forcing variables to 1 or 0

%      % FF for lb=0 & ub=1 + Normalised
result.FF_sum = 16*sum(abs((input.d-1).*input.d))/(input.dimension*0.25);

end

end

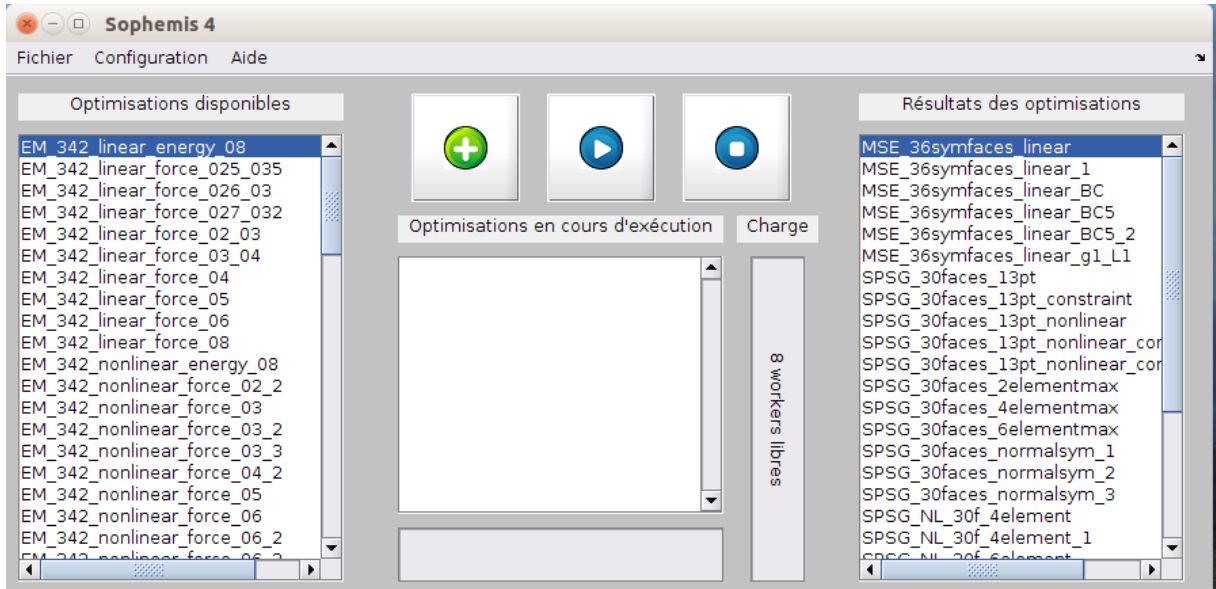
end

```

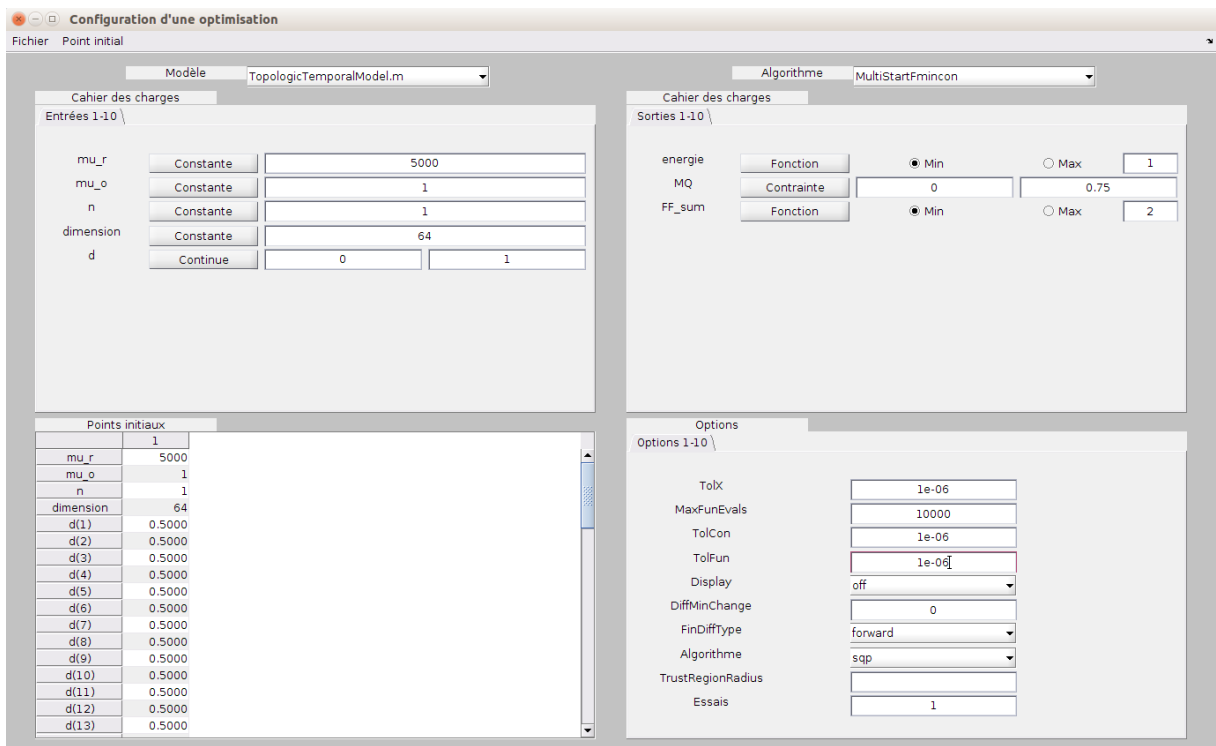
## Appendix C

### Example of Sophemis windows

#### Sophemis window



#### Optimisation of a model





# Appendix D

## Example of files where force is extracted

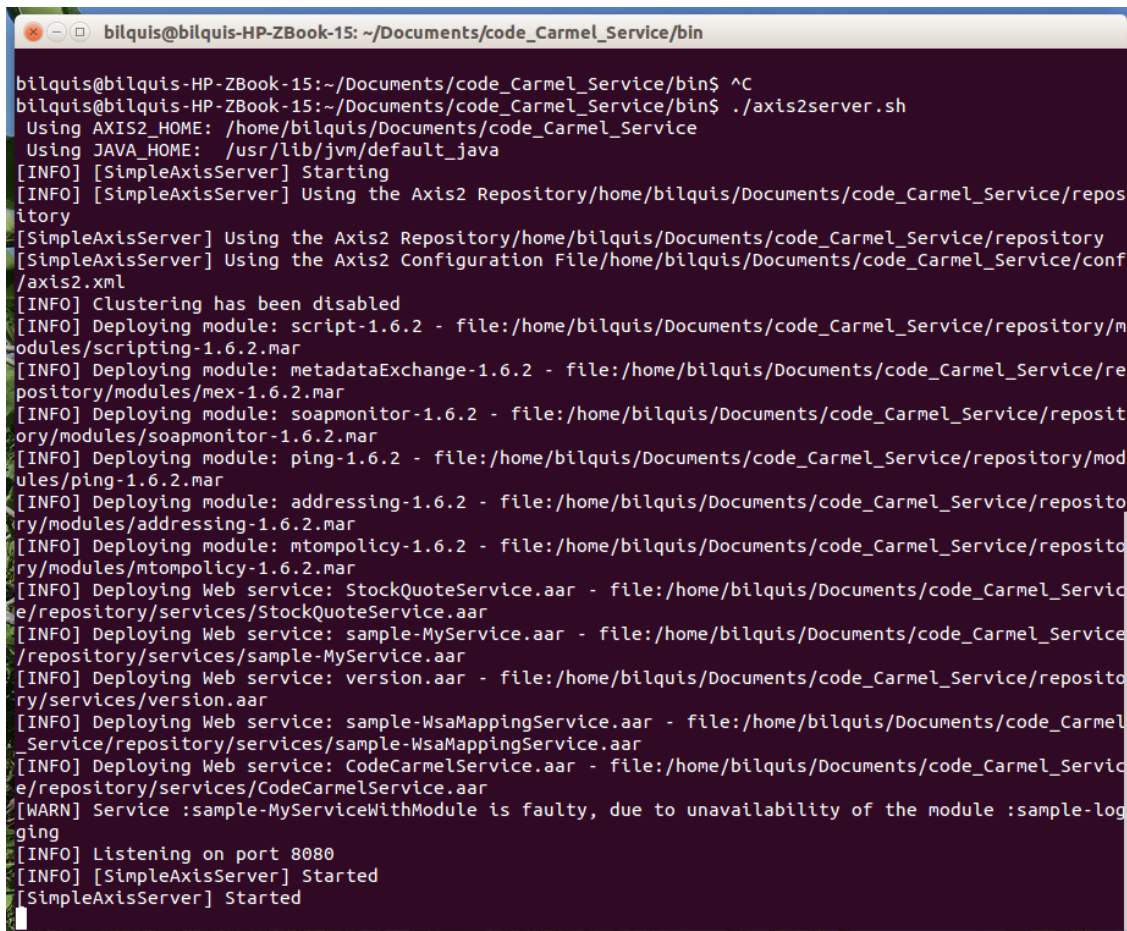
```
# Nom du champ : forceTV_Hsom
# Description du champ : densite surfactque de force
# Aucune description supplementaire
# Unite du champ : N/m2
# Temps du Champ (pas de temps 1) : 0.000000000000E+00 s
# (c) L2EP, 2014
# Indice element dans le maillage: barycentre element : x, y, z; champ : x, y, z, module
4476 5.05000000000000E-02 3.00000000000000E-02 0.00000000000000E+00 7.704110824459948E-05 0.00000000000000E+00 0.00000000000000E+00 7.704110824459948E-05
4477 5.05000000000000E-02 3.00000000000000E-02 0.00000000000000E+00 -2.48369320623300E-05 2.17319697822100E-07 1.472269181122197E-06 2.488147896225321E-05
4478 5.05000000000000E-02 0.00000000000000E+00 6.00000000000000E-02 -9.41426380726511E-05 -6.859633775099625E-06 2.579430715003352E-06 9.442745617064563E-05
4479 5.05000000000000E-02 0.00000000000000E+00 0.00000000000000E+00 -3.12794534116294E-06 0.00000000000000E+00 6.180988138803444E-06 7.012789886863833E-06
4480 5.05000000000000E-02 2.611240682318374E-02 0.00000000000000E+00 3.629368113769489E-04 -8.45591093355654E-06 -4.321077798607937E-05 6.35597827084453E-04
4489 5.05000000000000E-02 2.222481204000744E-02 0.00000000000000E+00 3.044616674426873E-04 3.38826283381626E-06 7.05629135254797E-06 3.045617244660389E-04
4490 5.05000000000000E-02 1.833721806955125E-02 0.00000000000000E+00 2.93884088084599E-04 -1.385935531847530E-05 -2.465763202797054E-06 2.9423355636997E-04
4491 5.05000000000000E-02 1.547853147101305E-02 0.00000000000000E+00 1.7534502716852E-04 -1.153297511252994E-05 4.776644506889172E-06 1.75789185559689E-04
4492 5.05000000000000E-02 1.335425808169140E-02 0.00000000000000E+00 8.959422422929794E-05 -3.76592902367793E-06 6.468323909209390E-06 8.990594388099736E-05
4493 5.05000000000000E-02 1.133689836221108E-02 0.00000000000000E+00 3.69626376085575E-05 -4.06665798580800E-06 2.34721699782095E-05 4.397406696046520E-05
4494 5.05000000000000E-02 9.928296927518954E-03 0.00000000000000E+00 -2.115271069168680E-05 9.74976584398212E-06 3.897626717788744E-05 4.54033566601875E-05
4495 5.05000000000000E-02 6.652410186234045E-03 0.00000000000000E+00 -3.293446311835500E-05 -1.46589355712667E-05 2.848762808931325E-05 4.59467975787034E-05
4496 5.05000000000000E-02 6.742381753592322E-03 0.00000000000000E+00 -2.73028619679201E-08 1.693415717363563E-06 1.38560276971371E-05 1.395915132608871E-05
4497 5.05000000000000E-02 4.421270120280990E-03 0.00000000000000E+00 -5.75125988778328E-06 -2.525345817460729E-06 1.094881398859976E-05 1.262263406261701E-05
4498 5.05000000000000E-02 2.46626243827968E-03 0.00000000000000E+00 -1.138470858677052E-05 -9.395716963687147E-06 1.557431655063103E-05 2.14581085799422E-05
4499 5.05000000000000E-02 1.115140259239224E-03 0.00000000000000E+00 -1.458933428375834E-05 -2.59664457208309E-06 2.370056984878304E-05 2.795192300649186E-05
4500 5.05000000000000E-02 3.00000000000000E-02 3.99999999999999E-02 6.817451276811538E-04 2.855246145191940E-05 2.135655484415105E-04 7.149838499249404E-04
4501 5.05000000000000E-02 3.00000000000000E-02 7.99999999999999E-02 2.78823734261812E-04 -1.43388380910462E-06 2.60497148478376E-04 3.815919871487848E-04
4502 5.05000000000000E-02 3.00000000000000E-02 1.19999999999999E-02 1.36573909257104E-04 -5.632399164688276E-07 3.062828172623288E-04 3.3532341668029277E-04
4503 5.05000000000000E-02 3.00000000000000E-02 1.59999999999999E-02 1.034433641812488E-05 -1.085345712351763E-05 3.11295502460391E-04 3.116563094932155E-04
4504 5.05000000000000E-02 3.00000000000000E-02 1.99999999999999E-02 -9.942882412993661E-05 -1.021646360299878E-05 2.68265697546762E-04 2.862811200167563E-04
4505 5.05000000000000E-02 3.00000000000000E-02 2.39999999999999E-02 -1.58821247869305E-04 1.569401451122901E-05 2.313226316921802E-04 2.818349505760064E-04
4506 5.05000000000000E-02 3.00000000000000E-02 2.79999999999999E-02 -1.1256856090219E-04 -7.11373948462454E-06 1.216852932386387E-04 1.65920471527590E-04
4507 5.05000000000000E-02 3.00000000000000E-02 3.19999999999999E-02 -2.01580997437330E-04 1.767118546391301E-05 1.55921533329990E-04 2.554578123566012E-04
4508 5.05000000000000E-02 3.00000000000000E-02 3.59999999999999E-02 -1.89322368333355E-04 9.382419546514808E-06 1.17626324428209E-04 2.230850587929237E-04
4509 5.05000000000000E-02 3.00000000000000E-02 3.99999999999999E-02 -1.07254883908662E-04 7.328222656757607E-07 5.549648890212326E-05 1.207640916152596E-04
4510 5.05000000000000E-02 3.00000000000000E-02 4.39999999999999E-02 -9.6238996779395109E-05 2.791858747598154E-06 4.659495906566471E-05 1.06961818278839E-04
4511 5.05000000000000E-02 3.00000000000000E-02 4.79999999999999E-02 -8.14697740825759E-06 -1.0836357553676E-06 3.5293770416641E-05 8.879493885737837E-05
4512 5.05000000000000E-02 3.00000000000000E-02 5.19999999999999E-02 -6.980328988871085E-05 -4.723360435304019E-08 1.879587299882527E-05 7.22896058085634E-05
4513 5.05000000000000E-02 3.00000000000000E-02 5.59999999999999E-02 -6.395750592799363E-05 3.417033488390608E-07 5.965671929540147E-06 6.4234245109533E-05
4514 5.05000000000000E-02 0.00000000000000E+00 1.14987615655081E-03 -3.899454531704960E-05 -3.970536509286911E-06 2.176894588421449E-05 3.80104754368673E-05
4515 5.05000000000000E-02 0.00000000000000E+00 2.299753033118155E-03 -7.7942723136745E-05 1.90977801990881E-06 3.15293458811145E-05 8.407362891044034E-05
4516 5.05000000000000E-02 0.00000000000000E+00 3.4496299665236E-03 -4.49083561758188E-04 7.362904663916740E-06 1.77914286215927569E-06 2.3261211876591E-05
4517 5.05000000000000E-02 0.00000000000000E+00 4.60664286916868E-03 -4.16584413593693E-04 6.854629754568782E-06 1.051394656120196E-04 4.29720675154623E-04
4518 5.05000000000000E-02 0.00000000000000E+00 5.782196493614528E-03 -8.6726546385480E-04 1.684244550927981E-05 2.63880413347836E-04 9.061629376110668E-04
4519 5.05000000000000E-02 0.00000000000000E+00 6.890155570833768E-03 -1.814925768643699E-02 -2.855887467406411E-05 5.61100944698174E-04 1.899896149795171E-04
4520 5.05000000000000E-02 0.00000000000000E+00 8.04803208738884E-03 -8.778345804494143E-03 7.750582396073788E-04 3.2302776836673788E-04 9.358581113438019E-03
4521 5.05000000000000E-02 0.00000000000000E+00 9.189986603943898E-03 -3.096582404729233E-02 3.24736764925137E-04 1.154201117284409E-02 3.20610903871807E-02
4522 5.05000000000000E-02 0.00000000000000E+00 1.034650648404783E-02 -6.46585513623707E-02 1.15229585556910E-03 4.769520991115118E-02 8.48444630811195E-02
4523 5.05000000000000E-02 0.00000000000000E+00 1.149204432223931E-02 -6.366760395849420E-02 6.114421146649286E-05 2.51137936823791E-04 3.326813651875181E-04
4524 5.05000000000000E-02 0.00000000000000E+00 1.266477632680237E-02 -5.783185159547898E-02 -5.679496298570040E-06 1.439954191013555E-04 5.78320314102799E-04
4525 5.05000000000000E-02 0.00000000000000E+00 1.382847094086808E-02 -5.83399988510977E-02 -3.15110872511876E-06 1.356965259202764E-04 5.834006778301300E-02
4526 5.05000000000000E-02 0.00000000000000E+00 1.497952943578733E-02 -5.88186274942587E-02 -3.205715824925397E-06 1.29479551357934E-04 5.881870998187554E-02
4527 5.05000000000000E-02 0.00000000000000E+00 1.616122121161045E-02 -4.98242217841085E-02 -3.28733828017161E-06 1.281673329210187E-04 5.612801365465113E-04
4528 5.05000000000000E-02 0.00000000000000E+00 1.727668546395400E-02 7.72668546395400E-02 4.442267948187021E-06 1.067992531649270E-04 7.06618282325874E-02
4529 5.05000000000000E-02 0.00000000000000E+00 1.842673983270962E-02 -7.637711564608808E-02 -2.587611445376438E-06 1.567884640097104E-04 7.63772766189318E-02
```

## Example of file where B is extracted

```
# Nom du champ : B_HsOmega
# Description du champ : Induction magnetique
# Aucune description supplementaire
# Unite du champ : T
# Temps du Champ (pas de temps 1) : 0.000000000000E+00 s
# (c) L2EP, 2014
# Indice element dans le maillage: barycentre element : x, y, z; champ : x, y, module
6426 9.545423727273202E-03 4.421248195357433E-03 4.8036746950657731E-03 9.848545173304881E-03 -2.451069002713841E-06 -3.361786873059156E-04 8.954856039272638E-03
6427 9.557272219770003E-03 4.496118196346947E-04 4.964810179355766E-03 1.036169754313128E-02 3.193168226356561E-07 -3.424732611049393E-04 1.036735569942885E-02
6428 9.5727695475918E-03 8.969239572633467E-03 7.442925227451857E-03 1.029679914591400E-02 3.8588851545666522E-03 8.02225919769815E-03 1.361137749681861E-02
6429 6.211945172432986E-03 8.58004096683329E-03 6.927514087748792E-03 1.454499314031071E-02 -4.259633710309588E-03 4.07727862481116E-03 1.56947603882767E-02
6430 6.03273626485884E-02 1.211848021766524E-03 1.068682462485280E-02 -7.447061546704652E-02 7.99430700718666E-03 1.245729922457639E-08 1.245768832616599E-06
6431 1.098435110226216E-03 4.701248747434314E-03 5.597129786665574E-03 6.89995789591908E-03 -4.66680857229927E-04 1.686190493808844E-02 8.03817325828197E-02
6432 5.641193836069999E-03 9.599537075144499E-03 8.296046021925366E-03 1.302193440428405E-02 -5.09482872421568E-03 4.633443548257407E-03 1.473081141899169E-02
6433 9.64715260943139E-03 2.576973276179969E-03 9.061055446797198E-03 1.68679468823106E-02 -6.27415810212210E-04 6.341330502547591E-03 1.803145060643488E-02
6434 5.426946430371025E-03 3.33171587422894E-03 1.466208722041580E-02 -2.458730273422819E-01 2.992548807873314E-02 1.17115722763308E+00 1.197062372303209E+00
6435 3.048843228021271E-03 4.0505787065729302E-04 9.633370184196615E-03 1.949908914252804E-02 -3.772471497620375E-04 3.236345694970007E-03 1.976845785065085E-02
6436 5.170114718577520E-02 6.116761840414042E-03 1.537698164548164E-02 -3.422950441428382E-01 6.478027750266740E-02 1.128421943192211E+00 1.180684938727462E-02
6437 9.947576176361407E-03 5.154642189889580E-03 3.407683702463810E-03 7.090387035289149E-03 4.099622439137588E-05 -1.98914954301270E-04 7.09329155265085E-03
6438 7.410914512103643E-03 4.371577375962702E-04 7.690793174344585E-03 1.88099167535539E-02 9.690761066828349E-05 2.845141296313648E-03 1.409994763302422E-04
6439 4.276208876184477E-04 4.36685724598354E-03 9.878184680082875E-03 1.195576116061753E-02 -4.280620912124599E-02 1.430942024599382E-02 1.865162110541852E-02
6440 3.9428732955295918E-03 7.79846472082659E-03 9.505922955389242E-03 1.682474743883465E-02 -1.62876846908779E-04 9.42046961020929E-02 1.725457309431340E-02
6441 8.38891453467760E-03 8.561643423865142E-03 9.15268733032325E-03 2.80885859280415E-02 -4.931178357996347E-02 2.21392762407906E-04 2.13599572387023E-02
6442 5.818636478253893E-03 6.859458005432384E-03 3.658538642108708E-03 5.30796695447133E-03 -8.86995950615392E-04 3.867885631144832E-04 7.64179364574908E-03
6443 6.32381861739688E-03 2.251244070562152E-03 9.511854615866108E-03 1.85436604574030E-02 -1.067769126796895E-03 6.94583832862863E-03 1.983124775159659E-02
6444 8.593071401782566E-03 7.799122895767595E-03 9.15268733032325E-03 2.293265678944267E-02 -2.694580926190534E-03 1.900399811650366E-03 2.26341949593051E-02
6445 3.9428732955295918E-03 7.79846472082659E-03 9.505922955389242E-03 1.682474743883465E-02 -1.62876846908779E-04 9.42046961020929E-02 1.725457309431340E-02
6446 8.38891453467760E-03 8.561643423865142E-03 9.15268733032325E-03 2.80885859280415E-02 -4.931178357996347E-02 2.21392762407906E-04 2.13599572387023E-02
6447 2.613790282240130E-03 9.396908111886251E-03 4.520349785304406E-03 5.044077911287232E-03 -1.933298226770752E-03 1.192942229583831E-02 1.309545756682135E-02
6448 1.01382866677982E-03 5.822899122975440E-03 4.422915279543629E-03 4.6554273116107E-03 -1.45865069803115E-03 1.82044175927048E-02 1.906245978224487E-02
6449 8.969380288884311E-03 2.481979529361563E-03 3.572944052244210E-03 6.877108077223091E-03 1.57129589829599E-05 3.347340489165300E-04 6.79563670823930E-03
6450 7.71362531454083E-02 4.435435506779289E-04 5.96861652335243E-03 1.983996066331699E-02 -8.11003826096219E-05 2.904216256726980E-04 1.22331120131303E-02
6451 5.02354724871267E-03 8.79125049001480E-03 4.03740904340103E-03 7.991116630887730E-03 -2.166121598259340E-03 8.0433248380997E-03 1.15431832368586E-02
6452 4.226225424347893E-04 4.073513233540573E-04 9.268758800431317E-03 1.52349608936741E-02 -1.549769405412681E-04 1.02224080335138E-02 8.8347395463697E-02
6453 5.13155813290799E-02 1.335818108007167E-03 2.766586619337066E-03 3.1504759515628E-01 1.714544095784865E-02 5.97965750350354E-02 1.674007847018347E-01
6454 1.588400742585085E-05 5.69820228483250E-03 5.374050227995339E-03 4.162311883548339E-03 -8.466694602364029E-04 1.460267171933362E-02 1.52078837880809E-02
6455 3.589262458440010E-03 8.875644521230023E-03 5.629877126140111E-03 8.547578518525183E-03 -2.83294338947687E-03 8.902809288479988E-03 1.26280276151835E-02
6456 5.267955869559492E-02 6.01459542008701E-02 2.360686743611799E-02 -2.9250030197274E-01 6.22008841298718E
```

## Appendix E

### Example of server showing running of code\_Carmel-Sophemis coupling



```
bilquis@bilquis-HP-ZBook-15: ~/Documents/code_Carmel_Service/bin
bilquis@bilquis-HP-ZBook-15:~/Documents/code_Carmel_Service/bin$ ^C
bilquis@bilquis-HP-ZBook-15:~/Documents/code_Carmel_Service/bin$ ./axis2server.sh
Using AXIS2_HOME: /home/bilquis/Documents/code_Carmel_Service
Using JAVA_HOME: /usr/lib/jvm/default_java
[INFO] [SimpleAxisServer] Starting
[INFO] [SimpleAxisServer] Using the Axis2 Repository/home/bilquis/Documents/code_Carmel_Service/repo
itory
[SimpleAxisServer] Using the Axis2 Repository/home/bilquis/Documents/code_Carmel_Service/repository
[SimpleAxisServer] Using the Axis2 Configuration File/home/bilquis/Documents/code_Carmel_Service/conf
/axis2.xml
[INFO] Clustering has been disabled
[INFO] Deploying module: script-1.6.2 - file:/home/bilquis/Documents/code_Carmel_Service/repository/m
odules/scripting-1.6.2.mar
[INFO] Deploying module: metadataExchange-1.6.2 - file:/home/bilquis/Documents/code_Carmel_Service/re
pository/modules/mex-1.6.2.mar
[INFO] Deploying module: soapmonitor-1.6.2 - file:/home/bilquis/Documents/code_Carmel_Service/reposit
ory/modules/soapmonitor-1.6.2.mar
[INFO] Deploying module: ping-1.6.2 - file:/home/bilquis/Documents/code_Carmel_Service/repository/mod
ules/ping-1.6.2.mar
[INFO] Deploying module: addressing-1.6.2 - file:/home/bilquis/Documents/code_Carmel_Service/reposito
ry/modules/addressing-1.6.2.mar
[INFO] Deploying module: mtompolicy-1.6.2 - file:/home/bilquis/Documents/code_Carmel_Service/reposito
ry/modules/mtompolicy-1.6.2.mar
[INFO] Deploying Web service: StockQuoteService.aar - file:/home/bilquis/Documents/code_Carmel_Servic
e/repository/services/StockQuoteService.aar
[INFO] Deploying Web service: sample-MyService.aar - file:/home/bilquis/Documents/code_Carmel_Servic
e/repository/services/sample-MyService.aar
[INFO] Deploying Web service: version.aar - file:/home/bilquis/Documents/code_Carmel_Service/reposito
ry/services/version.aar
[INFO] Deploying Web service: sample-WsaMappingService.aar - file:/home/bilquis/Documents/code_Carmel
_Service/repository/services/sample-WsaMappingService.aar
[INFO] Deploying Web service: CodeCarmelService.aar - file:/home/bilquis/Documents/code_Carmel_Servic
e/repository/services/CodeCarmelService.aar
[WARN] Service :sample-MyServiceWithModule is faulty, due to unavailability of the module :sample-log
ging
[INFO] Listening on port 8080
[INFO] [SimpleAxisServer] Started
[SimpleAxisServer] Started
```

## Appendix F

### Different mesh sizes for 3D FE electromagnet model

*Energy obtained using  $A$  and  $\Omega$  formulations with  $3.0 \text{ A/mm}^2$*

No. of Tetrahedra	Energy in $A$	Energy $\Omega$
2433	1.75e-2	2.93e-2
3011	1.67e-2	2.76e-2
3482	1.78e-2	2.70e-2
3733	1.85e-2	2.78e-2
3928	1.97e-2	2.83e-2
4514	1.96e-2	2.76e-2
4805	1.92e-2	2.75e-2
5559	2.00e-2	2.68e-2
8463	2.03e-2	2.64e-2
10588	2.05e-2	2.61e-2
17461	2.19e-2	2.56e-2



*Force obtained using  $A$  and  $\Omega$  formulations with  $3.0 A/mm^2$*

<b>Force Face nodes</b>	<b>Force in <math>A</math></b>	<b>Force <math>\Omega</math></b>
33	11.8	39.2
43	10.9	38.1
51	13.5	34.7
53	15.4	37.0
58	19.3	38.4
65	19.2	37.4
75	17.4	38.1
79	20.0	36.7
85	20.7	36.2
96	21.4	35.1
165	26.1	34.3

# Optimisation Topologique de Dispositifs Electromagnétiques

---

## *Introduction*

Nous vivons actuellement à l'ère de l'exigence technologique, poussant l'intelligence humaine vers de nouvelles inventions plus surprenantes et l'amélioration des anciennes, en quête d'optimalité ; les chercheurs scientifiques étant les acteurs principaux de cette mission. A l'aide d'autres outils, notamment des processeurs et d'ordinateurs qui sont maintenant devenus incontournables, nous pouvons à présent réaliser des calculs et simulations plus fastidieux, nous rapprochant de notre but essentiel. Ceci a permis de révolutionner l'ingénierie en général, y compris le génie électrique qui est notre principal préoccupation.

Le laboratoire de génie électrique (Laboratoire d'Électrotechnique et d'Électronique de Puissance, L2EP), au sein duquel cette thèse a été réalisé, dispose de beaucoup de travaux en cours sur l'optimisation de dispositifs électromagnétiques, plus particulièrement des machines électriques. Cette thèse est donc orientée vers la même thématique. L'optimisation des machines électriques est un sujet vaste qui s'étend d'un paramètre d'une machine à la machine entière. Communément, les ingénieurs se basent sur les structures existantes et optimisent les dimensions afin d'en faire émerger de meilleures. De ce fait, les optimisateurs se retrouvent souvent contraints par la forme initiale de la structure, et réduisent ainsi le degré de liberté. De plus, ces mêmes formes initiales, bien qu'elles soient convenables, obstruent souvent notre sens de l'innovation en quête de formes plus optimales. De ce fait, nous utiliserons une approche différente à ce type de problème : l'Optimisation Topologique (OT).

L'OT est une méthode originale pour retrouver des structures innovantes sans aucun a priori. Ceci sous-entend une définition du problème d'optimisation sans que la structure existante ne soit prise en compte dans le problème, et ainsi laissant libre choix au processus d'OT de retrouver la structure jugée optimale, relatif aux informations spécifiées. Les chercheurs scientifiques en mécanique structurelle sont les pionniers en OT, ayant pris des décennies avant de présenter un travail abouti. Ces résultats intéressants ont poussé les chercheurs d'autres filières à s'y intéresser, l'électromagnétisme en faisant partie.

L'OT demeure à ce jour l'une des formes les plus complexes d'optimisation car il requiert une multiple expertise en algorithmes d'optimisation, modélisation numérique (en Eléments Finis dans notre cas) et aussi en électromagnétisme dans notre cas pour pouvoir interpréter les

résultats. Le but de cette thèse est d'acquérir et de développer le savoir-faire et l'expertise nécessaire pour pouvoir optimiser la topologie d'un quelconque dispositif électromagnétique, simple ou complexe. Pour atteindre ce but, nous procéderons en fixant une suite d'objectifs.

Le premier objectif est de développer et tester un outil fonctionnel pour l'OT de dispositifs électromagnétiques basé sur les outils 'faits-maison' disponible au L2EP, notamment *code\_Carmel* et *Sophemis*. Le second objectif est de développer une méthodologie pour l'OT, basée sur la Méthode de Densité. La méthodologie proposée devra nous permettre d'avoir une méthode de densité plus efficace et surmonter les problèmes fréquemment rencontrés avec ce dernier. Un cas test académique est utilisé pour tester et valider la méthodologie et les outils. Le troisième objectif est d'adapter notre outil OT pour prendre en compte le comportement non-linéaire des matériaux, et ainsi analyser ses différents effets. En dépit de son importance en électromagnétisme, ce dernier est souvent négligé en OT dans la littérature dû à sa complexité de mise en œuvre et long temps de calcul. Enfin, le quatrième objectif est de valider la méthodologie et les outils OT développés avec des dispositifs plus complexes, notamment un électroaimant 3D et une Génératrice Synchrone à Pôles Saillants (GSPS).

### *Etat de l'Art*

Pour faire de l'OT en général, nous nécessitons d'une méthode de distribution de matière, d'un algorithme d'optimisation et d'un modèle numérique.

Parmi les méthodes de distribution de matière existants dans la littérature, on peut compter la Méthode d'Homogénéisation, la Méthode de Densité, la Méthode ON/OFF, et la Méthode Level-set. Pour ce travail de thèse, nous utilisons la Méthode de Densité pour sa facilité d'application et sa compatibilité avec nos logiciels. Cette méthode consiste à discrétiser le domaine à optimiser, et en utiliser chaque discrétisation comme variable d'optimisation. Chaque discrétisation prendra une densité artificielle qui sera assimilé à une présence ou absence de matériaux à cette position spatiale. Le lien entre les caractéristiques à varier dans le modèle et la densité artificielle est régi par une équation d'interpolation, communément appelé 'Mapping'. La caractéristique utilisée dans notre cas est la perméabilité magnétique des matériaux car nous optimisons des topologies fait de fer (et air).

L'algorithme d'optimisation choisi est *fmincon SQP* (Sequential Quadratic Programming), qui est à base de gradient. Ce choix d'algorithme repose sur l'utilisation de la méthode de densité, car celle-ci traite les variables continues (entre 0 et 1). L'algorithme est utilisé via la plateforme d'optimisation *Sophemis*, développée au sein du L2EP. Cette plateforme permet

l'utilisation des algorithmes disponibles sous Matlab<sup>®</sup>, mais aussi d'autres algorithmes programmés.

Pour la modélisation numérique, nous choisissons la méthode des Eléments Finis (EF), et résolvons les problèmes avec *code\_Carmel*, un code de calcul co-développé au L2EP et à EDF R&D pour les dispositifs électromagnétiques 2D et 3D. *code\_Carmel* se base sur les équations de Maxwell pour résoudre les problèmes électromagnétiques. En ce qui concerne le comportement non-linéaire des matériaux ferromagnétiques, il est pris en compte dans le code de calcul en utilisant la courbe de Marrocco. La méthode Newton-Raphson ou Point-Fixe est utilisée, en fonction de la formulation requise, c.à.d. A- $\phi$  ou T- $\Omega$  respectivement. Néanmoins, la méthode en tant que telle ne peut être utilisée directement en OT. En conséquence, les modifications apportées pour prendre en compte la non-linéarité de matériaux durant l'OT sont aussi abordées dans ce mémoire.

#### *Développement de Méthodologie et Outils OT*

Les outils *code\_Carmel* et *Sophemis* sont couplés afin de réaliser une évaluation d'optimisation et une résolution du modèle EF successivement dans une boucle jusqu'à convergence à une solution optimale. Les matériaux étant distribués avec la Méthode de Densité, le modèle initial est soumis au couplage *code\_Carmel-Sophemis* afin de trouver la topologie optimale. Une fois trouvée, et la convergence vers une solution optimale obtenue, le modèle final peut en être extrait. *code\_Carmel*, étant un solveur EF fonctionnel à part entière, propose plusieurs calculs, entre autres la force magnétique, l'énergie, le couple, le champ magnétique et l'induction magnétique. Celles-ci peuvent être utilisées pour diverses dispositifs électromagnétiques, mais d'autres peuvent aussi être rajoutées suivant les modèles. Le principal avantage d'utiliser *code\_Carmel* dans notre cas est la modélisation et le calcul EF relativement précis dont on bénéficie. D'autre part, avec la plateforme *Sophemis* nous pouvons facilement tester plusieurs algorithmes pour un même modèle sans beaucoup de modifications, et ainsi cette flexibilité nous permet d'analyser rapidement les résultats des algorithmes. Cette nouvelle approche permet de séparer l'outil solveur EF et l'outil d'optimisation pour préserver un aspect flexible, ce qui n'est pas habituellement le cas dans la littérature. La pratique commune est de plutôt rassembler les deux outils en un seul pour facilement passer de l'un à l'autre durant l'OT. Mais ceci a tendance à limiter l'utilisation à quelques méthodes seulement, contrairement au couplage *code\_Carmel-Sophemis* proposé.

Quant à la distribution de matière, nous utiliserons la Méthode de Densité comme indiqué précédemment. Cependant, cette méthode produit souvent des matériaux composites

indésirables dans la solution finale, plus particulièrement pour un grand nombre de variables, soit au-delà de 100, par exemple. Dans notre cas, nous recherchons des structures fait de fer (et air). Les matériaux composites sont des mélanges d'air et fer non définis dans notre problème d'optimisation, et qui ne peuvent donc pas être attribués dans la solution finale. Pour empêcher l'avènement de ces matériaux composites, nous introduisons une fonction mathématique qui les minimise, appelée Facteur de Faisabilité (FF). Cette fonction sera utilisée en objectif pondéré avec l'objectif principal du modèle, qui peut être l'énergie, la force magnétique, l'induction magnétique, et ainsi de suite. Un somme de ces deux objectifs sera optimisé dans le problème. Nous utilisons aussi un coefficient avec le FF pour lui attribuer un poids dans la fonction objectif. Ce poids permettra une transition plus progressive des variables vers des valeurs discrètes de 0 et 1 pour prendre les caractéristiques de fer et d'air, et ainsi générer une structure homogène et réalisable. La fonction FF ne sera pas utilisée comme contrainte dans le problème car la convergence vers une solution dans ce cas est assez brutale. Cela signifie que durant l'optimisation, la prise en compte de la contrainte est faite en premier, donnant lieu à des valeurs discrètes de 0 et 1 réparties dans la topologie pour satisfaire la contrainte. Une fois ses limites atteintes, l'algorithme poursuit avec l'optimisation de la fonction objectif, engendrant souvent des optimums locaux.

L'autre point clé de la méthodologie concerne la prise en compte du comportement non-linéaire des matériaux ferromagnétiques. Comme mentionné précédemment, celle-ci est prise en compte dans *code\_Carmel*. Cela dit, il nécessite une modification pour être appliqué à l'OT. En règle générale pour la non-linéarité, *code\_Carmel* utilise une méthode itérative pour aboutir à la bonne perméabilité, qui est de ce fait non fixée dans le problème à résoudre. Par ailleurs durant le processus d'optimisation, une perméabilité fixe est requise pour résoudre le problème EF à cet instant. Pour surmonter cette difficulté, nous introduisons la densité de la variable dans le code EF, qui est une valeur fixe, et nous combinons le 'Mapping' de densité à l'équation de Marrocco. Cette combinaison permet de renvoyer une densité fixe de l'optimisation au code EF, mais aussi de maintenir la méthode itérative pour retrouver la bonne perméabilité. On satisfait donc aux exigences de chaque outil utilisé pour un résultat cohérent suivant les deux, et ainsi nous permettant de mieux cerner les apports et les limites de la prise en compte de la non-linéarité dans un problème d'OT en électromagnétisme.

Afin de tester et valider la méthodologie, un modèle EF simple, logique et rapide est employé. Un cube électromagnétique avec une différence de potentiel appliquée aux surfaces servira de cas test pour investiguer les différents aspects et limites de la méthodologie. Au premier abord, un cube à 8 variables est utilisé pour obtenir des résultats exhaustifs de

différentes topologies possibles. Ceci servira à analyser le comportement de chaque variable dans le problème, mais aussi de comprendre leur évolution afin que notre méthodologie puisse être renforcée pour un plus grand nombre de variables. Ensuite, un cube à 64 variables est utilisé pour appliquer notre méthodologie et la comparer à d'autres dans la littérature. Nos analyses démontrent que notre méthode converge bien vers des solutions optimales, et que vis-à-vis des autres méthodes existantes, elle présente le meilleur compromis entre qualité des résultats et temps de calcul. Une comparaison est aussi faite entre la prise en compte ou pas de la non-linéarité des matériaux ferromagnétiques en OT. Plusieurs autres aspects du problème sont investigués, par exemple l'effet du maillage, les conditions initiales, ou encore la méthode de prise en compte des variables.

L'expérience acquise au fil de ces expérimentations nous permet dans une seconde étape de passer à une application électromagnétique plus réelle : un électroaimant 3D. La même méthodologie est donc utilisée.

#### *Application à un Electroaimant*

Le choix de l'électroaimant est fait car il demeure un problème relativement commun à l'électromagnétisme, nécessitant les lois de base de Maxwell. De plus, la tendance de sa forme optimale est connue dans la communauté, permettant une meilleure évaluation des résultats. Nous optimisons le dispositif en recherchant la topologie optimale du noyau de fer en appliquant un courant au bobinage de l'électroaimant. Ce dernier, engendrant une force magnétique servira à attirer une barre de fer dans le même modèle. Le tout est modélisé à l'intérieur d'une boîte d'air pour prendre en compte les flux de fuites. Un quart du modèle complet d'électroaimant est modélisé en prenant en compte la symétrie verticale et horizontale. Ceci permet de réduire le nombre de variable et ainsi diminuer le temps de calcul. La force magnétique du noyau pour attirer la barre de fer est maximisée, en contraignant la quantité de matière présente dans la topologie finale. La méthode de prendre en compte les variables dans le domaine à optimiser est aussi revue car elle diffère du cas test précédent.

Ce chapitre du manuscrit met plus l'emphase sur l'action de la non-linéarité des matériaux ferromagnétiques en OT. Les optimisations sont réalisées avec et sans comportement non-linéaire, et pour différentes contraintes sur la quantité de matière dans le domaine à optimiser. Les solutions sont ensuite analysées et comparées. A travers ces derniers, nous avons vu qu'avec la non-linéarité, nous n'avons pas les mêmes résultats en termes de fonction objectif et topologies, même si ces derniers avaient les mêmes tendances à un certain niveau mais pas forcément dans l'intégralité. La principale différence est la distribution de la matière dans

l'ensemble du domaine, qui est plus cohérente et réalisable avec la non-linéarité des matériaux. De plus, les valeurs d'induction magnétique obtenues avec ce dernier sont plus réalistes ( $< 2 T$ ) que ceux avec une linéarité des matériaux ( $> 2T$ ), et démontrant ainsi une prise en compte de la saturation dans le dispositif. Ceci engendre une force magnétique inférieure dans le cas de la non-linéarité, mais qui est physiquement correcte. Nous expliquons aussi l'effet que peut avoir la contrainte de quantité de matière sur les résultats, entre autres l'augmentation de la saturation en diminuant ce premier, ou encore le temps de calcul. Par ailleurs, d'autres aspects de l'OT relatifs au modèle sont examinés, entre autres la taille et la cohérence du maillage, la convergence des solutions et le temps de calcul. Une remarque pertinente est aussi ressortie de ces analyses concernant ce dernier : prendre en compte la non-linéarité des matériaux augmente certes le temps d'un calcul EF (et donc d'une évaluation du modèle), mais ceci ne produit pas un temps de calcul total excessif par rapport au linéaire comme nous aurions pu anticiper. Il se peut que le temps de calcul total en non-linéaire soit aussi moins long, dépendant du problème. Cela est naturellement dû à une meilleure position du problème électromagnétique, et ainsi une solution plus appropriée.

Suite à ces analyses, nous avons voulu traiter un cas plus 'électrotechnique', ceci étant notre cœur de métier. Une Génératrice Synchrone à Pôles Saillants (GSPS) a ainsi été choisie pour apporter un aspect concret à la mise en œuvre de notre méthodologie.

### *Application à une Génératrice Synchrone à Pôles Saillants (GSPS)*

La GSPS, disponible en prototype à Jeumont Electric, est prévue pour la génération d'énergie électrique à partir des éoliens. Avec une puissance nominale de 1 MVA, cette machine triphasé est composée de 8 pôles rotoriques et 96 encoches statoriques, mais on ne modélisera qu'un huitième de la machine en EF en prenant en compte les symétries, pour gagner en temps de calcul. Nous recherchons dans ce cas une distribution optimale de flux dans le stator de la machine, et ensuite une forme plus sinusoïdale de l'induction dans l'entrefer. Pour cela, nous choisissons la tête du rotor comme domaine d'optimisation. Les calculs sont fait avec et sans le comportement non-linéaire des matériaux ferromagnétiques, et les différentes topologies obtenues sont examinées.

Pour une première optimisation, nous ciblons quelques points dans le stator afin d'y maximiser le flux. Les formes optimales de la tête du rotor obtenues avec le comportement linéaire et non-linéaire sont analysées. Nous voyons que sans la non-linéarité prise en compte, la forme de la tête du rotor obtenue comporte beaucoup plus de matière, mais elle est aussi plus saturée, avec des valeurs d'induction magnétique étant non-réalisables physiquement

dans une machine. Quand la non-linéarité est prise en compte, nous voyons une baisse considérable de ces valeurs d'induction magnétique, mais aussi une forme différente du rotor.

En deuxième lieu, une forme sinusoïdale de l'induction magnétique dans l'entrefer est recherchée. L'induction magnétique à 73 points spatiaux dans l'entrefer est optimisée, de sorte à ce que la forme finale de ce premier soit un sinus. Mais ceci produit naturellement des harmoniques dû à l'effet de denture de la machine. En conséquence, nous choisirons seulement 13 points spatiaux dans l'entrefer à optimiser au lieu de 73 afin d'éviter l'effet de denture, ce qui donnera une meilleure cohérence dans nos analyses. Une fois de plus avec la non-linéarité, les topologies obtenues et leurs valeurs d'induction magnétique démontrent une meilleure cohésion avec la réalité physique ; ainsi ce premier ne peut être écarté durant l'OT.

### *Conclusion and Perspectives*

La thèse survole en détail différents aspects de l'OT, notamment les outils développés à cet effet, la méthodologie utilisée, ainsi que l'application à plusieurs cas tests. D'abord, nous abordons les outils EF et optimisation, basés sur *code\_Carmel* et *Sophemis*, tous deux développés au L2EP et couplés pour faire de l'OT. Cette nouvelle approche se démarque des outils classiques retrouvés dans la littérature, où le code EF et optimisation sont dans un même code. Notre approche permet donc d'être plus flexible pour changer de méthode d'optimisation ou résolution EF.

Pour ce qui est de la méthodologie, nous avons deux volets : la méthode de distribution de matière dans la topologie, et ensuite la prise en compte de la non-linéarité des matériaux ferromagnétiques. Pour le premier, nous nous sommes basés sur la méthode de densité avec un Mapping de Perméabilité, et nous avons proposé une technique pour éliminer les matériaux intermédiaires avec cette méthode. En comparaison avec d'autres méthodes de la littérature, nous avons vu que la nôtre présente le meilleur compromis en qualité de résultats et temps de calcul, pouvant donc être utilisée pour les cas tests. Pour la non-linéarité, nous avons mis en place une méthode en utilisant l'équation de Marrocco combiné au Mapping de Perméabilité. Nous l'avons aussi testé et validé sur nos 3 cas tests, démontrant ainsi son importance en OT afin de générer des solutions cohérentes avec la réalité et physiquement faisables.

Les trois cas tests employés présentent chacun une importance à cette thèse. D'abord, le cas test cubique, étant rapide et magnétiquement logique, a servi à comprendre le fonctionnement de l'OT dans son ensemble, ainsi que le comportement des variables. L'électroaimant a, quant à lui, été utile pour analyser l'effet de la prise en compte de la non-linéarité plus en



profondeur et ainsi voir les résultats en cas de saturation. Pour ce qui est de la Machine Synchrones à Pôles Saillants, il représente la concrétisation de la méthode sur une application électrotechnique réelle. Ceci nous a permis de voir les différentes topologies possibles en optimisant des paramètres de la machine.

Le travail effectué durant cette thèse peut bien évidemment servir de base pour apporter encore plus de progrès sur un certain nombre de points en OT en électromagnétisme. En ce qui concerne l'algorithme d'optimisation utilisé, elle pourrait par exemple être remplacée par un algorithme hybride pour aboutir à des solutions plus globales. Le nombre de variables en OT étant élevé, les méthodes classiques d'optimisation rencontrent des difficultés à trouver la solution optimale, d'autant plus qu'il en existe plusieurs dans certains cas. Pour les outils, ils pourraient être retravaillés afin d'être plus facilement utilisable, même par un non-expert. A son état actuel, il nécessite un certain temps d'adaptation pour la prise en main. A propos des applications, d'autres paramètres comme la force électromotrice (f.e.m) ou encore le couple pour la GSPS pourraient être investigués pour rechercher de nouvelles topologies du rotor. Une optimisation topologique pourraient aussi être faite sur les dents du stator pour atténuer les harmoniques, et rendre plus sinusoïdale la f.e.m ou encore l'induction magnétique dans l'entrefer.

Titre en français : Optimisation Topologique de Dispositifs Electromagnétiques

Résumé en français

L'Optimisation Topologique (OT) est un sujet en plein essor qui suscite l'intérêt de nombreux chercheurs depuis ces deux dernières décennies dans le domaine de l'électromagnétisme. L'OT représente une méthode très attrayante et originale car elle permet de trouver des structures innovantes sans aucun a priori. Ce travail de thèse est orienté vers l'OT des dispositifs électromagnétiques en approfondissant plusieurs aspects du sujet. Tout d'abord, un outil d'OT est développé et testé, à partir des outils existant au L2EP. En effet, l'OT requiert un outil d'éléments finis et un outil d'optimisation devant être couplés. Une méthodologie originale d'OT fondée sur les principes de la Méthode de Densité est développée et testée. Un cas test académique est utilisé afin de tester et valider le couplage des outils et la méthodologie. Une approche visant à prendre en compte le comportement non-linéaire des matériaux ferromagnétiques avec nos outils OT est également mise en place. Ensuite, la méthode est appliquée afin d'optimiser un électroaimant en 3 dimensions, représentant un cas test proche de la réalité. Ce cas test permet de comparer les résultats avec un comportement linéaire et non-linéaire des matériaux. Diverses topologies sont présentées, par rapport aux différentes formulations du problème. Par la suite, la méthodologie est appliquée à un dispositif électromagnétique plus complexe : une Génératrice Synchrone à Pôles Saillants. Cet exemple nous permet de voir comment la définition du problème d'optimisation peut grandement affecter les résultats d'OT. Quelques topologies sont présentées, et leur faisabilité est analysée.

Mots-clefs : Optimisation Topologique, Electromagnétisme, Méthode de Densité, Méthode Eléments Finis, Facteur de Faisabilité, Cas Test Cubique, Electroaimant, Génératrice Synchrone à Pôles Saillants

Titre en anglais : Topology Optimisation of Electromagnetic Devices

Résumé en anglais

Topology Optimisation (TO) is a fast growing topic that has been sparking the interest of many researchers for the past two decades in the electromagnetic community. Its attractiveness lies in the originality of finding innovative structures without any layout a priori. This thesis work is oriented towards the TO of electromagnetic devices by elaborating on various aspects of the subject. First of all, a tool for TO is developed and tested, based on the 'home-made' tools available at the L2EP. As TO requires a FE and an optimisation tool working together, a coupling is done using both. Furthermore, a TO methodology is developed and tested, based on the Density Method. An academic cubic test case is used to carry out all the tests, and validate the tools and methodology. An approach is also developed to consider the nonlinear behaviour of the ferromagnetic materials with our TO tools. Afterwards, the methodology is applied to a 3D electromagnet, which represents a more real test case. This test case also serves to compare the results with linear and nonlinear behaviour of the materials used. Various topologies are presented, for different problem formulations. Subsequently, the methodology is applied to a more complex electromagnetic device: a Salient Pole Synchronous Generator. This example allows us to see how the problem definition can largely affect TO results. Some topologies are presented and their viability is discussed.

Keywords : Topology Optimisation, Electromagnetism, Density Method, Finite Element Method, Feasibility Factor, Cubic Test Case, Electromagnet, Salient Pole Synchronous Generator